Fisheries and Oceans Canada | Pêches et Océans Canada
Ecosystems and Oceans Science | Sciences des écosystèmes et des océans

Canadian Science Advisory Secretariat (CSAS)

Research Document 2025/025

Maritimes Region

Calibration of Bottom Trawl Survey Vessels: Results of Comparative Fishing Between the CCGS *Teleost* and CCGS *John Cabot*/ CCGS *Captain Jacques Cartier* on the Scotian Shelf and Bay of Fundy in 2022 and 2023

Yihao Yin[1] , Hugues Benoît[2] and Ryan Martin[3]

Fisheries and Oceans Canada
[1]Bedford Institute of Oceanography
Fisheries and Oceans Canada
1 Challenger Drive
Dartmouth, NS B2Y 4A2

[2]Maurice Lamontagne Institute
Fisheries and Oceans Canada
850 Rte de la Mer
Mont Joli, QC G5H 3Z4

[3]St. Andrews Biological Station
Fisheries and Oceans Canada
125 Marine Science Drive
St. Andrews, NB, E5B 0E4

August 2025

Canada

Foreword

This series documents the scientific basis for the evaluation of aquatic resources and ecosystems in Canada. As such, it addresses the issues of the day in the time frames required and the documents it contains are not intended as definitive statements on the subjects addressed but rather as progress reports on ongoing investigations.

Published by:

Fisheries and Oceans Canada
Canadian Science Advisory Secretariat
200 Kent Street
Ottawa ON K1A 0E6

http://www.dfo-mpo.gc.ca/csas-sccs/
DFO.CSAS-SCAS.MPO@dfo-mpo.gc.ca

ISSN 1919-5044
ISBN 978-0-660-76841-0 Cat. No. Fs70-5/2025-025E-PDF

Correct citation for this publication:

Yin, Y., Benoît, H., and Martin, R. 2025. Calibration of Bottom Trawl Survey Vessels: Results of Comparative Fishing Between the CCGS *Teleost* and CCGS *John Cabot*/ CCGS *Captain Jacques Cartier* on the Scotian Shelf and Bay of Fundy in 2022 and 2023. DFO Can. Sci. Advis. Sec. Res. Doc. 2025/025. iv + 236 p.

Aussi disponible en français :

Yin, Y., Benoît, H. et Martin, R. 2025. Étalonnage des navires de relevé au chalut de fond : résultats de la pêche comparative entre le NGCC Teleost *et le NGCC* John Cabot *ou le NGCC* Captain Jacques Cartier *sur le plateau néo-écossais et dans la baie de Fundy en 2022 et 2023. Secr. can. des avis sci. du MPO. Doc. de rech. 2025/025. iv + 237 p.*

TABLE OF CONTENTS

ABSTRACT

Bottom-trawl surveys provide key inputs to stock assessments for groundfish stocks and other taxa, for ecosystem monitoring and reporting, and for research. These surveys can produce annual indices of abundance that are proportional to stock size, provided that the proportionality constant, typically called catchability, does not change over time. This is typically achieved through the use of standardized survey design and procedures. In the Maritimes Region, the Canadian Coast Guard Ship (CCGS) *Teleost* fishing a Western IIA bottom-trawl conducting the annual Summer Ecosystem Research Vessel Survey of the Scotian Shelf will be replaced by the CCGS *John Cabot* and CCGS *Captain Jacques Cartier* fishing the Northeast Fisheries Science Centre Ecosystem Survey Trawl and such a change in protocols required calibration experiments to estimate adjustments for possible changes in catchability. Hence, a comparative fishing experiment was conducted in the summers of 2022 and 2023 involving fishing by paired vessels and gears at a large number of locations to obtain data for catch required to estimate their relative fishing efficiency for a large number of fish and invertebrate taxa that are routinely sampled in this survey. This document briefly describes the comparative fishing experiment and the resulting catch data, followed by detailed analyses of the data for 108 fish and invertebrate taxa routinely sampled by the RV survey for which there were sufficient data from the experiment. The analyses employed a suite of contemporary statistical models used previously in comparative fishing analyses in the eastern United States as well as the Atlantic regions in Canada. Recommendations for vessel calibrations of catch numbers based on the results of the analyses were provided for these taxa, where 22 taxa had length-dependent conversion factors using length-disaggregated analysis, 14 taxa had length-independent conversion factors using length-disaggregated analysis, 40 taxa had length-independent conversion factors using length-aggregated analysis, and calibration for 21 taxa is recommended as not necessary. Complementary results were also provided for 59 taxa using length-aggregated analysis of catch biomass, of which 42 taxa appear to require a conversion factor, while 15 taxa do not.

1. INTRODUCTION

Bottom-trawl surveys provide key inputs to stock assessments for groundfish and some shellfish stocks worldwide. These surveys can produce annual indices of abundance that are proportional to stock size, provided that the proportionality constant, often called catchability, does not change over time. If this consistency is not achieved via proper sampling design and standardization, then there is a risk that changes in abundance will be confounded with changes in catchability. Maintaining consistency in survey protocols, and the survey vessel and gear, is key to maintaining constant catchability. However, periodically it becomes necessary or desirable to change one or more of these aspects and calibration experiments are required to estimate adjustments for possible changes in catchability. The most common and effective form of these experiments is comparative fishing, which usually involves paired trawling of the former and replacement vessel/gear/protocol as close together as safety permits. This design minimizes the difference in fish population densities sampled by the trawls, such that differences in catches over replicates of paired-trawl sampling will reflect the difference in catchability.

Fisheries and Oceans Canada (DFO) undertook a comparative fishing experiment in the Maritimes Region bottom-trawl survey (Figure 1) on the Scotian Shelf and Bay of Fundy in the summers of 2022 to 2023 to calibrate two new offshore fisheries survey vessels, Canadian Coast Guard Ship (CCGS) John Cabot and CCGS Captain Jacques Cartier (hereafter, the Cabot and the Cartier) that will replace the retiring longstanding vessels, CCGS Teleost and CCGS Alfred Needler. The Cabot and the Cartier are identical in design and build, and are considered to have equivalent fishing efficiency when identical trawls and protocols are employed. Paired trawls were conducted between the new vessels and the Teleost during 2022 and 2023 as a comparative fishing experiment like one undertaken between the Teleost and the Needler in 2005. The change in vessels will also be accompanied by a change in survey trawl from the Western IIA (WIIA) to the NEST (Northeast Fisheries Science Centre Ecosystem Survey Trawl), as well as in survey procedures (e.g., tow distance). The joint effect of all of these factors on relative catchability should be reflected in results of the comparative fishing experiments. Protocols for comparative fishing trawls were designed specifically to ensure paired trawls sample similar environmental conditions and fish aggregations, two factors that directly affect catch or catchability, such that the resulting data could provide a foundation for estimating conversion factors for calibrating historical survey catches for taxa of concern.

This document briefly introduces the comparative fishing experiment protocols first, followed by a description of the methods used for processing, validating and subsequently, analyzing the comparative fishing data. These methods have been employed by the Gulf, Québec, and Newfoundland Regions to analyze their current comparative fishing experiments from 2021 to 2023 (Benoît et al. 2024 for the Québec Region in the northern Gulf of St. Lawrence, Benoît and Yin 2023 for the Gulf Region in the southern Gulf of St. Lawrence, and Trueman et al. 2023 for the Newfoundland Region). Methods for validation of paired comparative fishing sets are detailed in Ricard et al. 2023. Methods for analyses of paired sets include contemporary statistical models used previously in extended comparative fishing analyses in the eastern United States (Miller et al. 2010, Miller 2013), and applied recently to analyses of past comparative fishing data for some stocks in the Gulf of St. Lawrence (Yin and Benoît 2022a, Benoît et al. 2022). These models were extensively tested in a simulation study and were confirmed appropriate for analyses (Yin and Benoît 2022b). Given considerable differences between the old and replacement survey protocols, which include a substantial change in the fishing gear and tow length, important differences in length-dependent and independent relative catchability were expected for this comparative fishing experiment. The analyses were only

applied to taxa with adequate data, based on which recommendations for conversion factors were provided.

2. METHODS

2.1. COMPARATIVE FISHING

2.1.1. Comparative fishing experiment protocols

Details of the comparative fishing and vessel-specific protocols used in this comparative fishing experiment largely followed those presented in Ricard et al. (2023) for similar experiments undertaken in the southern Gulf of St. Lawrence, and are therefore only briefly discussed here. In 2022 and 2023, the CCGS Teleost (hereafter referred to as the Teleost) served as the "primary" vessel which was responsible for carrying out the standard/full survey protocol. The CCGS John Cabot (2022, hereafter referred to as the Cabot) and CCGS Capt. Jacques Cartier (2023, hereafter referred to as the Cartier) were considered the "secondary" vessels and followed a reduced sampling protocol to fulfill the data collection requirements for the calibration analyses; mainly total catch weight and length frequencies, although in many cases additional parameters such as specimen weight and sex were also collected.

At pre-selected stations, the primary and secondary vessels fished side-by-side along parallel tracks as close together in space and in time as was safe and practical. The distance separating the vessels was typically 0.5 nautical miles (nm), and effort was made to ensure both tow tracks occupied similar depths. Across stations, vessels alternated between having the other vessel on their port or starboard side. The primary (Teleost) and secondary (Cabot/Cartier) vessels used different fishing gear and protocols. The Western IIA trawl (WIIA) was used for the Summer RV Surveys since 1982. Tows were conducted for 30 minutes at a speed of 3.5 knots covering 1.75 nautical miles over ground. Tow durations of at least 20 minutes were considered acceptable. The duration of tows was measured according to the elapsed time between locking the trawl winches following gear deployment and the initiation of hauling back the trawl. The secondary vessels were equipped with the Northeast Fisheries Science Centre Ecosystem Survey Trawl (NEST), a research trawl designed to better capture various sizes of specimens from a variety of taxa compared to the WIIA. The target tow duration was 20 minutes at a speed of 3 knots with an expected tow distance of 1.0 nautical mile. Tow durations of at least 16 minutes were considered acceptable. In contrast to the primary vessel protocol, the duration of tows was measured between the time the trawl touched down on bottom, indicated by the trawl positioning data from Scanmar trawl sensors, and when the winches engaged for hauling back the trawl. The data from Scanmar sensors were additionally used to monitor trawl performance for both the WIIA and NEST trawls, and aided in the validation of a successful tow. Scanmar data was not used to calculate the swept area of each tow for use in the data analyses. Instead, tow distance was used as the sole standardizing factor for swept area. Further details on comparative fishing protocols are available in Ricard et al. (2023).

2.1.2. Data collection and pre-processing

ANDES (A New Data Entry System) was the primary data collection program used during the comparative fishing experiment. This system has built-in checks for a suite of information collected during a fishing set. Actual fishing location in relation to the stratum boundaries and the randomly selected site ensures that the appropriate station is being sampled. In the processing lab, the catch is sorted by species and a total weight by species is entered. A list of species that are more common for the occupied location is used in the data entry system to check against each species entered. If a species that is not on the list is entered, a notification

will appear and the identification can be re-checked, and corrected if necessary. ANDES uses predetermined ‘a’ and ‘b’ values to calculate length-weight regression curves for many of the species requiring length and weight data. A notification is generated if the weight of a specimen at a given length falls outside the +/-25% buffer of an expected weight. This can then be immediately re-checked and corrected or confirmed. Finally, once sampling on a species is deemed complete, the sum of individual specimen weights is compared with the total weight of the sampled baskets for that species, to ensure the appropriate amount was represented.

Upon completion of the survey, all data are extracted from ANDES and formatted to align with data tables in the Oracle database where Ecosystem Research Vessel Surveys data is stored. A second round of scrutiny is performed using Structured Query Language (SQL) scripts to run checks on tow distance, speed, duration, and also on the catch and detail information.

In some rare instances, several baskets might be recorded as a “mixed catch” in ANDES (such as large catches of various shrimp species). In such cases, one “parent basket” will be identified, and this basket will be carefully examined. All species are accurately identified, weighed, and counted, and the relative proportion of each species will be determined. With the underlying assumption that all mixed baskets of a single parent have a similar mixture of species, these ratios are then applied to all of the child baskets.

2.1.3. Validation of paired sets

Comparative fishing experiments were conducted in the summers of 2022 and 2023 using the CCGS Teleost (2022, 2023), CCGS John Cabot (2022), and CCGS Jacques Cartier (2023) in order to calibrate data from historic research vessel (RV) surveys. The Cartier was originally planned to conduct comparative fishing with the Teleost in 2022, but due to delays in maintenance of the vessel, it was not available at the time of the survey. Instead, the Cabot was made available for comparative fishing for a limited number of sea days in 2022. The Cabot and Cartier are sister ships with identical designs and are thus considered interchangeable platforms. Comparative fishing between the Teleost and Cabot was conducted between July 20 and August 5, 2022 and comparative fishing between the Teleost and Cartier was conducted between June 29 and August 7, 2023. A total of 93 comparative fishing sets were completed in 2022 by the Teleost and Cabot, and an additional 189 comparative fishing sets were completed in 2023 by the Teleost and Cartier, totaling 282 comparative fishing sets (Tables 1 and 2). In 2022, comparative fishing was restricted to Northwest Atlantic Fisheries Organization (NAFO) Divisions 4X, western 4W, and the Canadian portion of 5YZ. No comparative fishing was completed in NAFO Divisions 4V, the eastern portion of 4W, or any of the deep water slope strata in 2022 (Table 2; Figures 1 and 2). In 2023, comparative fishing was completed throughout the survey range (NAFO Divisions 4VWX5c) with the exception of the Bay of Fundy in NAFO Division 4X and Canadian portion of Georges Bank in NAFO Division 5Z (Table 2; Figure 2). Between 2022 and 2023, all NAFO Divisions within the Summer RV Survey range received comparative fishing coverage, however, some gaps remain in the areas near Halifax and the Eastern Shore of Nova Scotia, the southern Laurentian Channel, and the deeper waters on the Scotian Shelf edge (Table 1; Figure 2).

In order to determine the validity of comparative fishing sets, further review of the comparative fishing data was conducted based on a number of criteria as listed below (see Ricard et al., 2023 for details of set validation methods and criteria):

1. Timing difference between sets in a pair: the timing difference was calculated as the difference between the starting times of the two paired tows,

2. Distance between vessels: the starting and ending locations were recorded for each tow; assuming the vessels tracked a straight line in each tow, the minimum/maximum distance was calculated as the minimum/ maximum distance between the two tracks,
3. Depth differences between sets: depths were recorded at the start and end of each tow and differences between start and end depths were calculated; average depth was calculated and assumed as the tow depth and the difference between sets in a pair was calculated,
4. Side of vessel: the side on which the Cartier/Cabot fished in each set pair was identified using the method from Ricard et al., 2023 and cross-validated with notes from captains; the sides sequenced with regard to dates and tested for statistical randomness using a Wald–Wolfowitz runs test (Wald and Wolfowitz 1940, Wu and Zhao 2013),
5. Duration of tows: the duration of tows were examined and significant deviation from vessel-specific protocols was identified.

2.2. COMPARATIVE FISHING ANALYSIS MODELS

2.2.1. Binomial models

In the analysis of comparative fishing data, the goal is to estimate the relative fishing efficiency between a pair of vessel-gear combinations (referred to as vessel in this section for simplicity). The expected catch from vessel v ($v \in \{A, B\}$) at length l and at station i is assumed as

$$E[C_{vi}(l)] = q_{vi}(l)D_{vi}(l)f_{vi}$$

where, $q_{vi}(l)$ is the catchability of vessel v, D_{vi} is the underlying population density sampled by vessel v, and f_{vi} is a standardization term which usually includes the swept area of a tow, and if applicable, the proportion of sub-sampling for size measurement on-board. In a binomial model (e.g., Miller 2013), the catch from vessel A at station i, conditioning on the combined catch from both vessels at this station, $C_i(l) = C_{Ai}(l) + C_{Bi}(l)$, is binomial-distributed

$$C_{Ai}(l) \sim BI(C_i(l), p_{Ai}(l))$$

where $p_{Ai}(l)$ is the expected proportion of catch from vessel A. Tows in a pair are generally assumed to fish the same underlying densities at the station, as the paired vessels typically fish within a small distance of each other: $D_{Ai}(l) = D_{Bi}(l) = D_i(l)$. Then the logit-probability of catch by vessel A is

$$logit(p_{Ai}(l)) = log(\frac{E[C_{Ai}(l)]}{E[C_{Bi}(l)]}) = log(\rho_i(l)) + o_i$$

Where $\rho_i(l)$ is the ratio of catchabilities between vessels A and B at length l and at station i, or the conversion factor, the quantity of interest,

$$\rho_i(l) = q_{Ai}(l)/q_{Bi}(l)$$

and $o_i = log(f_{Ai}/f_{Bi})$ is an offset term derived from known standardization terms for tow length relative to the standard tow lengths and for subsampling.

For a length-based conversion factor, a smooth length effect is assumed, based on a general additive smooth function,

$$log(\rho(l)) = \sum_{k=0}^{K} \beta_k X_k(l) = \mathbf{X}^T\boldsymbol{\beta},$$

where $\boldsymbol{\beta}$ are the coefficient parameters and are estimated, $\mathbf{X}$, or $\{X_k(l), k = 0,1,\cdots,K\}$, are a set of smoothing basis functions, and K is the dimension of the basis that controls the number of coefficient parameters and is usually pre-defined. Here a cubic spline smoother was used (Hastie et al. 2009), with the basis functions and penalty matrices generated by the mgcv (Wood 2011) R package (R core team 2021).

The estimation of a cubic spline smoother is based on the penalized sum of squares smoothing objective, but in practice, this is usually replaced by a penalized likelihood objective (Green and Silverman 1993):

$$\mathcal{L}(\boldsymbol{\beta}, \lambda) = f(\mathbf{Y}|\mathbf{X}, \boldsymbol{\beta}) e^{-\frac{\lambda}{2}\boldsymbol{\beta}^T \mathbf{S} \boldsymbol{\beta}}$$

$\mathcal{L}$ denotes the likelihood objective function. $f(\mathbf{Y}|\mathbf{X}, \boldsymbol{\beta})$ is the joint probability function of the survey data $\mathbf{Y}$ conditional on the basis functions and coefficient parameters. $\mathbf{S}$ is the penalty matrix defined by the smoother and the dimension of the basis, and λ is the smoothness parameter. This smoothness parameter is estimated by maximum likelihood along with other model parameters but may be sensitive to the data. In such cases, it can be determined by other criteria such as generalized cross-validation (Wood 2000).

The penalized maximum likelihood smoother can also be re-parameterized into a mixed effects model (Verbyla et al. 1999, Wood 2017) to facilitate implementation as well as incorporation of additional random effects:

$$log(\rho_i(l)) = \mathbf{X}_f^T \boldsymbol{\beta}_f + \mathbf{X}_r^T \mathbf{b}$$

where $\boldsymbol{\beta}_f$ are fixed effects and $\mathbf{b}$ are random effects. $\mathbf{X}_f$ and $\mathbf{X}_r$ are transformed from the basis functions $\mathbf{X}$ and an eigen-decomposition of the penalty matrix $\mathbf{S}$, $\mathbf{X}_f = \mathbf{U}_f^T \mathbf{X}$ and $\mathbf{X}_r = \mathbf{U}_r^T \mathbf{X}$, where $\mathbf{U}_f$ and $\mathbf{U}_r$ are the eigenvectors that correspond to the zero and positive eigenvalues of $\mathbf{S}$. The random effects $b \sim \mathrm{N}(0, \mathbf{D}_+^{-\mathbf{1}}/\boldsymbol{\lambda})$ where D_+ is the diagonal matrix of the positive eigenvalues of $\mathbf{S}$. In the mixed effects model representation of the cubic spline smoother, the number of fixed effects is 2 and the number of random effects is bounded by $K - 2$. Smoothing effects are transformed into shrinkage of random effects in the fitting of random deviations, and can be integrated into complex mixed effects models commonly used in fisheries science (Thorson and Minto 2015).

Additional random effects can be incorporated into the mixed effects model to address variations in the relative catch efficiency related to each station,

$$log(\rho_i(l)) = \mathbf{X}_f^T(\boldsymbol{\beta}_f + \boldsymbol{\delta}_i) + \mathbf{X}_r^T(\mathbf{b} + \boldsymbol{\epsilon}_i).$$

where $\boldsymbol{\delta}_i \sim \mathrm{N}(\mathbf{0}, \boldsymbol{\Sigma})$ and $\boldsymbol{\epsilon}_i \sim \mathrm{N}(\mathbf{0}, \mathbf{D}_+^{-1}/\xi)$. From a similar re-parameterization of the cubic spline smoother, these random effects allow for deviations of the length-based conversion at each station. $\boldsymbol{\Sigma}$ is the covariance matrix of the random effects corresponding to the random deviations and contains three parameters. ξ controls the degree of smoothness of the random smoothers and the smoother at each station can differ.

A summary of the above binomial mixed model is as follows,

$$C_i(l) = C_{Ai}(l) + C_{Bi}(l)$$

$$C_{Ai}(l) \sim BI(C_i(l), p_{Ai}(l))$$

$$logit(p_{Ai}(l)) = log(\rho_i(l)) + o_i$$

$$log(\rho_i(l)) = \mathbf{X}_f^T(\boldsymbol{\beta}_f + \boldsymbol{\delta}_i) + \mathbf{X}_r^T(\mathbf{b} + \boldsymbol{\epsilon}_i)$$

The model is estimated via maximum likelihood and the marginal likelihood integrating out random effects is

$$\mathcal{L}(\boldsymbol{\beta}_f, \boldsymbol{\Sigma}, \lambda, \xi) = \int \left(\prod_{i=1}^{m} \int \int f(\mathbf{Y}_i | \mathbf{X}_f, \mathbf{X}_r, \boldsymbol{\beta}_f, \mathbf{b}, \boldsymbol{\delta}_i, \boldsymbol{\epsilon}_i) f(\boldsymbol{\delta}_i | \boldsymbol{\Sigma}) f(\boldsymbol{\epsilon}_i | \xi) \mathrm{d}\boldsymbol{\delta}_i \mathrm{d}\boldsymbol{\epsilon}_i \right) f(\mathbf{b}|\lambda) \mathrm{d}\mathbf{b}$$

The binomial mixed model can be adapted for various assumptions on the smoother and potential station variation to accommodate different underlying density of a species and data limitations especially in length measurements. A set of binomial models considered in the present analyses is provided in Table 3.

2.2.2. Beta-binomial models

The binomial assumption of the catch can be extended to a beta-binomial distribution to explain over-dispersion at the stations (Miller 2013):

$$C_{A,i}(l) \sim BB(C_i(l), p_{A,i}(l), \phi_i(l)).$$

The beta-binomial distribution is a compound of the binomial distribution and a beta distribution. More specifically, it assumes a beta-distributed random effect in the expected proportion of catch from vessel A across stations. As a result, the expected catch by vessel A has a variance of

$$var(C_{A,i}) = C_i p_i (1 - p_i) \frac{\phi_i + C_i}{\phi_i + 1}$$

where ϕ is the over-dispersion parameter that captures the extra-binomial variation.

The same smoothing length effect can be applied to the over-dispersion parameter,

$$log(\phi_i(l)) = \mathbf{X}_f^T \boldsymbol{\gamma} + \mathbf{X}_r^T \mathbf{g}$$

where $\boldsymbol{\gamma}$ are fixed effects and $\mathbf{g}$ are random effects, $\mathbf{g} \sim \mathrm{N}(0, \mathbf{D}_+^{-1}/\tau)$. This length effect models the variance heterogeneity and is particularly useful for projecting uncertainty to poorly sampled lengths. However, estimation of a length-based variance parameter typically requires sufficient catch at length data, which is usually not available for less abundant species.

A summary of the beta-binomial mixed model is as follows,

$$C_i(l) = C_{Ai}(l) + C_{Bi}(l)$$
$$C_{Ai}(l) \sim BB(C_i(l), p_{Ai}(l), \phi_i(l))$$
$$logit(p_{Ai}(l)) = log(\rho_i(l)) + o_i$$
$$log(\rho_i(l)) = \mathbf{X}_f^T(\boldsymbol{\beta}_f + \boldsymbol{\delta}_i) + \mathbf{X}_r^T(\mathbf{b} + \boldsymbol{\epsilon}_i)$$
$$log(\phi_i(l)) = \mathbf{X}_f^T \boldsymbol{\gamma} + \mathbf{X}_r^T \mathbf{g}$$

The marginal likelihood is

$$\mathcal{L}(\boldsymbol{\beta}_f, \boldsymbol{\gamma}, \boldsymbol{\Sigma}, \lambda, \xi, \tau)$$
$$= \int \int \left(\prod_{i=1}^{m} \int \int f(\mathbf{Y}_i | \mathbf{X}_f, \mathbf{X}_r, \boldsymbol{\beta}_f, \mathbf{b}, \boldsymbol{\gamma}, \mathbf{g}, \boldsymbol{\delta}_i, \boldsymbol{\epsilon}_i) f(\boldsymbol{\delta}_i | \boldsymbol{\Sigma}) f(\boldsymbol{\epsilon}_i | \xi) \mathrm{d}\boldsymbol{\delta}_i \mathrm{d}\boldsymbol{\epsilon}_i \right) f(\mathbf{b}|\lambda) f(\mathbf{g}|\tau) \mathrm{d}\mathbf{b} \mathrm{d}\mathbf{g}$$

Likewise, various smoothing assumptions can be applied to the variance parameter. Table 4 presents a set of beta-binomial mixed models.

2.2.3. Tweedie model for biomass data

The binomial and beta-binomial models are appropriate for data constituted of catch counts, but are not appropriate for catch weight or biomass. Biomass indices are routinely derived from survey data for population trend monitoring. For taxa that are measured, biomass values adjusted for the change in relative catchability are most reliably derived by applying the results of the analyses described above to length specific catch numbers and employing a length-weight conversion. However, individual measurements are not made for numerous invertebrate taxa, and were not made for some years or some specific survey hauls for many of the remaining taxa. Estimates of relative catchabilities were therefore required for size-aggregated catch weights for all taxa.

The analysis of catch weights required a probability distribution with a mass at zero, but that is otherwise continuous and can accommodate some overdispersion in catch weights. Unlike the models for catch counts, it was not possible to condition model estimates on the total catch. The following model was employed, which assumed Tweedie (TW) distributed error:

$$W_{i,v} \sim TW(\mu_{i,v}, \varphi, \rho)$$

$$E\left[W_{i,v}\right] = \mu_{i,v} = \exp\left(v + S_i + o_{i,v}\right)$$

$$\varepsilon_{i,v} \sim TW\left(0, Var\left[W_{i,v}\right]\right)$$

$$Var\left[Y_{i,v}\right] = \varphi(\mu_{i,v})^{\tau}$$

where $W_{i,v}$ is the catch weight at station *i* by vessel *v*, $\mu_{i,v}$ is the expected catch weight at station *i* for vessel *v,* φ is the dispersion parameter of the Tweedie distribution,τ is a power parameter, restricted to the interval 1< τ <2 (Dunn and Smyth 2005), *v* is the fixed vessel effect, where *exp*(*v*) = ρ, S_i is a fixed effect that accounts for the biomass at station *i*, and $o_{i,v}$ is the offset. Unlike the model for catch numbers in which the offset term was the log of the ratio of sampling effort (tow distance and catch sampling fraction), the offset term in the Tweedie model is the log of sampling effort at station *i* for vessel *v*, relative to the standard effort for that vessel.

A version of the model in which the station effect was treated as a random effect of the following form was initially investigated:

$$E\left[W_{i,v}\right] = \mu_{i,v} = \exp\left(v + \delta_i + o_{i,v}\right)$$

$$\delta_i \sim N(0, \sigma^2)$$

However, the assumed normal distribution for the random effect in the linear predictor was found to be inappropriate.

2.2.4. Model fitting, selection, and validation

The binomial and beta-binomial models in Tables 3 and 4 for analyses of length-disaggregated catches were implemented using the Template Model Builder (TMB) package (Kristensen et al. 2016). TMB uses the Laplace approximation to integrate the joint negative loglikelihood (nll) over the random effects to calculate the marginal nll (mnll). Optimization of the mnll is then undertaken in R using the *nlminb()* function. The basis functions for the cubic smoothing spline and the corresponding penalty matrices were generated using the R package mgcv (Wood 2011) based on 10 equally-spaced knots ($K = 9$) within the pre-specified length range depending on the range of lengths observed proper to each taxon. TMB automatically calculates a standard error for the maximum likelihood estimation of the conversion factor via the delta method (Kristensen et al. 2016).

Analyses were also undertaken for length-aggregated catch numbers, for those taxa or instances where length-aggregated conversion factors are required. Contrary to the analyses described above that treat the catch of a taxon at a station and in a length class as the basic datum, these length-aggregated analyses model the total catch numbers at each station. For simplicity, these analyses were implemented using the glmmTMB function from the homonymous R package (Brooks et al. 2017). Models BI0, BI1, BB0 and BB1 (Tables 3 and 4) were fitted by specifying family=binomial(link="logit") or family=betabinomial(link="logit"), as appropriate. Note that conversion factor estimates for these four models obtained from the length-disaggregated analyses are likely to differ from those obtained from the length-aggregated analyses when there are strong underlying length-dependent effects on relative catchability between the two vessels.

The analyses of catch weights were also implemented using the glmmTMB function. The option family="tweedie" was specified.

Length-disaggregated models were fitted only for taxa for which there were data for, (1) at least 10 relevant set pairs (i.e., where each vessel within the pair had at least one catch), (2) at least 30 catches from each vessel, and (3) an observed length range spanning at least 10 cm (or mm depending on the measuring unit in record). Length-aggregated models were fitted for taxa for which there were data for, (1) at least 5 relevant set pairs, and (2) at least 15 catches from each vessel. These criteria were used as minimum requirements to determine a list of taxa to attempt analyses and some taxa did not receive scientific recommendations after further scrutiny of the results. Note that these criteria were updated for this study and thus slightly different from the analyses in other regions (Benoît et al. 2024 for the Québec Region in the northern Gulf of St. Lawrence, Benoît and Yin 2023 for the Gulf Region in the southern Gulf of St. Lawrence, and Trueman et al. 2023 for the Newfoundland Region). Table 5 listed all taxa considered for model-based analyses.

In addition, a ratio estimator (i.e., sample ratio between total catches from paired vessels) was calculated and reported for taxa for which there were data for at least 5 relevant set pairs. The ratio estimator can be used as a reference for comparison with model-estimated conversion factors. However, this sample ratio was not recommended for vessel calibration and therefore its associating confidence interval (CI) was not provided. While these thresholds are somewhat arbitrary, they are reasonable in light of the complexity of the models (number of fixed and random parameters estimated), the total number of taxa, and are consistent with minimum sample size requirements evident from the simulation study of Yin and Benoît (2022b). Table 5 provided a summary of data to illustrate sample sizes available for each taxon. Table 6 provided a summary of spatial distributions and population levels for all encountered taxa in the comparative fishing experiment.

There were in total 13 candidate models of length-disaggregated catches for estimating the conversion factors, although convergence could not be attained for any of the taxa for the most complex model BB7. There were four candidate models for length-aggregated catch numbers. The best model for each set of analyses was selected by BIC (Bayesian information criterion) to maximize model fitting, while avoiding over-fitting of more complicated models, especially in cases without adequate data. Values were also examined for AIC (Akaike information criterion), which tends to select slightly more complex models compared to BIC. In the present applications, AIC largely supported decisions based on BIC.

In each length-disaggregated analysis, the estimated μ function (length-dependent expected proportion of catch by vessel A) from all converged models were compared along with the sample proportions (aggregated by stations and averaged for each length) to provide a more rigorous interpretation of the results. The estimated $\rho(l)$ (expected relative catch efficiency, or

conversion factor function) and associated approximate 95% confidence interval (95% CI) from the best model is then shown over the range of lengths contained in the input data. Normalized quantile model residuals (Dunn and Smyth 1996) were produced and plotted using boxplots against length and survey station to visually assess the adequacy of model fit. Finally, model residuals were plotted against depth and the time at which a station was fished, two factors known to affect catchability (e.g., Benoît and Swain 2003), to evaluate whether these effects might interact with the vessel effect under study.

The fit of catch-aggregated analyses for counts and weights was assessed by plotting the conversion factor and associated approximate 95% CI in biplots of the catch of one vessel over the other. Additionally, the scaled quantile residuals obtained using the R package DHARMa (Hartig 2021) were examined. Unlike the normalized quantile residuals used in the length-disaggregated analyses above, which have an expected Gaussian distribution when model fit is adequate, the quantile residuals from DHARMa have an expected uniform distribution. The choice was dictated in part by the fact that it was easier to examine residuals using boxplots in the former case, which has more residual values. Residuals for the catch-aggregated analyses were examined for uniformity and possible overdispersion, and plotted as a function of the fitted values, station depth and time. The evaluation of residuals was in size-aggregated analyses was limited to a visual inspection.

2.2.5. Data treatment prior to analysis

Data for some taxa were grouped prior to analysis due to perceived inconsistencies in identification during the surveys or due to small sample sizes amongst related and morphologically similar taxa. *Gadus* sp. (code 251) individuals ≤ 20 cm are processed separately during catch sampling because of difficulties in distinguishing *G. morhua* and *G. ogac* at these sizes in the field. Normally samples are brought back to the laboratory for identification; however, such lab-based identification was not available in time for the comparative fishing data analyses. Given the relative prevalence of Atlantic Cod in the ecosystem, the fact that confirmed catches of *G. ogac* were not sufficiently frequent to include in any of the analyses, and the assumption that the catchability of small *Gadus* sp. should be the same as that of same-sized individuals of the specific species, these data were combined with the catches for *G. morhua*. This and the other taxonomic groupings are outlined in Table 7.

In a very small number of instances, the catch of one or two individuals at the very smallest or very largest lengths had undue influence on the shape of the length-dependent conversion factor function at and around those lengths. This results from the flexibility inherent in the cubic spline functions and is a known problem for these models (Cadigan et al. 2022). Although Cadigan et al. (2022) present an alternative and likely more robust approach, it is only applicable to monotonic length-dependent relative catchability functions and was not appropriate for the results of this comparative fishing where more complex, non-monotonic, functions were prevalent. Instead, the catches for these extreme lengths were excluded from the analysis. These cases are summarized in Table 8.

2.2.6. Interpretation of results and application of conversion factors

Although automatic model selection via BIC was used in the analyses, results were reviewed thoroughly and scrutinized. For a small number of taxa, the best model selected by BIC was rejected and analyses were downgraded from length-disaggregated models to length-aggregated models (i.e., re-analyzed using simpler models). Data and/or results for these taxa were not sufficient to support length-dependency in the conversion factors even though the models could be fit. Similarly, for a small number of taxa where estimated conversion factors are unrealistic (<0.05 or >20, i.e., difference between vessels exceeds 20 times), the length-

disaggregated models were rejected and no conversion factors could be estimated or recommended with confidence. These cases usually resulted from lack of effective data for analyses, especially when one vessel had predominantly zero catches compared to the other vessel. The taxa where analyses results were rejected for the reasons above are summarized in Table 8. Besides, for both model-based analyses, failure in model convergence or parameter estimation indicates insufficient data and results were not included in this document. However, for taxa where estimated conversion factors did not show significant difference between paired vessels (i.e., the 95% CI encompass a conversion factor of one), result figures were included for reference.

Two general patterns observed in the model selection and model results motivated the adoption of additional screening criteria in determining whether a conversion factor (function) should be applied, and which should be chosen for application in future analyses of the survey data. First, there were some taxa for which the 95% CI for a length-dependent conversion factor function overlapped with a value of one across all lengths, indicating absence of statistical significance for either length-dependency or the difference between vessel catchability, despite a length-dependent model being selected. This likely resulted from the use of marginal AIC and BIC values, for which the effective number of parameters may not be correctly calculated for the model random effects, causing more complex models with smoothed length effects to be favoured. Therefore, adopting conversion factor functions when the CI overlaps unity over the range of length is not recommended. In these cases, the results for non-length dependent analyses were examined, however, it was found that these were not statistically significant either.

As noted above, the estimation of length-specific conversion factor functions can be sensitive to the sparseness of data in the tails of the length frequencies. Despite eliminating some extreme lengths, there were still cases where conversion factor values diverged considerably from the overall length-dependent trend as lengths tended toward the smallest and largest lengths. Therefore, the following procedure was adopted. First, lengths were identified that constituted the 0.5^{th} and 99.5^{th} percentiles of the taxon-specific total length frequency distribution for the 2022–2023 experiment for taxa with at least 20 length classes, and used the 2.5^{th} and 97.5^{th} percentiles for taxa with fewer classes. Then, the conversions factor function values at these percentiles were identified for each taxon, and these values were assumed to be constants for lengths below and above these percentiles, respectively. These constant values were projected respectively to the taxon-specific smallest and largest lengths observed since 1984 in the survey (Ecosystem Research Vessel Surveys). Note that these data were from the Needler and the Teleost with Western IIA gear and may not be consistent with resultant data from comparative fishing in 2022 and 2023 using new vessels and gears.

3. RESULTS

3.1. VALIDATION OF PAIRED SETS

All successful and paired sets in the 2022–2023 comparative fishing experiment (282 pairs in total; Table 2) were validated after pre-processing to clean data. Six pairs (station numbers 249, 978, 123, 135, 254 and 6) had a time difference greater than 60 minutes, but were all within 90 minutes (Figure 3). There were 10 pairs where depth difference was greater than 20 meters but, as a percentage, all depth differences were within 15% (Figure 3; percentage calculated using the average depths from both vessels and both starting and ending locations); start depth differences and end depth differences were both consistently within protocol (Figure 4). Distance between vessels from all paired sets was within 3 nm (nautical miles), indicating close proximity between tows in a pair (Figure 3). The Cartier/Cabot were on the port side in 141 pairs

and the starboard side in 141 pairs (Figure 4); the sequence of sides was tested using a Wald–Wolfowitz runs test and results showed statistical significance for randomness (p-value < 0.001). Durations of tows for the three vessels did not show significant deviations even though a small number of tows were a few minutes shorter than standard (Figure 4; standard in protocol is 30 minutes for the Teleost and 20 minutes for the Cabot/Cartier). Overall, no serious concerns were identified, and hence, all sets were retained for analyses.

3.2. SUMMARY OF RESULTS

Results of analyses were summarized in Tables 6–9 and aggregated in Figures 5 and 6 with details explained and presented in Table 5 and Figures 7–109.

In total, the comparative fishing experiment recorded 417 encountered taxa (although some taxa code were designated to hard-to-identify situations). After data cleaning and grouping of taxa (Table 7) 384 taxa remained, but only 108 taxa met the minimum data requirements (>5 effective paired sets; Section 2.2.4) for analyses. A summary of data availability, sample sizes and the sample conversions (calculated as ratio between total catch numbers and biomass) for each taxon are listed in Table 5. Due to concerns in data reliability and/or model suitability, analyses for two taxa (codes 64 and 4321) were rejected and therefore, no recommendations were provided.

There were 46 taxa that met the minimum data requirements (Section 2.2.4) for length-disaggregated models (LDM; see Section 2.2 for details). LDM results for four taxa (codes 204, 340, 610, 701) were rejected for lack of confidence in estimated length-dependency and analyses were downgraded. In total, five taxa were removed, and detailed data visualization and results presentation for 40 taxa were included in Figures 11–50. Model selection and relative evidence based on AIC and BIC values are included in Table 10. BB7 did not converge for any taxon, and therefore, was not included. For most taxa, selection criteria preferred models with random station effects; this is likely due to wide variations among stations where different gears performed differently depending on environmental conditions such as bottom types, etc., and species population densities. The station effects were also indicated by the divergence between the aggregated versus averaged sample proportions in the data figures. Table 5 provides a reference to the resultant figures for these taxon and the final recommendation of conversion factors for application to vessel calibration. Table 9 provides a summary of recommendations of conversion factors for application based on results of analyses.

There were 106 taxa that meet the minimum data requirements (Section 2.2.4) for length-aggregated models (LAM). Taxa with successful model fits were reviewed and five (codes 150, 1812, 6113, 6121, 6413) were rejected due to insufficient information in data and/or lack of confidence in results. In addition, two more taxa with unrealistic results (codes 8367, 8600) were rejected for LAM for catch numbers, while two more taxa with insufficient data (codes 2809, 2893) were rejected for LAM for catch biomass (see Table 8 for details of rejections). Results for LAM for both catch numbers and biomass and for all taxa are listed in Table 11. Excluding the 41 taxa where LDM results were provided and the rejected instances, in total, 59 taxa with accepted and detailed results (LAM for catch numbers and/or biomass) are presented in Figures 51–109 and Table 5 provides a reference to these figures for each taxon. Table 9 also provides a summary of recommendations of conversion factors for application based on results of analyses.

Overall, estimated conversions indicated a significant difference in catchabilities between the old and replacement vessels with different protocols (Figure 5). For most groundfish, the Cartier and Cabot were more efficient than the Teleost after accounting for fishing effort. For taxa coded in the 2000s, 4000s, and 8000s, the difference in vessel catchabilities were less

pronounced (the 2000s represent mostly crustaceans, the 4000s represent mostly mollusks, bivalves, and cephalopods, while the 8000s are largely sponges and jellyfishes. For taxa coded in the 6000s (echinoderms), the Teleost was more efficient than the replacement vessels. Furthermore, most taxa with adequate data of length measurements indicated a significant shift in size selectivity likely introduced by the difference between NEST (used by the Cartier and Cabot) and WIIA (used by the Teleost) (Figure 6). For taxa with wide size ranges (from under 20 cm to over 50 cm), the estimated length-dependent conversion factor showed a declining trend for small sizes and an increasing trend for larger sizes; this shape resembles the ratio between two logistic selectivity curves with different L50 (50% retention length). For some crustaceans (e.g., crabs) with size range mostly under 20 cm, the wavy shape of estimated conversion factors resembles the ratio between two dome-shaped selectivity curves. Across various taxa that resulted in length-dependent conversions, the patterns were consistent and as expected.

3.3. PRESENTATION OF RESULTS

Results of the various analyses for the numerous taxa covered in this document are simply too voluminous to interpret in detail. Instead, the detailed results presented in figures and tables to support decisions for the application of conversion factors, and provide some interpretation of results only for key harvested species and species of conservation concern. These are species for which reporting on survey results is likely to be most consequential and frequent, and therefore where the need for careful examination and interpretation of comparative fishing results is arguably greatest. Below is an outline of how the results are summarized and presented, followed by the results for key species, as well as other cases.

The following tables and figures provide summaries of analyses results:

- Table 8 includes a summary of special considerations for some taxon, including reasons to reject/downgrade analytical methods.
- Table 9 provides a summary of results of comparative fishing analyses and an overview of recommended approaches to analyses.
- Figure 5 provides an overview of estimated conversion factors from length-disaggregated models for both catch numbers and biomass.
- Figure 6 provides an overview of estimated conversion factors from length-aggregated models for catch numbers.

The following tables and figures provide taxon-specific results:

- Table 5 provides a list of taxa that meet the minimum requirements for analysis, a summary of available data including the sample sizes (including the number of stations where a taxon was encountered by either vessel, the number of stations where a taxon was encountered by the Teleost and by the Cartier or Cabot, respectively, the number of effective sets where both vessels within the set had at least one catch, and the total number of length measurements) and sample conversions (for both catch numbers and biomass) for these taxa, and finally, an indexing of figures for reference to detailed data and results figures for each taxon. This table also highlights the recommended method for conversion factor for each taxon.
- Table 10 provides details of model selection (ΔAIC and ΔBIC values) for the length-disaggregated analyses.
- Table 11 provides details of the model evidence and selection (AIC and BIC values) for the length-aggregated analyses of catch numbers and biomass, and the estimated conversion factors with 95% confidence intervals (95% CI) from the analyses for taxa that meet the

minimum data requirements. Note that the recommended approach for these taxa is not necessarily the length-aggregated analysis.

- Figures 7 to 9 provide an explanation of the content within each figure for reference to taxon-specific data and results figures in Figures 11-50. Plots for the results of the length-disaggregated analyses are presented in multiple panels across three pages for each taxon. Briefly, the first page (labelled a.) provides a summary of the data from a spatial, size-aggregated and length-specific perspective (details in Figure 7). Results for the size-aggregated analyses are plotted in one of the panels in an effort to reduce the total number of figures contained in this report. The second page (labelled b.) provides a plot of the fit of all converged models and a plot of the selected conversion factor function and 95% CI, along with the projected constant values proposed for the smallest and largest lengths (details in Figure 8). Finally, the third page (labelled c.) provides various boxplots for the normalized quantile residual values for the selected model (details in Figure 9).
- Figure 10 provides an explanation of the content within the figure for reference to taxon-specific data and results figures in Figures 51-109. Plots for the results of the length-aggregated analyses, including the fitted model and model quantile residuals, are presented on a single page for each taxon for the analyses of catch counts (left column) and catch weights (right column) for measured taxa, and catch numbers or weights only (single column) for taxa where analyses of the other failed. Figures are presented only for taxa that were not subjected to length-disaggregated analyses to reduce the total number of figures in this report. Nonetheless, fits of the selected length-aggregated model for catch for the remaining taxa are presented in the plots for length-disaggregated analyses and the estimated conversion factor values are in Table 11.

3.4. TAXON-SPECIFIC RESULTS AND INTERPRETATIONS

3.4.1. *Gadus morhua*

For Atlantic Cod (*Gadus morhua*), there was strong station effect in the length-disaggregated analysis using Binomial and Beta-Binomial models where catch of large fish predominantly came from three large tows. The analysis models were able to smooth out this effect and provide an “averaged” calibration across the survey area and across various different conditions for application to historical catches; however, more detailed analysis is recommended for this species in order to improve estimation precision. Besides, the analysis could not provide reasonable calibration for large sizes due to lack of catches during the comparative fishing experiment and therefore, resulted in large confidence intervals in this size range. Consequently, caution is recommended when applying the conversion factor to large Atlantic Cod.

3.4.2. *Melanogrammus aeglefinus*

Similar to Atlantic Cod, caution is recommended when applying the conversion factor to large sized Haddock (*Melanogrammus aeglefinus*) given high model uncertainty in this size range.

3.4.3. *Triglops murrayi*

There were concerns with data sufficiency for mailed sculpin (*Triglops murrayi*) as catches resulted from the new vessels predominantly. Beside, applicability of the conversion factors was questioned during peer review since they are benthic and have specific habitats resulting in less occurrences of catches during surveys. The conversion factor was retained, however, caution is recommended when using this result.

3.4.4. *Homarus americanus*

The best model for American Lobster (*Homarus americanus*) was manually selected (BB5). LDM results indicated BB5 had the lowest AIC while BI1 had the lowest BIC. Model results differ in the conversion for small Lobsters. This uncertainty was mainly due to the fact that small individuals are found closer to Scotian shore off western side of Nova Scotia and the survey may not have good access to these area. With recommendation from the peer review meeting, BB5 was selected as the best model to be more consistent with other comparative fishing experiments and surveys employing same or similar gears (Benoît 2024) and to better represent conversions for the small size range.

3.4.5. *Alosa aestivalis*

Although the comparative fishing experiment did not have concerns in differentiating blueback herring (*Alosa aestivalis*) and Atlantic Herring, this could be an issue in historical surveys and data. Caution is recommended when applying the conversion to historical data.

3.4.6. *Parathemisto* sp*., Nymphon* sp.

Biomass conversion factors for *Parathemisto* sp*.* and *Nymphon* sp*.* are unreliable due to segmented animals in the survey and LAM for catch biomass were rejected for the two taxa.

3.4.7. *Pennatula aculeata,* Porifera

Abundance conversion factors for *Pennatula aculeata* and Porifera*.* were rejected due to unrealistic results (and likely unreliable data) but LAM for catch biomass were retained.

3.4.8. *Vazella pourtalesi*

Analysis for Russian Hats (*Vazella pourtalesi*) were conducted separately from the taxa group 8600 (Table 7) with recommendation from the peer review meeting.

4. DISCUSSION

Overall, the comparative fishing experiment between the CCGS Teleost and CCGS John Cabot/ CCGS Capt. Jacques Cartier during 2022 and 2023 for the Summer RV Survey in the Maritimes Region was successful. Data from the experiment was sufficient for most taxa of interest for estimating the difference in relative catch efficiencies between old and replacement vessels. Results were provided for 40 taxa using the length-disaggregated analysis and for 59 taxa using the length-aggregated analysis of catch numbers. As a result of the analyses, estimates and recommendations of length-dependent conversion factors were provided for 22 taxa, length-independent conversion factors using length-disaggregated analysis were recommended for 14 taxa, length-independent conversion factors using length-aggregated analysis were recommended for 40 taxa, whereas calibration of 21 taxa were recommended as not necessary. Results were also provided for 59 taxa using length-aggregated analysis of catch biomass, where 42 taxa received recommendations of conversion factors and calibration of 15 taxa were recommended as not necessary.

In practice, in order to apply these conversion factors properly, analysts should carefully examine their interested taxa to avoid mis-interpretations. For example, conversion factors for Atlantic Cod and Haddock may not well represent large-sized animals due to absence of these individuals in recent years and during the comparative fishing experiment. Some deepwater strata were not adequately covered during the 2022–2023 comparative fishing experiment, and while most species commonly captured at these depths had sufficient catches in other areas to

allow for data analyses, it is possible catch efficiency differs at greater depths. Further analysis is recommended, if applicable to the interested taxa, to assess the abovementioned situations, and explore potential spatial heterogeneity that may further explain variability in the relative catch efficiency, and therefore, improve estimation precision. Model estimation uncertainty was also calculated in this study for each accepted conversion factor and analysts are encouraged to consider this uncertainty in their further analysis.

5. ACKNOWLEDGEMENT

Numerous DFO Science and CCG staff participated in the planning and implementation of comparative fishing. We wish to thank Jordan Ouellette-Plante for providing R Markdown code for compiling the numerous figures into the document, to Paul Regular and Andrea Perreault for identifying and correcting an error in the calculation of AIC and BIC values in earlier analyses, to Jamie Emberley, Mike McMahon, and Ryan Martin for quality control and guidance for the interpretation of the data, and to everyone that participated and contributed to discussions on the analyses.

6. REFERENCES CITED

Benoît, H.P., and Swain, D.P.. 2003. Accounting for length and depth-dependent diel variation in catchability of fish and invertebrates in an annual bottom-trawl survey. ICES J. Mar. Sci. 60: 1297-1316.

Benoît, H.P., Ouellette-Plante, J., Yin, Y, and Brassard, C. 2022. Review of the assessment framework for Atlantic cod in NAFO 3Pn4RS: Fishery independent surveys. DFO Can. Sci. Advis. Sec. Res. Doc. 2022/049. xiii + 130 p.

Benoît, H.P., and Yin, Y. 2023. Results of Comparative Fishing Between the CCGS Teleost Fishing the Western IIA Trawl and CCGS Capt. Jacques Cartier Fishing the NEST Trawl in the Southern Gulf of St. Lawrence in 2021 and 2022. DFO Can. Sci. Advis. Sec. Res. Doc. 2023/083. xiii + 183 p.

Benoît, H.P., Yin, Y, and Bourdages, H. 2024. Results of comparative fishing between the CCGS Teleost and CCGS John Cabot in the Estuary and Northern Gulf of St. Lawrence in 2021 and 2022. DFO Can. Sci. Advis. Sec. Res. Doc. 2024/007. ix + 229 p.

Brooks, M.E., Kristensen, K., van Benthem, K.J., Magnusson, A., Berg, C.W., Nielsen, A., Skaug, H.J., Mächler, M., Bolker, B.M. (2017). glmmTMB balances speed and flexibility among packages for zero-inflated generalized linear mixed modeling. R Journal, 9(2):378-400.

Cadigan, N.G., Yin, Y., Benoît, H.P., and Walsh, S.J. 2022. A nonparametric-monotone regression model and robust estimation for paired-tow bottom-trawl survey comparative fishing data. Fish. Res. 254: 106422.

Dunn, P.K. and Smyth, G.K. 1996. Randomized quantile residuals. J. Comput. Graph. Stat 5: 236-244.

Dunn, P.K., and Smyth, G.K.. 2005. Series evaluation of Tweedie exponential dispersion model densities. Statis. Comput. 15:267-280.

Green, P.J., and Silverman, B.W. 1993. Nonparametric regression and generalized linear models. Chapman and Hall/CRC, 184 p.

Hartig, F. 2021. DHARMs: Residual diagnostics for hierarchical (multi-level.mixed) regression models. R package version 0.4.1

Hastie, T., Tibshirani, R. and Friedman, J., 2009. The elements of statistical learning: data mining, inference, and prediction. Springer Science and Business Media.

Kristensen, K., Nielsen, A., Berg, C.W., Skaug, H., and Bell, B.M. 2016. TMB: Automatic differentiation and Laplace approximation. J. Stat. Softw. 70: 1-21.

Miller, T.J. 2013. A comparison of hierarchical models for relative catch efficiency based on paired-gear data for US Northwest Atlantic fish stocks. Can. J. Fish. Aquat. Sci. 70: 1306-1316.

Miller, T.J., Das, C., Politis, P.J., Miller, A.S., Lucey, S.M., Legault, C.M., Brown, R.W., and Rago, P.J. 2010. Estimation of Albatross IV to Henry B. Bigelow calibration factors. Fish. Sci. Cent. Ref. Doc. 10-05; 233 p.

R Core Team. 2021. R: A language and environment for statistical computing. R Foundation for Statistical Computing, Vienna, Austria.

Ricard, D., Fishman, D., Rolland, N., Sylvain, F.-É., Turcotte, F. and Vergara, P. 2023. Validation of the paired sets from the comparative fishing experiments conducted between CCGS Teleost and CCGS Capt. Jacques Cartier in the southern Gulf of St. Lawrence, September 2021 and 2022. Can. Tech. Rep. Fish. Aquat. Sci. 3547: v + 274 p.

Thorson, J.T. and Minto, C. 2015. Mixed effects: a unifying framework for statistical modelling in fisheries biology. ICES J. Mar. Sci. 72:1245-1256.

Trueman, S., Wheeland, L., Benoît, H., Munro, H. Nguyen, T., Novaczek, E., Skanes, K., and Yin, Y. 2025. Results of comparative fishing between the CCGS Teleost and CCGS Alfred Needler with the CCGS John Cabot and CCGS Capt. Jacques Cartier in the Newfoundland and Labrador Region in 2021 and 2022. DFO. Can. Sci. Advis. Sec. Res. Doc. 2025/021. ix + 229 p.

Verbyla, A.P., Cullis, B.R., Kenward, M.G, and Welham, S.J. 1999. The analysis of designed experiments and longitudinal data by using smoothing splines. J. Royal Stat. Soc. Ser. C 48: 269-311.

Wald, A. and Wolfowitz, J. 1940. On a test whether two samples are from the same population. Ann. Math Statist. 11:147-162.

Wood, S.N. 2000. Modelling and smoothing parameter estimation with multiple quadratic penalties. J. Royal Stat. Soc. Ser. B Stat. Methodol. 62: 413–428.

Wood, S.N. 2011. Fast stable restricted maximum likelihood and marginal likelihood estimation of semiparametric generalized linear models. J. Royal Stat. Soc. Ser. B Stat. Methodol. 73: 3– 36.

Wood, S.N. 2017. Generalized additive models: An introduction with R, 2nd ed. Chapman and Hall/CRC Press, 496 p.

Wu, X. and Zhao, B. 2013. Nonparametric Statistics (Fourth Edition ed). China Statistics Press. pp. 40-42.

Yin, Y. and Benoît, H.P. 2022a. Re-analysis of comparative fishing experiments in the Gulf of St. Lawrence and other analyses to derive stock-wide bottom-trawl survey indices beginning in 1971 for 4RST Greenland halibut, Reinhardtius hippoglossoides. DFO Can. Sci. Advis. Sec. Res. Doc. 2022/002. vii + 45 p.

Yin, Y. and Benoît, H.P. 2022b. A Comprehensive Simulation Study of A Class of Analysis Methods for Paired-Tow Comparative Fishing Experiments. Can. Tech. Rep. Fish. Aquat. Sci. 3466: vi + 99 p.

7. TABLES

Table 1. Number of comparative fishing sets in 2022 and 2023 by NAFO Division.

Year	4X	4W	4V	5Z	Total
2022	**56**	**16**	**0**	**21**	**93**
2023	**45**	**73**	**70**	**1**	**189**
Total	**101**	**89**	**70**	**22**	**282**

Table 2. Details for paired comparative fishing sets in 2022 and 2023, where columns indicated by TEL represent values for the CCGS Teleost and those indicated by CA represent values for the CCGS Jacques Cartier and John Cabot. Date is that of the beginning of the tow by the CCGS Teleost, tow start times (Time) are expressed in decimal hours, tow depths (Depth) are in meters and were calculated as the average between start and end depths, Distance values represent the trawled distance for each vessel in nm, longitudes and latitudes are expressed in decimal degrees and were recorded by the Teleost in each pair.

Date	Station	Time CA	Time TEL	Depth CA	Depth TEL	Distance CA	Distance TEL	Longitude	Latitude
2022-07-20	138	21:07	20:07	62.16	78.5	0.95	1.7	-64.76	43.46
2022-07-20	978	17:07	19:07	85.5	83.5	1.05	1.7	-64.68	43.33
2022-07-21	141	15:07	15:07	68	80.5	1.01	1.67	-64.81	42.96
2022-07-21	143	00:07	00:07	132.5	133.5	0.82	1.73	-65.22	43.35
2022-07-21	144	12:07	11:07	158.5	157.5	1.02	1.77	-65.32	42.96
2022-07-21	146	03:07	03:07	124.15	121	1.04	1.74	-65.31	43.22
2022-07-21	166	10:07	10:07	144.5	142	1.06	1.78	-65.38	42.9
2022-07-22	157	15:07	15:07	80	81	0.99	1.81	-65.96	42.82
2022-07-22	158	09:07	09:07	89	90.5	0.98	1.73	-65.45	42.62
2022-07-22	161	12:07	12:07	91.5	90.5	1.03	1.77	-65.75	42.69
2022-07-22	168	23:07	23:07	180.3	170	1.01	1.69	-66.69	42.76
2022-07-23	172	03:07	03:07	252.25	247.5	1.06	1.76	-66.85	42.54
2022-07-23	175	06:07	06:07	247	239.5	0.92	1.73	-67.18	42.68

Date	Station	Time CA	Time TEL	Depth CA	Depth TEL	Distance CA	Distance TEL	Longitude	Latitude
2022-07-23	179	09:07	09:07	217.5	225.5	0.87	1.76	-67.11	42.77
2022-07-23	181	12:07	12:07	237.5	238.5	1.02	1.73	-67.2	42.9
2022-07-23	182	21:07	21:07	204.65	207	0.98	1.5	-66.99	43.43
2022-07-23	186	15:07	15:07	180	187.5	1.02	1.58	-66.93	42.94
2022-07-23	189	18:07	18:07	120.35	123	0.99	1.75	-66.71	43.31
2022-07-24	190	09:07	09:07	159.5	164.5	1.02	1.76	-66.93	43.97
2022-07-24	194	19:07	19:07	77.33	78	0.98	1.75	-66.46	44.25
2022-07-24	199	16:07	16:07	178	181.5	0.88	1.79	-66.7	44.23
2022-07-25	195	07:07	07:07	93	91	1.02	1.71	-65.89	44.75
2022-07-25	196	05:07	05:07	97	97	0.83	1.72	-66.09	44.67
2022-07-25	197	11:07	10:07	106.5	98.5	0.97	1.79	-66	44.84
2022-07-25	198	02:07	02:07	167.1	157.5	1.03	1.7	-66.37	44.63
2022-07-25	209	18:07	18:07	48.55	58.5	0.97	1.75	-65.43	45.25
2022-07-25	210	21:07	21:07	53.05	56	1.03	1.43	-65.1	45.32
2022-07-25	211	15:07	15:07	81	81.5	1	1.77	-65.73	45.08
2022-07-25	601	00:07	23:07	49.53	49	0.87	1.36	-65.18	45.39
2022-07-26	208	02:07	02:07	50.16	51	0.83	1.53	-65.33	45.32
2022-07-27	205	20:07	20:07	92.12	95	0.84	1.73	-65.92	45.05
2022-07-27	214	15:07	15:07	73.5	74	1	1.81	-65.62	44.91
2022-07-27	215	13:07	13:07	77.5	78	0.84	1.84	-65.55	45.04
2022-07-28	201	13:07	13:07	179	179.5	0.96	1.73	-66.86	44.31
2022-07-28	1003	16:07	16:07	87	91	0.99	1.76	-66.57	44.14
2022-07-29	176	20:07	19:07	355.6	354.5	1.02	1.76	-66.96	42.43
2022-07-29	177	22:07	22:07	341.5	339.5	0.96	1.82	-66.75	42.4
2022-07-29	178	17:07	17:07	319.75	319.5	1.01	1.75	-67.22	42.53

Date	Station	Time CA	Time TEL	Depth CA	Depth TEL	Distance CA	Distance TEL	Longitude	Latitude
2022-07-29	180	11:07	11:07	221.5	224.5	1.02	1.74	-67.56	42.9
2022-07-29	183	03:07	03:07	224.85	219.5	0.85	1.29	-67.07	43.44
2022-07-29	184	13:07	13:07	231.5	222.5	1.01	1.76	-67.47	42.84
2022-07-29	191	08:07	08:07	161	161.5	1.02	1.75	-67.32	43.11
2022-07-30	230	05:07	05:07	170.5	134	1.1	1.7	-66.83	42.16
2022-07-30	235	09:07	09:07	64.5	64.5	1.03	1.69	-66.89	42.09
2022-07-30	237	15:07	15:07	73.5	78.5	0.96	1.71	-66.52	41.92
2022-07-30	238	13:07	13:07	68	70	1.07	1.81	-66.71	41.94
2022-07-30	240	23:07	23:07	84.53	87.5	1.02	1.73	-66.25	41.65
2022-07-30	242	17:07	17:07	67.27	67	0.91	1.77	-66.62	41.77
2022-07-30	243	21:07	21:07	80.42	80.5	1.02	1.77	-66.42	41.69
2022-07-30	244	19:07	19:07	70.5	74	0.98	1.77	-66.51	41.77
2022-07-30	247	02:07	02:07	272.65	263	1.04	1.69	-67.16	42.28
2022-07-31	229	19:07	19:07	94.74	97	1.04	1.74	-66.01	41.85
2022-07-31	232	10:07	10:07	105	116.5	0.85	1.55	-66.32	41.21
2022-07-31	233	13:07	13:07	124.5	127	1.04	1.8	-66.12	41.43
2022-07-31	234	16:07	16:07	133.7	140	1.08	1.77	-65.78	41.76
2022-07-31	241	06:07	06:07	91	90.5	1.04	1.76	-66.46	41.38
2022-07-31	625	03:07	03:07	76	77.5	1.07	1.63	-66.63	41.6
2022-08-01	228	04:08	04:08	176	167	1.08	1.78	-65.88	41.98
2022-08-01	231	01:08	01:08	94.11	93.5	0.91	1.77	-66.09	41.98
2022-08-01	245	18:08	18:08	231.5	232.5	1.02	1.78	-66.22	42.34
2022-08-01	248	08:08	08:08	230	234.5	1.07	1.72	-66.04	42.21
2022-08-01	249	10:08	12:08	203.5	206	1.06	1.79	-66.22	42.2
2022-08-01	623	13:08	13:08	87	91.5	1.02	1.73	-66.37	42.11

Date	Station	Time CA	Time TEL	Depth CA	Depth TEL	Distance CA	Distance TEL	Longitude	Latitude
2022-08-02	154	19:08	19:08	88.54	88.5	1.04	1.76	-65.7	42.52
2022-08-02	156	11:08	11:08	62	64	1.11	1.81	-66.21	42.62
2022-08-02	160	17:08	17:08	91.11	92	1.04	1.8	-65.57	42.57
2022-08-02	170	22:08	22:08	108.5	109.5	1.07	1.73	-65.66	42.28
2022-08-02	174	09:08	09:08	200.5	197	0.84	1.29	-66.35	42.56
2022-08-03	149	07:08	07:08	145	141	1.07	1.69	-65.03	42.37
2022-08-03	169	01:08	01:08	116.5	119.5	1.05	1.26	-65.55	42.15
2022-08-03	171	04:08	04:08	116.95	116.5	1.04	1.76	-65.46	42.21
2022-08-03	569	23:08	23:08	150.9	156	0.88	1.82	-63.48	43.31
2022-08-03	570	17:08	17:08	81.74	83.5	1.04	1.76	-64.22	43.1
2022-08-03	575	14:08	14:08	98	99	1.01	1.77	-64.58	42.87
2022-08-03	576	12:08	12:08	126.5	129	1.01	1.76	-64.59	42.63
2022-08-03	976	19:08	19:08	88.95	89.5	1.04	1.8	-64.03	43.19
2022-08-03	985	09:08	09:08	138.5	140.5	1.04	1.77	-64.85	42.47
2022-08-04	101	08:08	08:08	204	214.5	1.03	1.72	-63.1	43.54
2022-08-04	120	05:08	05:08	116	118	0.93	1.79	-63.08	43.27
2022-08-04	121	21:08	21:08	268.2	283.5	1.05	1.76	-61.74	42.99
2022-08-04	122	16:08	16:08	121.5	119	1.02	1.75	-62.29	43.03
2022-08-04	123	19:08	19:08	197.85	196.5	1.04	1.75	-61.95	42.98
2022-08-04	560	02:08	02:08	143.6	146	1.05	1.78	-63.22	43.15
2022-08-04	965	14:08	14:08	101.5	103	1.02	1.73	-62.41	43.11
2022-08-04	967	11:08	11:08	96.5	97	1.03	1.6	-62.6	43.45
2022-08-05	99	20:08	20:08	203.1	203	1.05	1.75	-62.71	43.86
2022-08-05	106	17:08	17:08	132.35	132.5	1.05	1.77	-62.26	43.81
2022-08-05	115	00:08	00:08	106.75	105.5	1.04	1.82	-61.79	43.07

Date	Station	Time CA	Time TEL	Depth CA	Depth TEL	Distance CA	Distance TEL	Longitude	Latitude
2022-08-05	117	14:08	14:08	90.5	91.5	1.04	1.78	-62.08	43.64
2022-08-05	118	03:08	03:08	95.27	95.5	1.08	1.83	-62.01	43.24
2022-08-05	124	12:08	12:08	96.5	100	1.04	1.81	-62.34	43.59
2022-08-05	960	10:08	10:08	80.5	81	1.1	1.51	-62.49	43.52
2022-08-05	961	07:08	07:08	86	93	1.04	1.74	-62.34	43.33
2023-06-29	565	16:06	15:06	165.51	157.28	1.02	1.77	-63.52	44.12
2023-06-29	135	20:06	19:06	195.68	196.6	1	1.76	-63.45	43.85
2023-06-30	150	16:06	16:06	152.7	154.53	1.03	1.78	-65.11	43.1
2023-06-30	154	03:06	03:06	149.96	148.13	0.99	1.74	-64.61	43.61
2023-06-30	145	07:06	07:06	70.41	67.67	1.07	1.78	-64.65	43.43
2023-06-30	978	10:06	09:06	90.53	87.78	1.03	1.78	-64.65	43.32
2023-06-30	151	14:06	14:06	160.93	160.02	1.01	1.8	-64.98	43.09
2023-06-30	152	18:06	18:06	141.73	143.56	1.06	1.82	-65.24	43.18
2023-06-30	153	20:06	20:06	156.36	158.19	1.01	1.77	-65.23	43.06
2023-06-30	175	23:06	23:06	134.42	131.67	1.03	1.75	-65.48	42.91
2023-07-01	167	09:07	09:07	93.27	92.35	1.01	1.77	-65.77	42.59
2023-07-01	168	18:07	18:07	54.86	52.12	1.08	1.24	-66.21	42.78
2023-07-01	166	14:07	14:07	85.95	86.87	1.09	1.8	-65.9	42.73
2023-07-01	165	16:07	16:07	71.32	69.49	1.04	1.82	-66.08	42.73
2023-07-01	176	21:07	21:07	160.02	161.85	1.03	1.55	-66.16	42.87
2023-07-02	188	09:07	09:07	236.83	235.92	1.01	1.81	-67.23	43.04
2023-07-02	199	11:07	11:07	179.22	180.14	0.95	1.78	-66.99	43.19
2023-07-02	187	14:07	14:07	216.71	207.57	1.02	1.8	-67.09	43.25
2023-07-02	194	17:07	16:07	149.05	149.05	1.07	1.82	-66.78	43.31
2023-07-02	198	20:07	19:07	169.16	162.76	1.01	1.8	-66.89	43.56

Date	Station	Time CA	Time TEL	Depth CA	Depth TEL	Distance CA	Distance TEL	Longitude	Latitude
2023-07-03	200	02:07	02:07	143.56	142.65	0.92	1.41	-66.68	43.68
2023-07-03	196	13:07	13:07	107.9	106.98	1	1.33	-66.51	44.17
2023-07-05	212	12:07	12:07	139.9	135.33	1.03	1.77	-67.03	44.33
2023-07-05	206	16:07	15:07	170.99	169.16	0.91	1.74	-66.93	44.03
2023-07-05	195	18:07	18:07	168.25	162.76	0.98	1.79	-67.16	43.81
2023-07-05	186	22:07	21:07	223.11	219.46	0.99	1.79	-67.36	43.59
2023-07-06	190	02:07	01:07	204.83	202.08	0.98	1.71	-67.47	43.25
2023-07-06	191	06:07	05:07	194.77	189.28	1.02	1.76	-67.58	43.02
2023-07-06	179	10:07	10:07	206.65	205.74	0.98	1.75	-67.48	42.68
2023-07-06	184	22:07	22:07	307.24	314.55	0.92	1.75	-67.08	42.54
2023-07-07	182	01:07	01:07	258.78	246.89	0.96	1.8	-66.92	42.64
2023-07-08	254	05:07	07:07	235	227.69	0.9	1.42	-66	42.21
2023-07-08	170	13:07	13:07	126.19	119.79	0.99	1.83	-65.48	42.18
2023-07-08	986	16:07	16:07	200.25	203	0.98	1.77	-65.29	42.26
2023-07-08	583	19:07	19:07	113.39	111.56	0.99	1.8	-65.29	42.43
2023-07-08	172	21:07	21:07	97.84	96.01	1.01	1.79	-65.32	42.6
2023-07-09	575	05:07	05:07	106.07	100.58	0.97	1.76	-65.01	42.74
2023-07-09	572	09:07	09:07	82.3	79.55	1.03	1.76	-64.79	42.99
2023-07-09	147	11:07	11:07	91.44	88.7	1	1.8	-64.69	42.99
2023-07-09	155	14:07	14:07	130.76	126.19	0.99	1.78	-64.4	42.96
2023-07-14	144	17:07	16:07	85.95	85.95	1.02	1.76	-64.16	43.11
2023-07-14	158	21:07	20:07	107.9	104.24	1.01	1.78	-64.51	42.87
2023-07-15	157	00:07	00:07	124.36	120.7	1.01	1.83	-64.26	42.79
2023-07-15	142	02:07	02:07	101.5	98.76	1.01	1.8	-64.13	42.93
2023-07-15	141	07:07	07:07	160.93	155.45	1.03	1.84	-63.44	43

Date	Station	Time CA	Time TEL	Depth CA	Depth TEL	Distance CA	Distance TEL	Longitude	Latitude
2023-07-15	569	13:07	13:07	162.76	155.45	0.99	1.74	-63.39	42.93
2023-07-15	560	15:07	15:07	158.19	153.62	1.01	1.73	-63.18	43.01
2023-07-15	121	18:07	18:07	134.42	131.67	0.83	1.78	-62.96	42.91
2023-07-15	129	22:07	21:07	239.57	235.92	1.02	1.74	-62.63	42.86
2023-07-16	128	02:07	01:07	235	231.34	1.01	1.84	-62.26	42.95
2023-07-16	124	07:07	07:07	105.16	103.33	1.03	1.82	-62.57	43.16
2023-07-16	119	10:07	10:07	116.13	116.13	1.01	1.8	-62.87	43.12
2023-07-16	122	13:07	13:07	141.73	138.07	1.02	1.75	-63.11	43.2
2023-07-16	125	15:07	15:07	118.87	119.79	1.08	1.82	-63.06	43.33
2023-07-16	120	17:07	17:07	117.96	114.3	1.03	1.74	-62.79	43.56
2023-07-16	112	19:07	19:07	84.12	81.38	1.01	1.77	-62.52	43.6
2023-07-16	111	22:07	21:07	81.38	79.55	0.98	1.73	-62.36	43.47
2023-07-17	123	01:07	00:07	100.58	98.76	1	1.8	-62.2	43.39
2023-07-17	114	07:07	07:07	96.01	95.1	1	1.8	-62.05	43.56
2023-07-17	115	10:07	10:07	81.38	79.55	1.02	1.83	-61.82	43.57
2023-07-18	104	03:07	03:07	136.25	136.25	1.01	1.76	-62.56	44.07
2023-07-18	105	07:07	07:07	160.02	158.19	1.02	1.79	-62.29	44.11
2023-07-18	106	11:07	11:07	175.56	168.25	1.03	1.81	-61.87	44.2
2023-07-18	107	14:07	13:07	93.27	89.61	0.98	1.75	-61.7	44.18
2023-07-18	110	16:07	16:07	128.02	117.04	1.01	1.73	-61.44	44.02
2023-07-18	113	18:07	18:07	53.95	55.78	1.03	1.79	-61.47	43.94
2023-07-18	73	21:07	21:07	44.81	45.72	1.01	1.75	-60.92	43.9
2023-07-19	75	01:07	01:07	56.69	58.52	0.99	1.81	-60.49	43.76
2023-07-19	72	03:07	03:07	64.92	63.09	1.02	1.78	-60.37	43.63
2023-07-19	71	06:07	06:07	63.09	60.35	1.01	1.85	-60.66	43.66

Date	Station	Time CA	Time TEL	Depth CA	Depth TEL	Distance CA	Distance TEL	Longitude	Latitude
2023-07-19	70	07:07	07:07	60.35	59.44	1.02	1.81	-60.79	43.63
2023-07-19	74	10:07	09:07	65.84	66.75	1.01	1.76	-60.8	43.54
2023-07-19	535	12:07	12:07	109.73	116.13	1.01	1.81	-60.6	43.43
2023-07-19	934	17:07	16:07	195.68	219.46	1.08	1.74	-60.27	43.43
2023-07-19	63	20:07	20:07	218.54	194.77	1.02	1.73	-59.92	43.56
2023-07-19	66	23:07	23:07	108.81	123.44	1.01	1.76	-60.05	43.59
2023-07-20	67	02:07	02:07	58.52	56.69	0.96	1.82	-60.23	43.69
2023-07-20	68	04:07	04:07	58.52	56.69	1.01	1.78	-60.15	43.78
2023-07-20	69	07:07	07:07	44.81	45.72	0.97	1.8	-59.95	43.84
2023-07-20	65	12:07	12:07	96.01	94.18	1.05	1.77	-59.19	43.81
2023-07-20	58	16:07	16:07	228.6	202.08	1.01	1.78	-58.82	43.92
2023-07-20	59	20:07	20:07	234.09	204.83	1	1.76	-58.51	44.05
2023-07-20	56	23:07	23:07	101.5	102.41	1.01	1.73	-58.31	44.23
2023-07-21	52	02:07	02:07	59.44	60.35	1.01	1.79	-58.52	44.29
2023-07-21	48	06:07	05:07	74.98	81.38	1.02	1.79	-58.56	44.2
2023-07-21	49	07:07	07:07	65.84	62.18	1.01	1.84	-58.7	44.27
2023-07-21	55	11:07	11:07	100.58	95.1	1.02	1.78	-58.75	44.11
2023-07-21	62	15:07	14:07	279.81	291.69	1.02	1.76	-59.09	44.16
2023-07-21	60	16:07	16:07	261.52	211.23	1.02	1.38	-59.24	44.17
2023-07-21	61	19:07	19:07	205.74	211.23	1.07	1.79	-59.17	44.32
2023-07-21	57	22:07	22:07	100.58	96.93	1.01	1.75	-59.25	44.32
2023-07-22	531	01:07	01:07	234.09	228.6	1.02	1.8	-59.4	44.28
2023-07-22	533	04:07	04:07	224.03	215.8	1.01	1.75	-59.54	44.23
2023-07-22	540	08:07	08:07	60.35	60.35	0.99	1.83	-59.82	44.08
2023-07-22	77	09:07	09:07	66.75	68.58	1	1.76	-59.94	44.09

Date	Station	Time CA	Time TEL	Depth CA	Depth TEL	Distance CA	Distance TEL	Longitude	Latitude
2023-07-22	541	13:07	12:07	71.32	70.41	1.04	1.75	-60.18	44.12
2023-07-22	539	15:07	15:07	71.32	70.41	1.06	1.8	-60.46	44.15
2023-07-22	81	18:07	18:07	160.02	155.45	1.05	1.77	-60.27	44.28
2023-07-22	524	22:07	22:07	58.52	56.69	1.01	1.75	-59.82	44.46
2023-07-23	85	03:07	03:07	62.18	64.01	1.01	1.8	-60.28	44.46
2023-07-23	83	05:07	05:07	32.92	32.92	0.99	1.78	-60.48	44.41
2023-07-23	84	09:07	08:07	33.83	33.83	1	1.76	-60.46	44.51
2023-07-23	546	11:07	11:07	74.07	69.49	1.02	1.77	-60.45	44.73
2023-07-23	82	13:07	13:07	41.15	41.15	0.99	1.71	-60.59	44.71
2023-07-23	86	17:07	17:07	72.24	67.67	1.01	1.75	-60.83	44.47
2023-07-23	80	20:07	20:07	122.53	105.16	1.01	1.74	-60.59	44.36
2023-07-23	76	23:07	22:07	27.43	26.52	1.01	1.77	-60.79	44.21
2023-07-24	78	03:07	02:07	55.78	54.86	1.01	1.82	-60.99	44.12
2023-07-24	543	04:07	04:07	64.92	65.84	1	1.77	-61.11	44.1
2023-07-24	536	08:07	08:07	51.21	50.29	0.98	1.85	-60.99	43.85
2023-07-24	961	11:07	11:07	49.38	47.55	0.94	1.79	-61.43	43.85
2023-07-24	117	13:07	13:07	72.24	69.49	1.02	1.81	-61.67	43.88
2023-07-24	553	16:07	16:07	137.16	134.42	1.01	1.78	-62.04	43.97
2023-07-24	957	19:07	19:07	95.1	90.53	1.02	1.76	-62.38	43.98
2023-07-24	552	23:07	23:07	268.83	259.69	1	1.76	-62.95	43.77
2023-07-27	91	08:07	08:07	178.31	174.65	0.99	1.78	-61.21	44.91
2023-07-27	89	12:07	12:07	155.45	149.96	1.02	1.76	-60.75	45.11
2023-07-27	92	15:07	15:07	168.25	160.93	1.02	1.75	-60.62	45.21
2023-07-27	87	18:07	18:07	70.41	71.32	1.01	1.76	-60.4	45.05
2023-07-27	90	20:07	20:07	78.64	72.24	1.02	1.68	-60.3	45.1

Date	Station	Time CA	Time TEL	Depth CA	Depth TEL	Distance CA	Distance TEL	Longitude	Latitude
2023-07-28	29	01:07	01:07	129.84	122.53	1.01	1.3	-59.78	45.09
2023-07-28	911	06:07	06:07	76.81	79.55	0.97	1.74	-59.63	45.29
2023-07-28	30	11:07	11:07	151.79	142.65	1	1.69	-59.32	45.52
2023-07-28	25	15:07	15:07	139.9	136.25	1.05	1.79	-59.66	45.75
2023-07-28	12	18:07	18:07	57.61	53.95	1.1	1.33	-59.71	45.97
2023-07-28	26	22:07	21:07	122.53	123.44	1.09	1.78	-59.52	45.76
2023-07-29	914	00:07	00:07	130.76	133.5	0.99	1.75	-59.35	45.8
2023-07-29	31	04:07	04:07	179.22	166.42	1.03	1.76	-58.99	45.87
2023-07-29	8	15:07	14:07	122.53	116.13	1.02	1.76	-59.36	46.3
2023-07-29	6	18:07	17:07	102.41	103.33	1.01	1.75	-59.49	46.27
2023-07-29	15	22:07	22:07	67.67	64.01	1.02	1.82	-59.78	46.36
2023-07-30	5	02:07	02:07	98.76	98.76	1.01	1.75	-60.12	46.48
2023-07-30	11	06:07	05:07	91.44	84.12	0.99	1.77	-60.31	46.47
2023-07-30	16	09:07	08:07	67.67	74.07	1	1.4	-60.3	46.66
2023-07-30	512	12:07	13:07	80.47	86.87	1.01	1.79	-59.99	46.57
2023-07-30	14	15:07	15:07	67.67	66.75	1	1.8	-59.74	46.59
2023-07-30	7	18:07	18:07	133.5	128.93	1.02	1.77	-59.89	46.77
2023-07-30	10	21:07	21:07	149.05	147.22	1.02	1.77	-60.08	46.77
2023-07-31	4	01:07	01:07	231.34	217.63	1.01	1.79	-60.1	47.05
2023-07-31	231	07:07	07:07	420.62	417.88	1.01	1.8	-59.88	47.18
2023-07-31	233	11:07	11:07	465.43	454.46	1.01	1.75	-59.63	47.16
2023-07-31	503	15:07	15:07	363.02	343.81	1.02	1.76	-59.68	46.85
2023-07-31	232	19:07	19:07	437.08	420.62	1.01	1.78	-59.36	46.8
2023-08-01	2	00:08	00:08	343.81	326.44	1.01	1.79	-59.12	46.47
2023-08-01	501	02:08	02:08	374.9	372.16	1.01	1.78	-58.96	46.47

Date	Station	Time CA	Time TEL	Depth CA	Depth TEL	Distance CA	Distance TEL	Longitude	Latitude
2023-08-01	505	06:08	06:08	149.05	141.73	1.01	1.75	-58.9	46.14
2023-08-01	3	10:08	10:08	347.47	337.41	1	1.75	-58.57	46.16
2023-08-01	1	13:08	13:08	290.78	272.49	1.04	1.76	-58.52	46.03
2023-08-01	33	17:08	16:08	275.23	270.66	1.04	1.78	-58.71	45.78
2023-08-01	517	20:08	20:08	237.74	242.32	1	1.76	-58.78	45.69
2023-08-02	27	03:08	03:08	168.25	152.7	1.02	1.62	-58.29	45.86
2023-08-02	36	06:08	06:08	306.32	318.21	1.01	1.76	-58.23	45.92
2023-08-02	235	11:08	11:08	468.17	454.46	1.03	1.75	-57.77	45.72
2023-08-02	22	18:08	17:08	160.02	170.99	0.84	1.38	-58.04	45.65
2023-08-02	1101	21:08	20:08	177.39	156.36	1.03	1.76	-57.99	45.56
2023-08-02	38	23:08	23:08	330.1	305.41	1	1.75	-57.87	45.53
2023-08-03	21	03:08	03:08	84.12	85.95	1.02	1.85	-58.25	45.41
2023-08-03	20	08:08	07:08	70.41	69.49	1.01	1.8	-58.86	45.44
2023-08-03	19	11:08	11:08	96.01	87.78	1.04	1.76	-59.1	45.3
2023-08-03	915	15:08	14:08	149.96	149.96	1.05	1.78	-59.36	45.08
2023-08-03	17	18:08	18:08	79.55	77.72	1.02	1.77	-59.11	45.09
2023-08-03	18	21:08	21:08	77.72	76.81	1.03	1.74	-58.72	45.13
2023-08-04	917	03:08	03:08	261.52	257.86	1.03	1.76	-58.86	44.8
2023-08-04	46	06:08	06:08	72.24	70.41	1.02	1.82	-58.89	44.65
2023-08-04	51	08:08	08:08	58.52	60.35	1	1.75	-59.05	44.59
2023-08-04	525	11:08	11:08	63.09	62.18	1.03	1.79	-58.84	44.54
2023-08-04	50	13:08	13:08	74.98	70.41	1.02	1.74	-58.59	44.64
2023-08-04	39	16:08	16:08	63.09	63.09	1.02	1.79	-58.19	44.75
2023-08-04	40	19:08	19:08	45.72	44.81	1.05	1.77	-57.85	44.76
2023-08-05	521	04:08	04:08	62.18	61.26	1.01	1.75	-57.36	44.66

Date	Station	Time CA	Time TEL	Depth CA	Depth TEL	Distance CA	Distance TEL	Longitude	Latitude
2023-08-05	44	06:08	06:08	57.61	56.69	1	1.75	-57.54	44.6
2023-08-05	41	08:08	08:08	68.58	68.58	0.96	1.74	-57.31	44.57
2023-08-05	54	11:08	11:08	100.58	104.24	1.02	1.78	-57.33	44.44
2023-08-05	527	15:08	15:08	101.5	105.16	1	1.75	-57.89	44.38
2023-08-05	53	17:08	17:08	125.27	105.16	1.03	1.75	-58.05	44.3
2023-08-05	930	21:08	21:08	122.53	141.73	0.97	1.77	-58.57	44.05
2023-08-06	937	02:08	02:08	109.73	104.24	1.01	1.84	-59.28	43.76
2023-08-06	538	05:08	05:08	63.09	64.92	1	1.8	-59.63	43.77
2023-08-06	939	07:08	06:08	56.69	53.95	1.01	1.81	-59.82	43.77
2023-08-06	936	11:08	11:08	129.84	138.07	1.03	1.8	-60.16	43.51
2023-08-06	64	15:08	14:08	203	218.54	1.03	1.75	-60.48	43.41
2023-08-06	941	18:08	18:08	67.67	65.84	1.02	1.77	-60.72	43.56
2023-08-06	537	20:08	20:08	82.3	75.9	1.05	1.81	-60.98	43.44
2023-08-06	534	23:08	23:08	211.23	189.28	1	1.78	-61.04	43.27
2023-08-07	962	04:08	04:08	73.15	74.07	1	1.77	-61.55	43.49
2023-08-07	558	05:08	05:08	71.32	72.24	1.01	1.79	-61.65	43.58
2023-08-07	963	09:08	09:08	96.93	94.18	0.82	1.81	-62.07	43.35
2023-08-07	959	13:08	13:08	98.76	96.01	0.94	1.78	-62.56	43.35
2023-08-07	964	17:08	17:08	125.27	123.44	1.02	1.77	-63.02	43.2

Table 3. A set of binomial models with various assumptions for the length effect and station effect in the relative catch efficiency. A smoothing length effect can be considered and the station effect can be added to the intercept, without interaction with the length effect, or added to both the intercept and smoother to allow for interaction between the two effects.

Model	$\boldsymbol{log(\rho)}$	Length Effect	Station Effect
$BI0$	β_0	constant	not considered
$BI1$	$\beta_0 + \delta_{0,i}$	constant	intercept
$BI2$	$\boldsymbol{X}_f^T\boldsymbol{\beta}_f + \boldsymbol{X}_r^T\boldsymbol{b}$	smoothing	not considered

Model	$log(\boldsymbol{\rho})$	Length Effect	Station Effect
$BI3$	$\boldsymbol{X}_f^T\boldsymbol{\beta}_f + \boldsymbol{X}_r^T\boldsymbol{b} + \delta_{0,i}$	smoothing	intercept
$BI4$	$\boldsymbol{X}_f^T(\boldsymbol{\beta}_f + \boldsymbol{\delta}_i) + \boldsymbol{X}_r^T(\boldsymbol{b} + \boldsymbol{\epsilon}_i)$	smoothing	intercept, smoother

Table 4. A set of beta-binomial models with various assumptions for the length effect and station effect in the relative catch efficiency, and the length effect on the variance parameter. A smoothing length effect can be considered in both the conversion factor and the variance parameter. A possible station effect can be added to the intercept, without interaction with the length effect, or added to both the intercept and the smoother to allow for interaction between the two effects.

Model	$log(\boldsymbol{\rho})$	$log(\boldsymbol{\phi})$	Length Effects	Station Effect
BB0	β_0	γ_0	constant/constant	not considered
BB1	$\beta_0 + \delta_{0,i}$	γ_0	constant/constant	intercept
BB2	$\boldsymbol{X}_f^T\boldsymbol{\beta}_f + \boldsymbol{X}_r^T\boldsymbol{b}$	γ_0	smoothing/constant	not considered
BB3	$\boldsymbol{X}_f^T\boldsymbol{\beta}_f + \boldsymbol{X}_r^T\boldsymbol{b}$	$\boldsymbol{X}_f^T\boldsymbol{\gamma} + \boldsymbol{X}_r^T\boldsymbol{g}$	smoothing/smoothing	not considered
BB4	$\boldsymbol{X}_f^T\boldsymbol{\beta}_f + \boldsymbol{X}_r^T\boldsymbol{b} + \delta_{0,i}$	γ_0	smoothing/constant	intercept
BB5	$\boldsymbol{X}_f^T\boldsymbol{\beta}_f + \boldsymbol{X}_r^T\boldsymbol{b} + \delta_{0,i}$	$\boldsymbol{X}_f^T\boldsymbol{\gamma} + \boldsymbol{X}_r^T\boldsymbol{g}$	smoothing/smoothing	intercept
BB6	$\boldsymbol{X}_f^T(\boldsymbol{\beta}_f + \boldsymbol{\delta}_i) + \boldsymbol{X}_r^T(\boldsymbol{b} + \boldsymbol{\epsilon}_i)$	γ_0	smoothing/constant	intercept, smoother
BB7	$\boldsymbol{X}_f^T(\boldsymbol{\beta}_f + \boldsymbol{\delta}_i) + \boldsymbol{X}_r^T(\boldsymbol{b} + \boldsymbol{\epsilon}_i)$	$\boldsymbol{X}_f^T\boldsymbol{\gamma} + \boldsymbol{X}_r^T\boldsymbol{g}$	smoothing/smoothing	intercept, smoother

Table 5. Details for data and results of comparative fishing analyses for taxa considered in this study. Taxa not included in the table indicate no recommendations due to lack of data for analyses. The scientific and common names are for taxa after grouping (see Table 5 for details of grouping). Summary of data include the number of stations where a taxon was encountered (#Stn), the number of stations where a taxa was encountered by the Teleost (#TEL) and by the Cartier or Cabot (#CA), respectively, the number of effective sets where both vessels within the set pair had at least one catch (#Pair), and the total number of length measurements (#Len). The sample conversion (Sample ratio) was calculated as the ratio between total catches (standardized by tow distances) and was provided for both catch numbers (N) and biomass (B) for reference. The sample conversion is not recommended for application to calibration. Analyses results for length-disaggregated model (LDM) and length-aggregated models (LAM) were provided for each taxon in figure(s) where Figure No. (Fig. No.) provides a reference to the figure. Shadings of the Result cells indicates final recommendation for each taxon, where green indicates no calibration is needed for catch numbers, orange indicates an LDM is recommended for application to calibration of catch numbers ($\rho(L)$ denotes recommendation of length-dependent conversion and $\rho \neq 1$ denotes recommendation of length-independent conversion that is not equal to 1), yellow indicates a LAM is recommended, and absence of shading in the table indicate no recommendations due to insufficient information for analyses. Results for calibration of catch biomass using LAM are found in Table 11. A dash (—) indicates taxon that did not have corresponding figures or recommendations of conversion.

Taxon Code	Scientific name	Common name	Summary of data #Stn	Summary of data #TEL	Summary of data #CA	Summary of data #Pair	Summary of data #Len	Sample ratio N	Sample ratio B	Fig. No. LDM	Fig. No. LAM	Result
10	*Gadus morhua*	Cod (Atlantic)	133	81	117	65	2971	0.18	0.22	11	—	LDM, $\rho(L)$
11	*Melanogrammus aeglefinus*	Haddock	193	172	177	156	24729	0.52	0.71	12	—	LDM, $\rho(L)$
12	*Urophycis tenuis*	White Hake	100	76	83	59	1136	0.37	0.48	13	—	LDM, $\rho \neq 1$
13	*Urophycis chuss*	Squirrel or Red Hake	172	142	162	132	6968	0.37	0.41	14	—	LDM, $\rho \neq 1$
14	*Merluccius bilinearis*	Silver Hake	255	226	246	217	46415	0.63	0.9	15	—	LDM, $\rho(L)$
16	*Pollachius virens*	Pollock	108	74	75	41	1265	1.92	1.66	16	—	$\rho = 1$
23	*Sebastes* sp.	redfish unseparated	167	136	146	115	21064	0.36	0.44	17	—	LDM, $\rho(L)$
30	*Hippoglossus hippoglossus*	Halibut(Atlantic)	87	72	56	41	338	0.95	1.42	18	—	$\rho = 1$
31	*Reinhardtius hippoglossoides*	Turbot,Greenland Halibut	24	23	16	15	275	0.97	0.94	19	—	$\rho = 1$
40	*Hippoglossoides platessoides*	American Plaice	135	94	121	80	7074	0.24	0.53	20	—	LDM, $\rho(L)$
41	*Glyptocephalus cynoglossus*	Witch Flounder	147	118	129	100	4400	0.67	0.69	21	—	LDM, $\rho(L)$
42	*Limanda ferruginea*	Yellowtail Flounder	102	84	99	81	7251	0.38	0.48	22	—	LDM, $\rho(L)$
43	*Pseudopleuronectes americanus*	Winter Flounder	72	57	63	48	2377	0.67	0.61	23	—	LDM, $\rho \neq 1$
44	*Citharichthys arctifrons*	Gulf Stream Flounder	74	41	69	36	1740	0.08	0.05	24	—	LDM, $\rho(L)$
60	*Clupea harengus*	Herring(Atlantic)	132	112	115	95	8450	0.37	0.37	25	—	LDM, $\rho(L)$
61	*Alosa sapidissima*	Shad American	40	32	23	15	198	1.37	2.17	26	—	LDM, $\rho(L)$
62	*Alosa pseudoharengus*	Alewife	43	37	39	33	1293	0.45	0.43	27	—	LDM, $\rho \neq 1$

Taxon Code	Scientific name	Common name	Summary of data #Stn	Summary of data #TEL	Summary of data #CA	Summary of data #Pair	Summary of data #Len	Sample ratio N	Sample ratio B	Fig. No. LDM	Fig. No. LAM	Result
112	*Urophycis chesteri*	Longfin Hake	33	20	31	18	526	0.22	0.17	28	—	LDM, $\rho \neq 1$
122	*Tautogolabrus adspersus*	Cunner	27	19	22	14	255	0.17	0.3	29	—	LDM, $\rho \neq 1$
123	*Helicolenus dactylopterus*	Rosefish (Black Belly)	64	36	61	33	3131	0.32	0.49	30	—	LDM, $\rho(L)$
142	*Hippoglossina oblonga*	Fourspot Flounder	39	19	32	12	154	0.27	0.27	31	—	LDM, $\rho \neq 1$
160	*Argentina silus*	Argentine (Atlantic)	58	26	52	20	458	0.29	0.82	32	—	LDM, $\rho(L)$
200	*Dipturus laevis*	Barndoor Skate	67	35	52	20	506	0.27	0.35	33	—	LDM, $\rho(L)$
201	*Amblyraja radiata*	Thorny Skate	71	44	62	35	581	0.33	0.27	34	—	LDM, $\rho \neq 1$
202	*Malacoraja senta*	Smooth Skate	82	49	64	31	368	0.36	0.33	35	—	LDM, $\rho \neq 1$
203	*Leucoraja erinacea*	Little Skate	74	53	65	44	1020	0.4	0.36	36	—	LDM, $\rho \neq 1$
220	*Squalus acanthias*	Spiny Dogfish	118	100	100	82	5564	0.81	0.88	37	—	LDM, $\rho(L)$
300	*Myoxocephalus octodecemspinosus*	Longhorn Sculpin	138	99	123	84	4783	0.34	0.35	38	—	LDM, $\rho(L)$
304	*Triglops murrayi*	Mailed Sculpin	36	15	35	14	998	0.14	0.14	39	—	LDM, $\rho \neq 1$
320	*Hemitripterus americanus*	Sea Raven	82	48	69	35	736	0.41	0.4	40	—	LDM, $\rho \neq 1$
400	*Lophius americanus*	Monkfish,Goosefish, Angler	129	61	111	43	531	0.27	0.19	41	—	LDM, $\rho(L)$
712	*Notolepis rissoi*	White Barracudina	36	22	29	16	223	0.28	0.26	42	—	LDM, $\rho \neq 1$
1191	*Leucoraja* sp.	skate; Little or Winter; unspecified	83	50	68	35	1191	0.39	0.4	43	—	LDM, $\rho(L)$
2511	*Cancer borealis*	Jonah Crab	144	134	56	48	1316	3.28	3.8	44	—	LDM, $\rho(L)$
2513	*Cancer irroratus*	Atlantic Rock Crab	85	70	63	48	1316	2.8	3.07	45	—	LDM, $\rho(L)$
2520	*Hyas* sp.	toad crab,unident.	115	98	62	46	1194	1.81	3.07	46	—	LDM, $\rho \neq 1$
2526	*Chionoecetes opilio*	Snow Crab (queen)	78	73	65	60	4283	2.1	1.58	47	—	LDM, $\rho(L)$
2550	*Homarus americanus*	American Lobster	157	145	138	126	4205	0.79	0.67	48	—	LDM, $\rho(L)$
4511	*Illex illecebrosus*	Short-fin Squid	203	157	147	101	2879	1.79	1.89	49	—	LDM, $\rho(L)$
4512	*Loligo pealeii*	Longfin Squid, Longfin Inshore Squid	37	33	22	18	1135	1.14	1.06	50	—	$\rho = 1$
50	*Anarhichas lupus*	Striped Atlantic Wolffish	32	22	21	11	86	0.4	1.18	—	51	LAM, $\rho \neq 1$
114	*Enchelyopus cimbrius*	Fourbeard Rockling	48	22	40	14	220	0.15	0.12	—	52	LAM, $\rho \neq 1$
143	*Scophthalmus aquosus*	Brill/Windowpane	13	10	10	7	102	0.23	0.24	—	53	LAM, $\rho \neq 1$
165	*Alosa aestivalis*	Blueback Herring	18	12	12	6	51	0.79	0.58	—	54	$\rho = 1$

Taxon Code	Scientific name	Common name	Summary of data #Stn	Summary of data #TEL	Summary of data #CA	Summary of data #Pair	Summary of data #Len	Sample ratio N	Sample ratio B	Fig. No. LDM	Fig. No. LAM	Result
204	*Leucoraja ocellata*	Winter Skate	48	34	33	19	1479	0.25	0.32	—	55	LAM, $\rho \neq 1$
241	*Myxine glutinosa*	Northern Hagfish	53	35	33	15	183	0.6	0.48	—	56	$\rho = 1$
280	Scorpaenidae	scorpion fishes	10	6	9	5	90	0.16	0.25	—	57	LAM, $\rho \neq 1$
323	*Artediellus* sp.	Hookear Sculpin (ns)	19	9	15	5	122	0.39	0.31	—	58	LAM, $\rho \neq 1$
340	*Aspidophoroides monopterygius*	Alligatorfish	69	24	64	19	379	0.27	0.21	—	59	LAM, $\rho \neq 1$
410	*Nezumia bairdii*	Marlin-spike Grenadier	36	15	32	11	274	0.1	0.12	—	60	LAM, $\rho \neq 1$
610	*Ammodytes dubius*	Northern Sand Lance	122	83	92	56	6428	0.54	3.61	—	61	LAM, $\rho \neq 1$
640	*Zoarces americanus*	Ocean Pout	76	41	58	23	289	0.17	0.27	—	62	LAM, $\rho \neq 1$
701	*Peprilus triacanthus*	Butterfish	91	70	73	52	1971	1.2	1.22	—	63	LAM, $\rho \neq 1$
1810	Tunicata	tunicates	44	31	20	8	0	1.34	0.64	—	64	$\rho = 1$
2211	*Pandalus borealis*	Northern Shrimp	35	30	30	25	0	0.57	0.47	—	65	$\rho = 1$
2212	*Pandalus montagui*	Striped shrimp	101	74	86	59	0	0.33	0.26	—	66	LAM, $\rho \neq 1$
2213	*Atlantopandalus propinqvus*	Atlantopandalus propinqvus	42	30	28	17	0	0.62	0.52	—	67	$\rho = 1$
2214	*Dichelopandalus leptocerus*	Dichelopandalus leptocerus	175	138	149	113	0	0.8	0.47	—	68	LAM, $\rho \neq 1$
2221	*Pasiphaea multidentata*	Pasiphaea multidentata	38	27	31	20	0	0.4	0.4	—	69	LAM, $\rho \neq 1$
2312	*Lebbeus polaris*	Lebbeus polaris	44	29	24	10	0	1.54	0.93	—	70	$\rho = 1$
2316	*Spirontocaris spinus*	Spirontocaris spinus	23	11	18	6	0	0.9	0.74	—	71	LAM, $\rho \neq 1$
2332	*Eualus fabricii*	Eualus fabricii	21	13	15	7	0	1.17	0.95	—	72	$\rho = 1$
2411	*Argis dentata*	Argis dentata	38	36	30	28	0	0.46	0.36	—	73	LAM, $\rho \neq 1$
2415	*Pontophilus norvegicus*	Pontophilus norvegicus	52	37	35	21	0	0.41	0.3	—	74	LAM, $\rho \neq 1$
2417	*Crangon septemspinosa*	Crangon septemspinosa	51	30	34	13	0	0.48	0.45	—	75	LAM, $\rho \neq 1$
2523	*Lithodes maja*	Northern Stone Crab	29	23	20	14	107	0.89	0.47	—	76	$\rho = 1$
2555	*Munida iris*	Munida iris	23	12	14	5	0	0.13	0.09	—	77	LAM, $\rho \neq 1$
2600	Euphausiacea	krill shrimp	159	122	130	93	0	0.82	0.71	—	78	LAM, $\rho \neq 1$
2809	*Parathemisto* sp.	Parathemisto sp.	57	25	44	13	0	0.47	0.5	—	79	LAM, $\rho \neq 1$
2893	*Nymphon* sp.	Nymphon sp.	33	24	14	7	0	0.92	1.28	—	80	$\rho = 1$
3000	*Annelida*	segmented worms	95	78	39	23	0	2.26	1.5	—	81	LAM, $\rho \neq 1$

Taxon Code	Scientific name	Common name	Summary of data #Stn	Summary of data #TEL	Summary of data #CA	Summary of data #Pair	Summary of data #Len	Sample ratio N	Sample ratio B	Fig. No. LDM	Fig. No. LAM	Result
4210	*Buccinum* sp.	whelks	43	43	15	15	0	5.85	5.57	—	82	LAM, $\rho \neq 1$
4400	Nudibranchia	sea slugs	104	86	65	47	0	1.09	0.85	—	83	$\rho = 1$
4508	*Bathypolypus* sp.	bathypolypus	72	61	46	36	1	1.05	1.03	—	84	$\rho = 1$
4536	Sepiolodae	bobtail squid	64	35	40	15	1	0.58	0.28	—	85	LAM, $\rho \neq 1$
6102	*Porania pulvilis*	Porania pulvilis	35	27	16	8	0	2.68	2.6	—	86	LAM, $\rho \neq 1$
6106	*Sclerasterias tanneri*	Sclerasterias tanneri	44	40	21	18	0	2.6	3.82	—	87	LAM, $\rho \neq 1$
6111	*Asterias rubens*	Asterias rubens	139	123	77	64	0	2.71	2.94	—	88	LAM, $\rho \neq 1$
6114	*Leptasterias* sp.	Leptasterias sp.	65	52	26	13	0	1.76	0.25	—	89	$\rho = 1$
6115	*Ctenodiscus crispatus*	Mud Star	39	33	28	22	0	2.67	1.98	—	90	LAM, $\rho \neq 1$
6117	*Hippasteria phrygiana*	Hippasteria phrygiana	60	55	24	21	0	1.79	1.35	—	91	LAM, $\rho \neq 1$
6118	*Henricia* sp.	blood star (genus)	136	122	81	68	0	2.25	1.6	—	92	LAM, $\rho \neq 1$
6123	*Crossaster papposus*	Spiny Sunstar	62	55	32	26	0	3.87	6.92	—	93	LAM, $\rho \neq 1$
6126	*Pteraster pulvillus*	Orange cushion star	54	46	21	14	0	4.15	3.85	—	94	LAM, $\rho \neq 1$
6136	*Astropecten americanus*	Astropecten americanus	49	40	33	24	0	3.29	3.7	—	95	$\rho = 1$
6200	Ophiuroidea	brittle stars	136	121	68	54	0	17.82	2.32	—	96	LAM, $\rho \neq 1$
6300	Gorgonocephalidae,*Asteronychidae*	basket stars	25	22	14	12	0	3.52	2.64	—	97	LAM, $\rho \neq 1$
6400	*Strongylocentrotus* sp.	sea urchins	60	55	39	34	0	3.38	4	—	98	LAM, $\rho \neq 1$
6511	*Echinarachnius parma*	Echinarachnius parma	67	46	36	15	0	13.24	2.91	—	99	$\rho = 1$
6600	Holothuroidea	Holothuroidea c.	68	61	40	34	0	2.25	2.42	—	100	LAM, $\rho \neq 1$
8100	Ctenophora	comb jellies	95	42	82	29	0	0.18	0.14	—	101	LAM, $\rho \neq 1$
8216	*Actinostola* spp.	Actinostola spp.	20	16	9	5	0	1.39	1.43	—	102	$\rho = 1$
8316	*Hormathia* sp.	Hormathia sp.	25	20	13	8	0	1.12	1.62	—	103	$\rho = 1$
8347	*Psilaster andromeda*	Psilaster andromeda	25	23	14	14	0	2.05	1.98	—	104	LAM, $\rho \neq 1$
8367	*Pennatula aculeata*	Pennatula aculeata	55	42	23	12	0	9.54	4.47	—	105	—
8500	Scyphozoa	jellyfishes	134	67	72	32	0	0.33	0.28	—	106	LAM, $\rho \neq 1$
8600	Porifera	sponges	152	58	49	22	0	0.26	0.88	—	107	—
8601	*Vazella pourtalesi*	Russian Hats	24	17	11	8	365	2.28	1.05	—	108	LAM, $\rho \neq 1$

Taxon Code	Scientific name	Common name	Summary of data #Stn	Summary of data #TEL	Summary of data #CA	Summary of data #Pair	Summary of data #Len	Sample ratio N	Sample ratio B	Fig. No. LDM	Fig. No. LAM	Result
8613	*Suberites ficus*	Fig Sponge	25	13	9	5	0	1.26	0.8	—	109	$\rho = 1$
15	*Brosme brosme*	Cusk	20	12	13	5	39	0.29	0.4	—	—	—
64	*Mallotus villosus*	Capelin	25	11	19	5	1140	0.11	0.2	—	—	—
150	*Myctophidae*	lanternfish (ns)	34	20	26	12	259	0.44	0.4	—	—	—
622	*Lumpenus lumpretaeformis*	Snake Blenny	9	7	7	5	115	0.88	0.61	—	—	—
1812	*Boltenia ovifera*	Boltenia ovifera	36	29	11	5	0	1.97	1.82	—	—	—
4321	*Placopecten magellanicus*	Sea Scallop	114	97	79	62	6117	0.38	0.76	—	—	—
6113	*Leptasterias polaris*	Leptasterias polaris	38	36	11	9	0	6.85	9.88	—	—	—
6121	*Solaster endeca*	Purple Sunstar	50	46	10	6	0	5.52	3.81	—	—	—
6413	*Brisaster fragilis*	Heart Urchin	12	10	9	7	0	8	6.43	—	—	—

Table 6. Summary of comparative fishing data, i.e., sample size for analyses. Taxa were tallied by the number of stations where they were encountered (i.e., spatial distribution) and the number of total catch numbers (i.e., population level). Each column corresponds to a range of number of effective sets (for example, there were 103 that had numbers of catches within 0–1 AND number of effective sets within 1–5).Most taxa were encountered in the comparative fishing experiment only sporadically and there were not sufficient data for analysis; a few species were both abundant and widely distributed.

Total number of catches	1-5 effective sets	5-50 effective sets	50-100 effective sets	>100 effective sets
0-1	103	119	22	7
1-10	52	7	1	0
10-100	7	34	1	0
100-1000	1	22	10	1
>1000	0	4	8	18

Table 7. Taxonomic groupings employed for the analyses of the comparative fishing data. The codes are those used routinely in DFO's Maritimes Region, commonly called RVAN codes.

Taxon	Taxon code	Codes in group
Merluccius bilinearis	14	14, 19
Artediellus sp.	323	323, 306, 880
Liparidae	500	500, 505, 512, 520, 868
Hyas sp.	2520	2520, 2521, 2527
Pagurus sp.	2560	2560, 2561, 2562
Euphausiacea	2600	2600, 2611
Polycheatae	3000	3000 - 3104
Aphrodita hastata	3200	3200, 3210
Buccinum sp.	4210	4209, 4210, 4211, 4212
Nudibranchia	4400	4400. 4410
Bathypolypus spp.	4508	4508, 4521
Pycnogonida	5100	5100, 5101, 5102
Ophiuroidea	6200	6200, 6211, 6213
Euryalida	6300	6300, 6310
Strongylocentrotus sp.	6400	6400, 6411
Holothuroidea	6600	6600, 6601, 6611
Scyphozoa	8500	8500, 8511
Porifera	8600	8600, 8602-8612, 8614, 8617-8623, 8628-8632, 8637-8699

Table 8. Summary of data and results treatment for specific taxa, including exclusion of certain lengths from the length-disaggregated analyses, rejection of automatic model selection results.

Taxa	**Taxa codes**	**Special considerations**
Urophycis tenuis	12	Small sizes (<20 cm) excluded for possible wrong coding
Squalus acanthias	220	Small sizes (<30 cm) excluded for data sparseness

Taxa	Taxa codes	Special considerations
Leucoraja sp.	1191	Large sizes (>40 cm) excluded for lack of confidence in data
Placopecten magellanicus	4321	Small sizes (<15 mm) excluded for data sparseness
Meganyctiphanes norvegica	2611	One outlier (station 87 in 2023) was excluded from analysis
Euphausiacea*, Meganyctiphanes norvegica* (Krills)	2600, 2611	Grouped due to concerns in species identification during survey
Bathypolypus spp.*,* Octopoda (Octopus and squid)	4508, 4521	Grouped due to concerns in species identification during survey
Hyas sp.*, Hyas coarctatus, Hyas araneus* (Toad crabs)	2520, 2521, 2527	Grouped due to concerns in species identification during survey
Vazella pourtalesi	8601	Russian hat was analyzed separately from taxa group 8600
Homarus americanus	2550	Manual model selection for lobster (BB5 was selected as recommended from the peer review meeting)
Mallotus villosus, Placopecten magellanicus	64, 4321	Both LDM and LAM rejected due to data concerns and model suitability, therefore, no recommendations were provided
Leucoraja ocellata, Aspidophoroides monopterygius, Ammodytes dubius, Peprilus triacanthus	204, 340, 610, 701	LDM rejected for wide CI indicating uncertainty in estimation and analysis downgraded to LAM
Pollachius virens, Hippoglossus hippoglossus, Reinhardtius hippoglossoides, Loligo pealeii	16, 30, 31, 4512	LDM resulted in CI covering 1, indicating no significant vessel difference
Urophycis tenuis, Urophycis chuss, Pseudopleuronectes americanus, Alosa pseudoharengus, Urophycis chesteri, Tautogolabrus adspersus, Hippoglossina oblonga, Amblyraja radiata, Malacoraja senta, Leucoraja erinacea, Triglops murrayi, Hemitripterus americanus, Notolepis rissoi, Hyas sp.	12, 13, 43, 62, 112, 122, 142, 201, 202, 203, 304, 320, 712, 2520	LDM resulted in length-independent conversion factors

Taxa	Taxa codes	Special considerations
Myctophidae, *Boltenia ovifera, Leptasterias polaris, Solaster endeca, Brisaster fragilis*	150, 1812, 6113, 6121, 6413	LAM results rejected due to insufficient information in data and/or lack of confidence in results, therefore, no conversion could be estimated
Pennatula aculeata, Porifera	8367, 8600	LAM for catch numbers rejected but LAM for catch biomass retained
Alosa aestivalis, Myxine glutinosa, Tunicata *, Pandalus borealis, Atlantopandalus propinqvus, Lebbeus polaris, Eualus fabricii, Lithodes maja, Nymphon* sp.*,* Nudibranchia*, Bathypolypus* spp., *Leptasterias* sp.*, Astropecten americanus, Echinarachnius parma, Actinostola* spp.*, Hormathia* sp., *Suberites ficus*	165, 241, 1810, 2211, 2213, 2312, 2332, 2523, 2893, 4400, 4508, 6114, 6136, 6511, 8216, 8316, 8613	LAM for catch numbers resulted in CIs covering 1, indicating no significant vessel difference
Parathemisto sp., *Nymphon* sp.	2809, 2893	LAM for catch biomass unavailable due to insufficient data but LAM for catch numbers retained
Anarhichas lupus, Alosa aestivalis, Ammodytes dubius, Tunicata s.p., Lebbeus polaris, Spirontocaris spinus, Eualus fabricii, Nudibranchia *, Bathypolypus* spp.*, Leptasterias sp., Actinostola* spp., Porifera, *Vazella pourtalesi, Suberites ficus*	50, 165, 610, 1810, 2312, 2316, 2332, 4400, 4508, 6114, 8216, 8600, 8601, 8613	LAM for catch biomass resulted in CIs covering 1, indicating no significant vessel difference

Table 9. Summary of results of comparative fishing analyses and recommendations for vessel calibration.

Type of analysis	Number of taxa	Details and comments
Length-disaggregated for catch numbers	Results for 40 taxa were provided in figures	4 instances indicated no significant difference in catchabilities 22 instances received length-dependent recommendations based on LDM 14 instances received length-independent recommendations based on LDM

Type of analysis	Number of taxa	Details and comments
Length-aggregated for catch numbers	Results for 59 taxa were provided in Figures	17 instances indicated no significant difference in catchabilities 40 instances received length-independent recommendations based on LAM LAM analysis for catch numbers was rejected for 2 instances
Length-aggregated for catch biomass	Results for 59 taxa were provided in numbers	15 instances indicated no significant difference in catchabilities 42 instances received length-independent recommendations based on LAM LAM analysis for catch biomass was rejected for 2 instances
No recommendations for conversion of catch numbers	285	Insufficient data for analysis.
Total taxa in analyses (after grouping)	384	See Table 5 for grouping of taxa.
Total encountered	417	Total number of species encountered in comparative fishing tows.

Table 10. Relative evidence for length-disaggregated binomial and beta-binomial models based on delta values of the Aikaike Information Criterion (∆AIC) and the Bayesian Information Criterion (∆BIC) values. Entries with '—' indicate models that did not converge properly. Models BB7 did not converge for any taxon and are not included in the table.

Taxon code	∆AIC BI0	∆AIC BI1	∆AIC BI2	∆AIC BI3	∆AIC BI4	∆AIC BB0	∆AIC BB1	∆AIC BB2	∆AIC BB3	∆AIC BB4	∆AIC BB5	∆AIC BB6	∆BIC BI0	∆BIC BI1	∆BIC BI2	∆BIC BI3	∆BIC BI4	∆BIC BB0	∆BIC BB1	∆BIC BB2	∆BIC BB3	∆BIC BB4	∆BIC BB5	∆BIC BB6
10	686	85	581	8	—	305	67	266	268	0	4	—	666	70	571	3	—	290	57	261	273	0	14	—
11	4198	994	3161	416	—	1266	363	940	938	42	0	—	4161	964	3137	398	—	1236	338	922	932	30	0	—
12	34	9	29	0	—	29	10	22	20	2	—	—	21	0	25	0	—	21	6	23	30	7	—	—
13	1090	29	1078	16	—	454	7	457	460	0	4	—	1072	16	1071	15	—	441	0	455	469	4	19	—
14	8266	562	7640	322	—	1625	189	1483	1476	42	0	—	8228	531	7615	303	—	1594	164	1465	1470	29	0	—
16	478	2	468	2	—	245	0	241	243	0	4	—	471	0	470	9	—	243	3	248	259	12	25	—
23	6594	1123	5622	475	—	1022	298	855	840	44	0	—	6562	1096	5600	459	—	995	276	839	835	33	0	—
30	6	8	0	2	—	5	7	0	—	2	—	—	0	6	2	8	—	3	9	5	—	11	—	—
31	0	2	4	6	—	0	2	4	—	6	—	—	0	5	10	15	—	3	8	13	—	18	—	—
40	1217	313	723	63	—	462	196	295	273	20	0	—	1186	286	702	48	—	436	175	280	267	10	0	—
41	527	53	432	11	200	204	31	185	188	0	2	—	507	38	422	6	210	189	21	180	193	0	13	—
42	799	331	472	0	—	554	293	328	331	0	—	—	784	321	467	0	—	544	288	328	341	5	—	—
43	378	10	319	8	—	210	1	192	193	0	4	—	368	5	318	12	—	205	0	196	206	8	21	—
44	174	26	70	0	—	58	21	35	37	1	—	—	162	18	66	0	—	50	17	35	44	5	—	—
60	3405	232	3248	135	—	1677	71	1621	1622	0	3	—	3382	214	3236	129	—	1660	59	1615	1628	0	15	—
61	13	6	0	0	—	15	—	2	6	2	6	—	7	3	0	3	—	12	—	5	15	8	18	—
62	105	4	75	0	—	56	—	45	45	—	—	—	98	0	75	3	—	52	—	48	56	—	—	—
64	1910	77	1655	46	—	76	2	73	76	0	3	32	1903	73	1653	46	—	72	0	72	81	2	9	40
112	61	4	50	6	—	23	0	19	23	2	—	—	54	0	50	10	—	20	0	23	33	9	—	—
122	51	1	32	0	—	44	—	30	33	—	—	—	47	0	34	5	—	43	—	35	44	—	—	—
123	823	91	445	40	—	204	50	132	134	0	0	—	806	78	436	35	—	191	42	128	138	0	9	—
142	10	0	13	4	21	—	—	—	—	—	—	—	7	0	16	9	35	—	—	—	—	—	—	—
160	215	7	60	0	—	55	8	36	24	—	—	—	205	0	57	0	—	49	5	36	30	—	—	—
200	75	25	46	0	51	59	22	44	48	1	—	—	64	17	42	0	63	51	19	44	55	5	—	—
201	20	5	18	1	—	14	0	14	16	0	4	—	12	1	18	5	—	10	0	18	28	8	19	—

Taxon code	ΔAIC BI0	ΔAIC BI1	ΔAIC BI2	ΔAIC BI3	ΔAIC BI4	ΔAIC BB0	ΔAIC BB1	ΔAIC BB2	ΔAIC BB3	ΔAIC BB4	ΔAIC BB5	ΔAIC BB6	ΔBIC BI0	ΔBIC BI1	ΔBIC BI2	ΔBIC BI3	ΔBIC BI4	ΔBIC BB0	ΔBIC BB1	ΔBIC BB2	ΔBIC BB3	ΔBIC BB4	ΔBIC BB5	ΔBIC BB6
202	41	0	44	4	—	37	—	40	43	—	9	—	38	0	48	11	—	37	—	48	58	—	28	—
203	150	4	149	0	—	90	5	88	88	2	—	—	142	0	149	4	—	86	6	92	100	10	—	—
204	397	56	281	2	—	202	37	171	174	0	—	—	383	47	275	0	—	192	31	169	181	3	—	—
220	685	114	577	55	—	336	24	322	—	6	0	—	658	92	560	44	—	314	7	311	—	0	4	—
300	770	72	738	18	—	299	37	298	—	0	—	—	750	57	728	13	—	284	27	293	—	0	—	—
304	254	4	256	3	—	54	0	57	59	1	—	—	248	1	256	6	—	51	0	60	68	7	—	—
320	70	0	71	4	—	66	—	70	74	—	—	—	66	0	75	12	—	66	—	78	90	—	—	—
340	93	7	77	0	—	38	8	33	36	2	5	—	84	1	74	0	—	31	5	33	42	5	15	—
400	30	23	6	1	—	26	20	4	—	0	4	12	17	14	1	0	—	17	16	4	—	3	15	28
610	6845	2173	3493	407	112	422	227	249	234	0	—	—	6827	2160	3484	402	121	409	218	244	239	0	—	—
701	703	88	703	47	—	141	12	132	136	0	3	—	688	77	695	43	—	129	4	128	140	0	11	—
712	14	4	15	0	—	7	3	8	6	0	2	—	7	0	13	1	—	3	1	10	13	4	12	—
1191	207	29	176	8	—	116	12	106	110	0	4	—	190	16	168	4	—	104	3	101	114	0	12	—
2511	187	24	160	0	—	173	23	152	154	2	—	—	173	14	155	0	—	163	18	152	164	6	—	—
2513	120	34	92	0	—	104	35	82	—	—	—	—	106	25	87	0	—	94	30	82	—	—	—	—
2520	175	9	172	1	—	105	8	98	101	0	—	—	161	0	167	0	—	96	4	98	109	4	—	—
2526	551	287	254	53	—	231	174	67	62	0	2	—	529	271	243	47	—	214	163	61	68	0	13	—
2550	241	7	226	9	—	172	5	167	157	7	0	—	229	0	225	14	—	165	4	172	173	18	22	—
4321	2541	665	1788	343	—	1089	241	724	719	19	0	—	2508	637	1765	327	—	1061	219	707	714	8	0	—
4511	2083	121	1729	74	—	212	20	204	154	2	0	—	2063	105	1718	68	—	196	9	197	157	0	7	—
4512	69	1	72	0	—	28	2	32	34	2	—	—	65	0	73	5	—	27	4	37	45	10	—	—

Table 11. Relative evidence for length-aggregated binomial and beta-binomial models for catch numbers based on Aikaike Information Criterion (AIC) and the Bayesian Information Criterion (BIC) values, and estimates of the conversion factor, and approximate 95% confidence intervals, for catches in numbers and in biomass. Results provided included taxa where length-disaggregated analyses were also undertaken. Decisions for recommended conversion factors for each taxa are in Table 7. A dash (—) indicates results were not available.

Taxon code	AIC BI0	AIC BI1	AIC BB0	AIC BB1	BIC BI0	BIC BI1	BIC BB0	BIC BB1	Numbers Model Conversion	AIC	BIC	Biomass Model Conversion
10	1104	489	484	486	1107	495	490	495	0.23 (0.18,0.3)	1293	1780	0.25 (0.2,0.33)
11	7856	1438	1433	1435	7859	1445	1440	1445	0.47 (0.41,0.54)	2698	3473	0.59 (0.53,0.66)
12	377	348	348	350	379	354	353	358	0.35 (0.29,0.43)	974	1314	0.46 (0.39,0.54)
13	2412	899	892	893	2415	905	898	903	0.26 (0.22,0.3)	1151	1824	0.26 (0.23,0.3)
14	54702	2117	2110	2112	54705	2124	2117	2123	0.37 (0.33,0.42)	2857	3950	0.41 (0.37,0.46)
16	952	350	344	346	954	356	350	354	0.69 (0.51,0.93)	1146	1521	0.97 (0.73,1.28)
23	24055	1213	1201	1203	24058	1219	1207	1212	0.41 (0.34,0.5)	1678	2326	0.41 (0.35,0.48)
30	204	206	206	208	207	211	211	216	0.95 (0.76,1.18)	991	1275	1.37 (0.98,1.91)
31	73	75	75	77	74	77	77	80	0.96 (0.76,1.23)	165	216	0.97 (0.67,1.41)
40	1844	617	619	621	1847	623	625	630	0.18 (0.14,0.23)	714	1211	0.32 (0.27,0.39)
41	1216	648	646	648	1219	654	652	657	0.48 (0.41,0.57)	894	1447	0.57 (0.5,0.66)
42	1107	622	620	622	1110	628	625	630	0.36 (0.29,0.43)	781	1129	0.46 (0.4,0.53)
43	762	362	360	362	764	367	365	369	0.48 (0.37,0.62)	703	926	0.58 (0.46,0.72)
44	394	245	249	247	396	250	254	254	0.05 (0.03,0.07)	-104	126	0.05 (0.04,0.07)
50	74	74	74	76	76	77	77	80	0.4 (0.26,0.61)	247	322	0.99 (0.5,1.93)
60	5242	832	819	820	5245	838	825	829	0.46 (0.37,0.57)	1222	1705	0.4 (0.33,0.5)
61	116	109	109	111	118	112	112	116	1.33 (0.83,2.12)	238	340	2.07 (1.41,3.04)
62	325	223	222	224	326	227	226	230	0.5 (0.38,0.65)	272	385	0.45 (0.37,0.56)
64	10810	103	104	106	10811	106	106	110	0 (0,0.09)	33	87	0.24 (0.12,0.46)
112	179	122	122	124	181	125	125	129	0.14 (0.08,0.26)	55	134	0.15 (0.1,0.23)
114	120	108	109	111	122	112	113	117	0.12 (0.06,0.25)	-13	118	0.13 (0.09,0.2)
122	148	98	99	101	150	101	101	105	0.21 (0.08,0.51)	156	216	0.3 (0.2,0.45)

Taxon code	AIC BI0	AIC BI1	AIC BB0	AIC BB1	BIC BI0	BIC BI1	BIC BB0	BIC BB1	Numbers Model Conversion	AIC	BIC	Biomass Model Conversion
123	1096	310	309	311	1099	314	313	317	0.18 (0.13,0.26)	348	539	0.27 (0.2,0.36)
142	102	92	92	94	104	96	96	99	0.24 (0.14,0.4)	209	308	0.24 (0.15,0.37)
143	55	47	47	49	55	48	48	50	0.25 (0.08,0.76)	62	82	0.32 (0.13,0.82)
150	221	109	106	108	222	112	109	113	0.48 (0.27,0.84)	-206	-124	0.46 (0.26,0.79)
160	360	149	151	153	362	153	155	159	0.1 (0.05,0.21)	80	248	0.21 (0.12,0.36)
165	51	48	48	50	52	50	49	52	0.65 (0.31,1.37)	27	60	0.56 (0.31,1.01)
200	221	171	170	172	224	175	174	179	0.27 (0.18,0.4)	845	1048	0.28 (0.2,0.4)
201	232	217	216	218	235	222	221	225	0.29 (0.21,0.39)	540	759	0.27 (0.2,0.37)
202	267	225	222	224	270	230	227	232	0.35 (0.25,0.48)	495	758	0.31 (0.22,0.43)
203	428	282	282	284	431	287	286	291	0.34 (0.25,0.44)	677	908	0.35 (0.29,0.43)
204	912	203	202	204	914	207	205	209	0.46 (0.3,0.71)	637	768	0.31 (0.23,0.43)
220	1374	623	619	621	1377	629	624	629	0.62 (0.51,0.74)	1688	2107	0.75 (0.66,0.85)
241	182	137	134	136	184	141	138	142	0.69 (0.44,1.08)	57	207	0.52 (0.36,0.74)
280	35	35	35	37	36	36	35	38	0.2 (0.08,0.53)	-15	-2	0.27 (0.16,0.44)
300	1346	618	616	618	1349	624	622	626	0.29 (0.24,0.35)	837	1348	0.31 (0.27,0.36)
304	360	110	109	111	362	113	112	116	0.09 (0.05,0.17)	-77	12	0.09 (0.06,0.15)
320	313	243	242	244	316	248	247	251	0.37 (0.28,0.5)	653	917	0.37 (0.27,0.5)
323	53	50	49	51	54	51	51	54	0.26 (0.12,0.54)	-132	-96	0.26 (0.16,0.41)
340	243	158	155	157	246	162	160	164	0.15 (0.1,0.24)	-526	-315	0.16 (0.11,0.22)
400	295	287	286	288	297	293	291	296	0.24 (0.18,0.31)	1257	1726	0.17 (0.13,0.22)
410	112	96	96	98	114	99	99	103	0.05 (0.02,0.14)	27	115	0.1 (0.06,0.17)
610	16261	682	674	676	16264	688	679	684	0.59 (0.44,0.78)	-286	137	1.29 (0.92,1.8)
640	220	187	184	186	223	192	188	193	0.27 (0.18,0.4)	253	492	0.25 (0.18,0.37)
701	1087	382	372	373	1089	387	377	380	0.63 (0.48,0.85)	282	584	0.92 (0.7,1.19)
712	114	104	103	105	116	107	106	109	0.3 (0.18,0.47)	-150	-65	0.25 (0.17,0.35)

Taxon code	AIC BI0	AIC BI1	AIC BB0	AIC BB1	BIC BI0	BIC BI1	BIC BB0	BIC BB1	Numbers Model Conversion	AIC	BIC	Biomass Model Conversion
1191	489	301	299	301	491	306	304	309	0.39 (0.29,0.54)	394	662	0.41 (0.31,0.54)
1810	249	119	116	118	251	122	120	124	1.05 (0.6,1.85)	-91	22	1.48 (0.75,2.89)
1812	123	73	77	79	125	76	81	84	2032.06 (25.04,164918.29)	29	114	2.59 (1.32,5.08)
2211	8987	335	330	332	8988	338	334	337	0.86 (0.55,1.35)	128	214	0.51 (0.39,0.67)
2212	10203	668	659	661	10206	673	664	669	0.48 (0.36,0.64)	-289	55	0.41 (0.32,0.52)
2213	1099	226	222	224	1100	229	225	229	0.68 (0.41,1.12)	-140	-34	0.56 (0.39,0.8)
2214	8984	1209	1194	1196	8987	1216	1201	1205	0.56 (0.46,0.69)	-684	-2	0.56 (0.47,0.68)
2221	2373	280	272	272	2374	284	276	277	0.39 (0.24,0.63)	-46	50	0.39 (0.27,0.56)
2312	270	137	132	134	272	140	135	139	0.85 (0.5,1.46)	-324	-211	0.94 (0.62,1.41)
2316	82	76	75	77	83	79	77	80	0.47 (0.22,0.99)	-185	-137	0.68 (0.44,1.07)
2332	104	75	74	76	105	77	76	79	0.64 (0.31,1.3)	-192	-150	0.88 (0.53,1.45)
2411	483	248	247	249	485	251	250	254	0.63 (0.45,0.88)	-197	-102	0.38 (0.32,0.45)
2415	497	212	207	209	499	216	211	215	0.54 (0.35,0.85)	-398	-256	0.32 (0.23,0.45)
2417	434	176	169	171	436	180	172	176	0.49 (0.31,0.8)	-393	-252	0.46 (0.3,0.7)
2511	533	362	359	360	536	368	365	369	2.8 (2.09,3.75)	410	939	3.94 (3.02,5.13)
2513	406	320	320	322	408	325	325	329	1.71 (1.27,2.3)	130	406	2.52 (1.96,3.23)
2520	532	348	345	347	535	353	350	355	1.24 (0.94,1.65)	-639	-238	2.72 (2.01,3.68)
2523	75	77	76	78	77	79	79	82	0.9 (0.61,1.32)	125	191	0.49 (0.31,0.78)
2526	758	441	441	443	760	445	446	450	2.2 (1.75,2.77)	253	500	1.78 (1.5,2.11)
2550	1326	678	677	679	1329	684	683	688	0.76 (0.66,0.86)	1929	2529	0.77 (0.68,0.87)
2555	79	56	55	57	80	58	57	60	0.38 (0.17,0.83)	-96	-54	0.15 (0.07,0.3)
2600	10211	1024	1009	1011	10215	1030	1015	1020	0.55 (0.44,0.7)	-1281	-672	0.64 (0.51,0.8)
2809	238	147	144	146	240	151	148	152	0.32 (0.2,0.51)	—	—	—
2893	104	77	76	78	105	80	79	82	1.19 (0.63,2.25)	—	—	—
3000	252	204	201	203	255	209	206	210	1.62 (1.11,2.38)	-905	-592	1.54 (1.15,2.05)

Taxon code	AIC BI0	AIC BI1	AIC BB0	AIC BB1	BIC BI0	BIC BI1	BIC BB0	BIC BB1	Numbers Model Conversion	AIC	BIC	Biomass Model Conversion
4210	136	110	108	110	137	114	112	115	7.78 (4.89,12.36)	10	123	6.69 (5.04,8.87)
4321	4531	612	605	607	4534	618	610	615	0.56 (0.43,0.74)	454	855	0.68 (0.51,0.91)
4400	632	358	354	356	635	363	359	364	0.93 (0.69,1.25)	-908	-551	0.99 (0.78,1.27)
4508	272	227	227	229	274	232	231	235	0.93 (0.69,1.27)	-266	-47	1.01 (0.8,1.27)
4511	6613	786	766	767	6616	793	773	777	0.69 (0.57,0.85)	577	1402	1 (0.83,1.21)
4512	216	148	148	150	218	151	151	155	0.91 (0.63,1.3)	44	137	1 (0.83,1.2)
4536	122	123	123	125	124	128	127	132	0.59 (0.42,0.82)	-396	-221	0.37 (0.25,0.53)
6102	78	77	77	79	80	80	80	83	2.65 (1.69,4.15)	23	109	2.08 (1.23,3.53)
6106	146	119	118	120	147	122	122	126	2.42 (1.52,3.84)	-227	-114	3.26 (2.18,4.87)
6111	1290	536	533	535	1293	542	539	544	1.72 (1.3,2.28)	-251	250	2.53 (1.95,3.28)
6113	111	71	77	79	113	75	80	84	50.67 (4.02,638.17)	87	182	12.39 (7.62,20.15)
6114	284	160	159	161	286	165	164	168	1.57 (0.97,2.54)	-433	-238	1.42 (0.78,2.58)
6115	690	223	224	226	691	226	227	230	1.73 (1.07,2.81)	-50	49	1.83 (1.43,2.33)
6117	129	119	119	121	131	123	123	127	2.03 (1.34,3.08)	78	246	1.67 (1.2,2.32)
6118	606	467	463	465	609	473	469	474	1.88 (1.48,2.4)	-1166	-670	1.83 (1.47,2.3)
6121	107	70	79	—	109	73	82	—	3501.78 (79.67,153914.38)	72	210	7.11 (3.48,14.53)
6123	192	163	165	167	194	167	169	173	3.42 (2.13,5.49)	-42	138	6.17 (4.23,9)
6126	176	123	123	125	178	127	127	131	2.21 (1.29,3.77)	-391	-241	3.44 (2.28,5.17)
6136	746	219	219	221	748	223	223	226	1.13 (0.72,1.79)	-176	-41	2.14 (1.45,3.16)
6200	5617	520	521	523	5620	526	527	531	10.47 (5.61,19.54)	-1036	-539	6.02 (4.58,7.9)
6300	72	74	74	76	73	76	76	79	3.51 (2.79,4.41)	85	135	2.82 (2.07,3.85)
6400	763	297	298	300	765	301	302	306	3.57 (2.51,5.06)	150	326	3.83 (2.99,4.9)
6413	89	54	55	57	89	55	56	59	2.59 (0.81,8.25)	-54	-36	4.39 (2.38,8.08)
6511	853	228	220	222	855	233	224	228	0.98 (0.62,1.54)	117	320	2.23 (1.38,3.6)
6600	819	278	280	282	821	283	284	288	3.58 (2.27,5.65)	544	747	2.76 (2.12,3.59)

Taxon code	AIC BI0	AIC BI1	AIC BB0	AIC BB1	BIC BI0	BIC BI1	BIC BB0	BIC BB1	Numbers Model Conversion	AIC	BIC	Biomass Model Conversion
8100	1449	333	332	334	1451	338	338	342	0.15 (0.1,0.22)	-422	-104	0.1 (0.08,0.14)
8216	66	55	54	56	67	57	56	59	1.3 (0.58,2.89)	62	101	1.42 (0.82,2.45)
8316	268	104	104	106	270	106	106	109	1.19 (0.64,2.19)	-20	34	1.81 (1.28,2.57)
8347	124	95	95	97	125	97	97	100	1.94 (1.16,3.24)	-20	27	2.19 (1.53,3.13)
8367	738	184	184	186	740	188	188	192	923.58 (9.26,92134.64)	-196	-47	4.97 (3.3,7.49)
8500	387	304	298	300	390	310	304	308	0.42 (0.31,0.58)	-8	362	0.27 (0.2,0.37)
8600	1864	305	296	298	1867	310	301	305	0.68 (0.47,0.99)	26	302	1.2 (0.85,1.7)
8601	146	87	84	85	147	89	86	88	2.06 (1,4.24)	87	126	1.31 (0.95,1.8)
8613	201	72	71	73	202	74	73	76	0.98 (0.42,2.27)	96	127	1.28 (0.67,2.44)

8. FIGURES

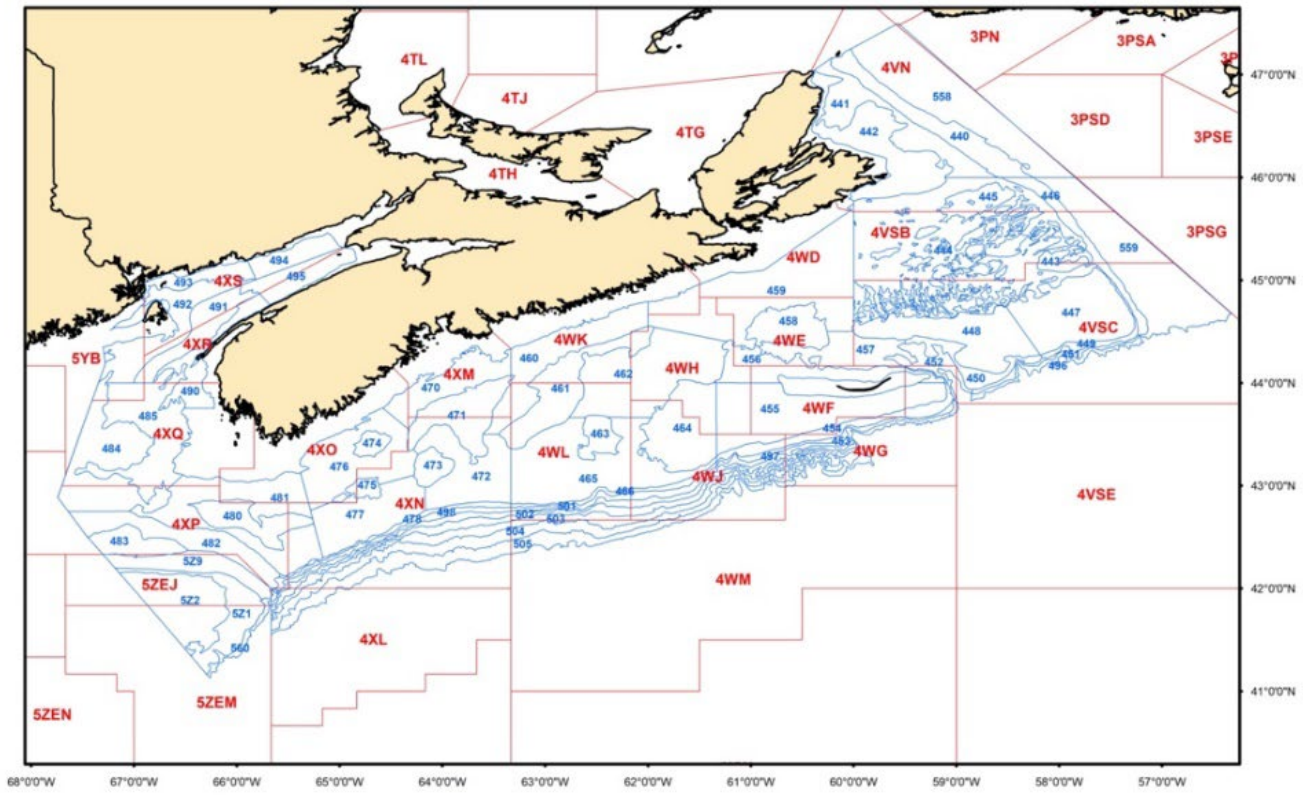

Figure 1. Stratification map for the Summer Research Vessel (RV) Survey in the Maritimes Region. The strata are labelled in blue and DFO unit areas are labelled in red. The strata design expanded over the years that the Needler was in service. From 1970–1995, sampling was generally concentrated in strata 440–495. Spatial coverage was extended to the Scotian Shelf slope (strata 496–498) in 1996 and the Fundian Channel (5Z1 & 5Z9) in 2011. The sampled area expanded to include strata 558 and 559 in 2014 and strata 5Z2 in 2016.

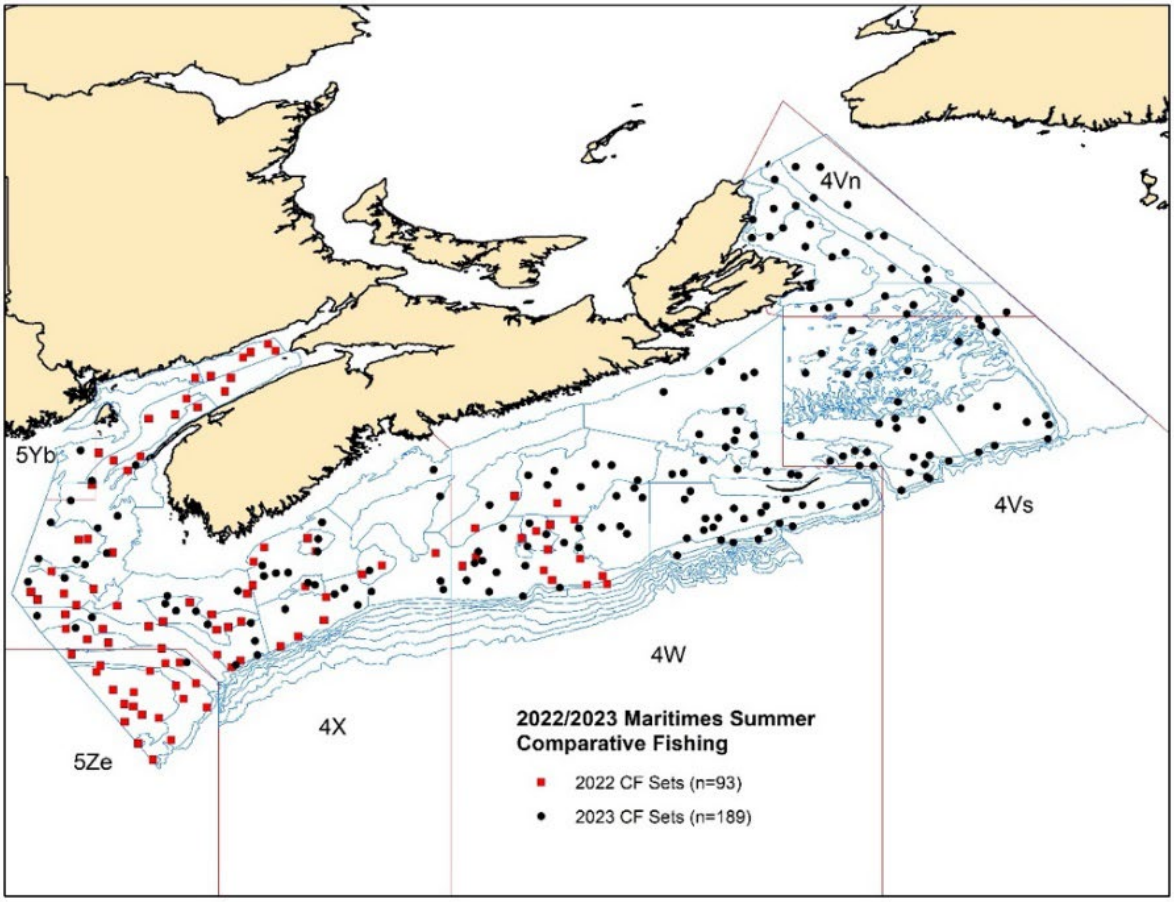

Figure 2. Locations of 2022 (red) and 2023 (black) comparative fishing sets (CF Sets; n=number of fishing sets) from the Maritimes Region summer comparative fishing experiment. Blue and red lines represent survey strata boundaries and NAFO Subdivisions within the Maritimes Region, respectively.

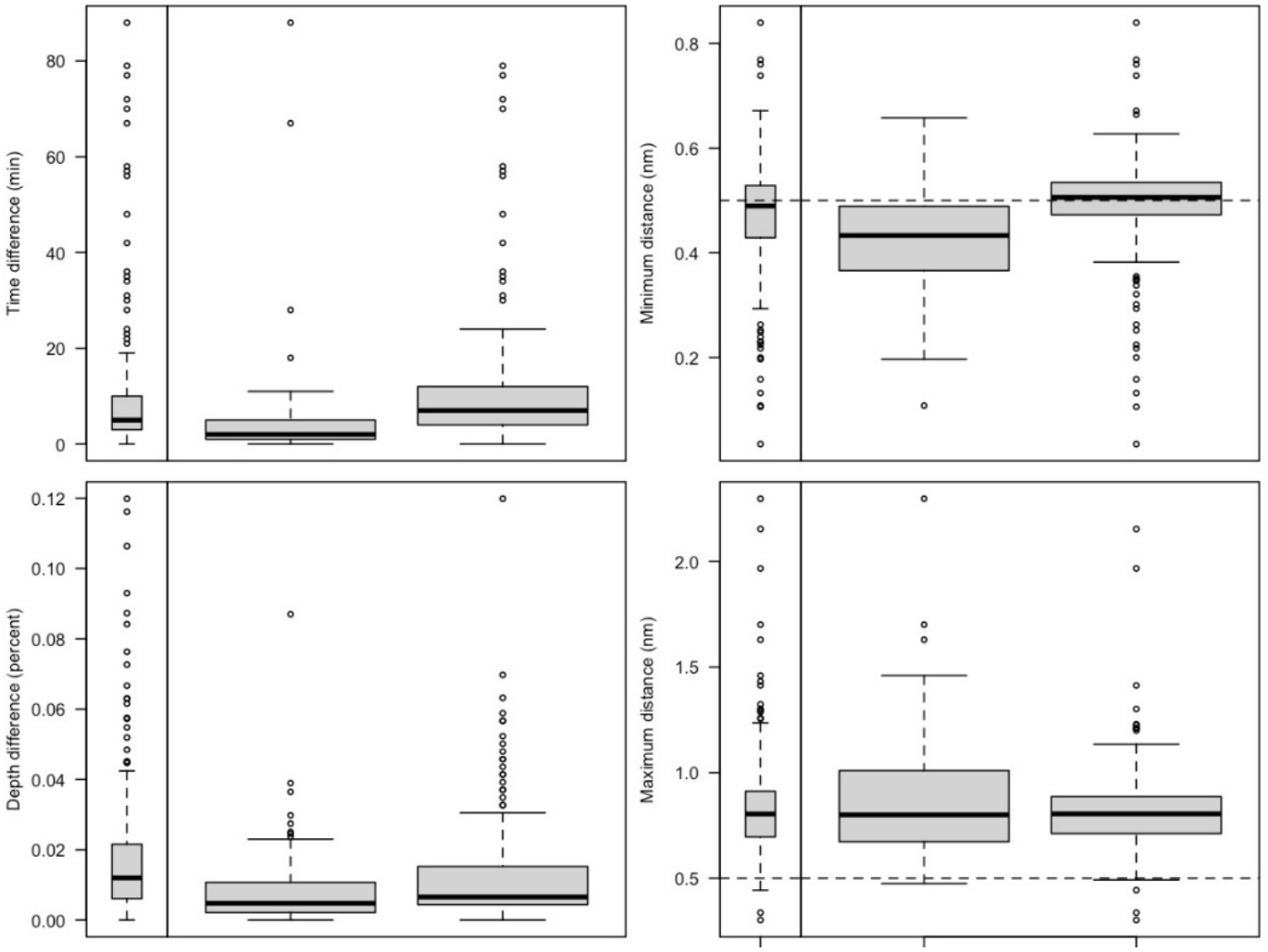

Figure 3. Boxplots showing the amount of time in minutes between the onset of fishing between vessels, the difference in depth in meters between vessels and the minimum and maximum distances between vessels in nautical miles (nm). Both years where comparative fishing took place are presented together in the left column, and separately in the right column.

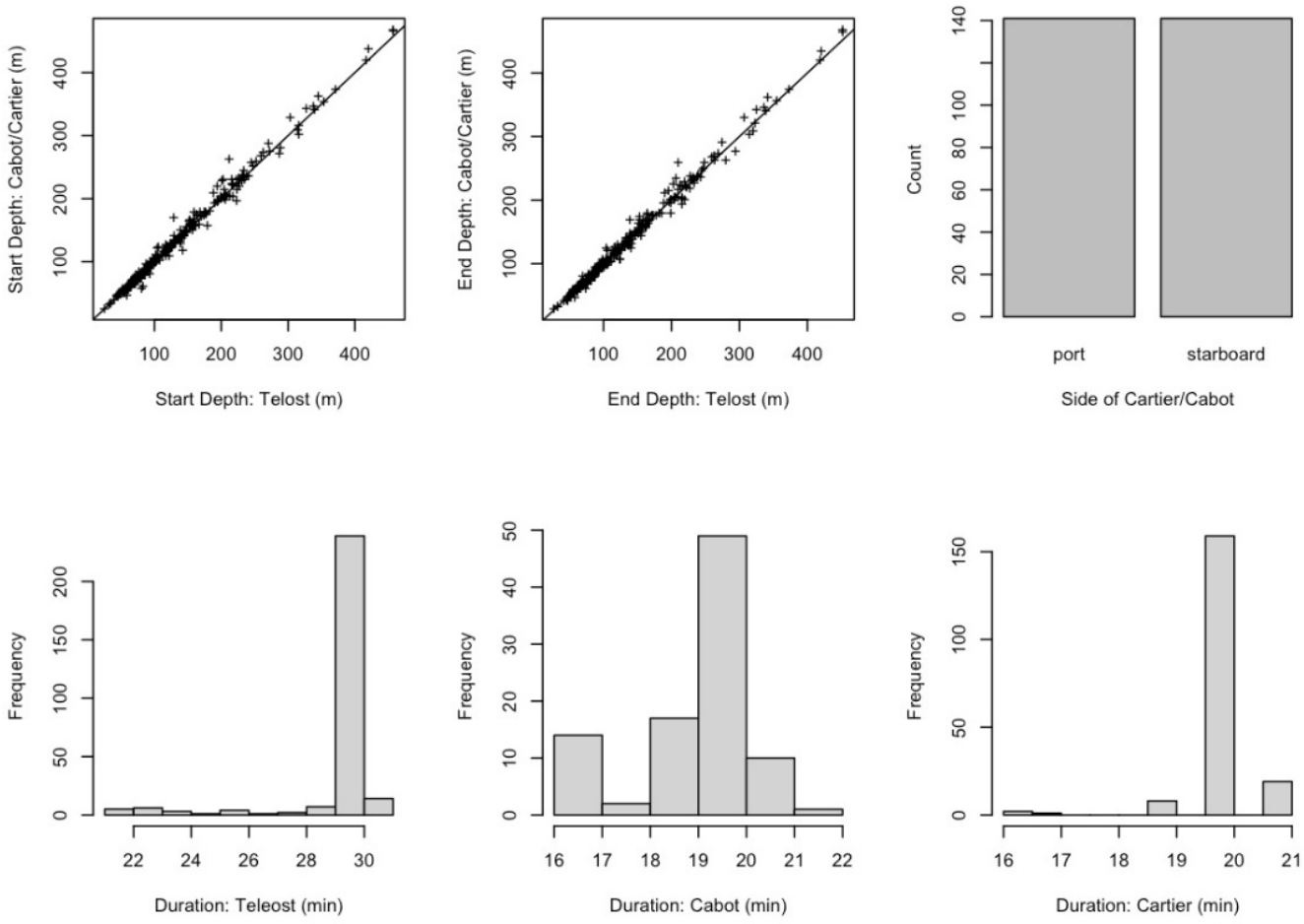

Figure 4. Top two panels on the left plot depths from starting and ending locations from each pair of tows in meters (m). Top right panel counts the number of pairs where Cartier/Cabot fished on each side. The bottom three panels summarize tow durations in minutes for all tows from the three vessels, respectively.

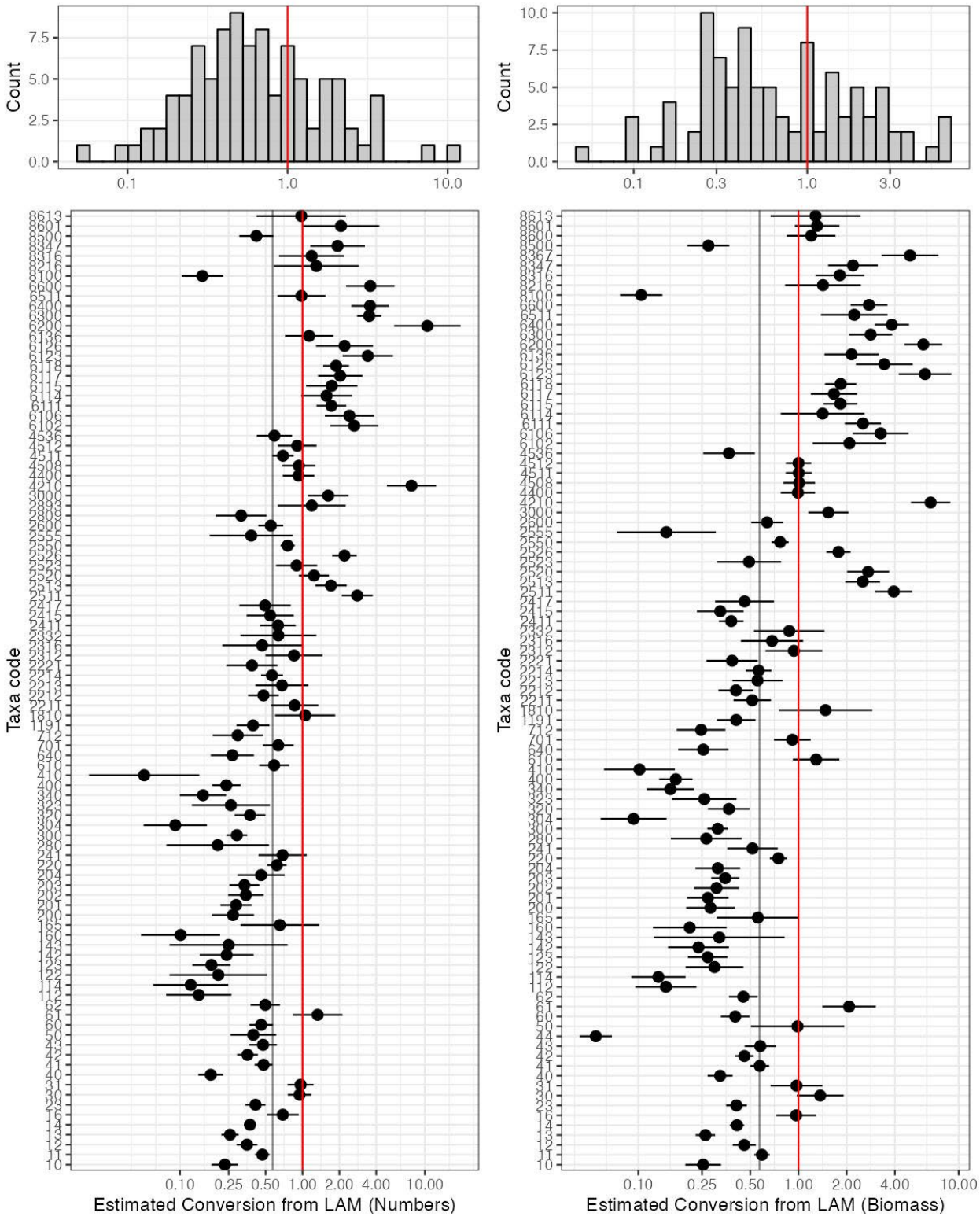

Figure 5. Estimated conversion factors and 95% confidence interval for taxa (see Table 5 for codes) catch numbers and biomass using length-aggregated models (LAM, see Section 2.2 for details) and histogram summaries for estimated conversion factors. Red and grey vertical lines indicate a conversion equal to one and 1/1.75 (ratio between protocol tow distances).

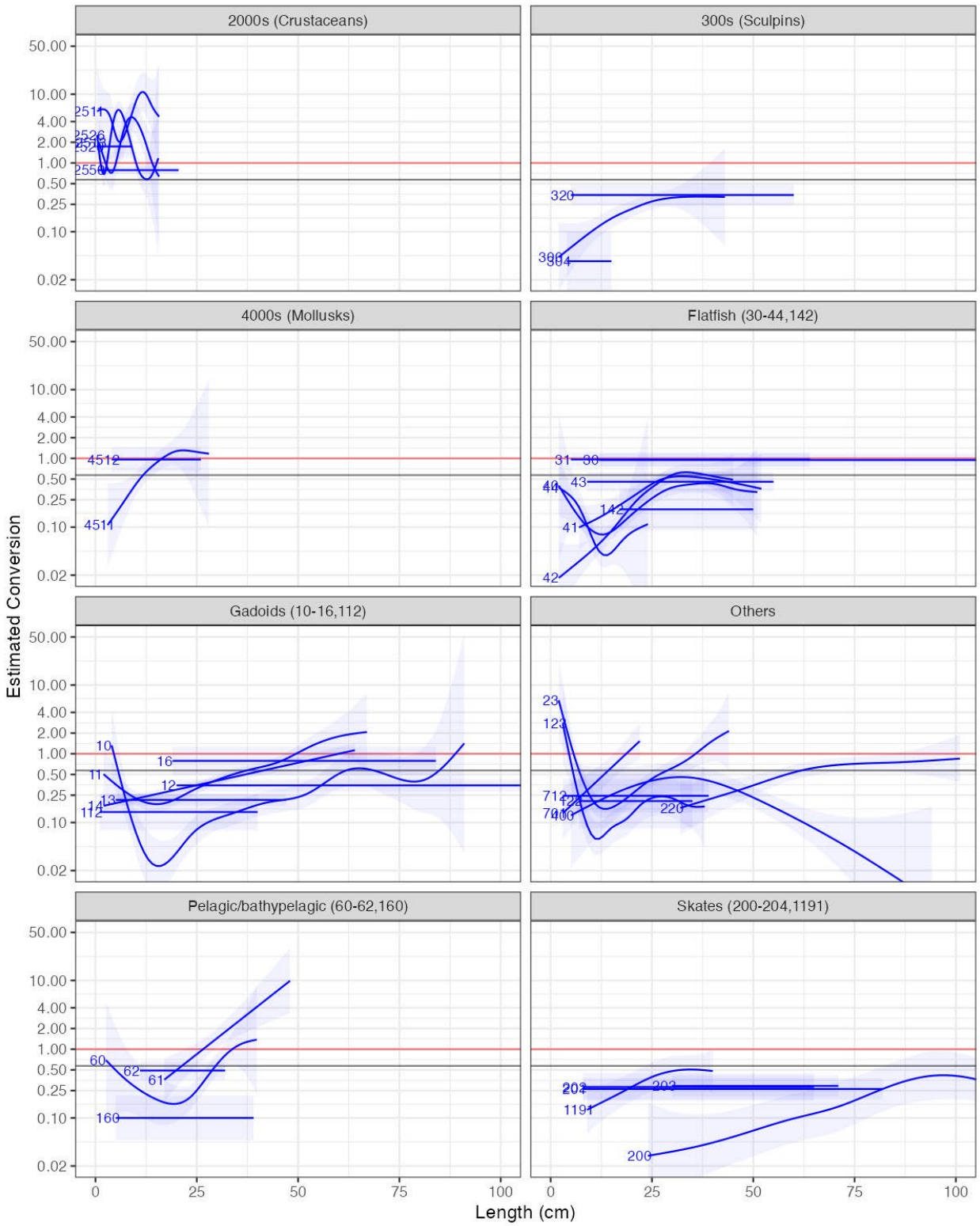

Figure 6. Estimated conversion factors and 95% confidence interval for taxa (see Table 5 for codes) catch numbers using length-disaggregated models (LDM, see Section 2.2 for details). Red horizontal lines indicate a conversion equal to one. Taxa were clustered roughly based on taxonomy (and identified using the taxon codes) in each panel.

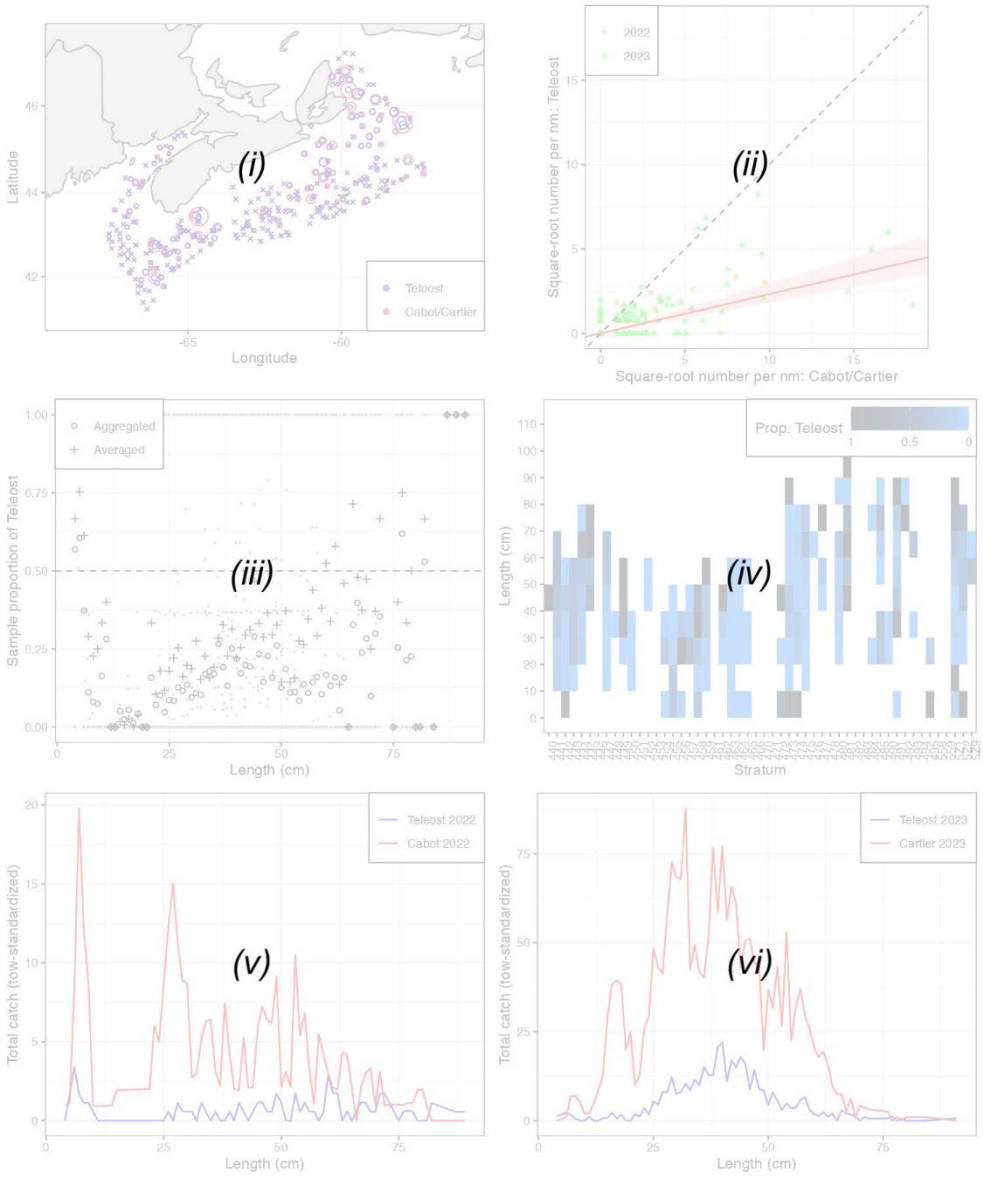

Figure 7. Interpretation for the first of three sets of figures presenting the data and results for taxa for which length-disaggregated analyses were undertaken. (i) Presents a map of catches by the Canadian Coast Guard Ship (CCGS) Teleost (red circles) and by the CCGS Jacques Cartier/CCGS John Cabot (blue circles) in comparative fishing sets, where circle size is proportional to the number caught and nil catches are indicated by x. (ii) Biplot of the square-root of Teleost catch numbers against the square-root of Cartier/Cabot catch numbers (orange for sets in 2022 and green for 2023), where the red line and shaded interval show the estimated conversion and approximate 95% confidence interval from the best length-aggregated model. (iii) Plot of the empirical proportions of catch in a pair made by the Teleost as a function of length for each set pair (grey dots), averaged across set pairs in each length interval (cross) and aggregated across set pairs (circles). (iv) compositions of catch proportions by Teleost where lengths were aggregated by 10 cm (or mm) intervals and stations were aggregated by strata (v) Total length frequencies for catches made by Teleost (blue line) and by Cartier/Cabot (red line) in 2022. (vi) Same as (v) except for 2023.

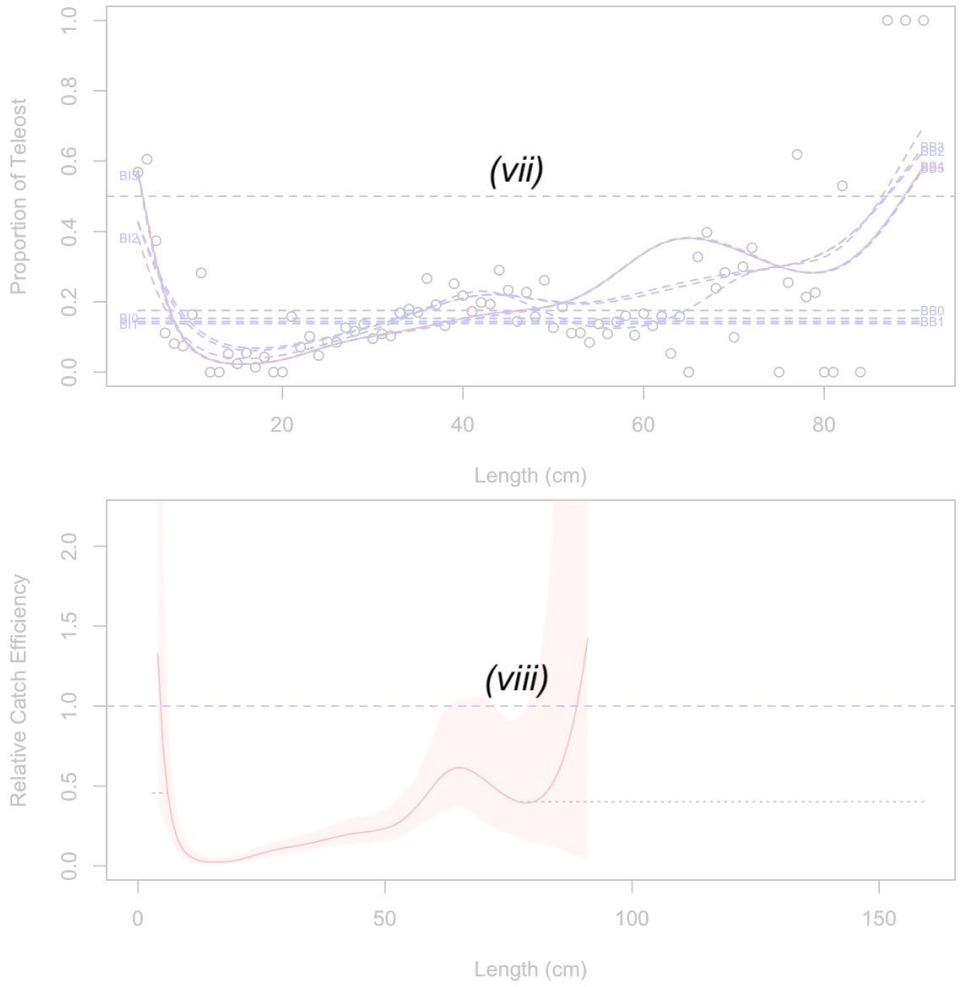

Figure 8. Interpretation for the second of three sets of figures presenting the data and results for taxa for which length-disaggregated analyses were undertaken. (vii) Estimated length-specific catch proportion functions, $logit(p_{Ai}(l))$, for each converged model, with the selected model plotted using a red line along with its approximate 95% confidence interval (95% CI) (shaded area), as well as the length class-specific mean empirical proportion of total catch in a pair made by the Canadian Coast Guard Ship Teleost (black circles). (viii) Estimated relative catch efficiency (conversion factor) function from the best model (with 95% CI). The horizontal dashed red line indicates equivalent efficiency between vessels and the dotted black line indicates the relative catch efficiency function that assumes a constant efficiency at small and large sizes (i.e., extended to minimum and maximum length measurements in the database of historical surveys).

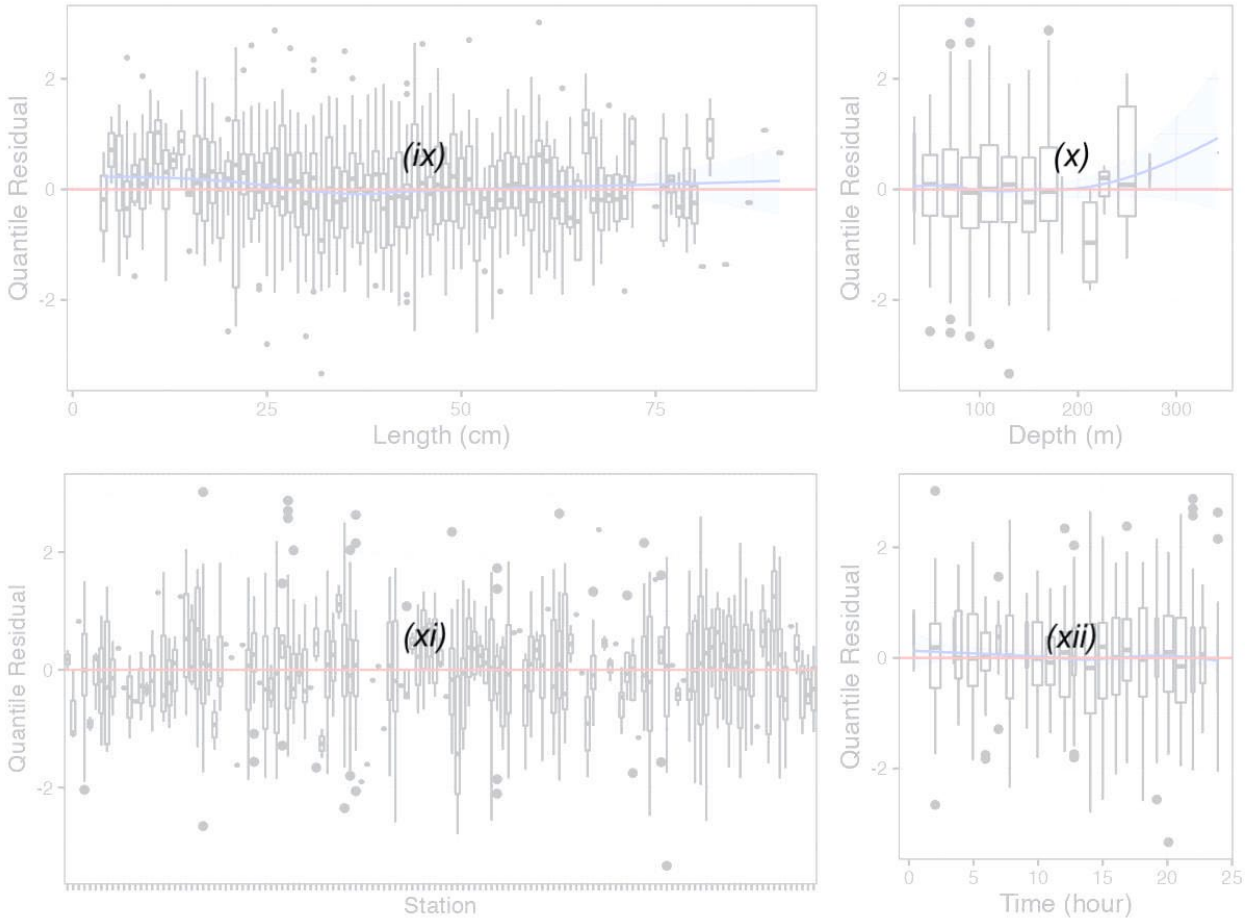

Figure 9. Interpretation for the third of three sets of figures presenting the data and results for taxa for which length-disaggregated analyses were undertaken. Boxplot of normalized quantile residuals as a function of (ix) length, (x) depth class, (xi) station, and (xii) hour.

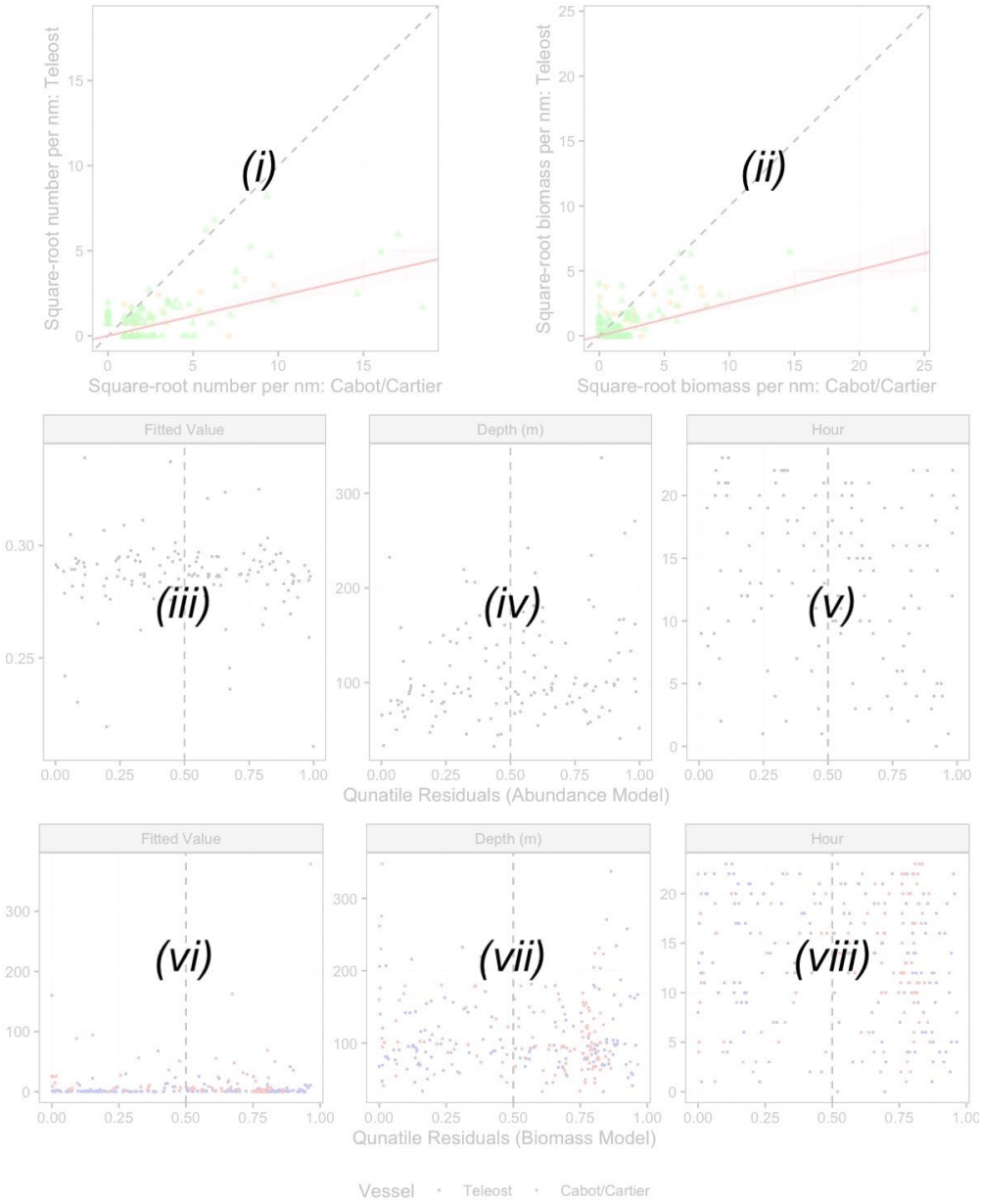

Figure 10. Interpretation for the figures presenting the data and results for taxa for which size-aggregated analyses were undertaken. (i) Biplot of the square-root of Cartier/Cabot catch numbers against the square-root of Teleost catch numbers, where the blue line and shaded interval show the estimated conversion and approximate 95% confidence interval from the best size-aggregated model, and where the pairs made in 2022 and 2023 are distinguished by colour (orange for 2022 and green for 2023). (ii) As in (i), except for catch weights. Quantile residuals from the analysis of catch numbers are plotted as a function of (iii) fitted values, and the (v) time and (vii) depth of the paired set (i). Similarly, quantile residuals from the analysis of catch weights are plotted as a function of (iv) fitted values, with values for Teleost plotted with blue circles and those for Cartier/Cabot in red, and the (vi) time and (viii) depth of the paired set. Note that for taxa that are not measured and depending on model conversion, only panels (ii), (iv), (vi) and (viii) are shown.

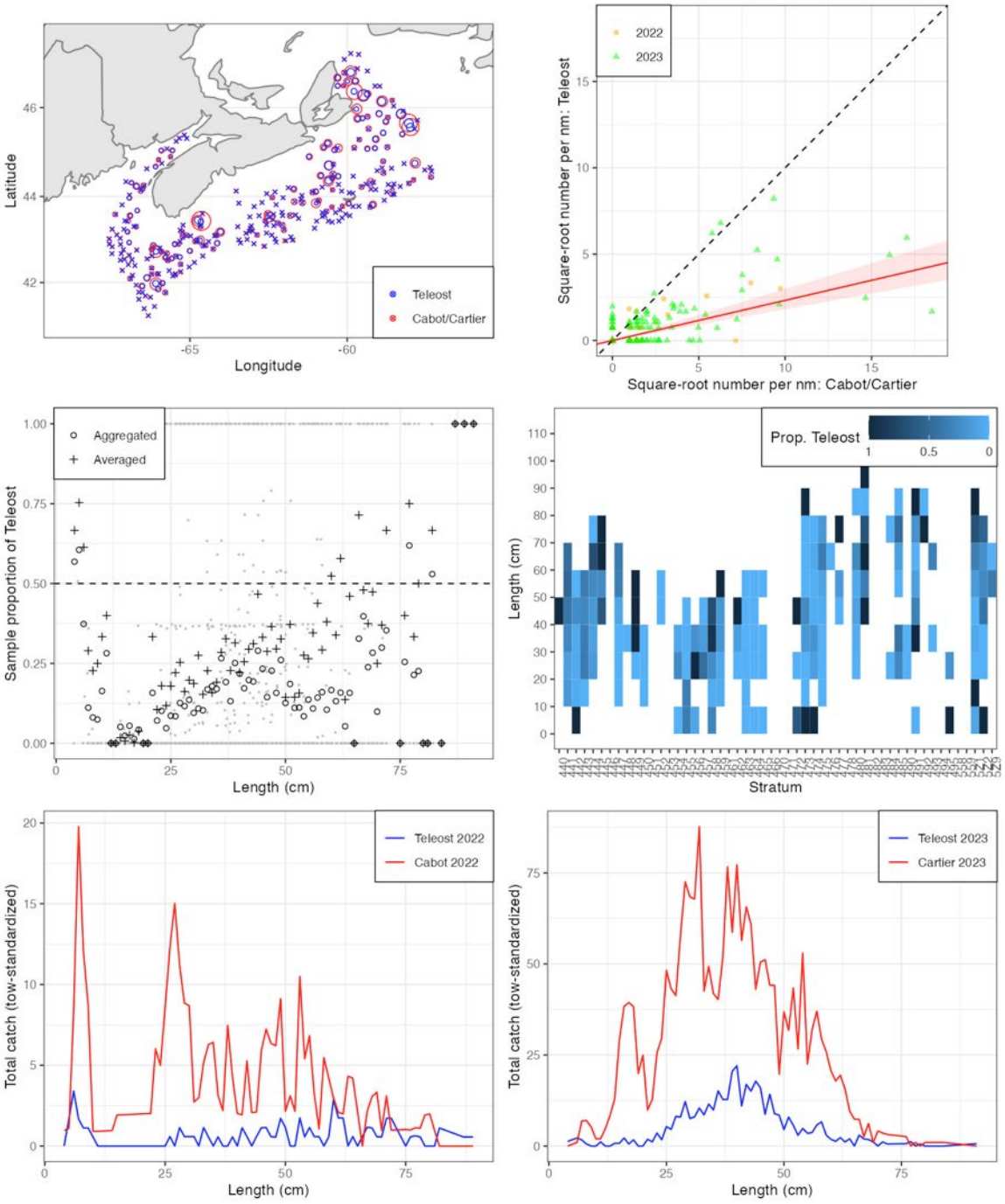

Figure 11a. Visualisation of comparative fishing data and size-aggregated model fit for Gadus morhua (10).

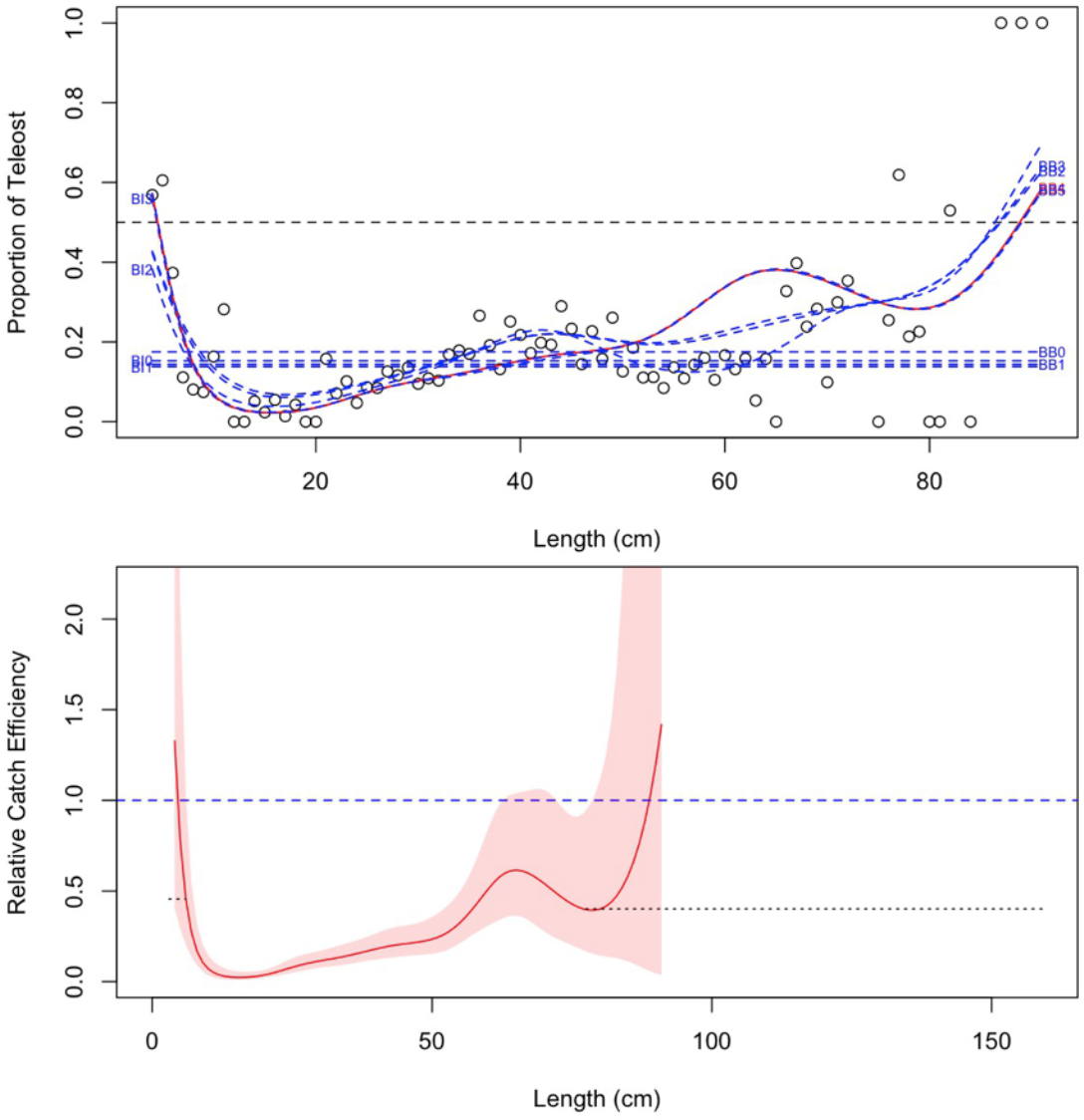

Figure 11b. Model fits and the selected length-based calibration for Gadus morhua (10).

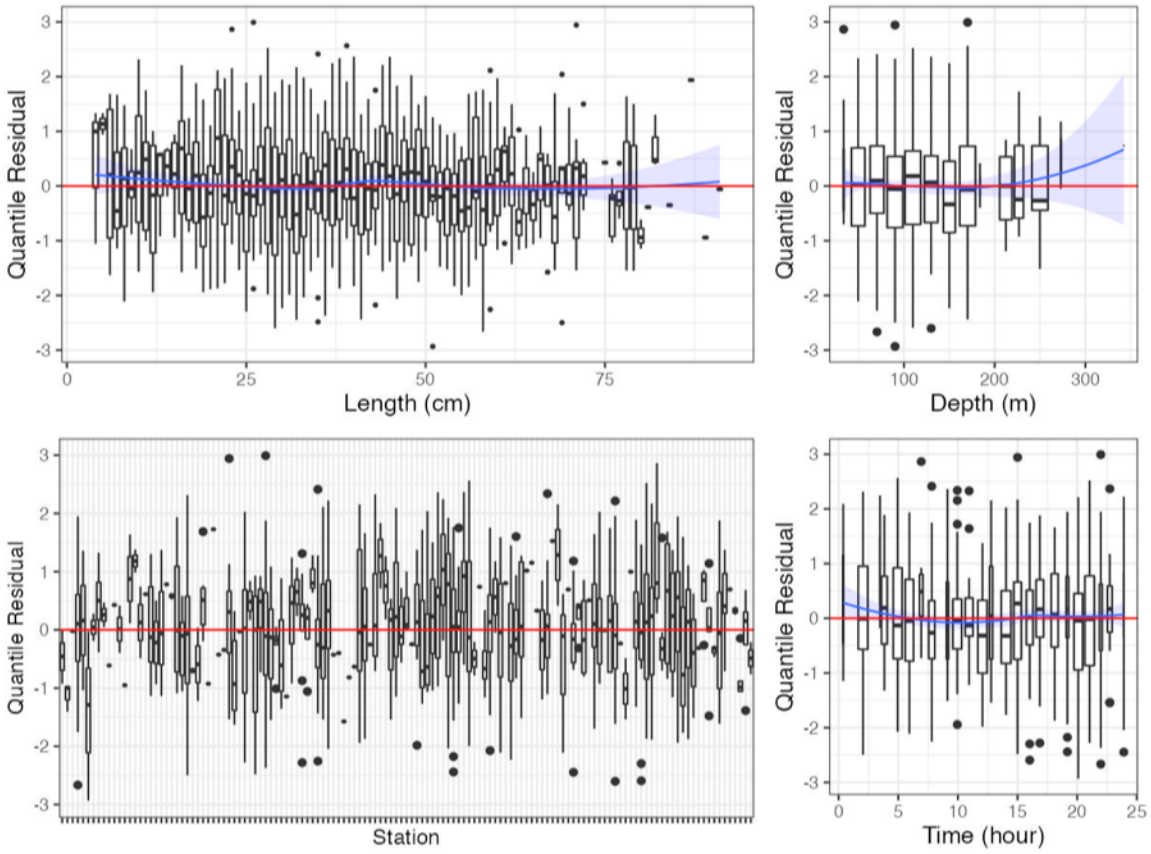

Figure 11c. Randomized and normalized quantile residuals for the selected model for Gadus morhua (10).

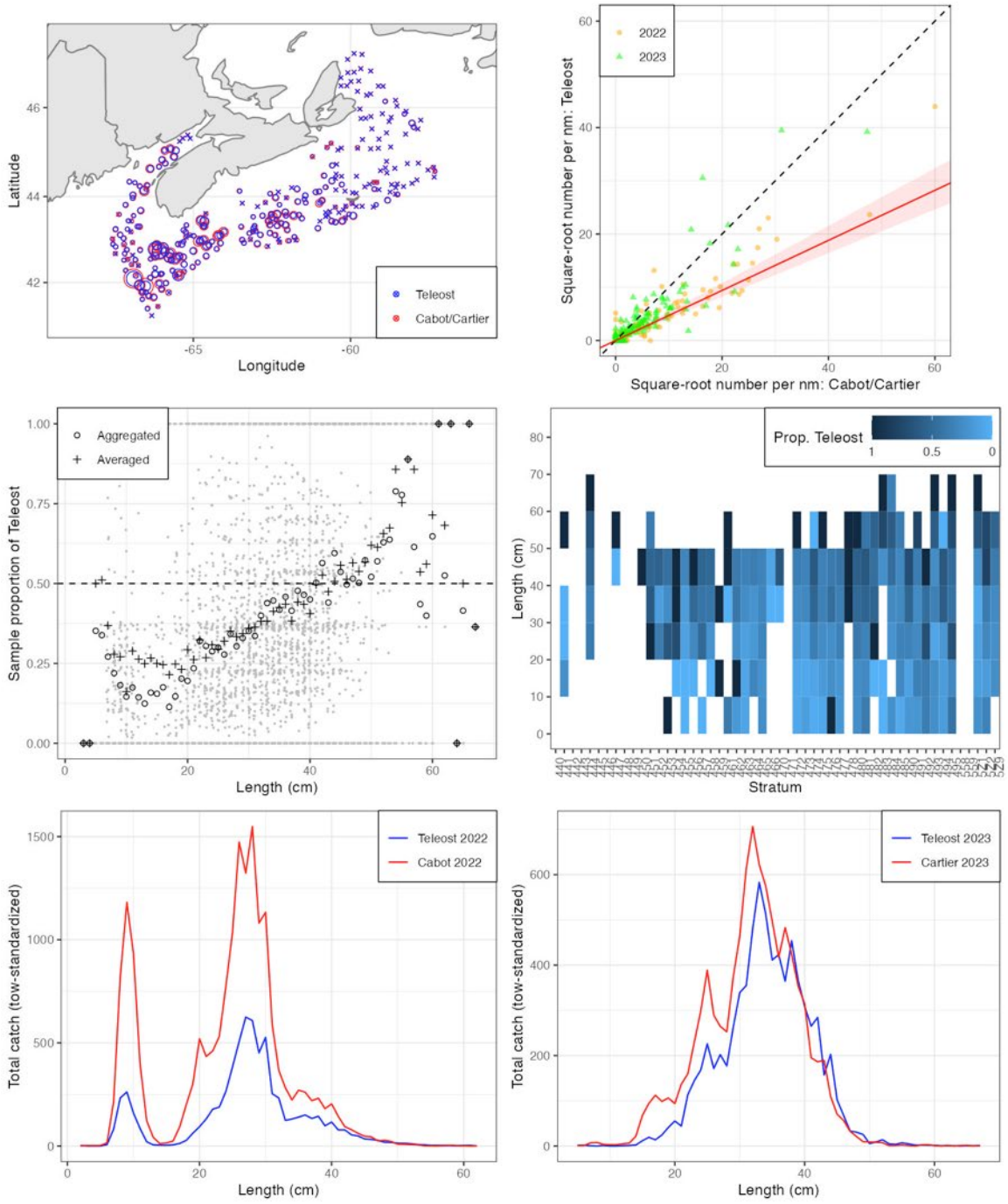

Figure 12a. Visualisation of comparative fishing data and size-aggregated model fit for Melanogrammus aeglefinus (11).

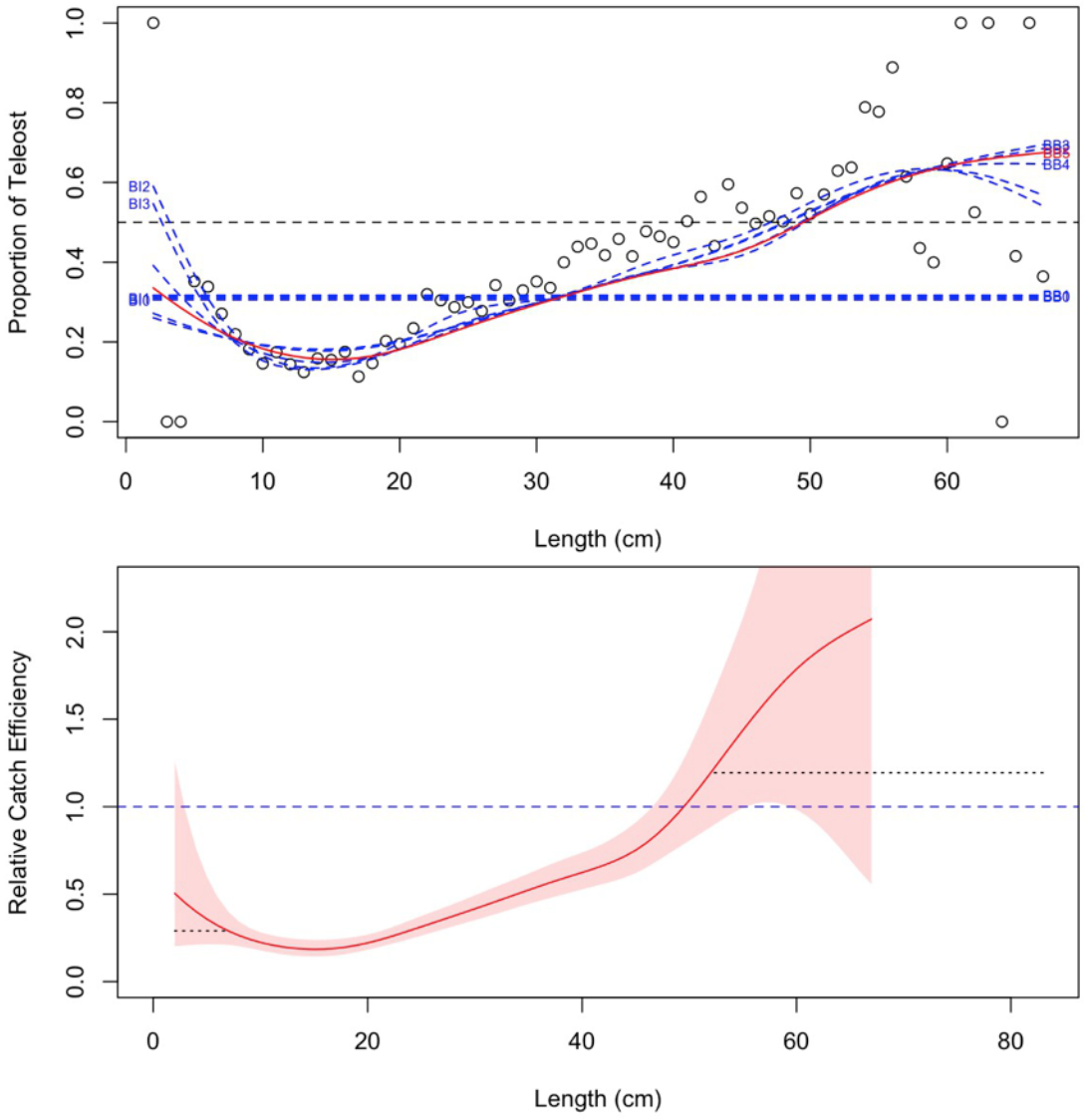

Figure 12b. Model fits and the selected length-based calibration for Melanogrammus aeglefinus (11).

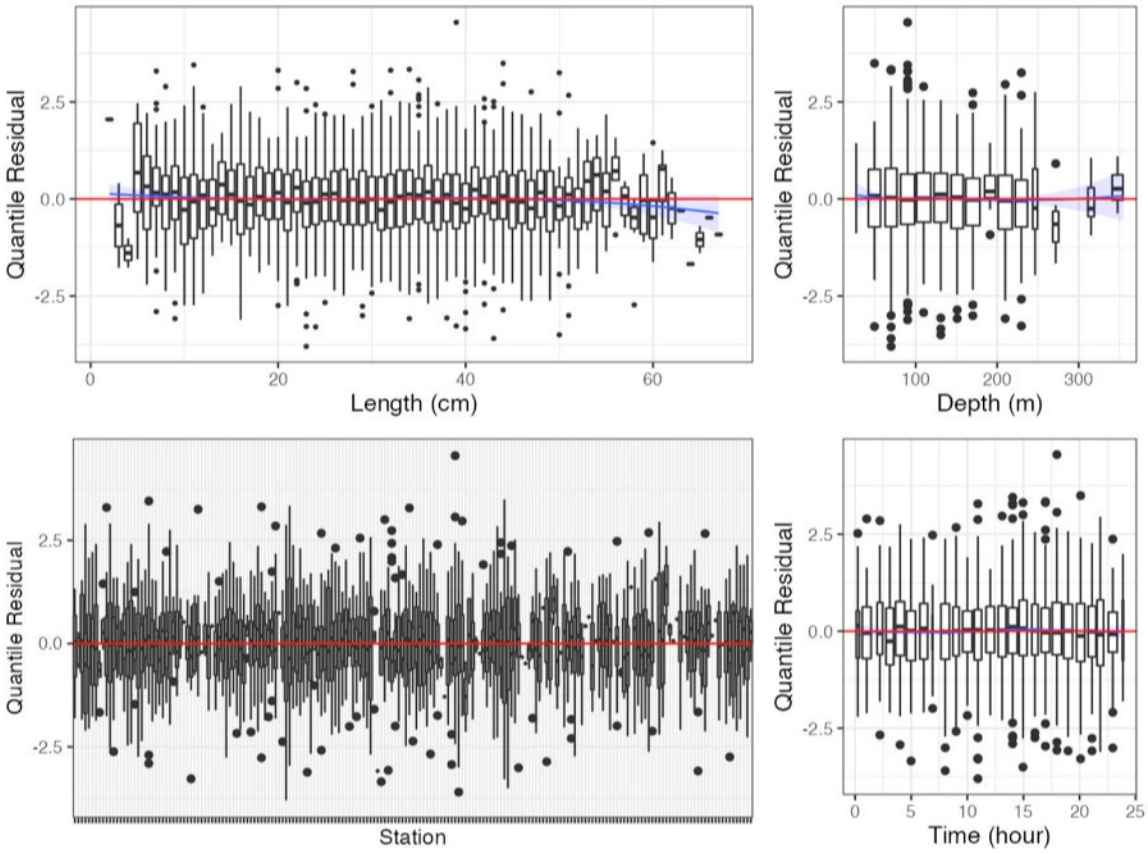

Figure 12c. Randomized and normalized quantile residuals for the selected model for Melanogrammus aeglefinus (11).

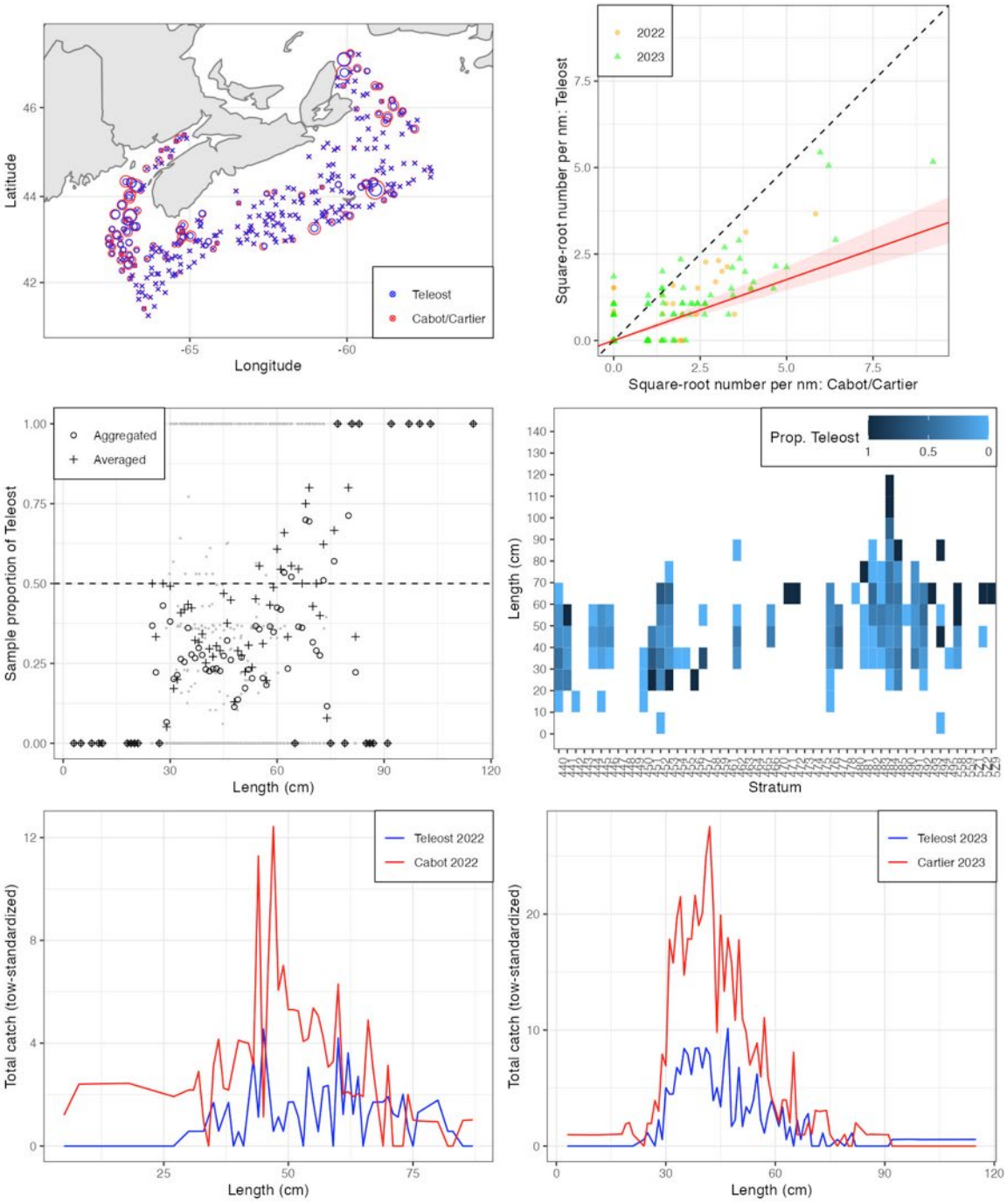

Figure 13a. Visualisation of comparative fishing data and size-aggregated model fit for Urophycis tenuis (12).

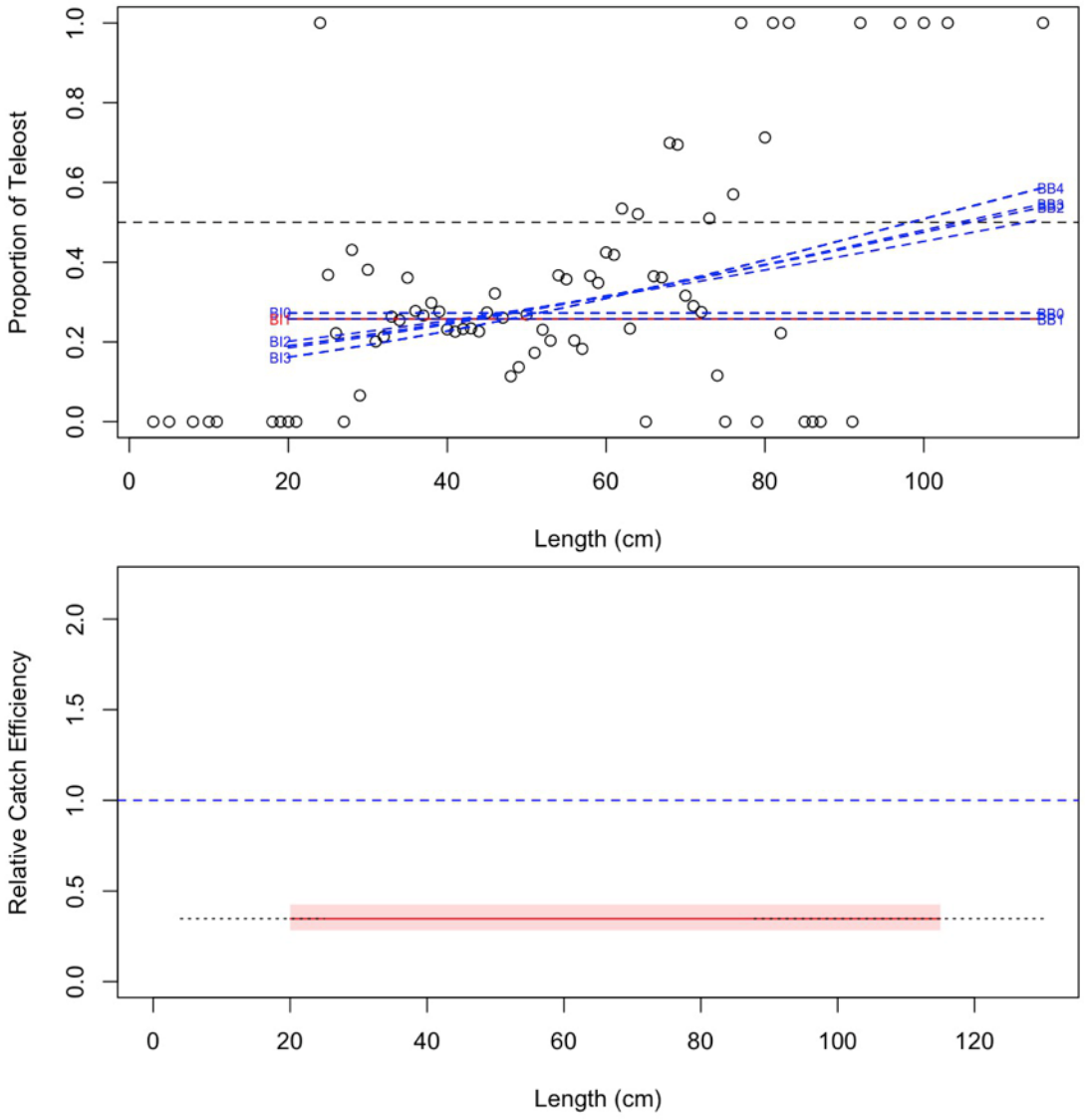

Figure 13b. Model fits and the selected length-based calibration for Urophycis tenuis (12).

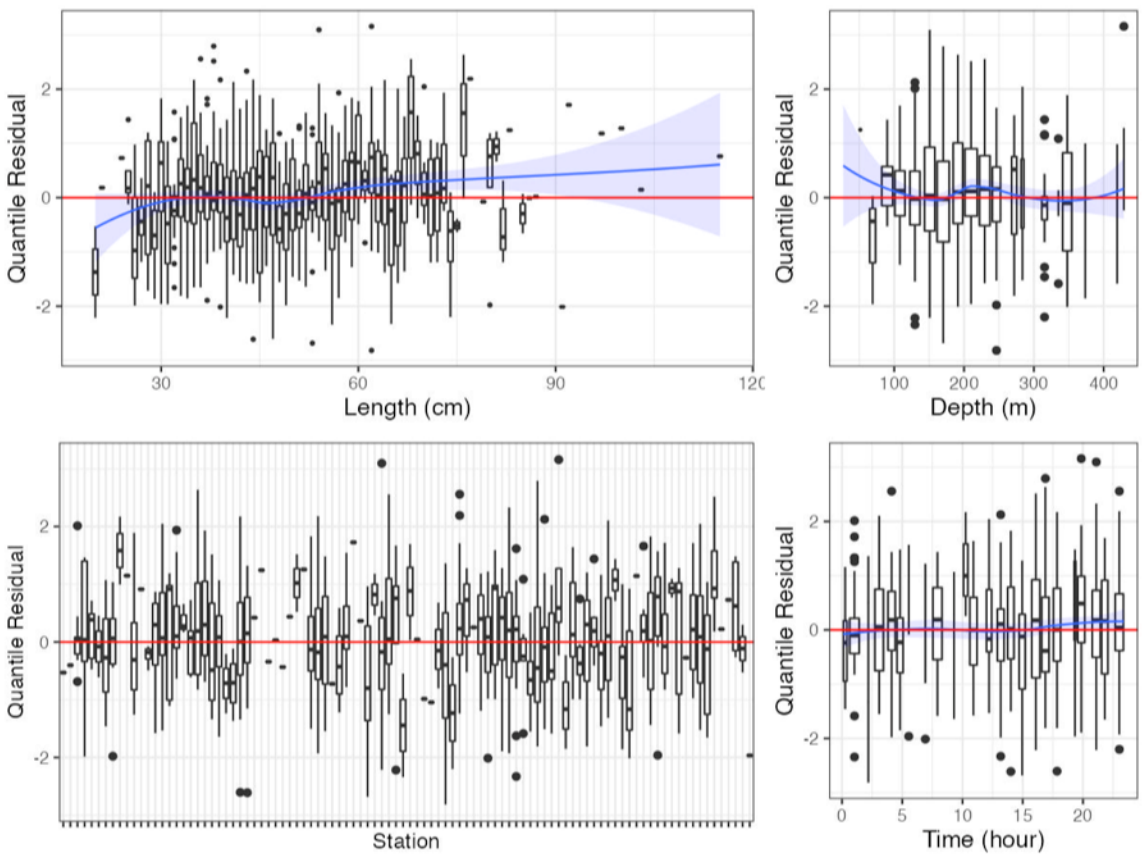

Figure 13c. Randomized and normalized quantile residuals for the selected model for Urophycis tenuis (12).

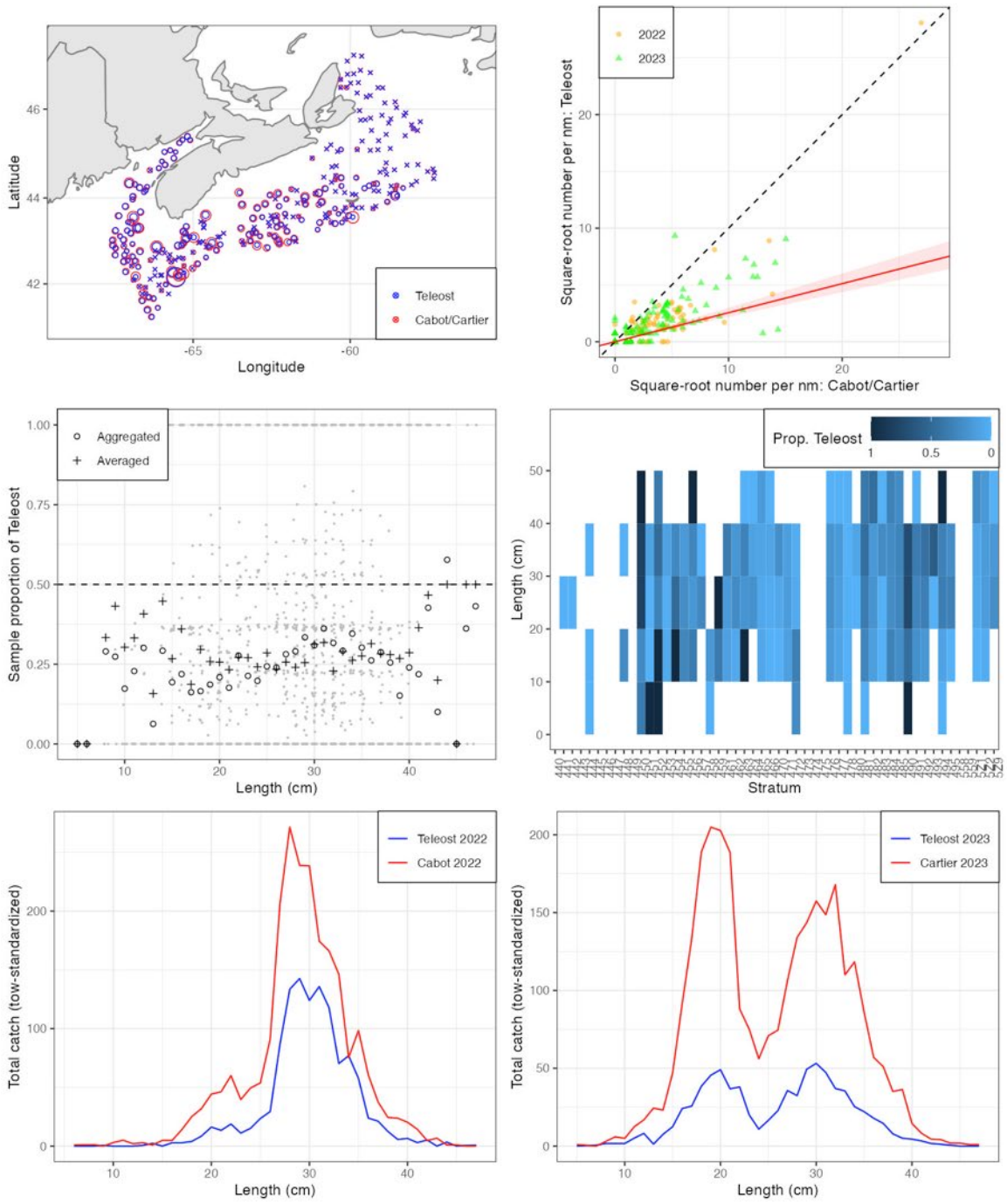

Figure 14a. Visualisation of comparative fishing data and size-aggregated model fit for Urophycis chuss (13).

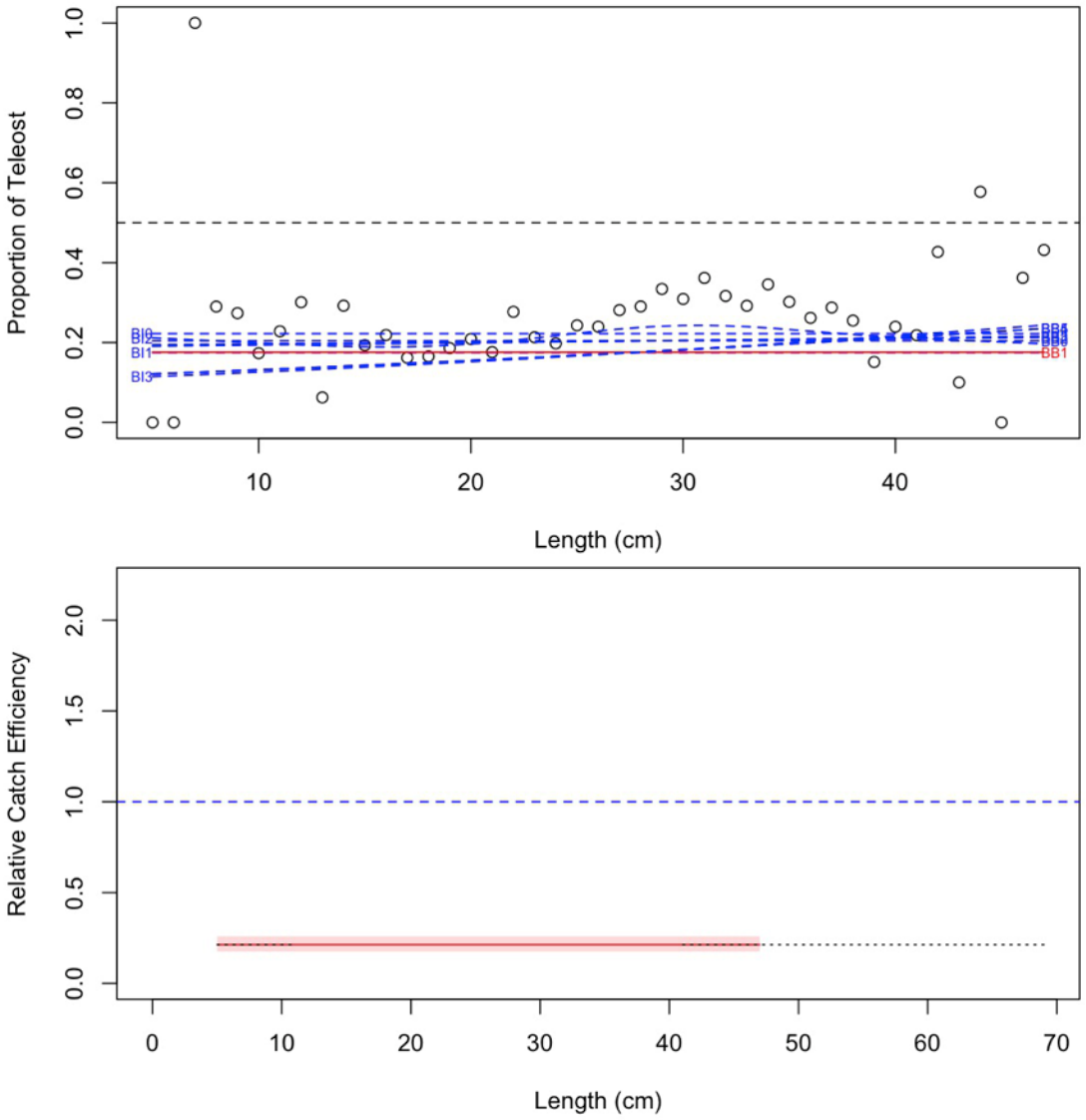

Figure 14b. Model fits and the selected length-based calibration for Urophycis chuss (13).

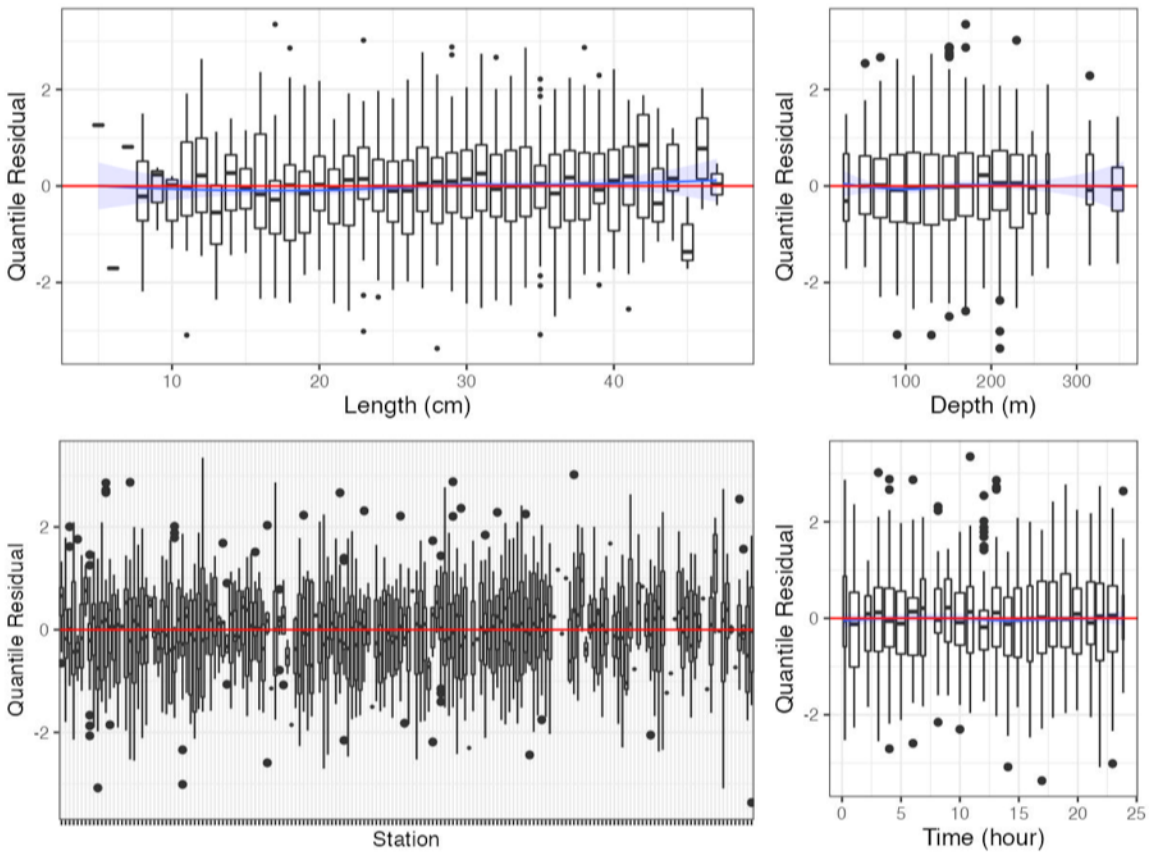

Figure 14c. Randomized and normalized quantile residuals for the selected model for Urophycis chuss (13).

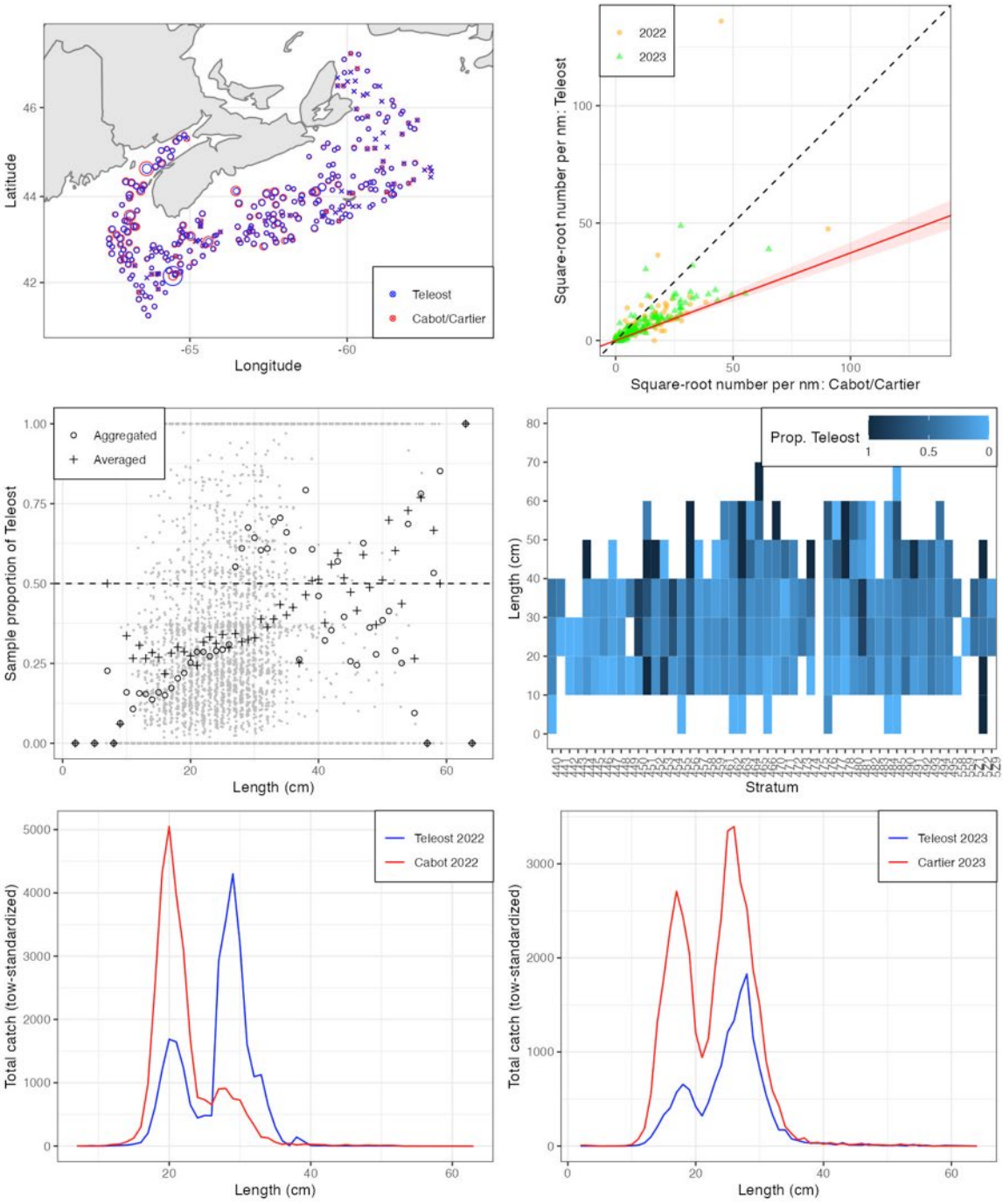

Figure 15a. Visualisation of comparative fishing data and size-aggregated model fit for Merluccius bilinearis (14).

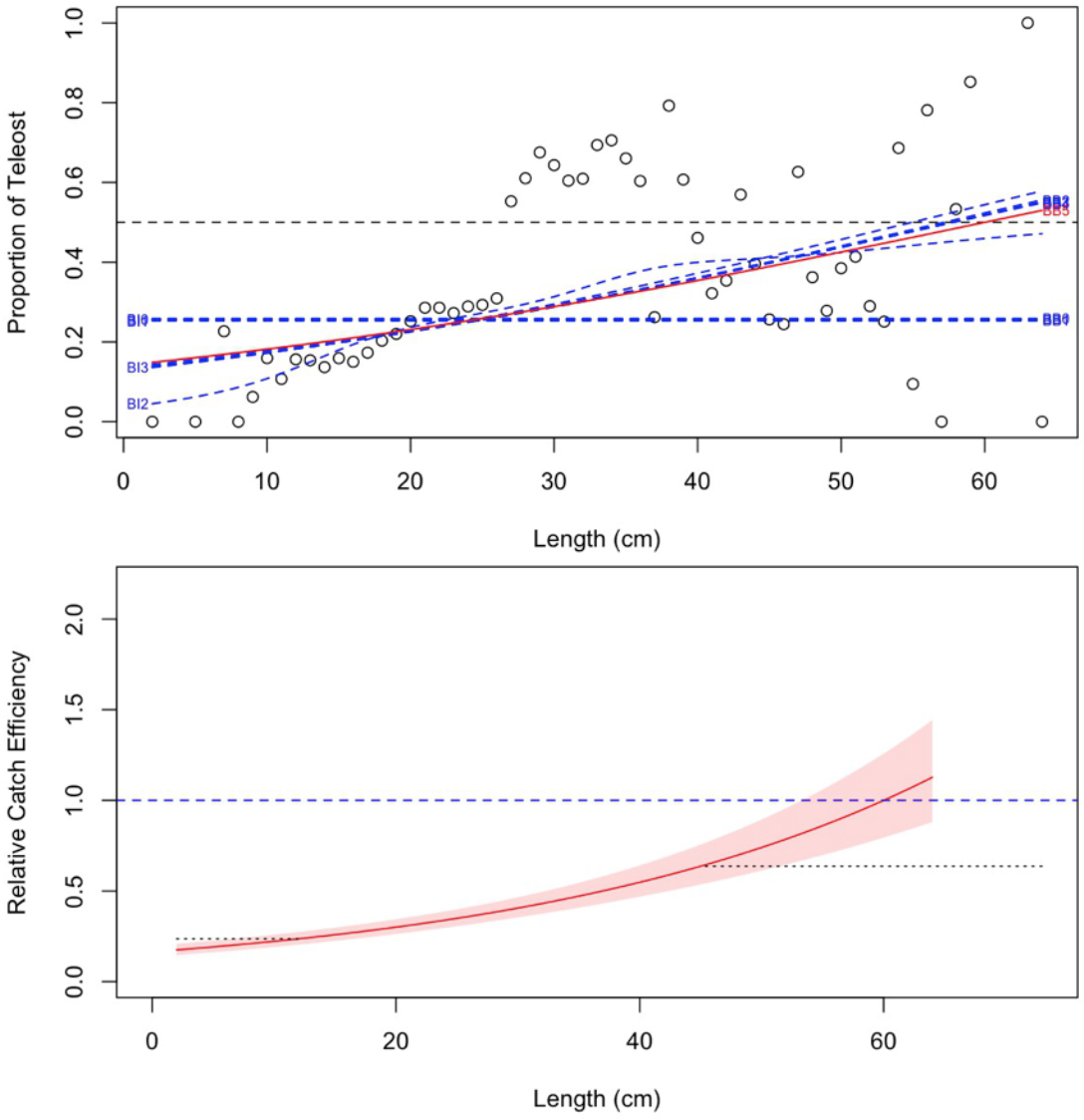

Figure 15b. Model fits and the selected length-based calibration for Merluccius bilinearis (14).

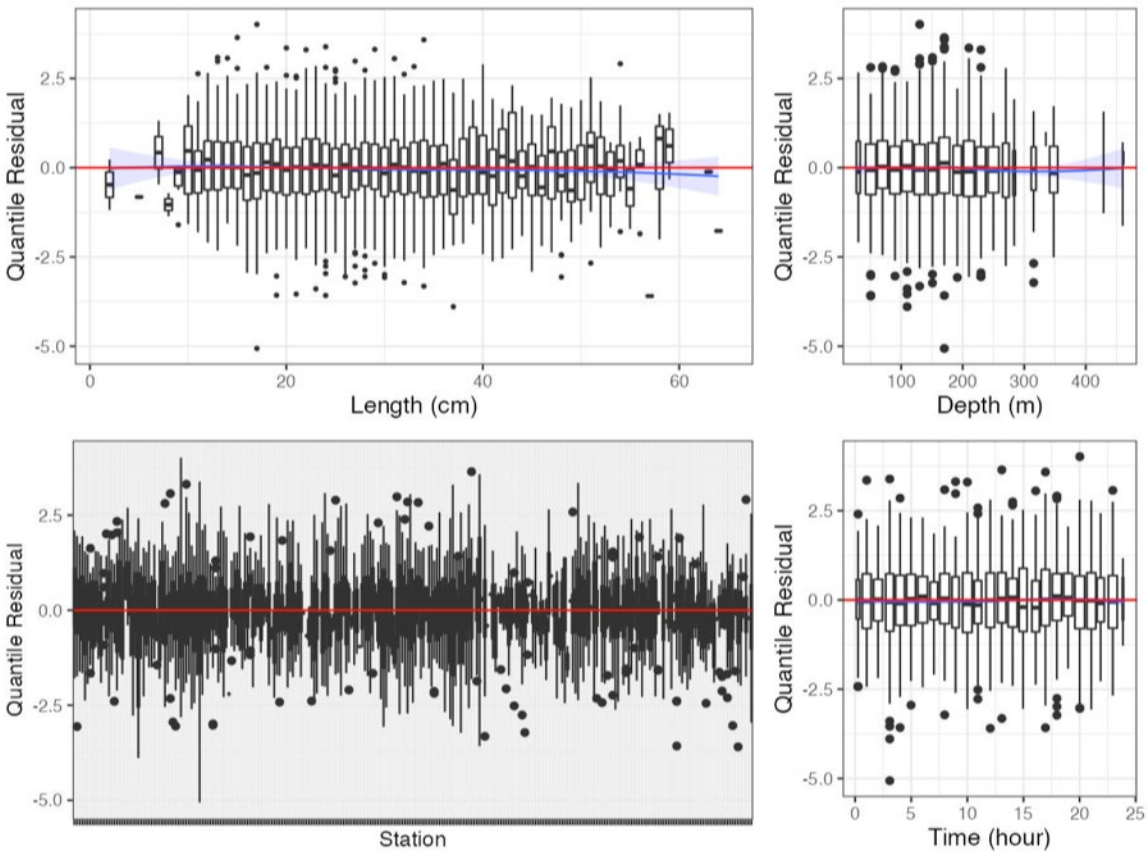

Figure 15c. Randomized and normalized quantile residuals for the selected model for Merluccius bilinearis (14).

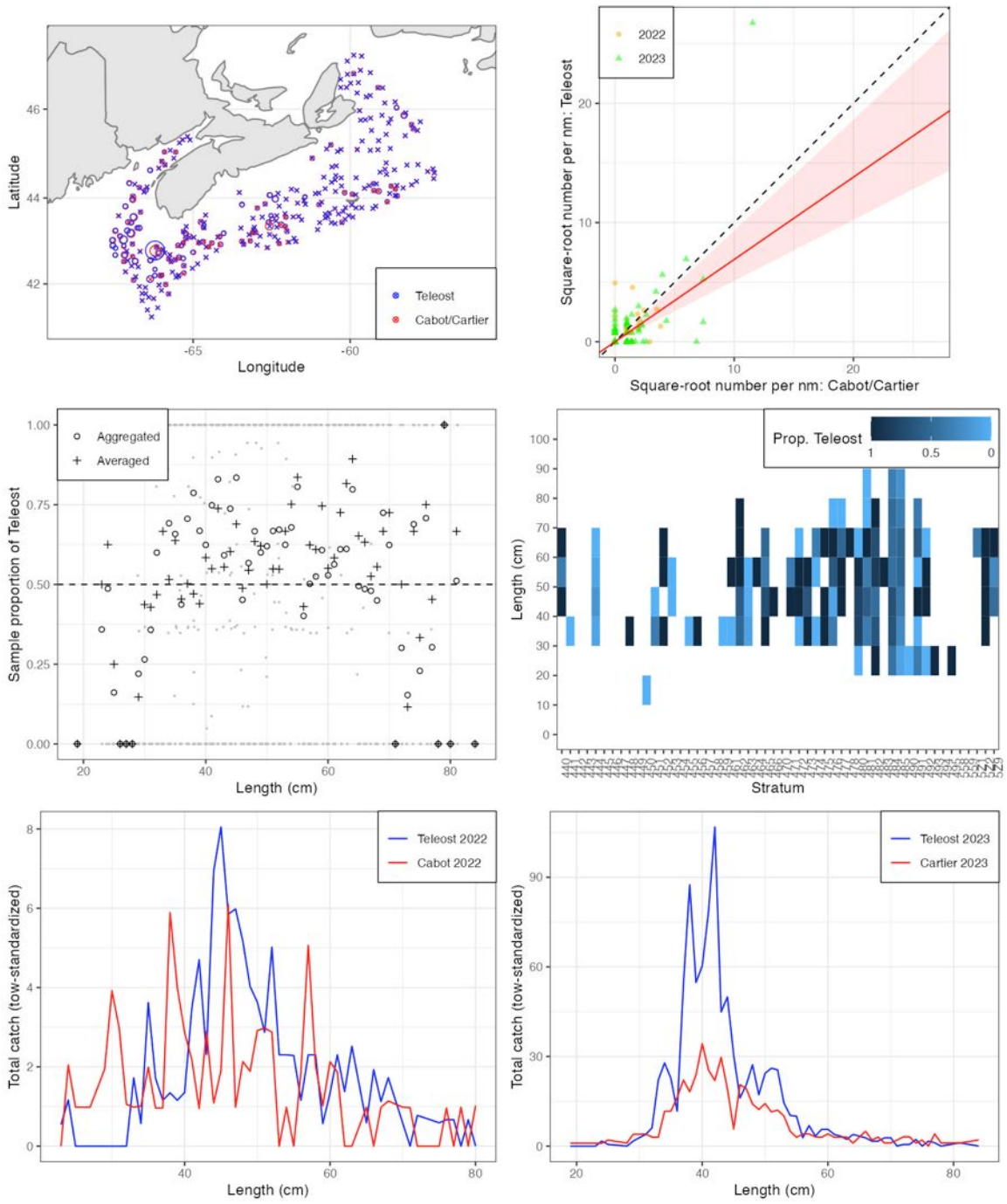

Figure 16a. Visualisation of comparative fishing data and size-aggregated model fit for Pollachius virens (16).

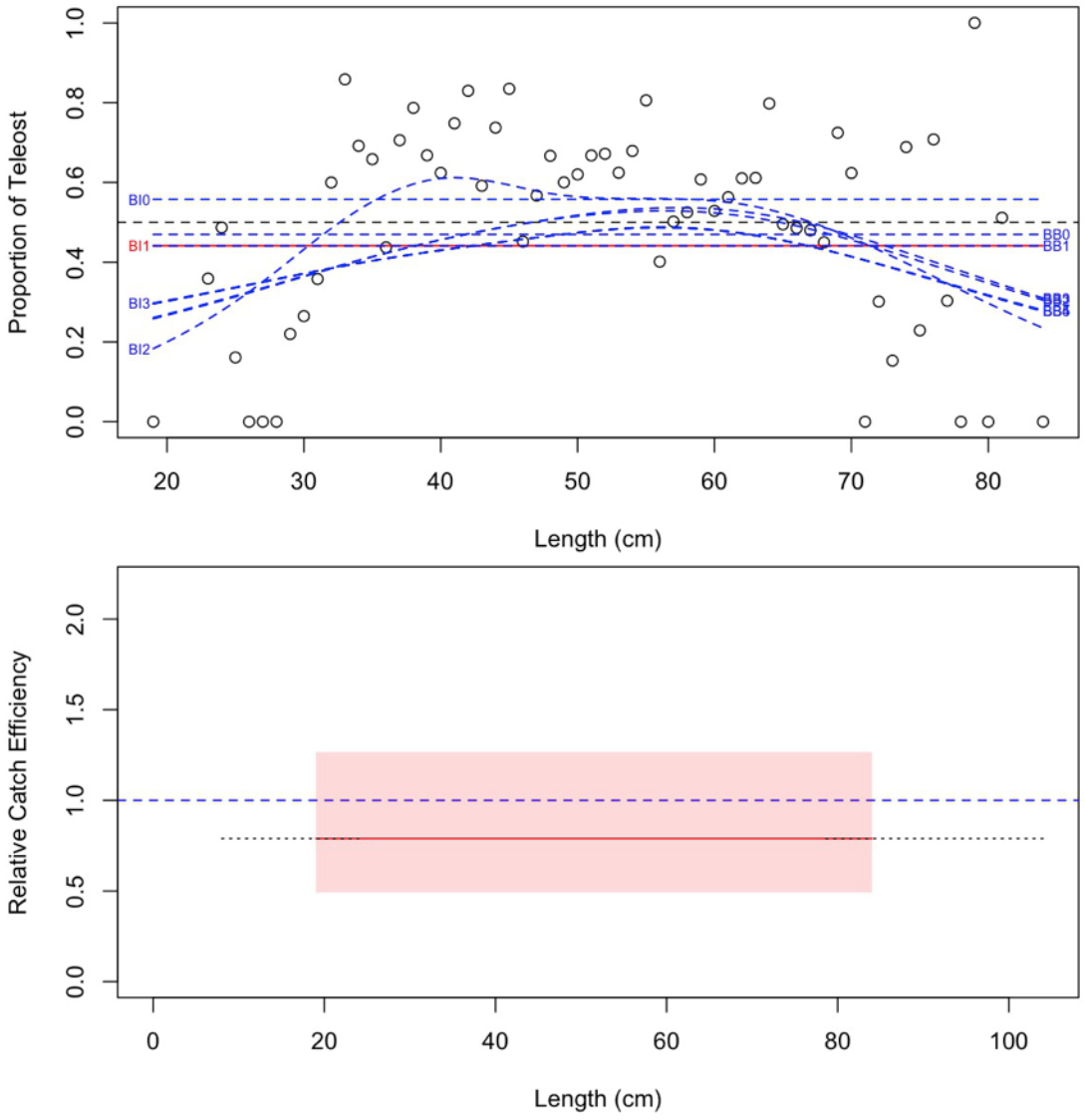

Figure 16b. Model fits and the selected length-based calibration for Pollachius virens (16).

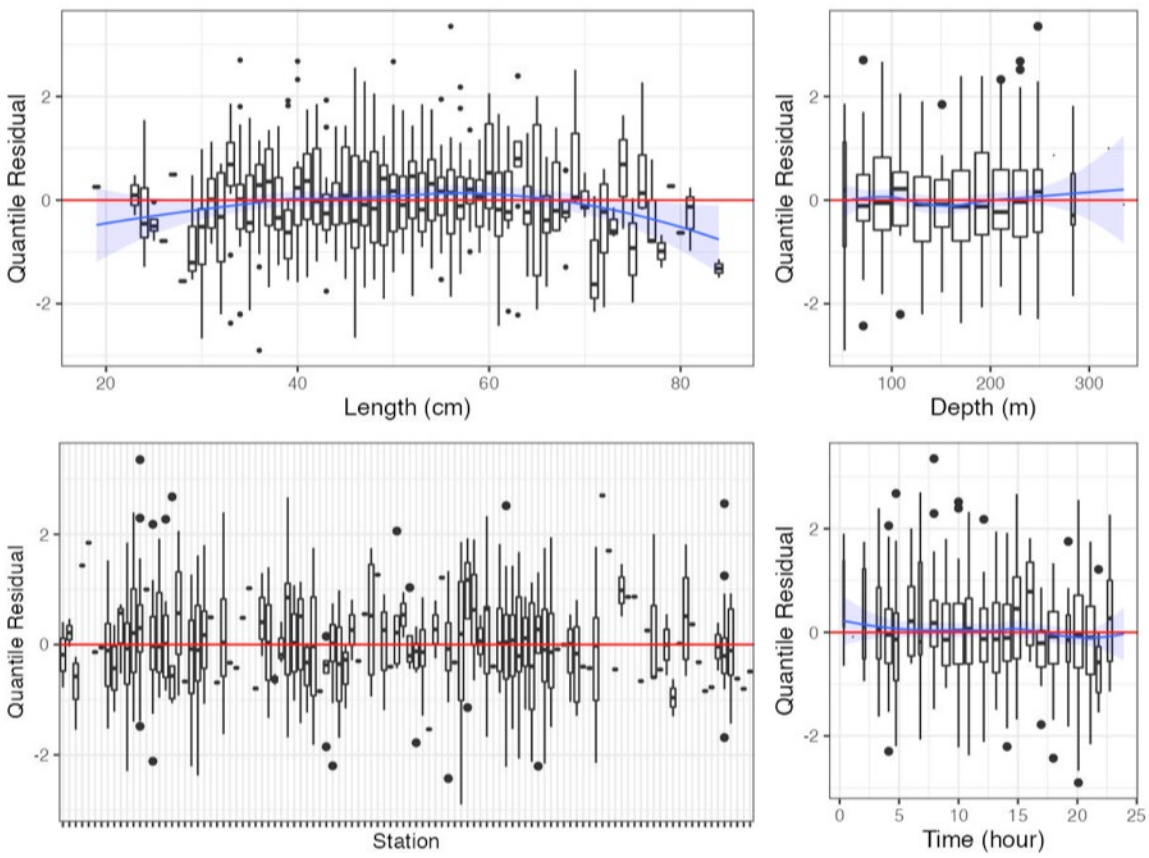

Figure 16c. Randomized and normalized quantile residuals for the selected model for Pollachius virens (16).

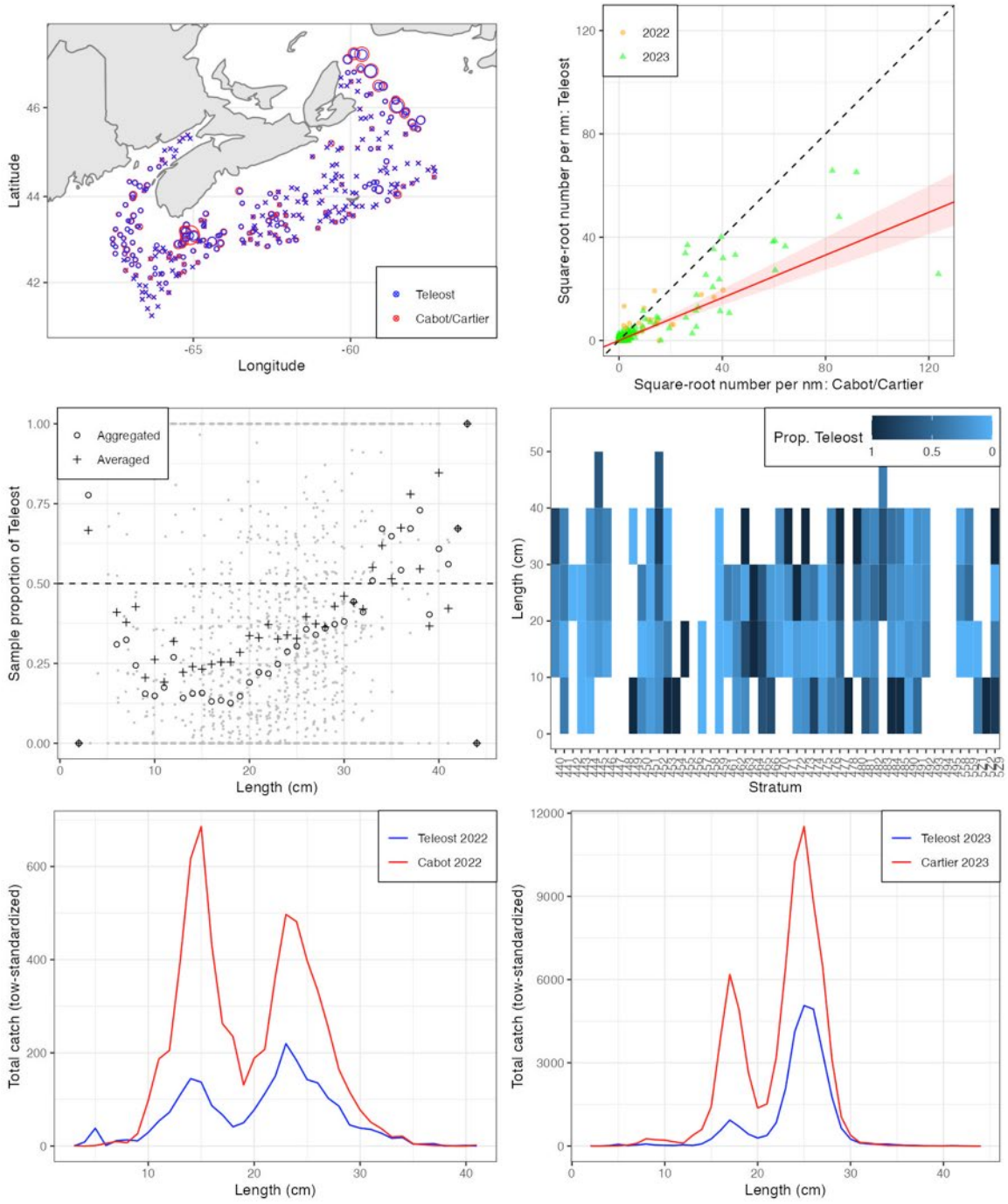

Figure 17a. Visualisation of comparative fishing data and size-aggregated model fit for Sebastes sp. (23).

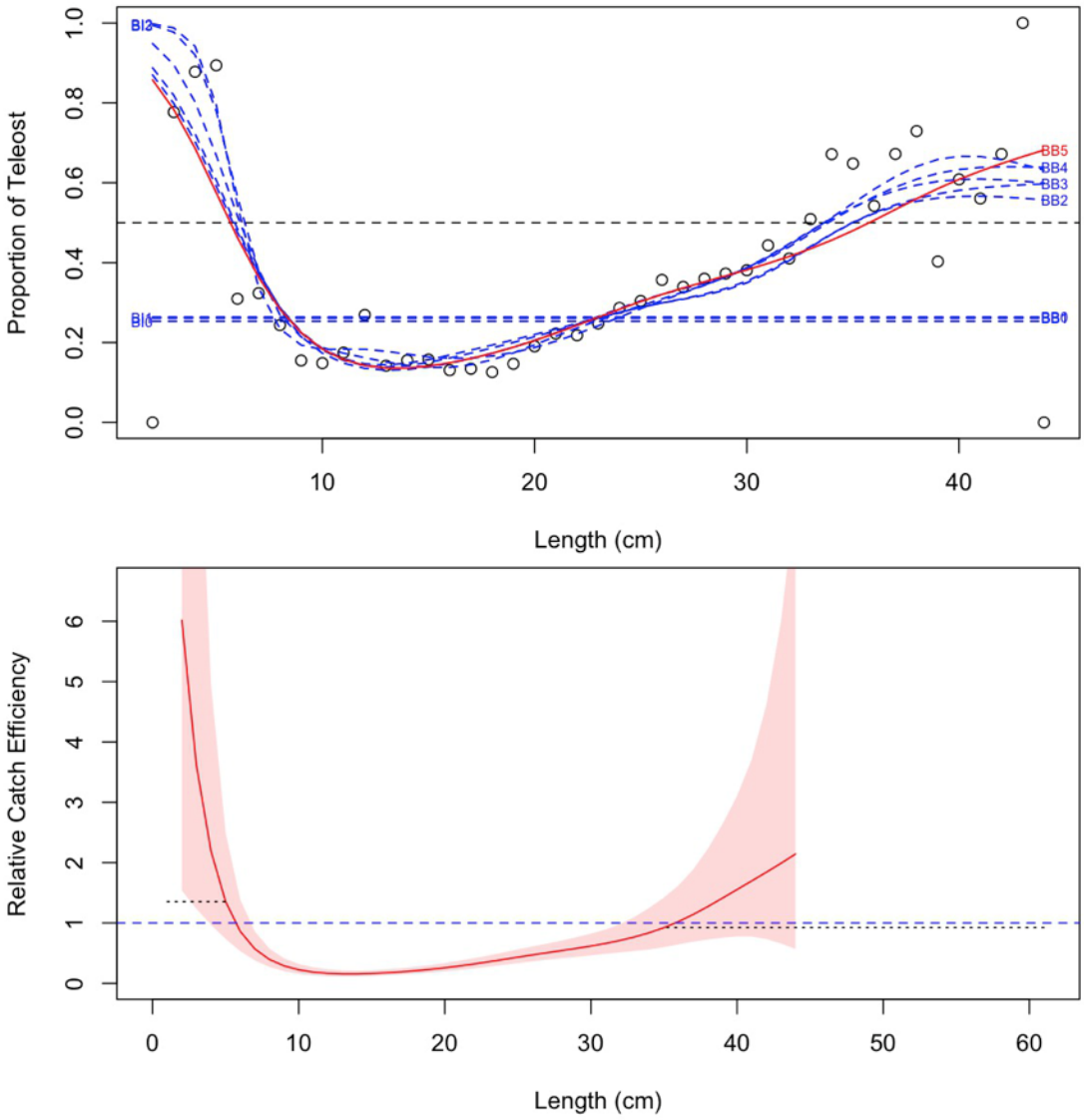

Figure 17b. Model fits and the selected length-based calibration for Sebastes sp. (23).

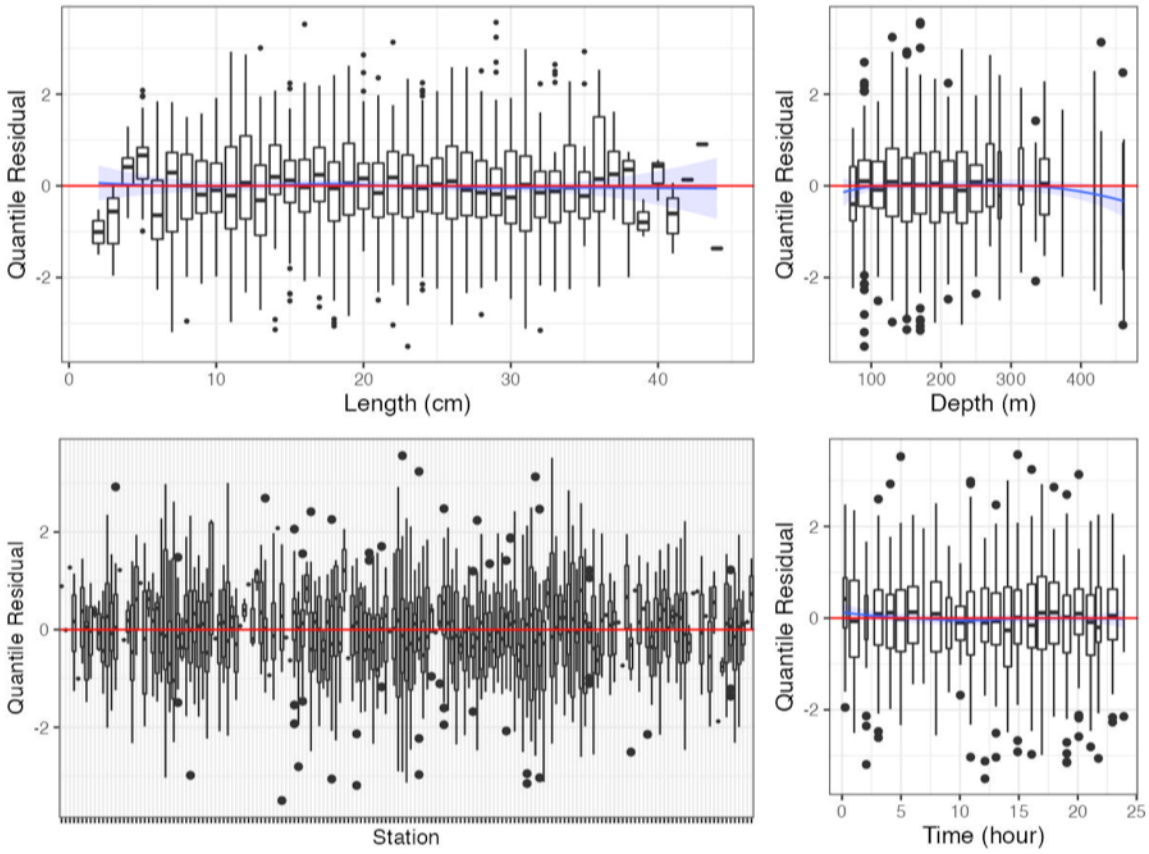

Figure 17c. Randomized and normalized quantile residuals for the selected model for Sebastes sp. (23).

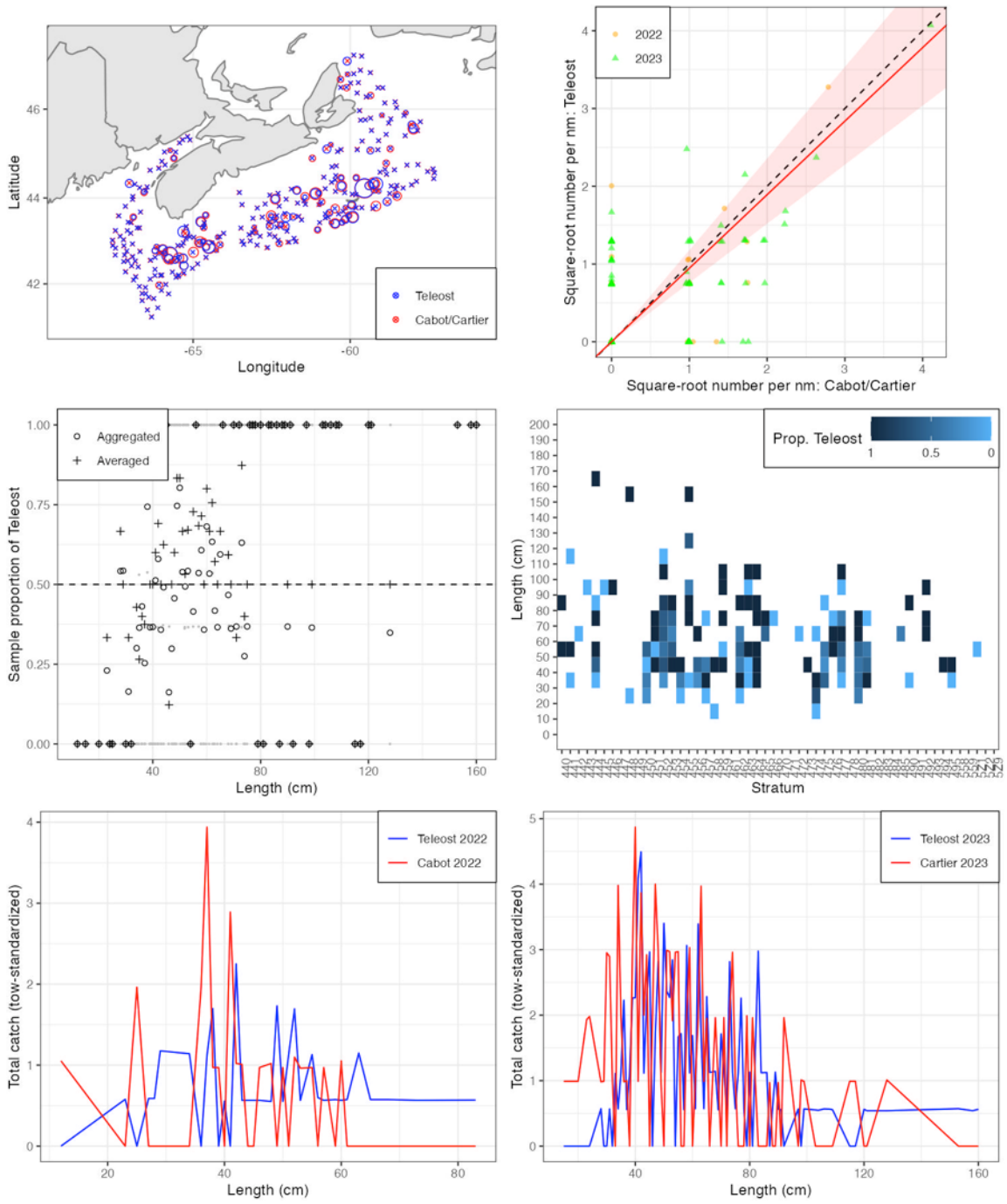

Figure 18a. Visualisation of comparative fishing data and size-aggregated model fit for Hippoglossus hippoglossus (30).

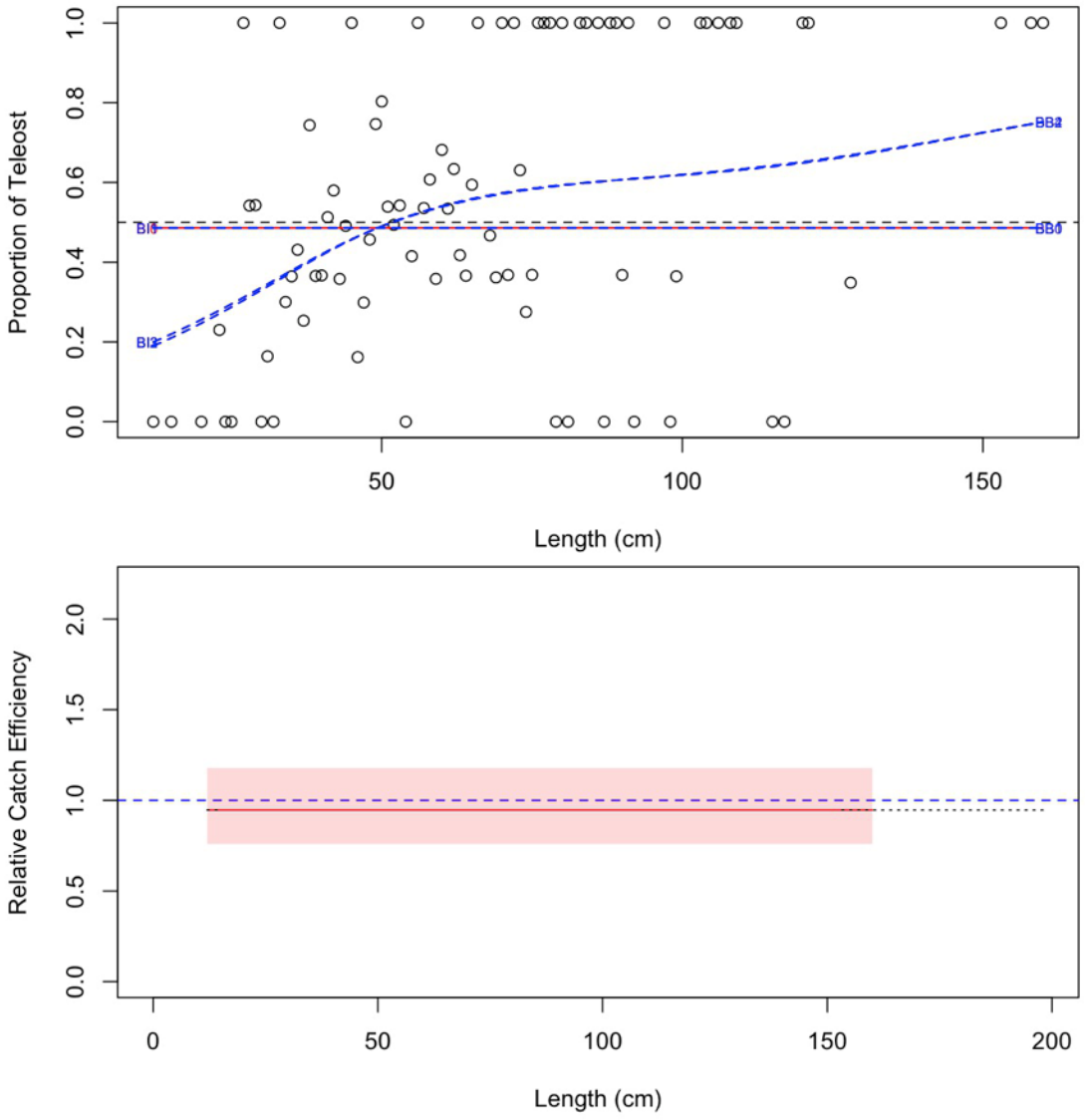

Figure 18b. Model fits and the selected length-based calibration for Hippoglossus hippoglossus (30).

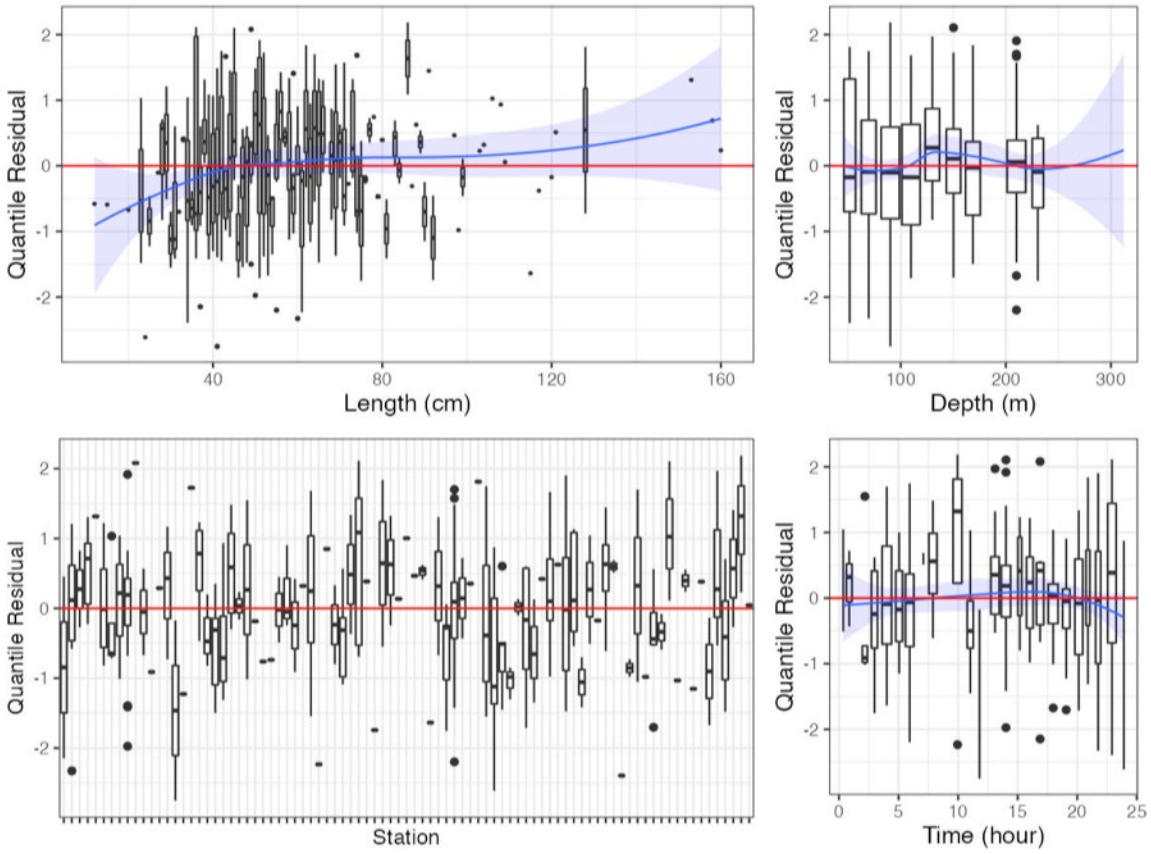

Figure 18c. Randomized and normalized quantile residuals for the selected model for Hippoglossus hippoglossus (30).

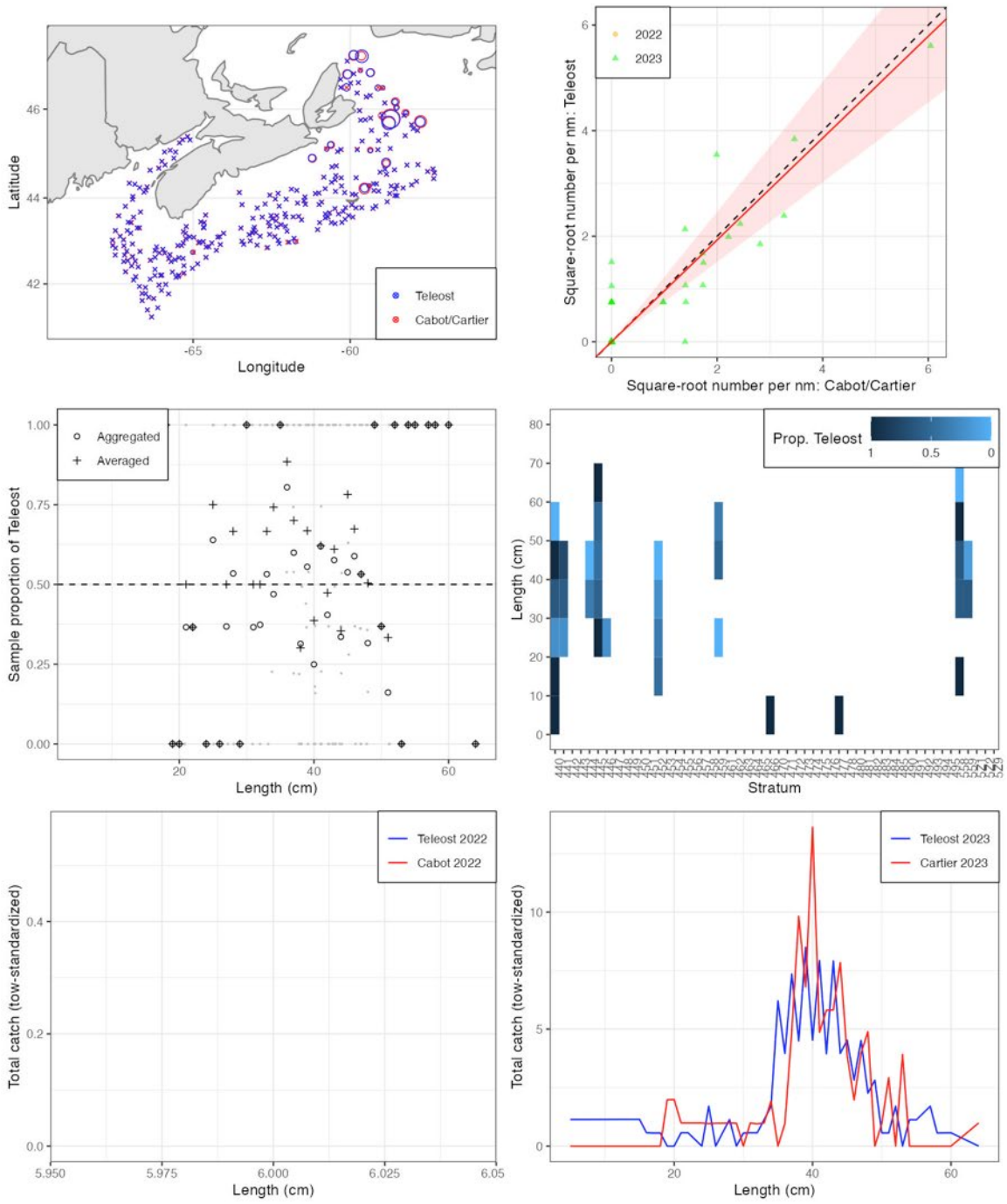

Figure 19a. Visualisation of comparative fishing data and size-aggregated model fit for Reinhardtius hippoglossoides (31).

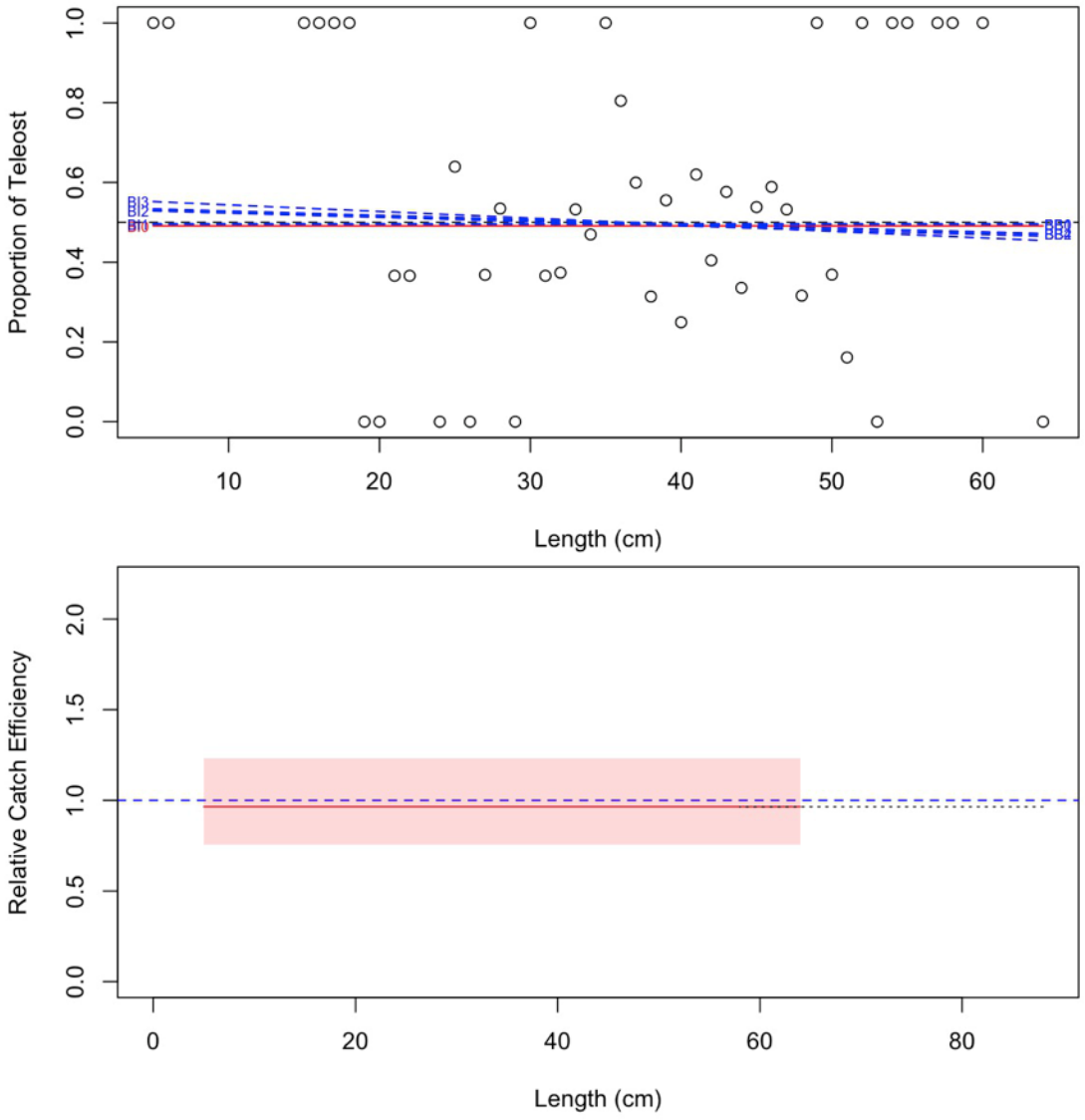

Figure 19b. Model fits and the selected length-based calibration for Reinhardtius hippoglossoides (31).

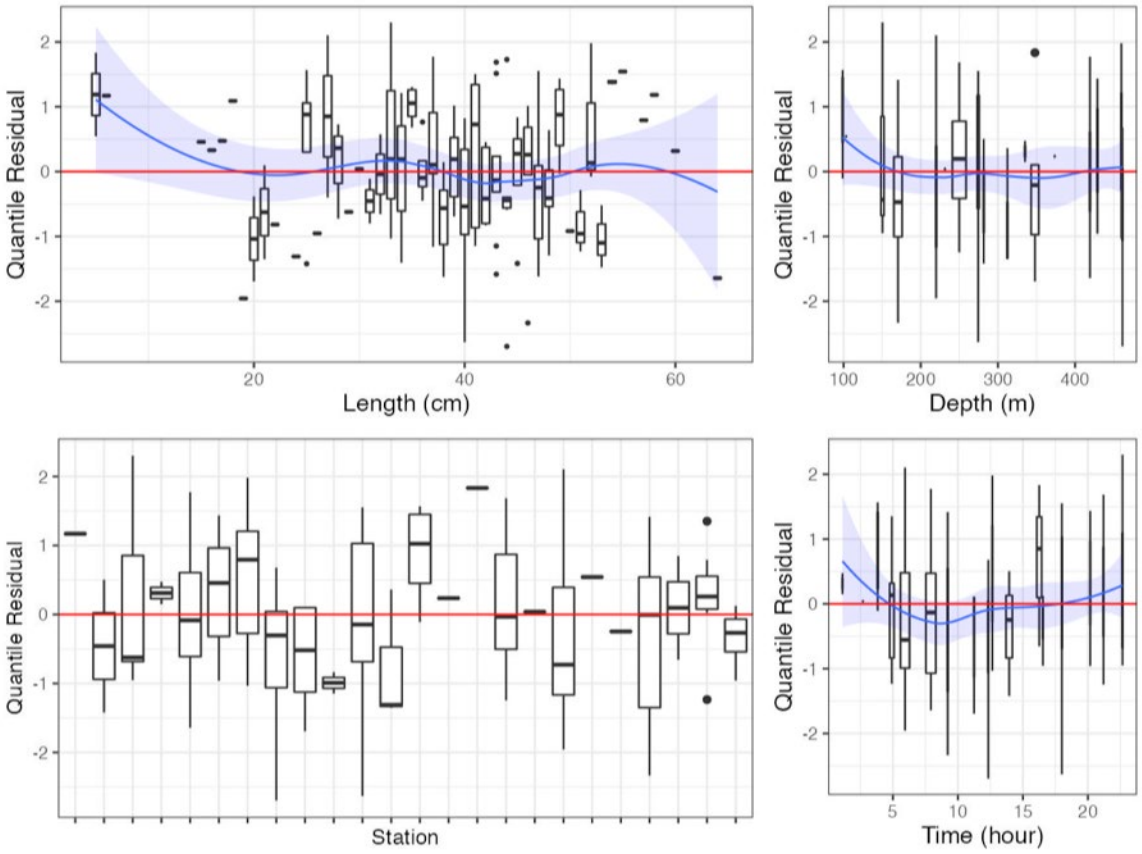

Figure 19c. Randomized and normalized quantile residuals for the selected model for Reinhardtius hippoglossoides (31).

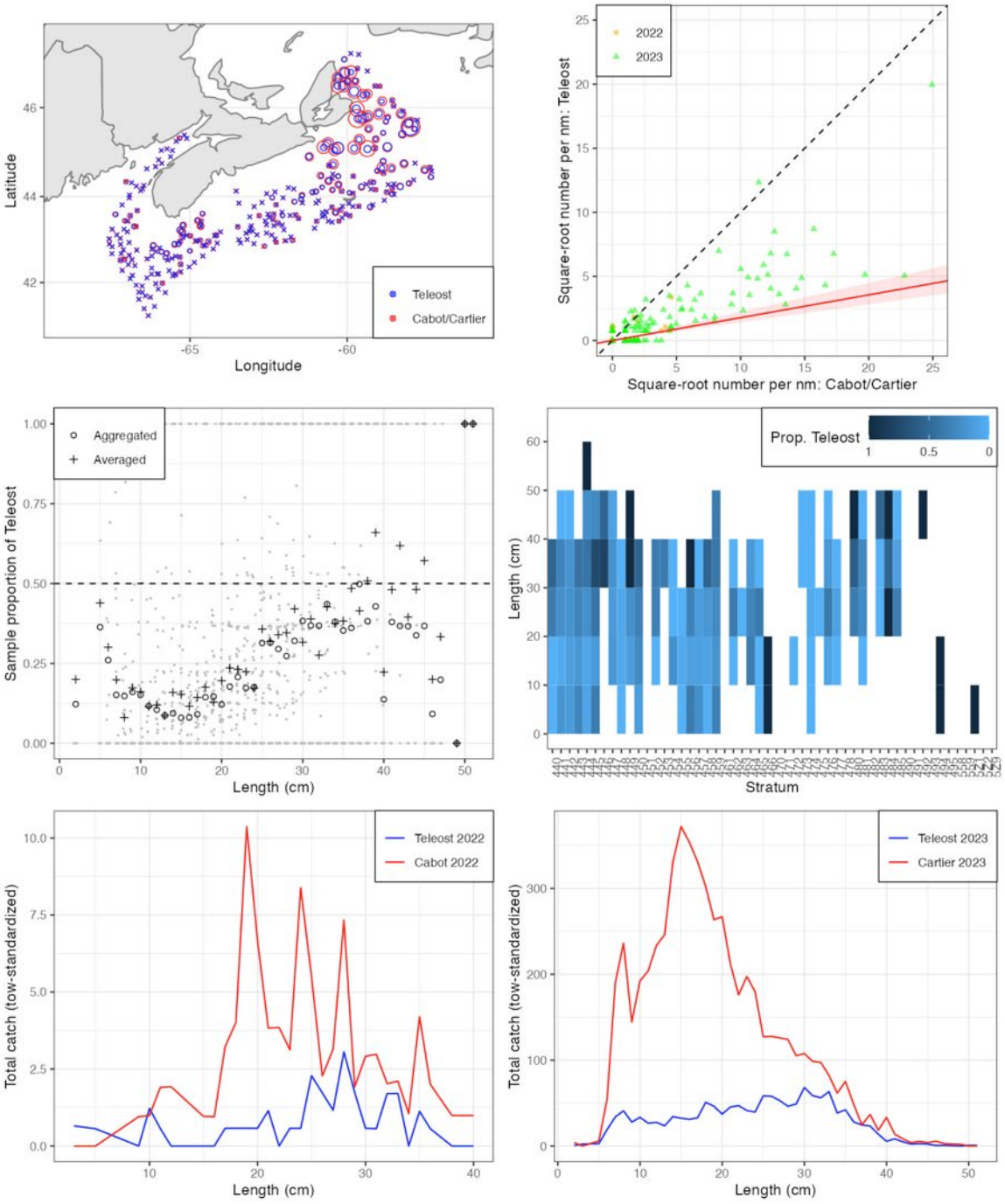

Figure 20a. Visualisation of comparative fishing data and size-aggregated model fit for Hippoglossoides platessoides (40).

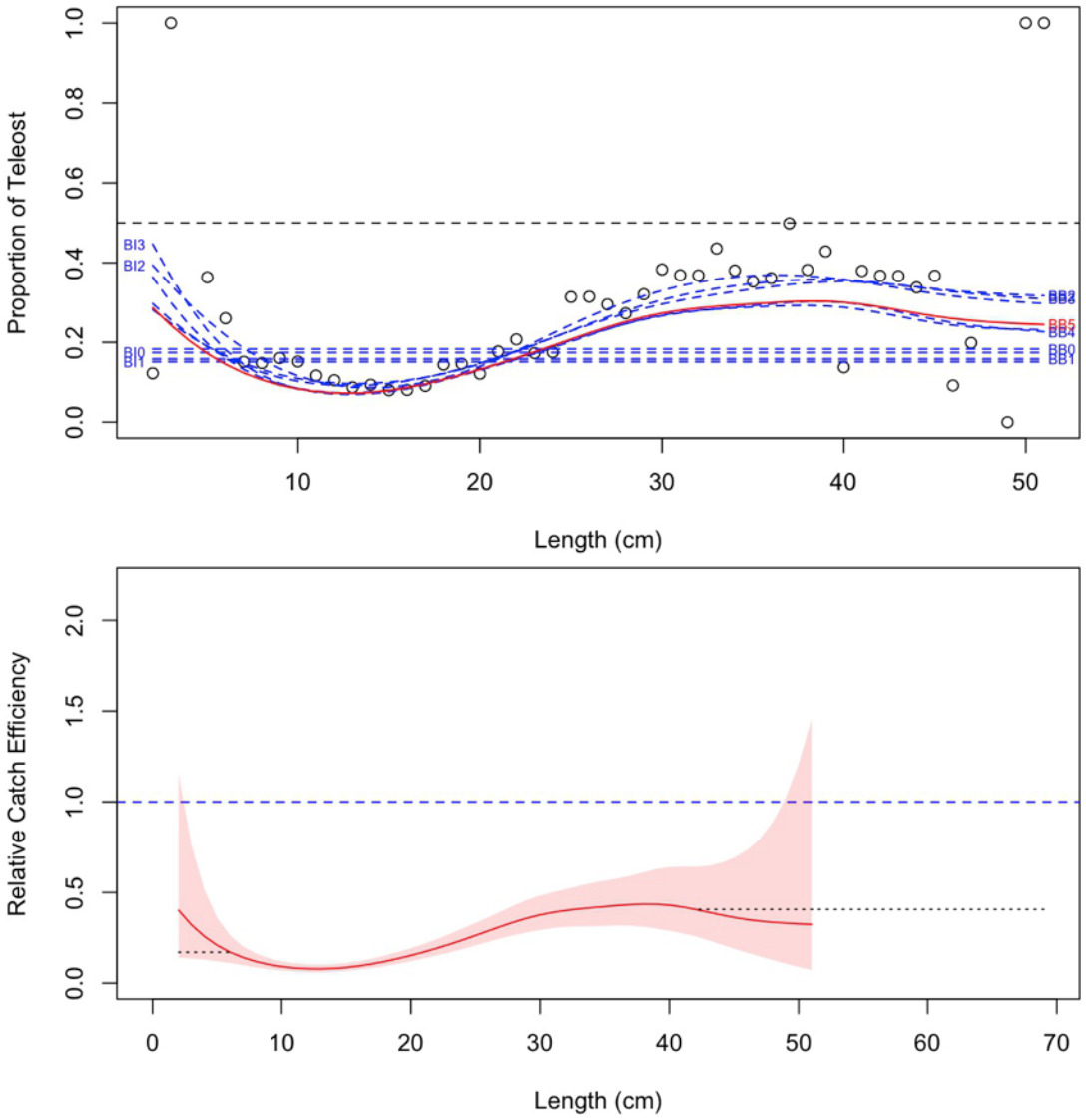

Figure 20b. Model fits and the selected length-based calibration for Hippoglossoides platessoides (40).

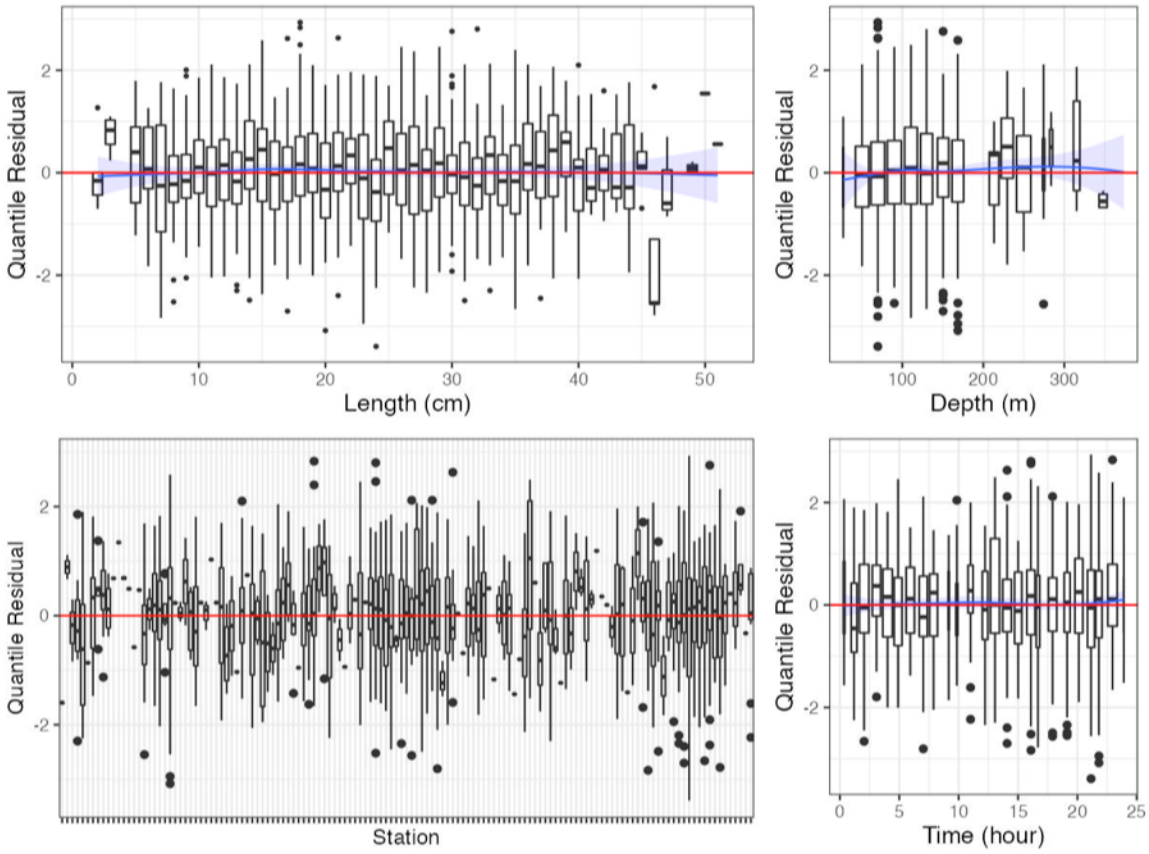

Figure 20c. Randomized and normalized quantile residuals for the selected model for Hippoglossoides platessoides (40).

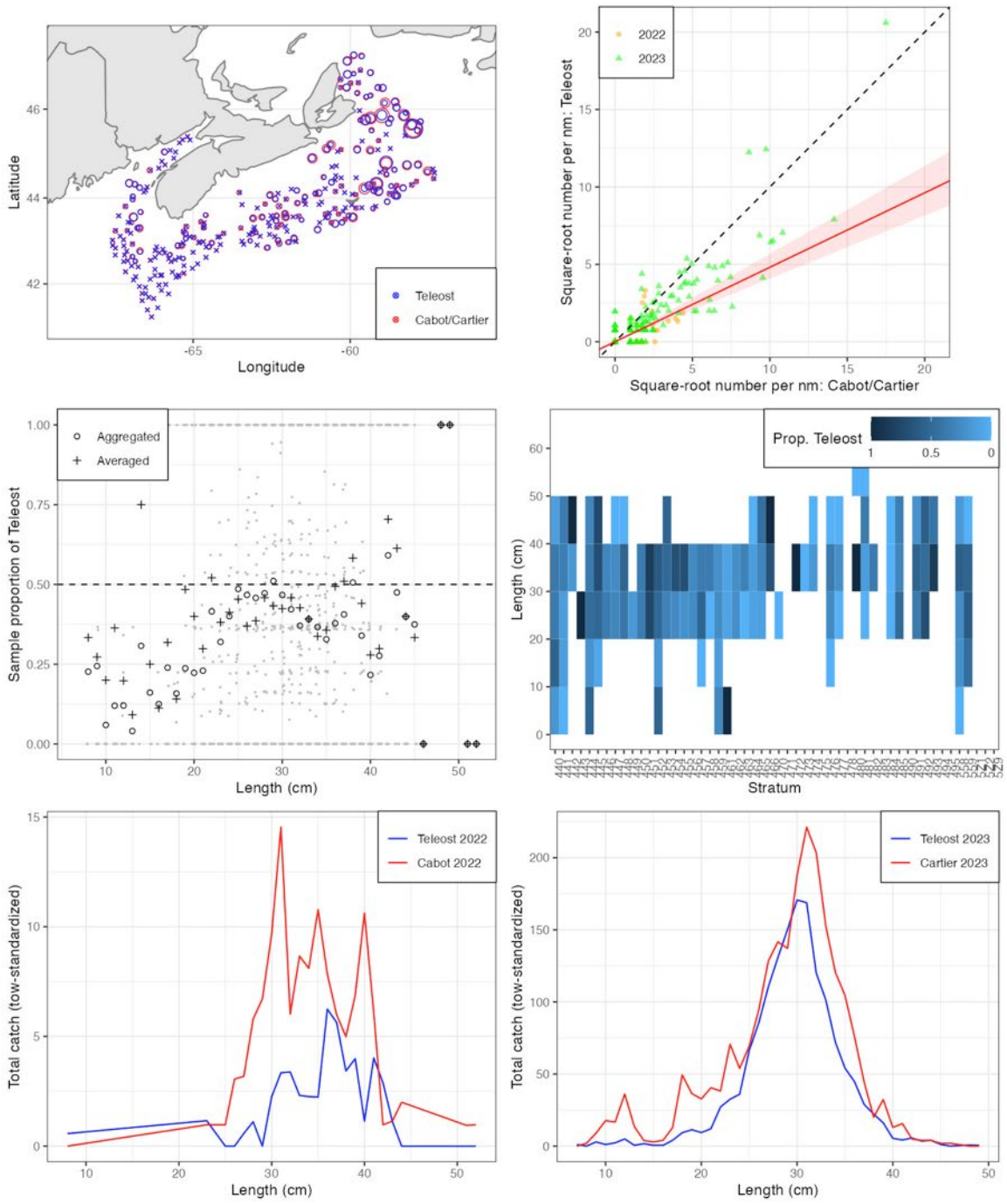

Figure 21a. Visualisation of comparative fishing data and size-aggregated model fit for Glyptocephalus cynoglossus (41).

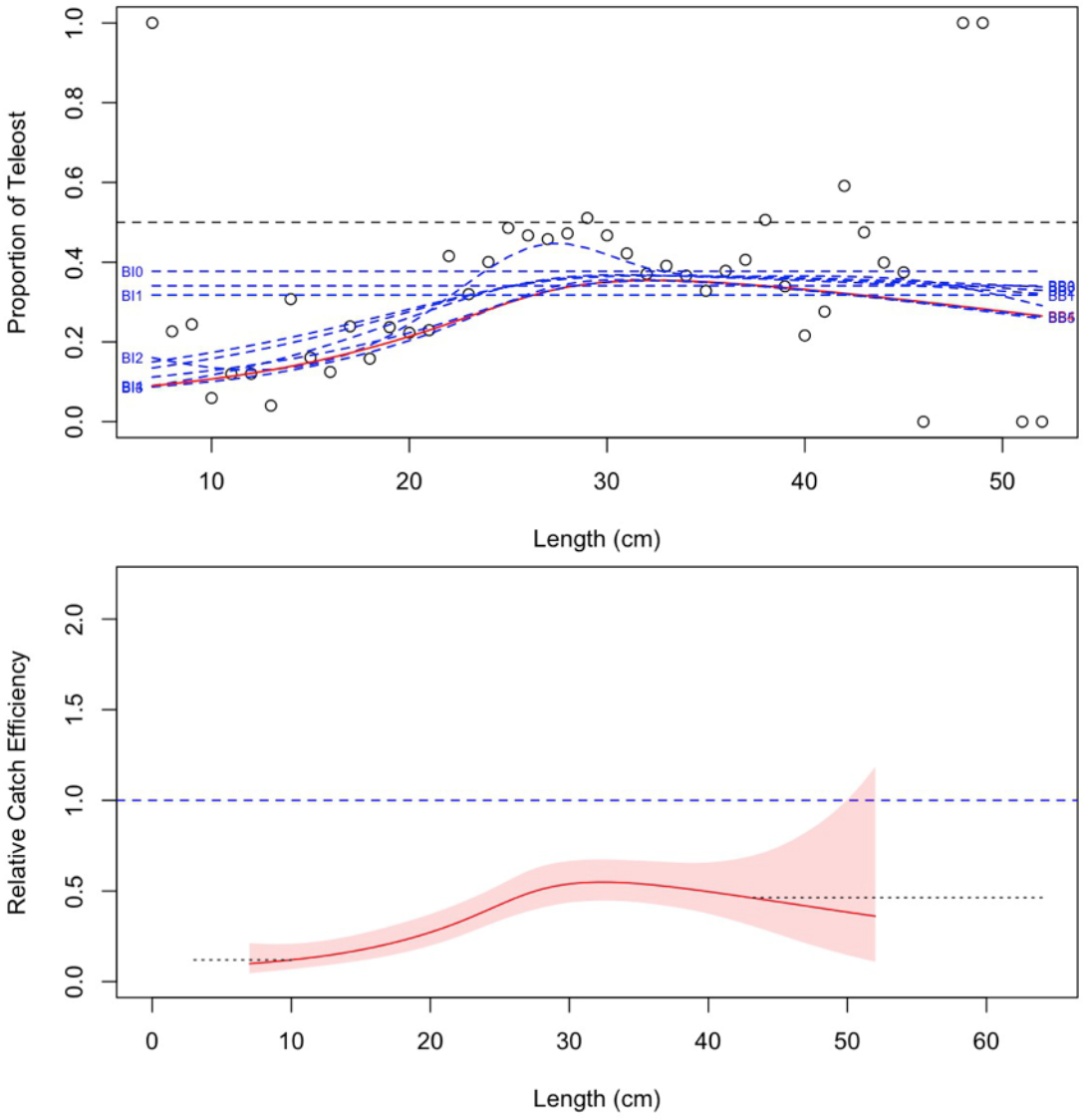

Figure 21b. Model fits and the selected length-based calibration for Glyptocephalus cynoglossus (41).

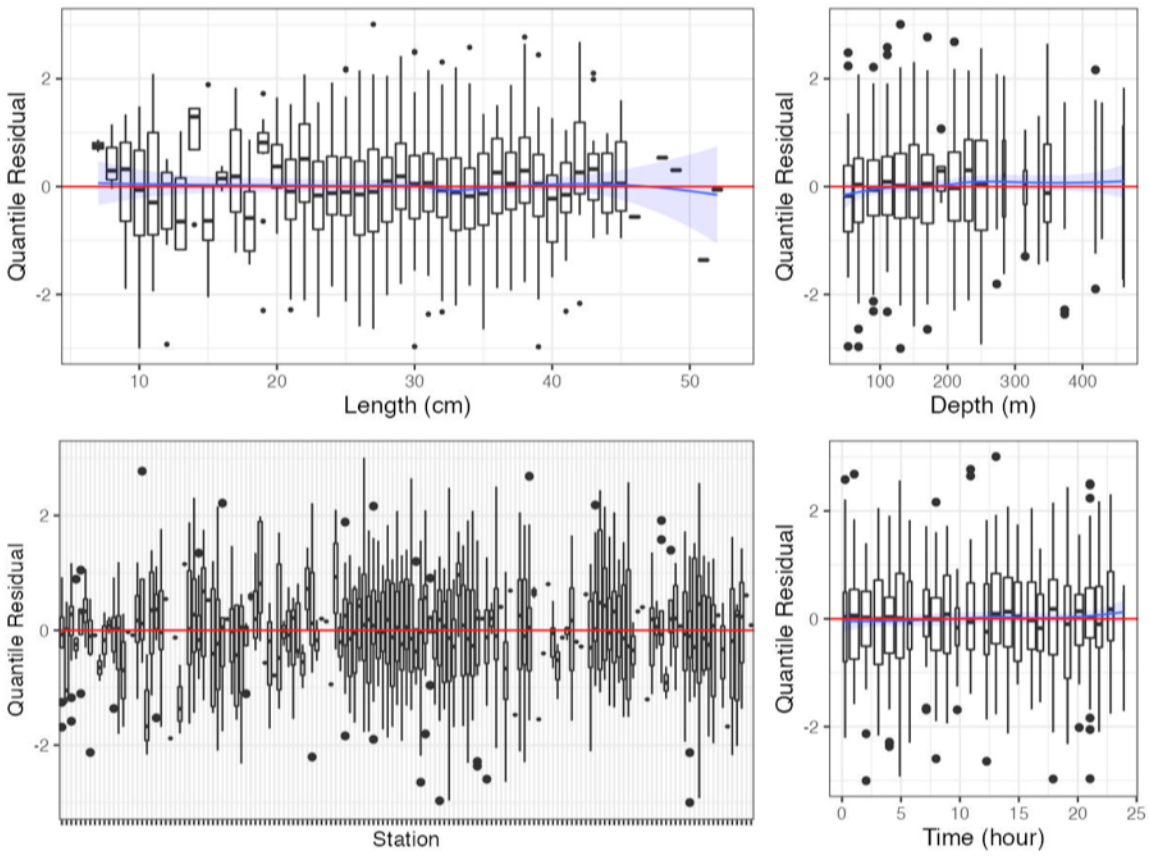

Figure 21c. Randomized and normalized quantile residuals for the selected model for Glyptocephalus cynoglossus (41).

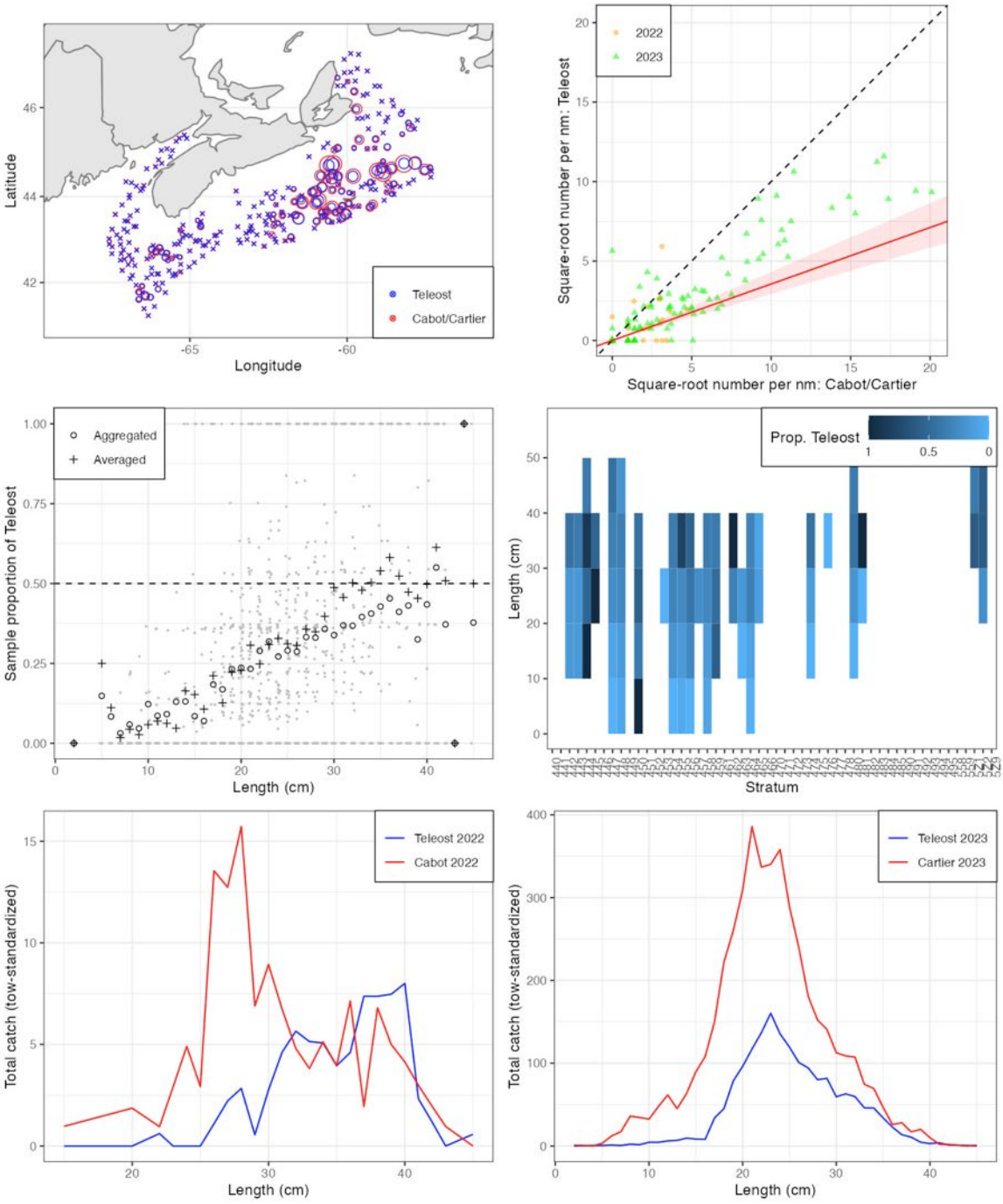

Figure 22a. Visualisation of comparative fishing data and size-aggregated model fit for Limanda ferruginea (42).

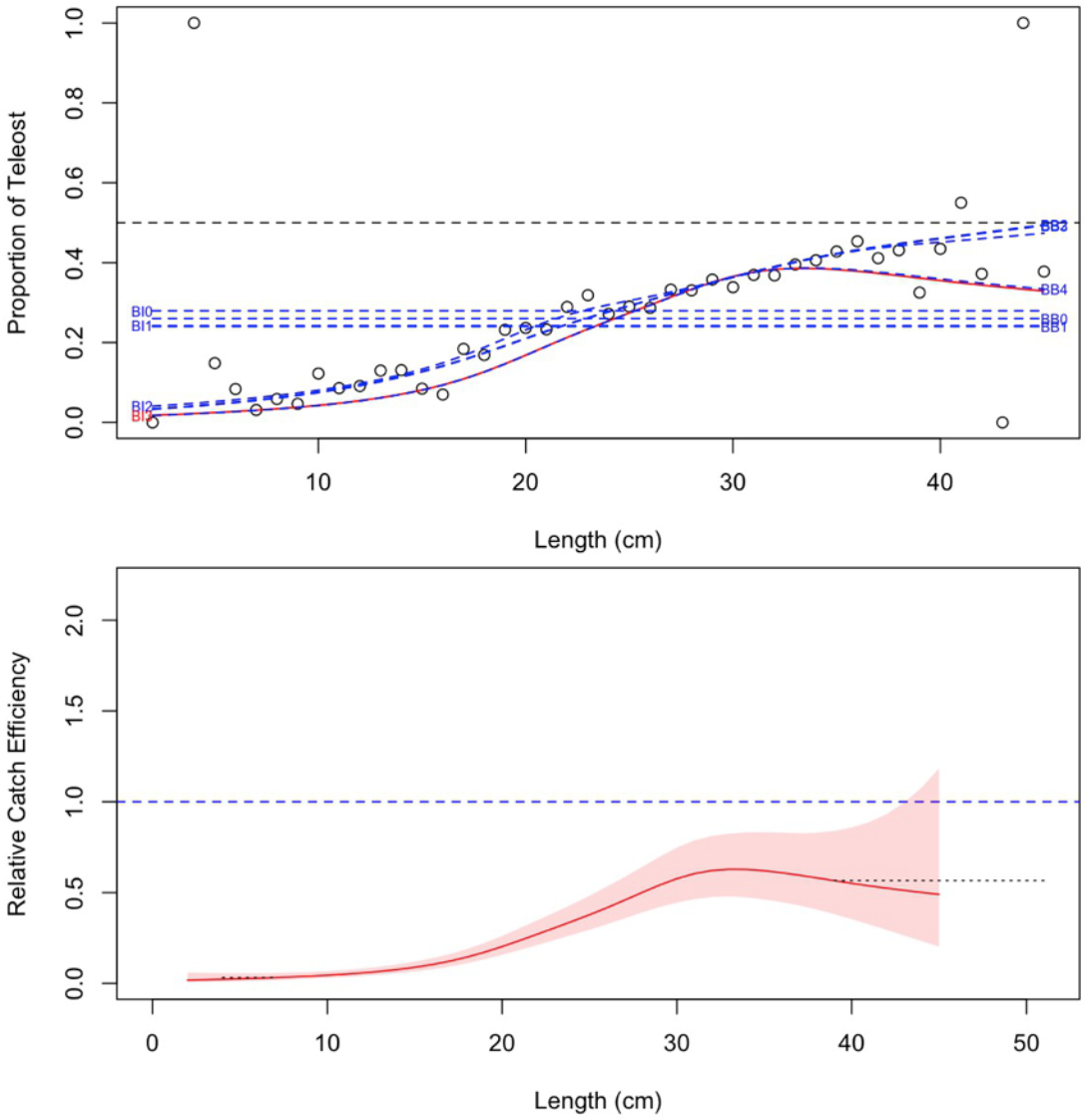

Figure 22b. Model fits and the selected length-based calibration for Limanda ferruginea (42).

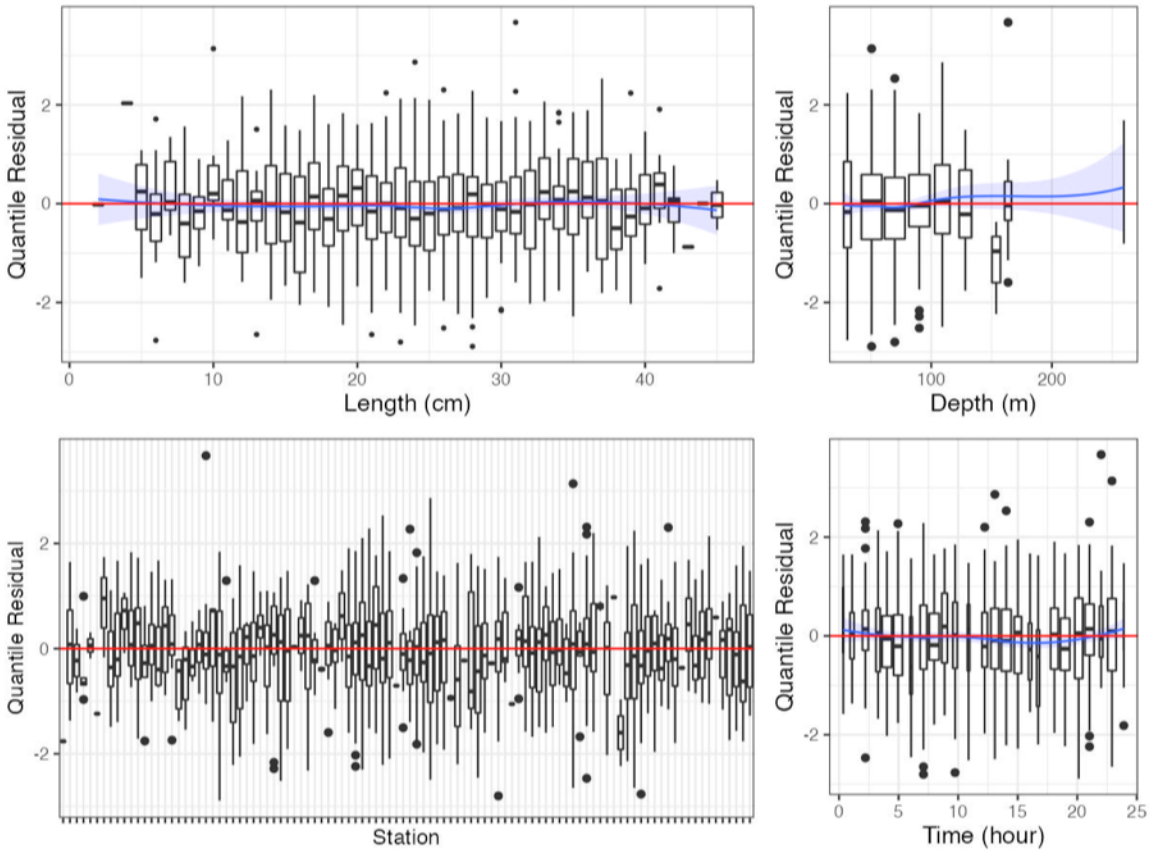

Figure 22c. Randomized and normalized quantile residuals for the selected model for Limanda ferruginea (42).

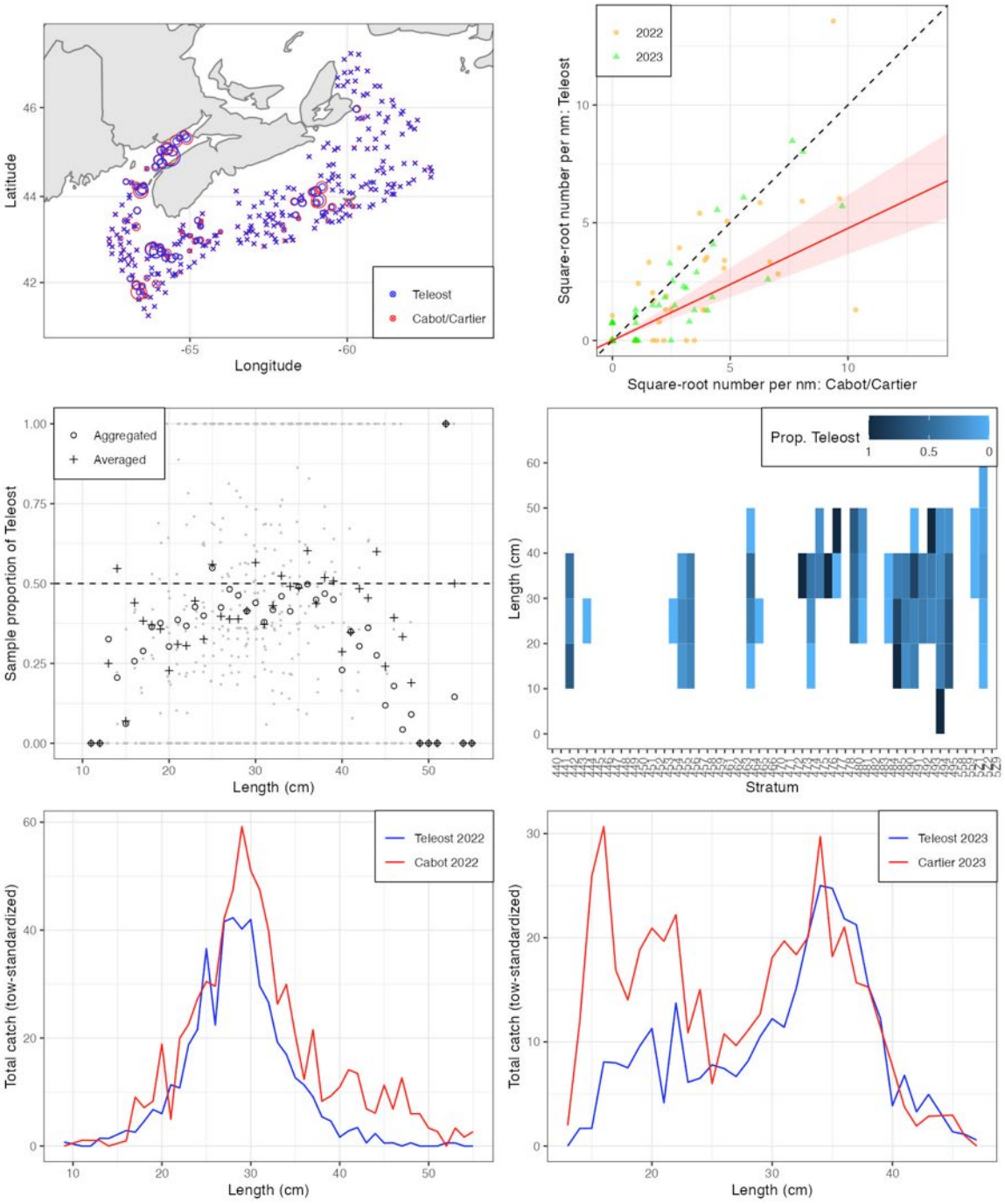

Figure 23a. Visualisation of comparative fishing data and size-aggregated model fit for Pseudopleuronectes americanus (43).

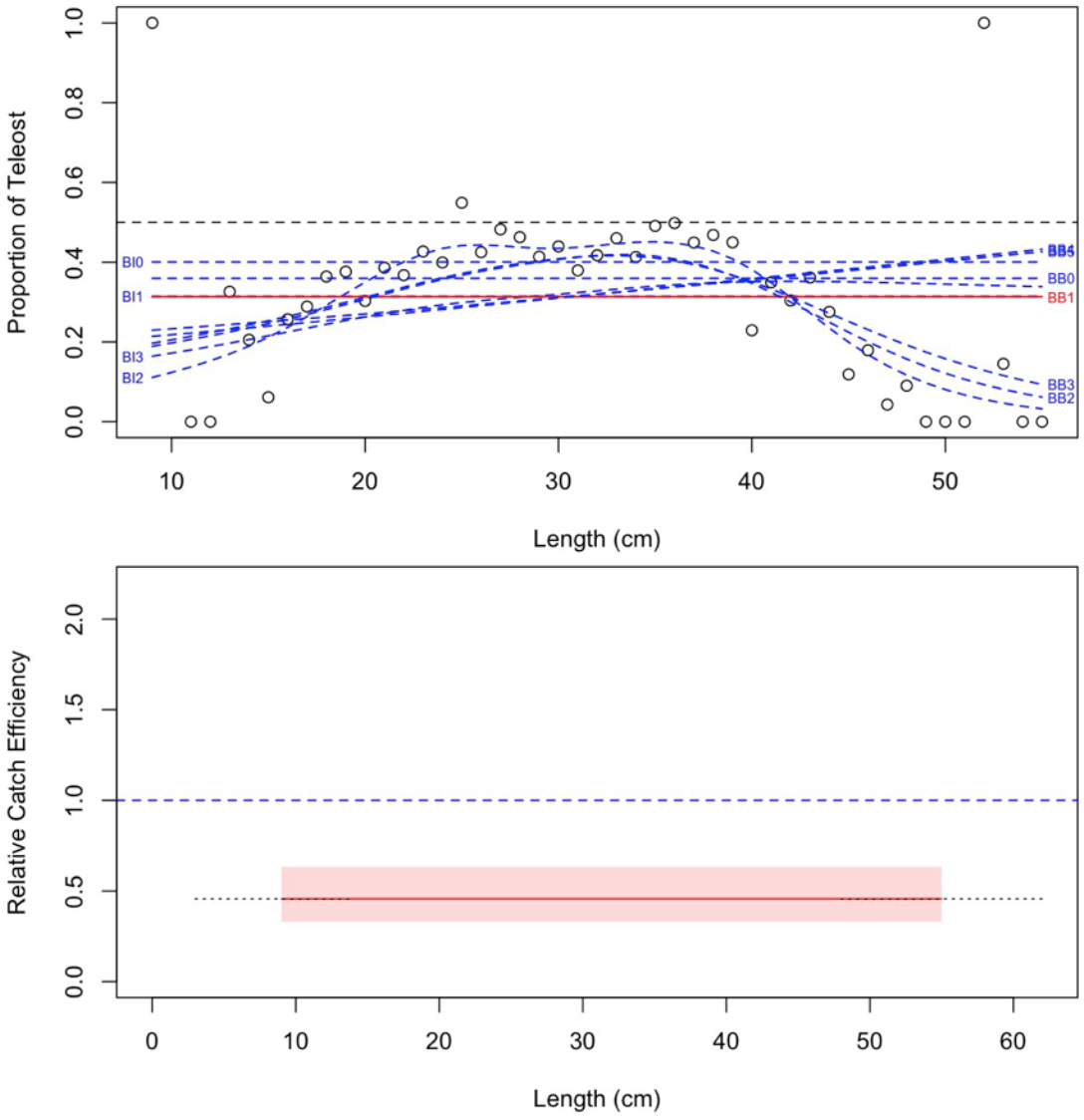

Figure 23b. Model fits and the selected length-based calibration for Pseudopleuronectes americanus (43).

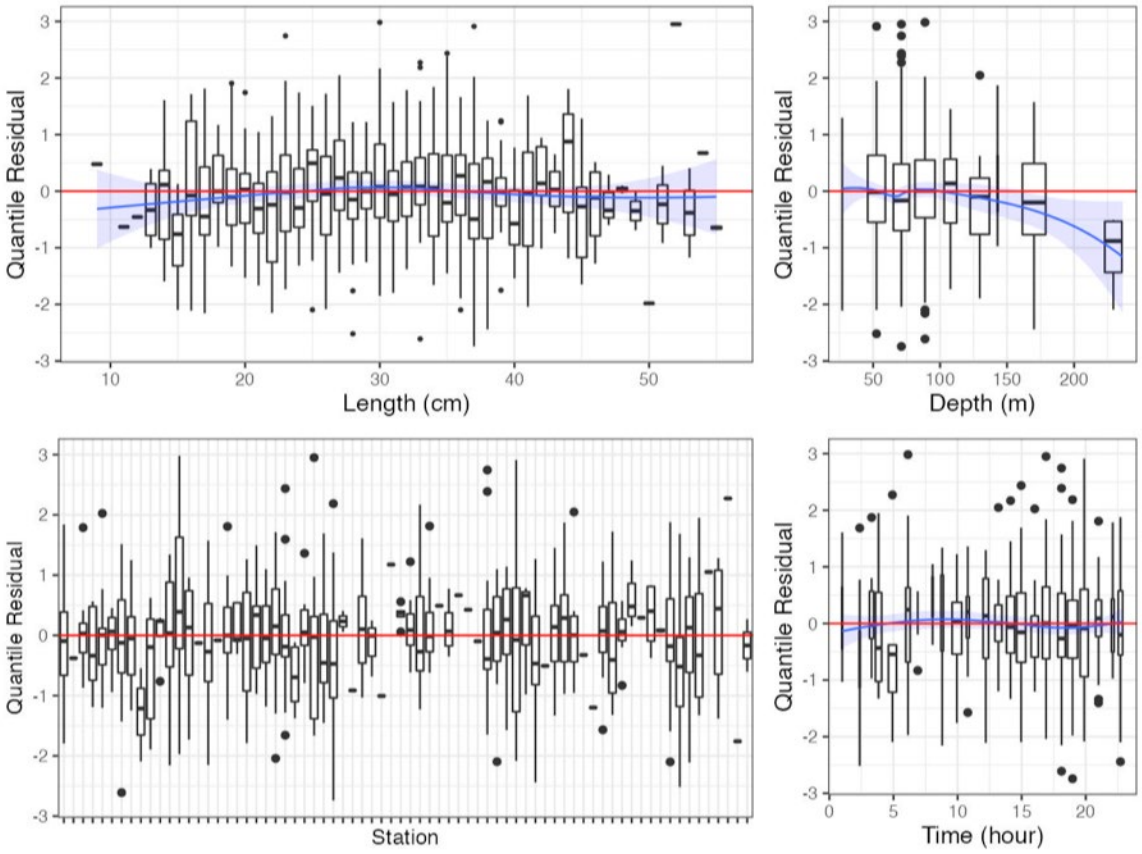

Figure 23c. Randomized and normalized quantile residuals for the selected model for Pseudopleuronectes americanus (43).

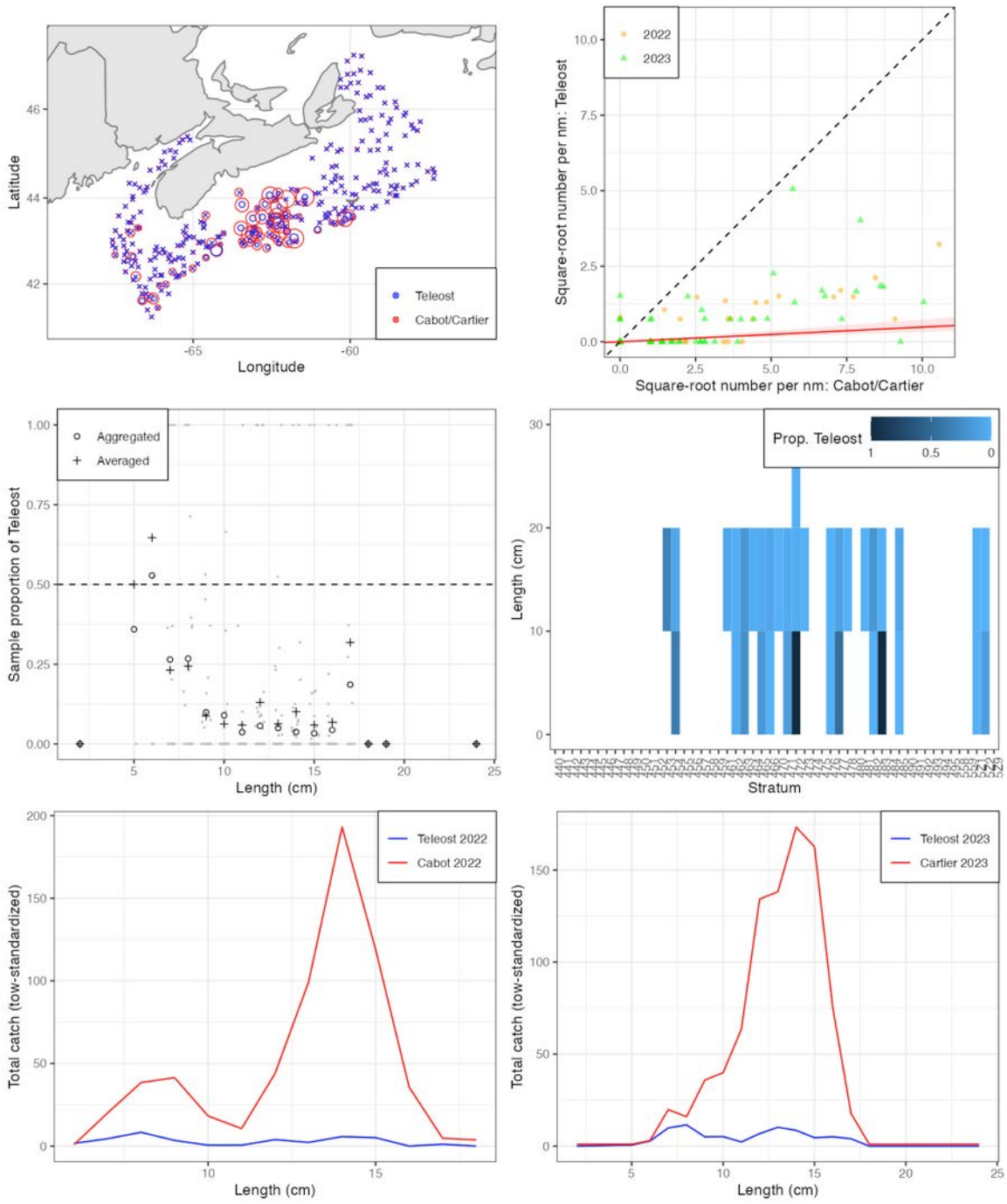

Figure 24a. Visualisation of comparative fishing data and size-aggregated model fit for Citharichthys arctifrons (44).

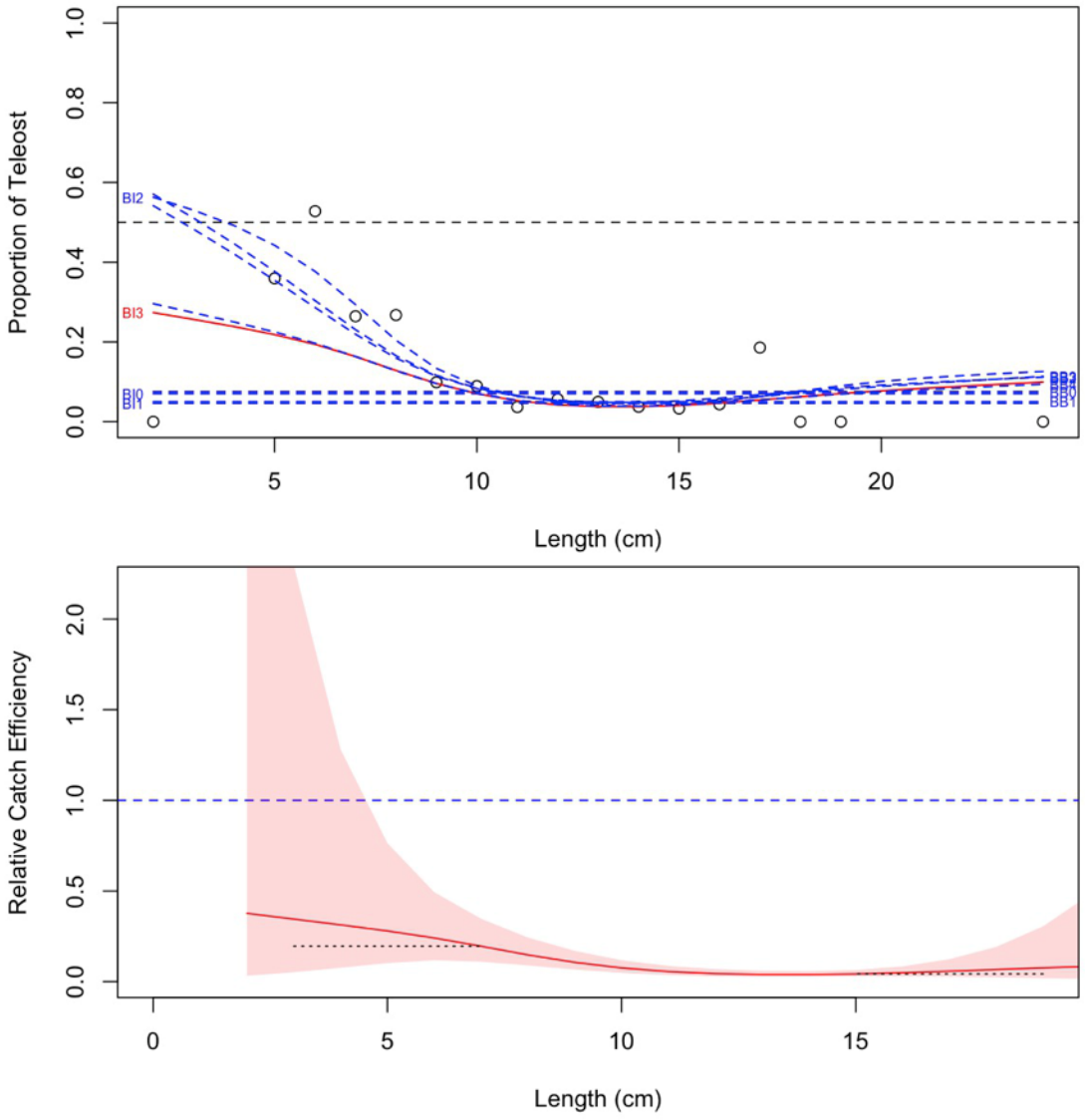

Figure 24b. Model fits and the selected length-based calibration for Citharichthys arctifrons (44).

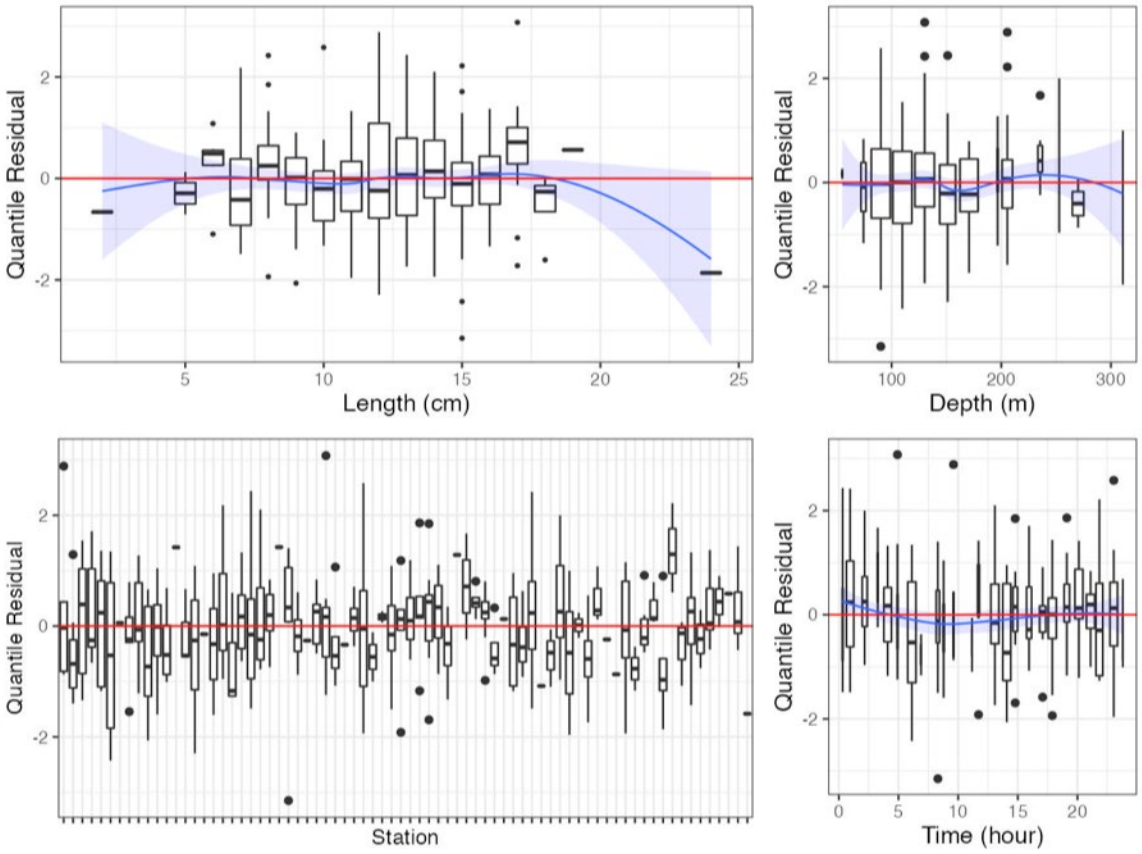

Figure 24c. Randomized and normalized quantile residuals for the selected model for Citharichthys arctifrons (44).

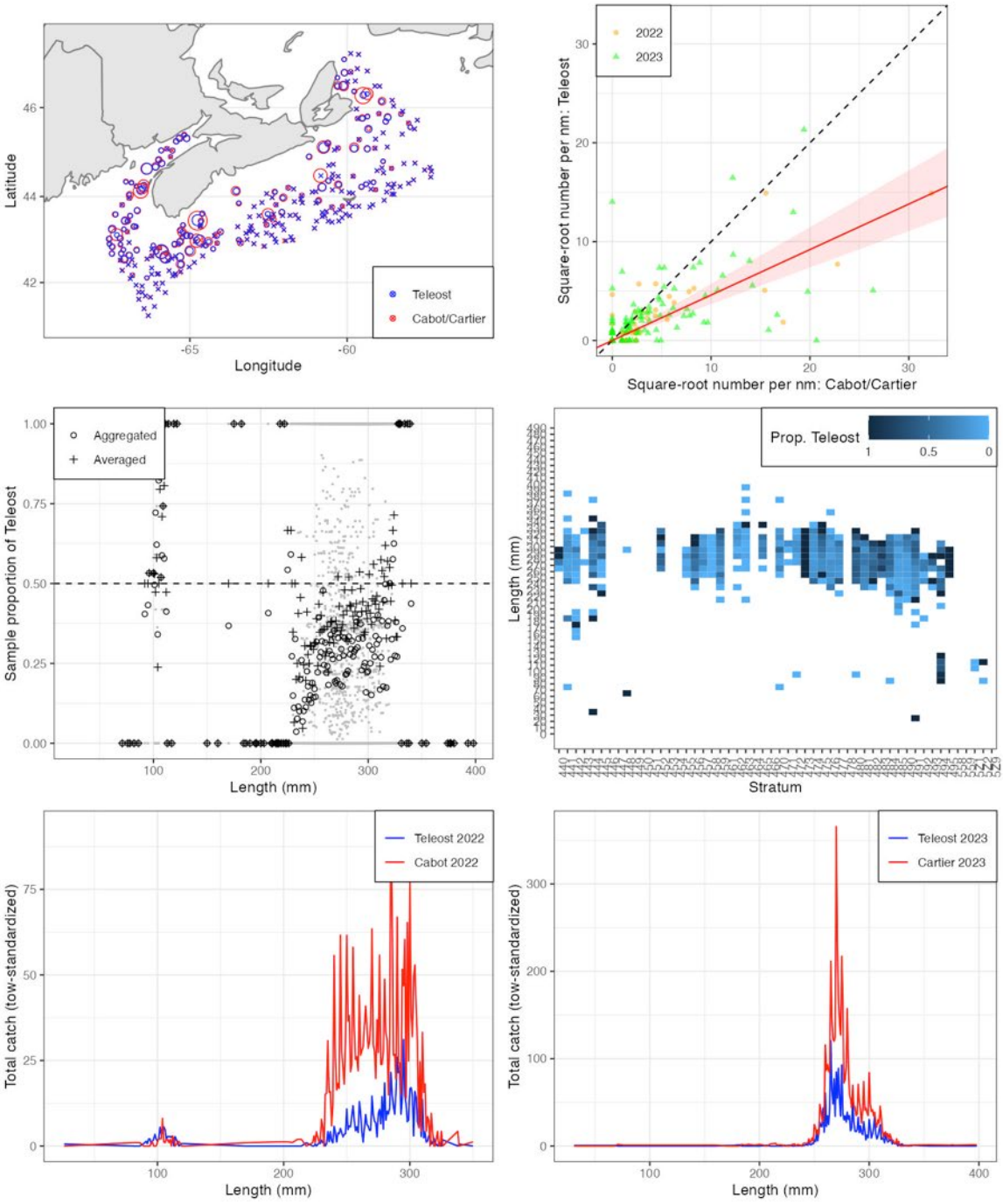

Figure 25a. Visualisation of comparative fishing data and size-aggregated model fit for Clupea harengus (60).

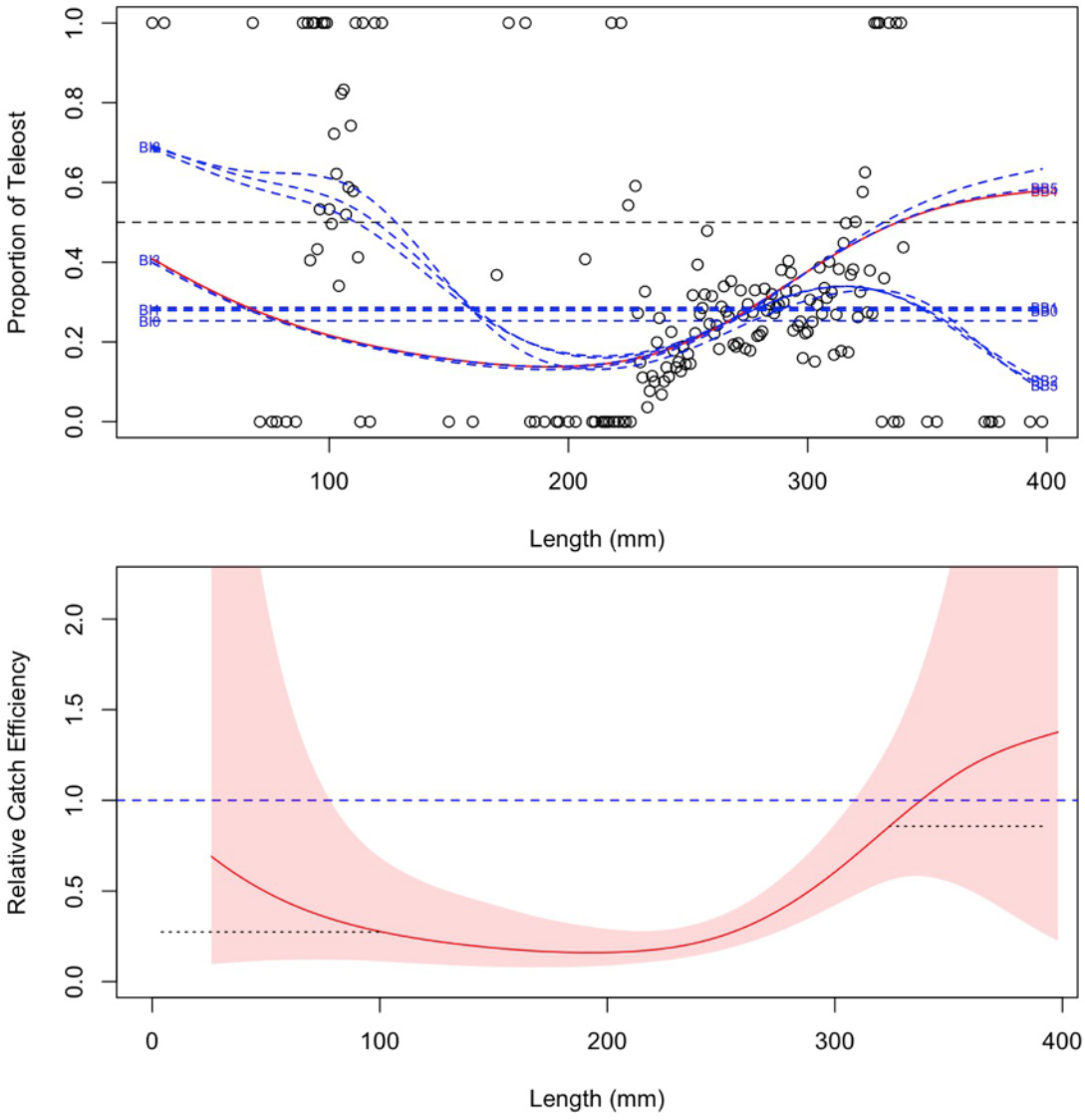

Figure 25b. Model fits and the selected length-based calibration for Clupea harengus (60).

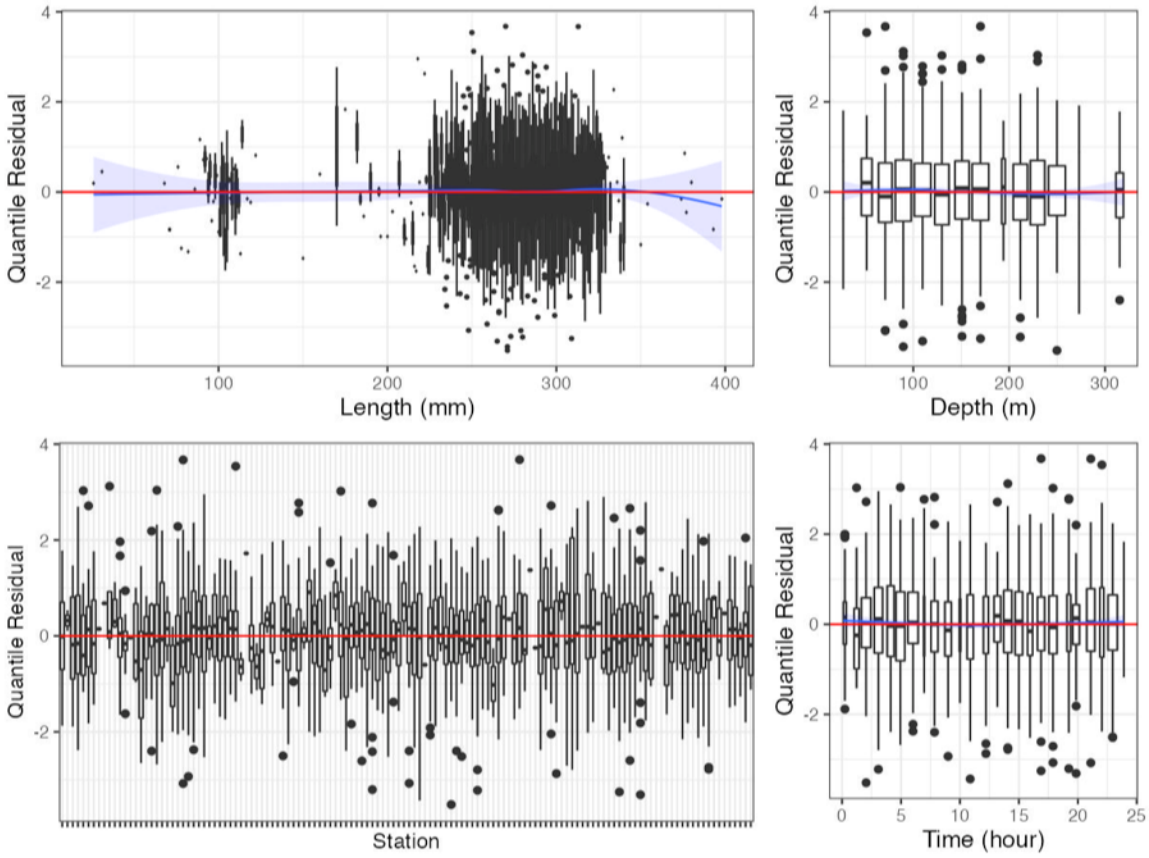

Figure 25c. Randomized and normalized quantile residuals for the selected model for Clupea harengus (60).

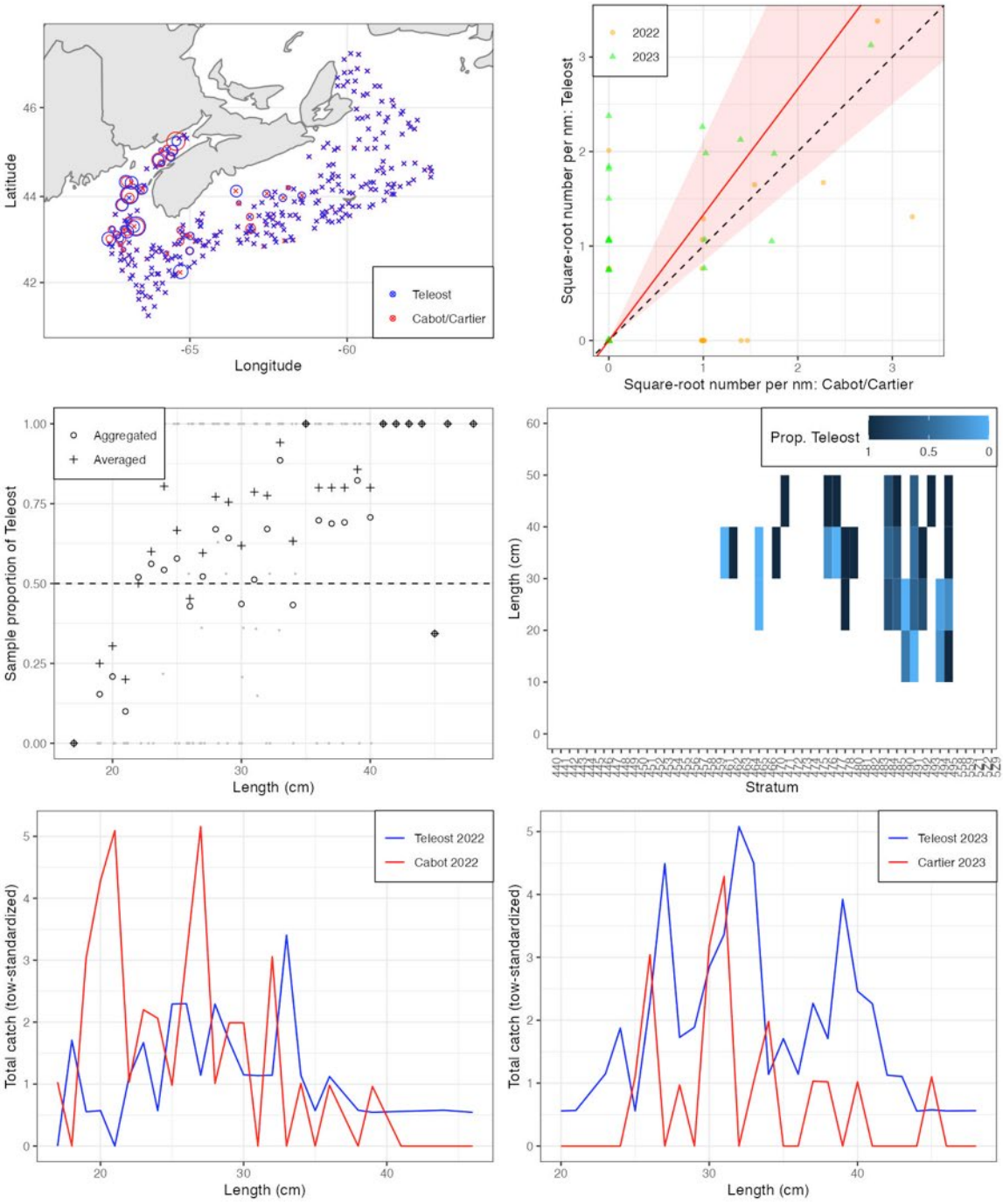

Figure 26a. Visualisation of comparative fishing data and size-aggregated model fit for Alosa sapidissima (61).

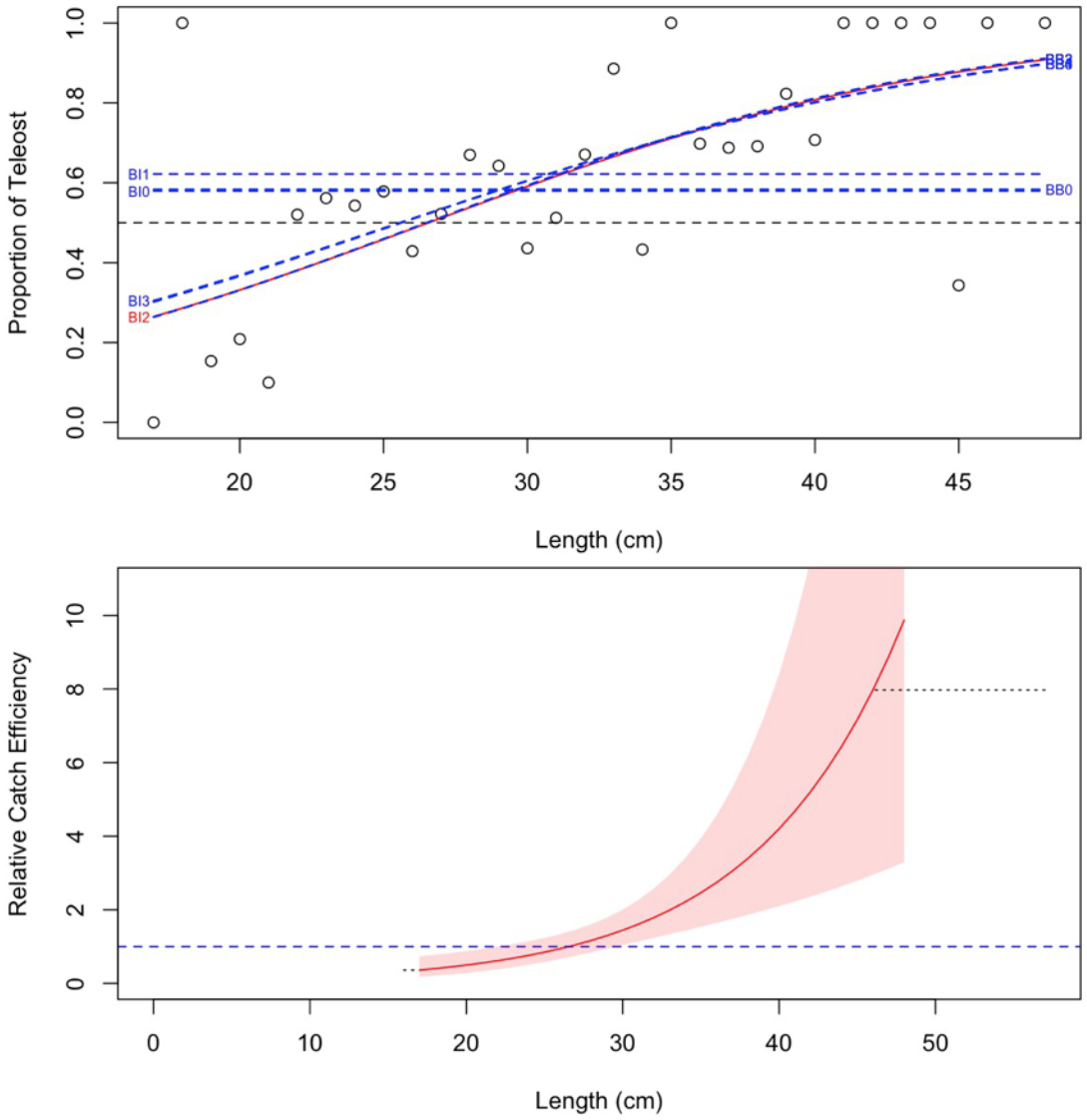

Figure 26b. Model fits and the selected length-based calibration for Alosa sapidissima (61).

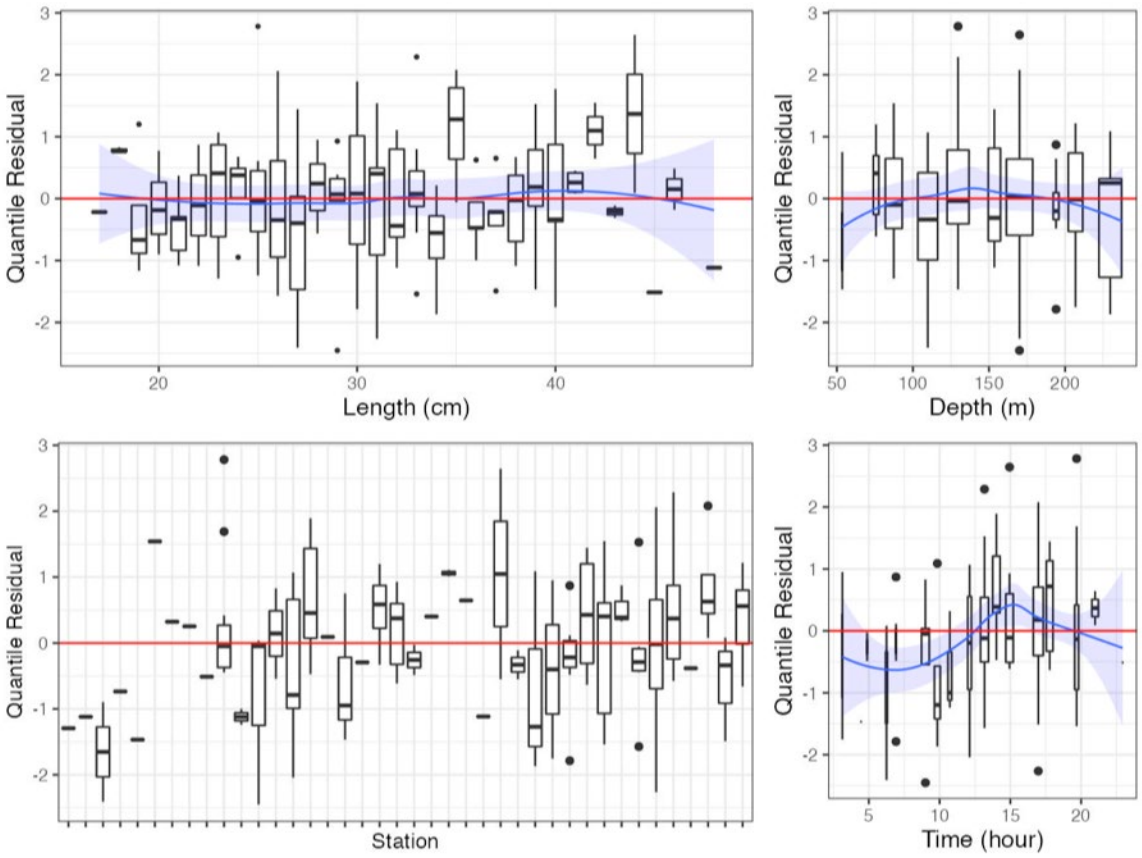

Figure 26c. Randomized and normalized quantile residuals for the selected model for Alosa sapidissima (61).

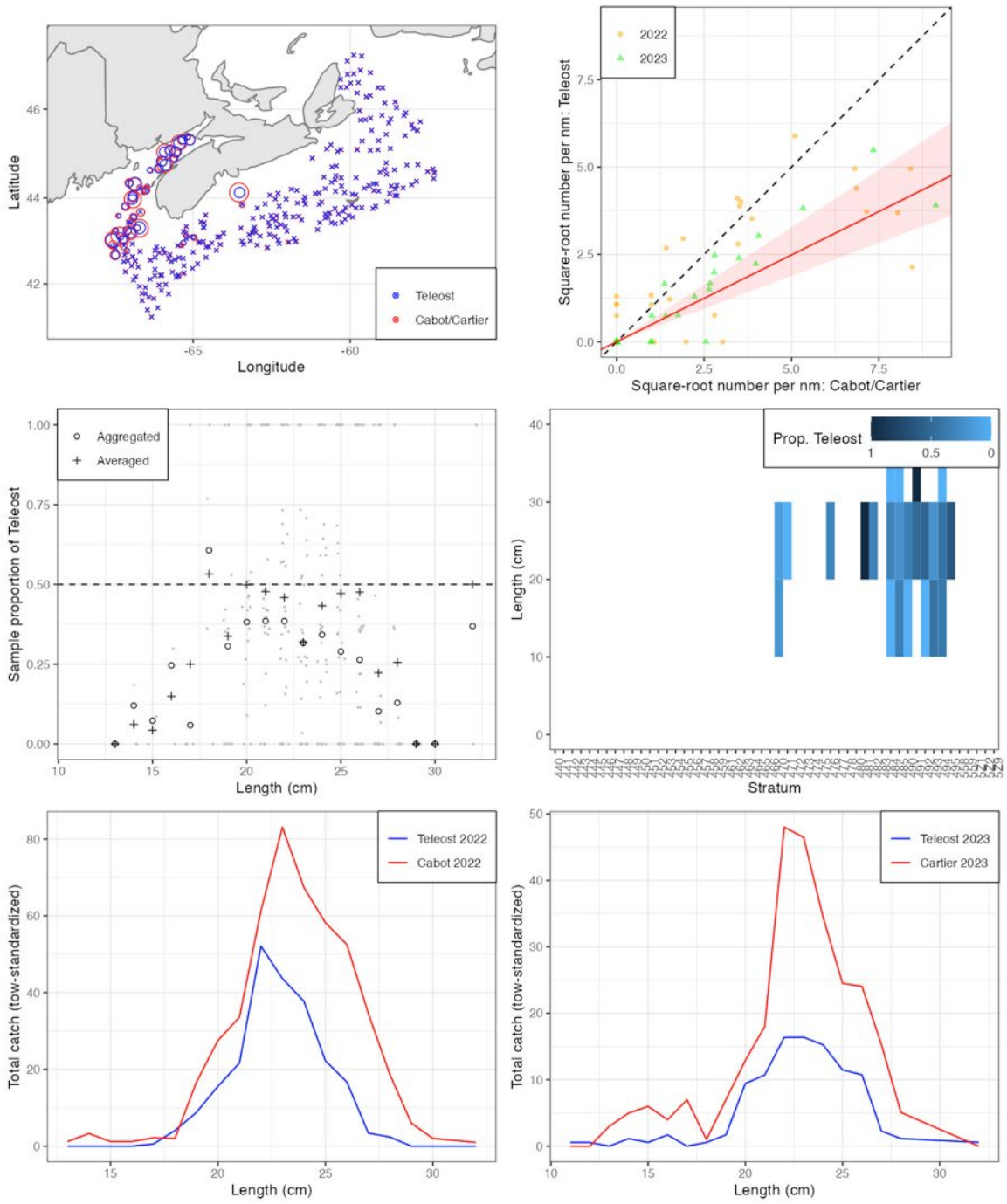

Figure 27a. Visualisation of comparative fishing data and size-aggregated model fit for Alosa pseudoharengus (62).

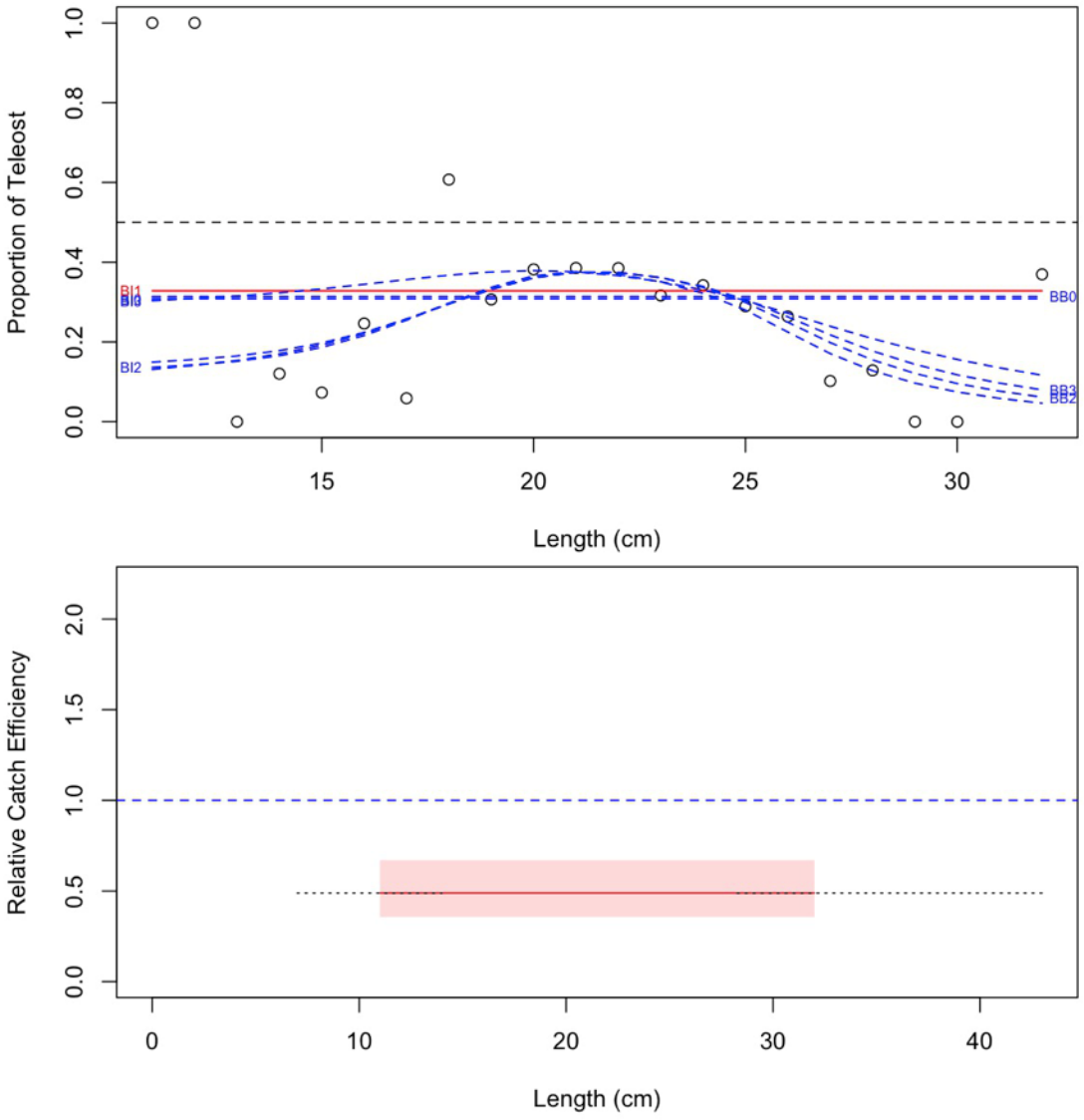

Figure 27b. Model fits and the selected length-based calibration for Alosa pseudoharengus (62).

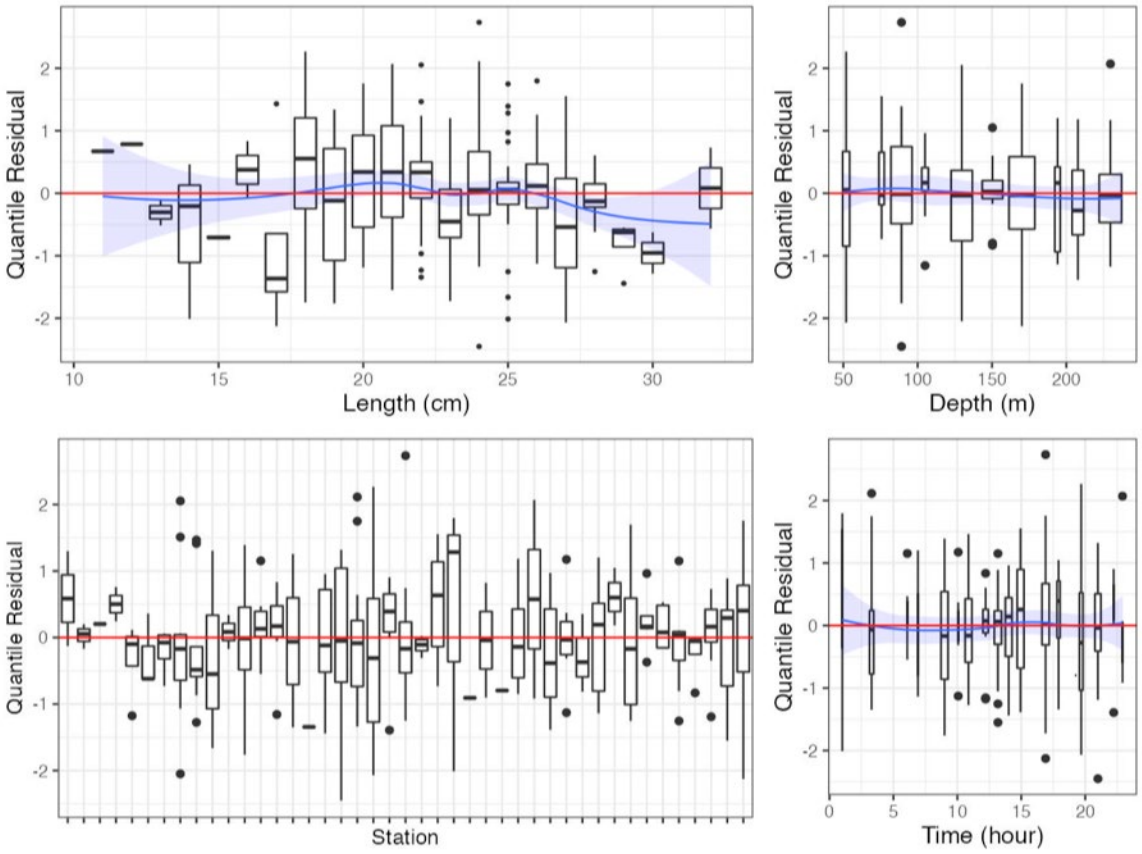

Figure 27c. Randomized and normalized quantile residuals for the selected model for Alosa pseudoharengus (62).

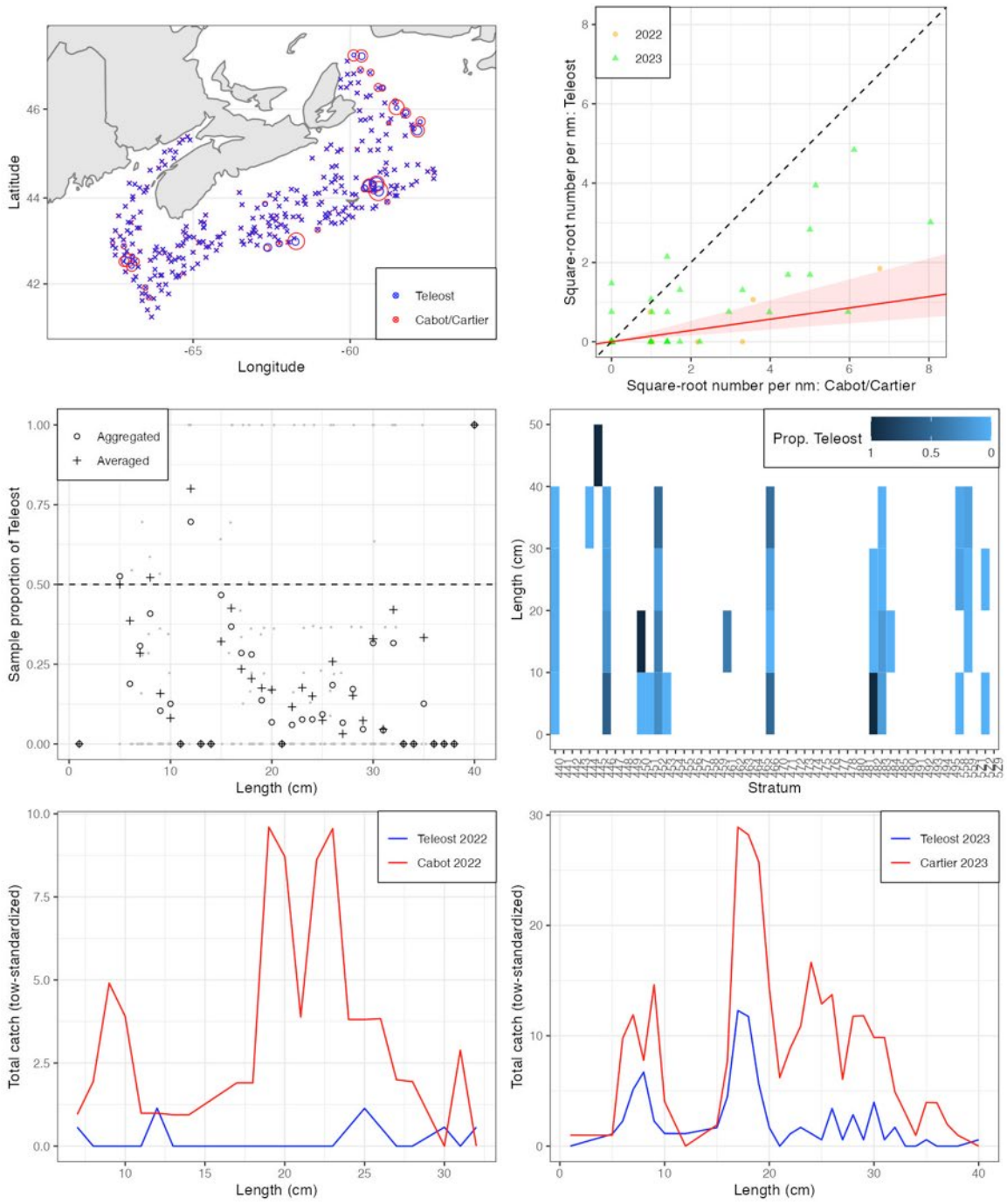

Figure 28a. Visualisation of comparative fishing data and size-aggregated model fit for Urophycis chesteri (112).

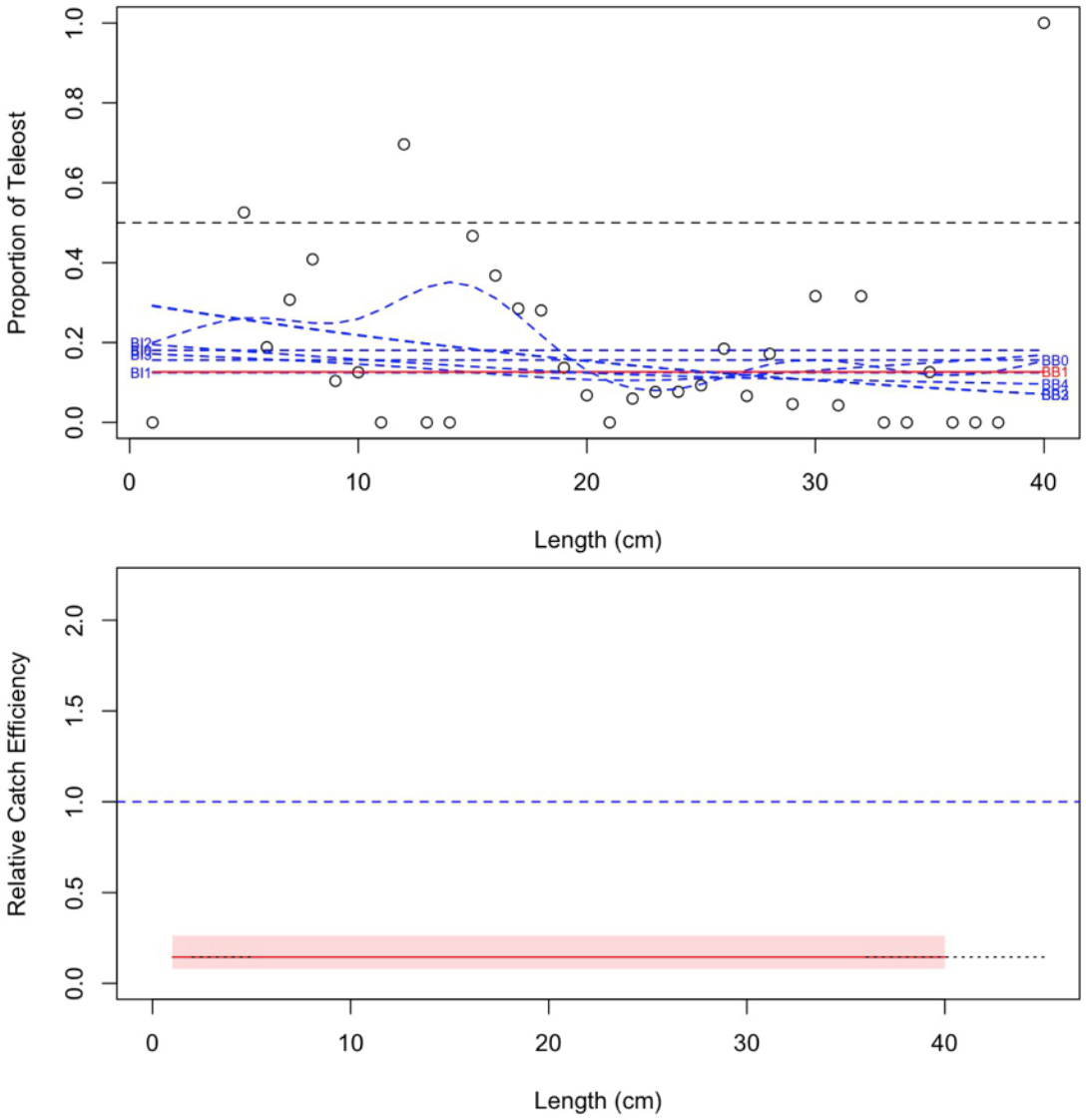

Figure 28b. Model fits and the selected length-based calibration for Urophycis chesteri (112).

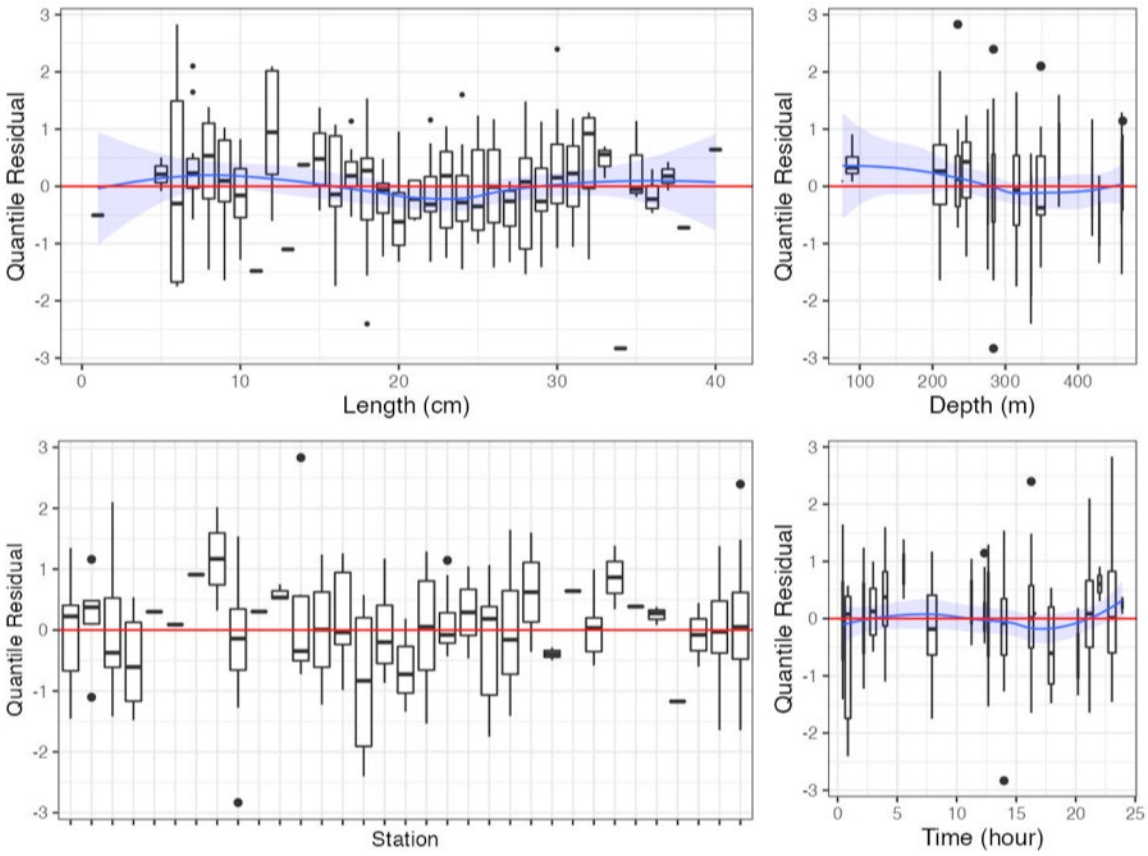

Figure 28c. Randomized and normalized quantile residuals for the selected model for Urophycis chesteri (112).

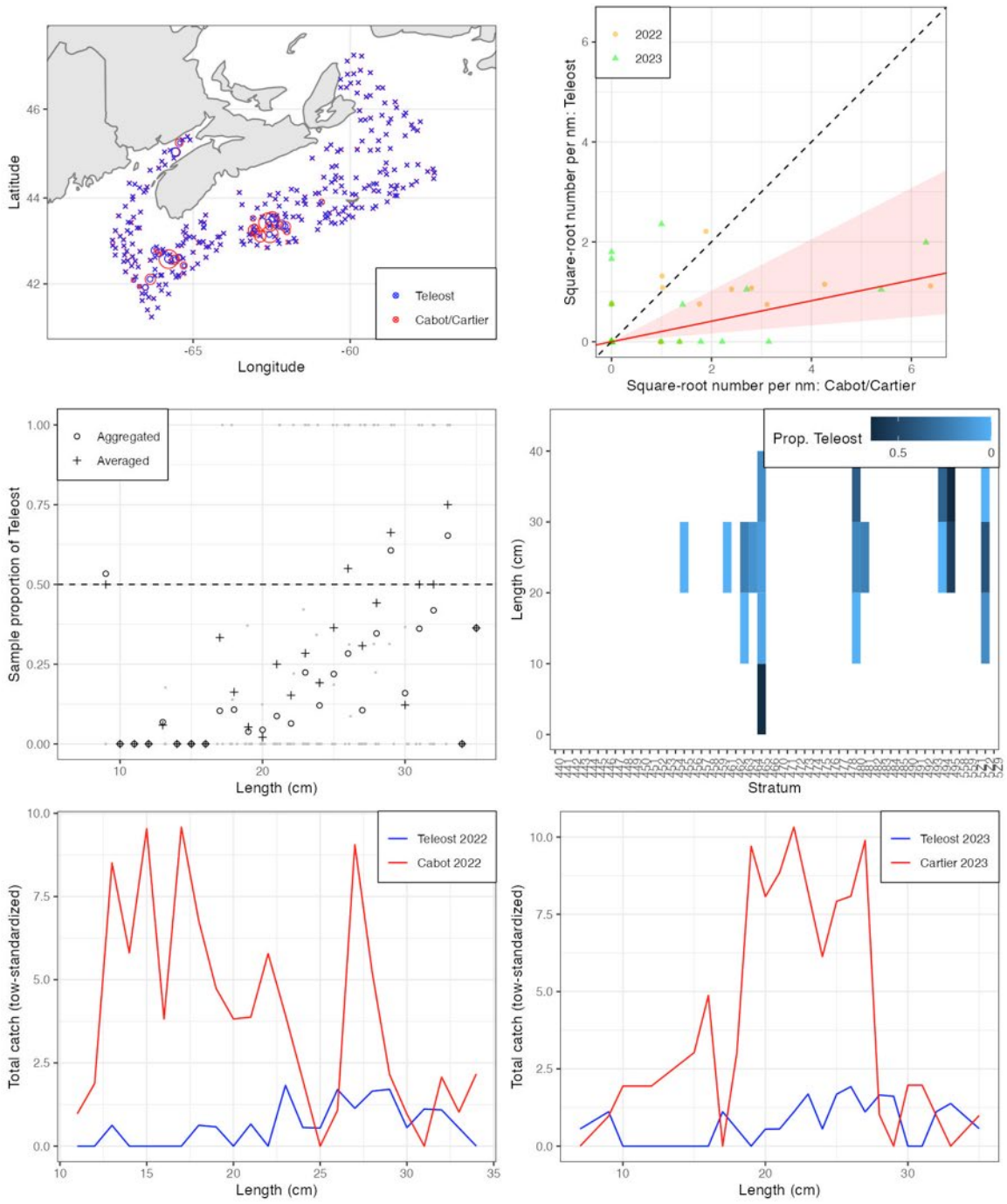

Figure 29a. Visualisation of comparative fishing data and size-aggregated model fit for Tautogolabrus adspersus (122).

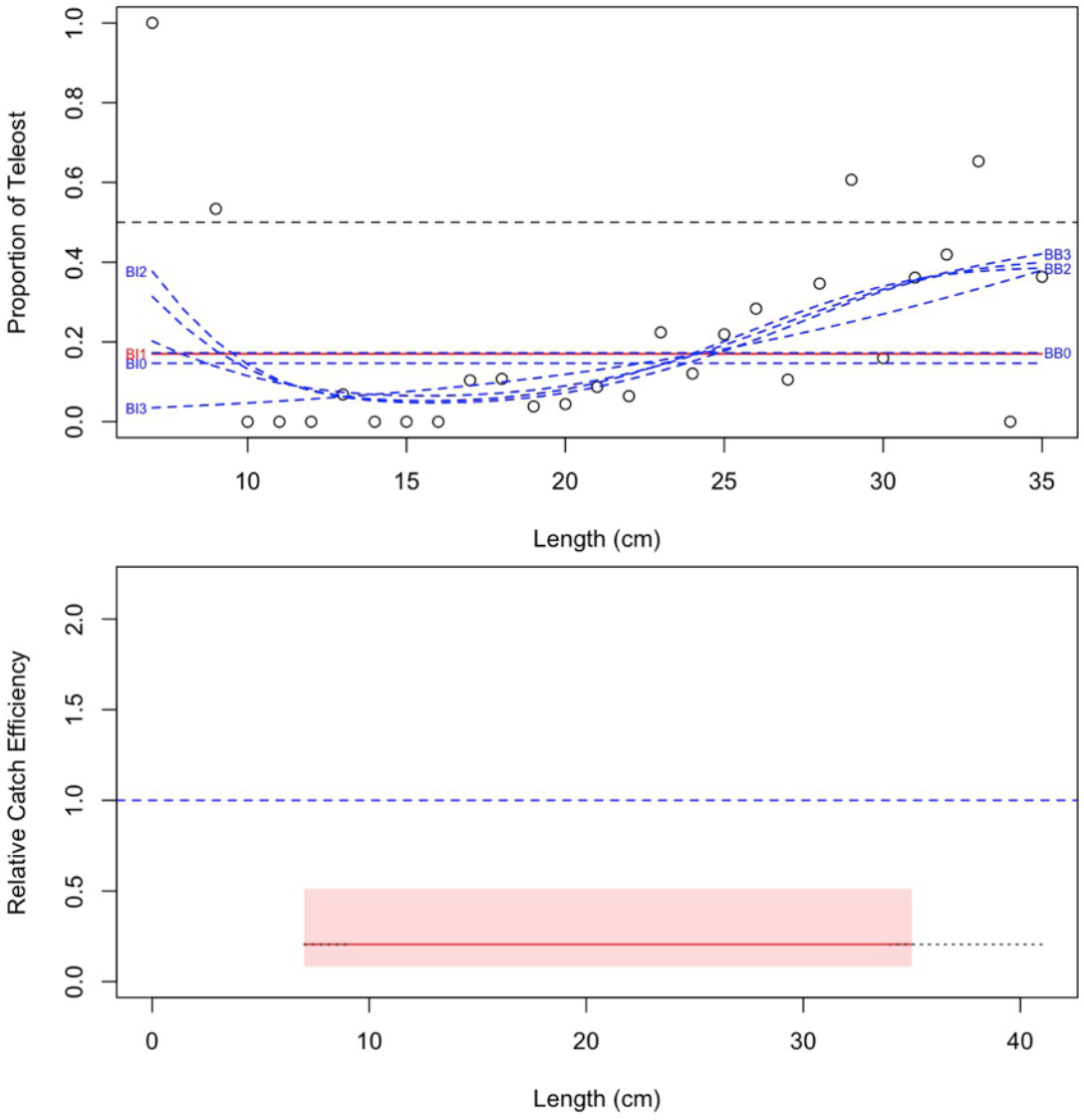

Figure 29b. Model fits and the selected length-based calibration for Tautogolabrus adspersus (122).

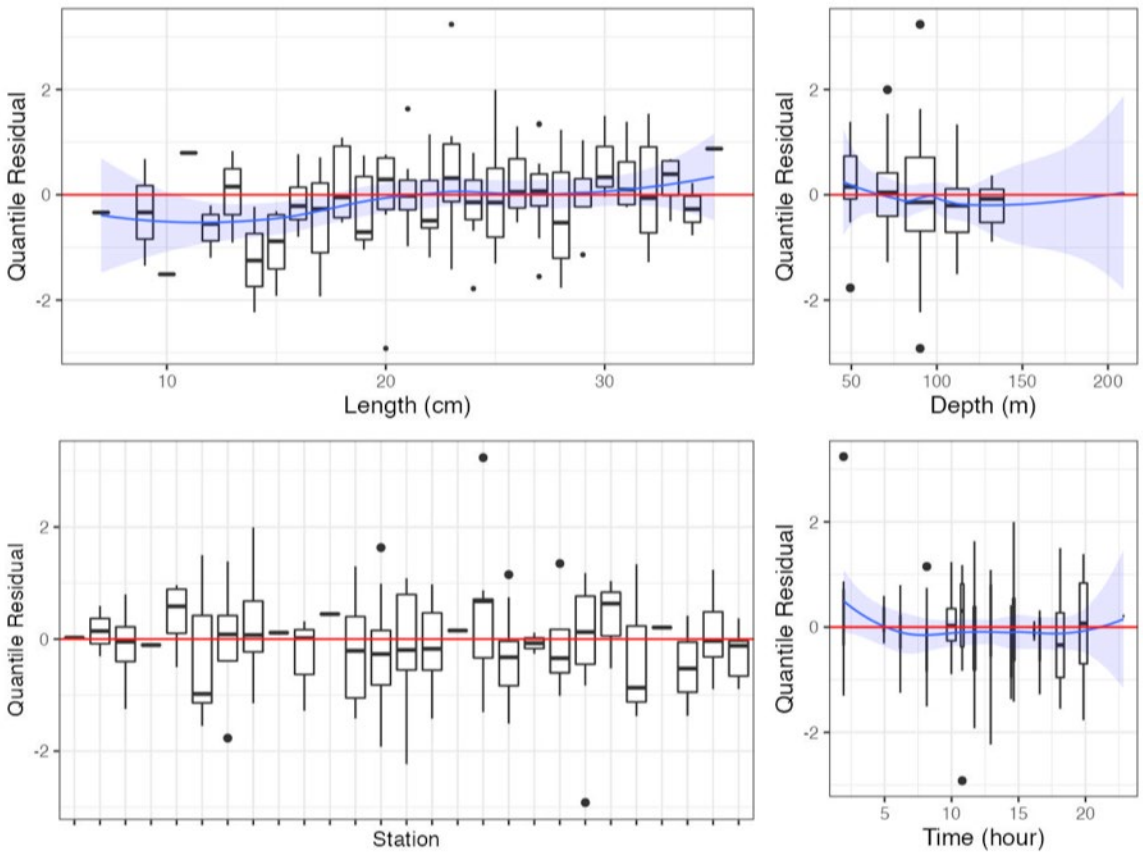

Figure 29c. Randomized and normalized quantile residuals for the selected model for Tautogolabrus adspersus (122).

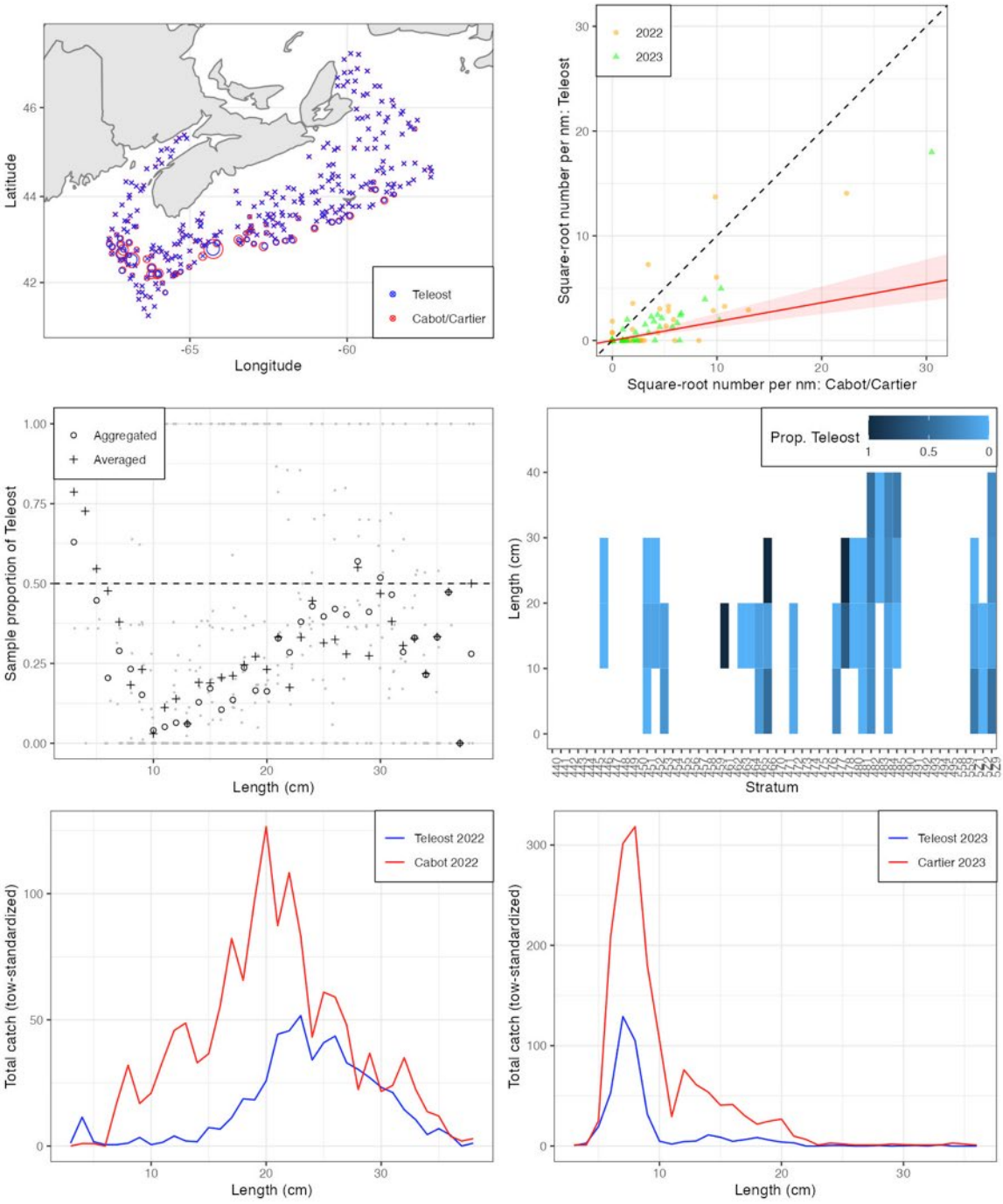

Figure 30a. Visualisation of comparative fishing data and size-aggregated model fit for Helicolenus dactylopterus (123).

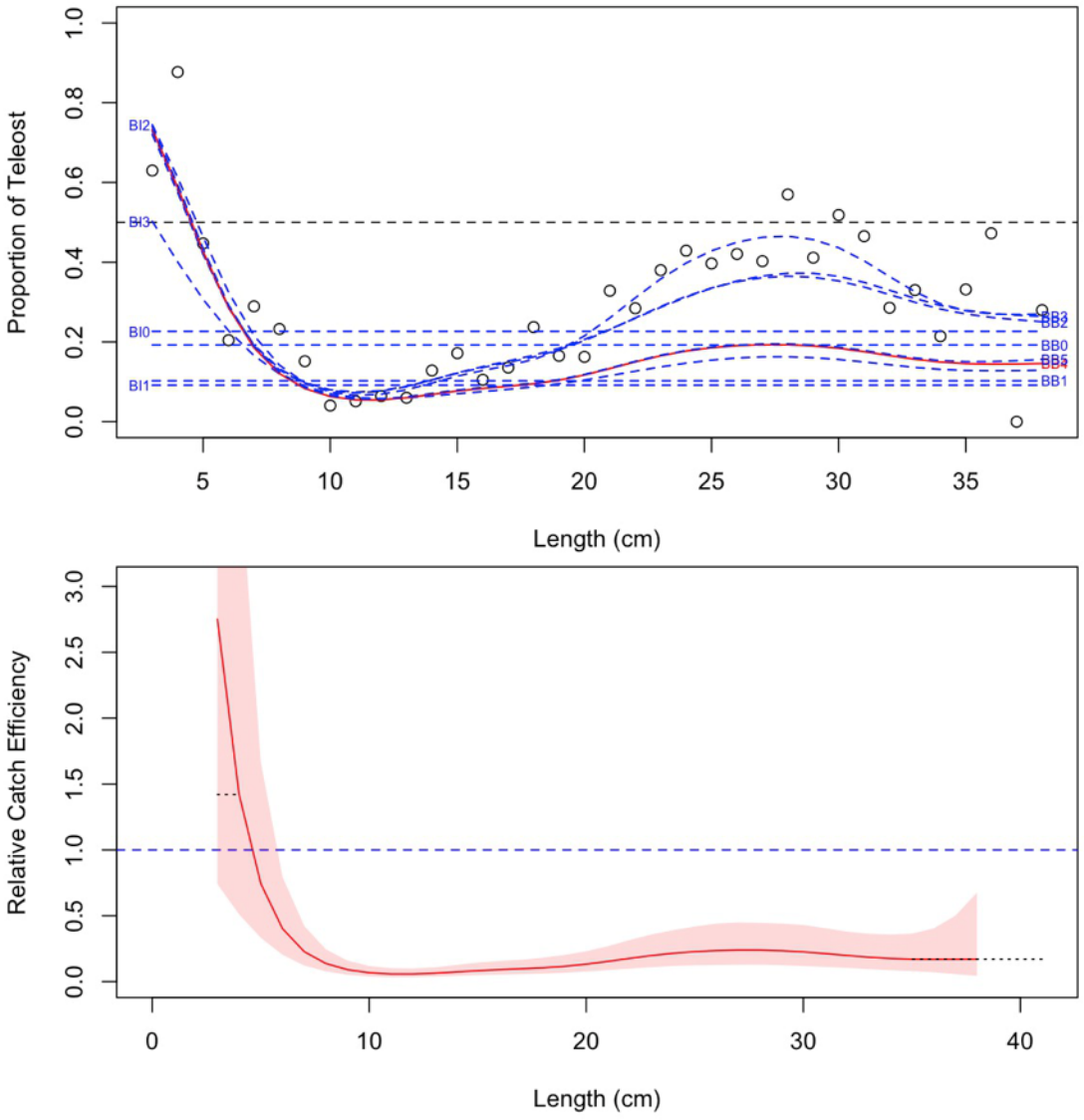

Figure 30b. Model fits and the selected length-based calibration for Helicolenus dactylopterus (123).

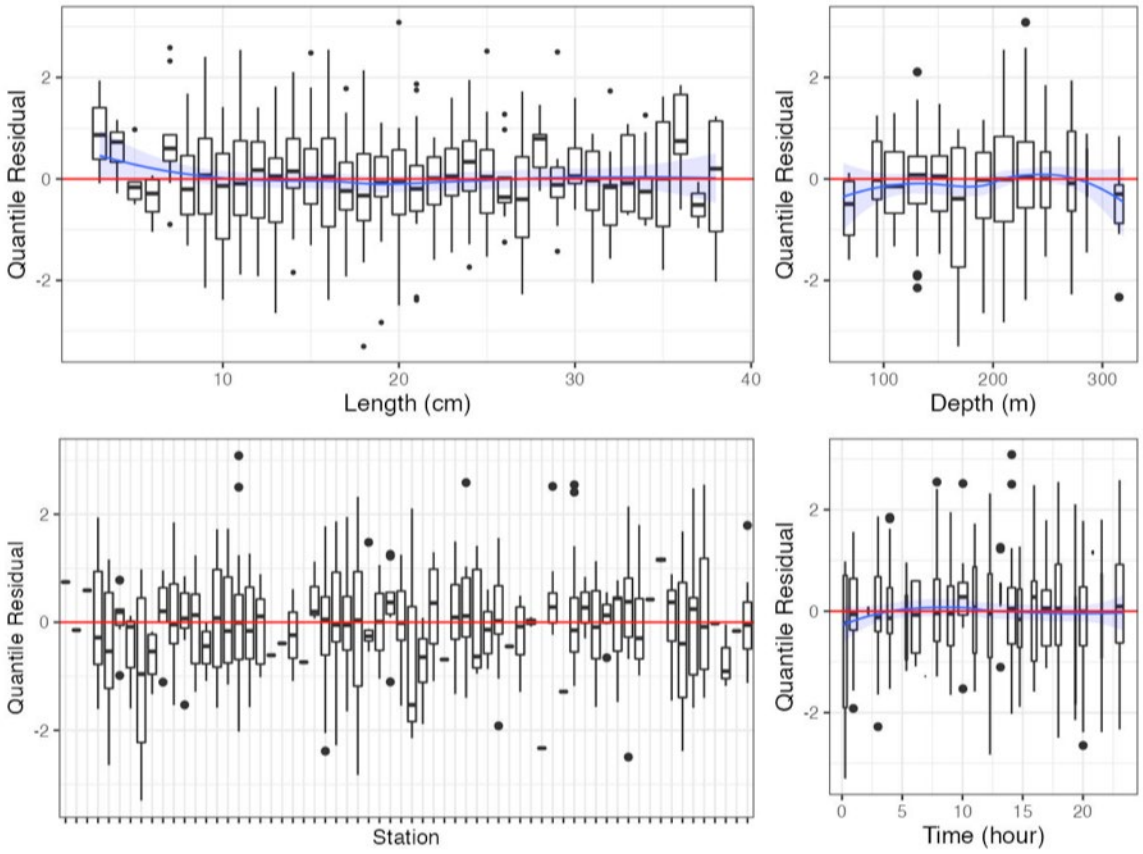

Figure 30c. Randomized and normalized quantile residuals for the selected model for Helicolenus dactylopterus (123).

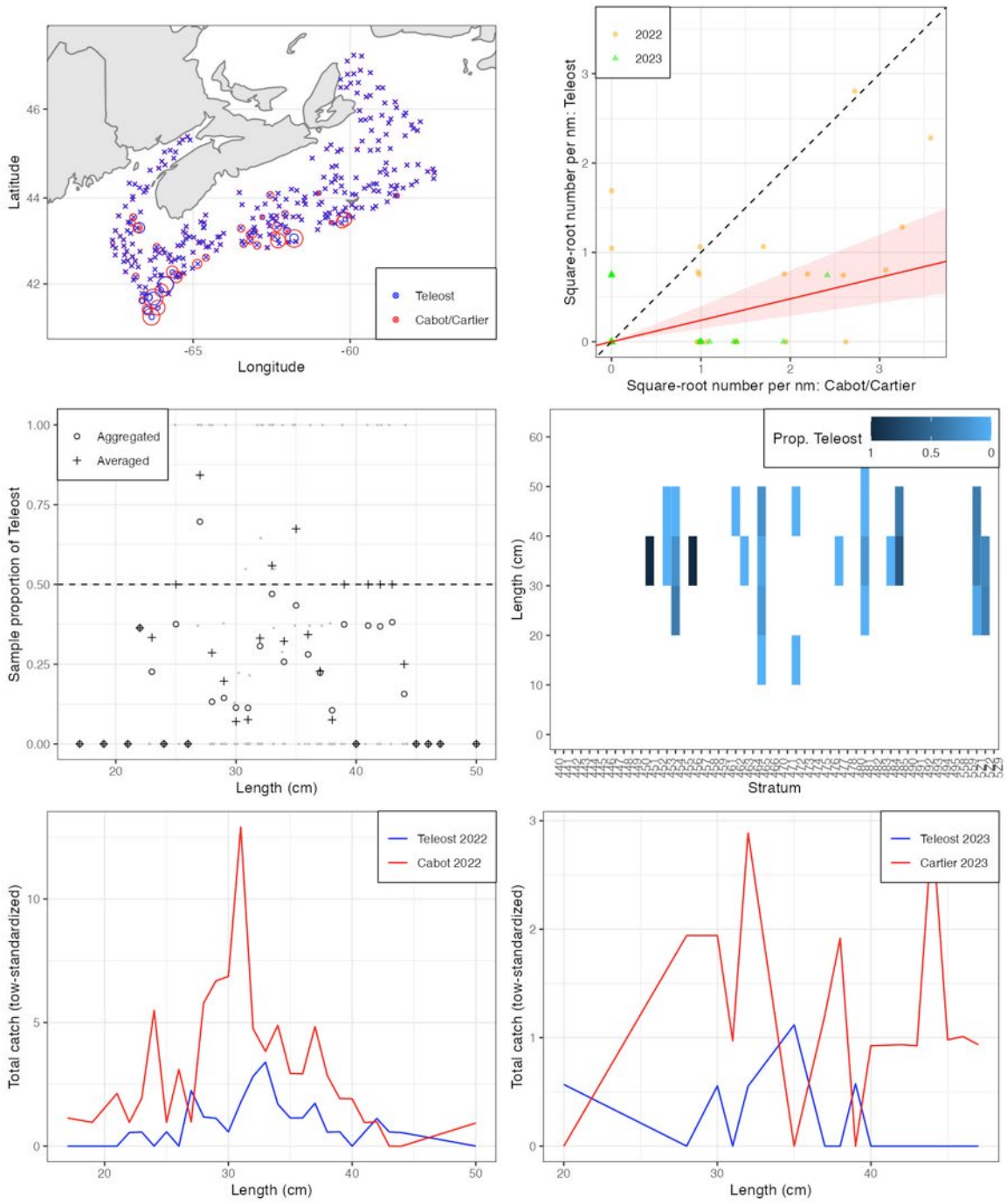

Figure 31a. Visualisation of comparative fishing data and size-aggregated model fit for Hippoglossina oblonga (142).

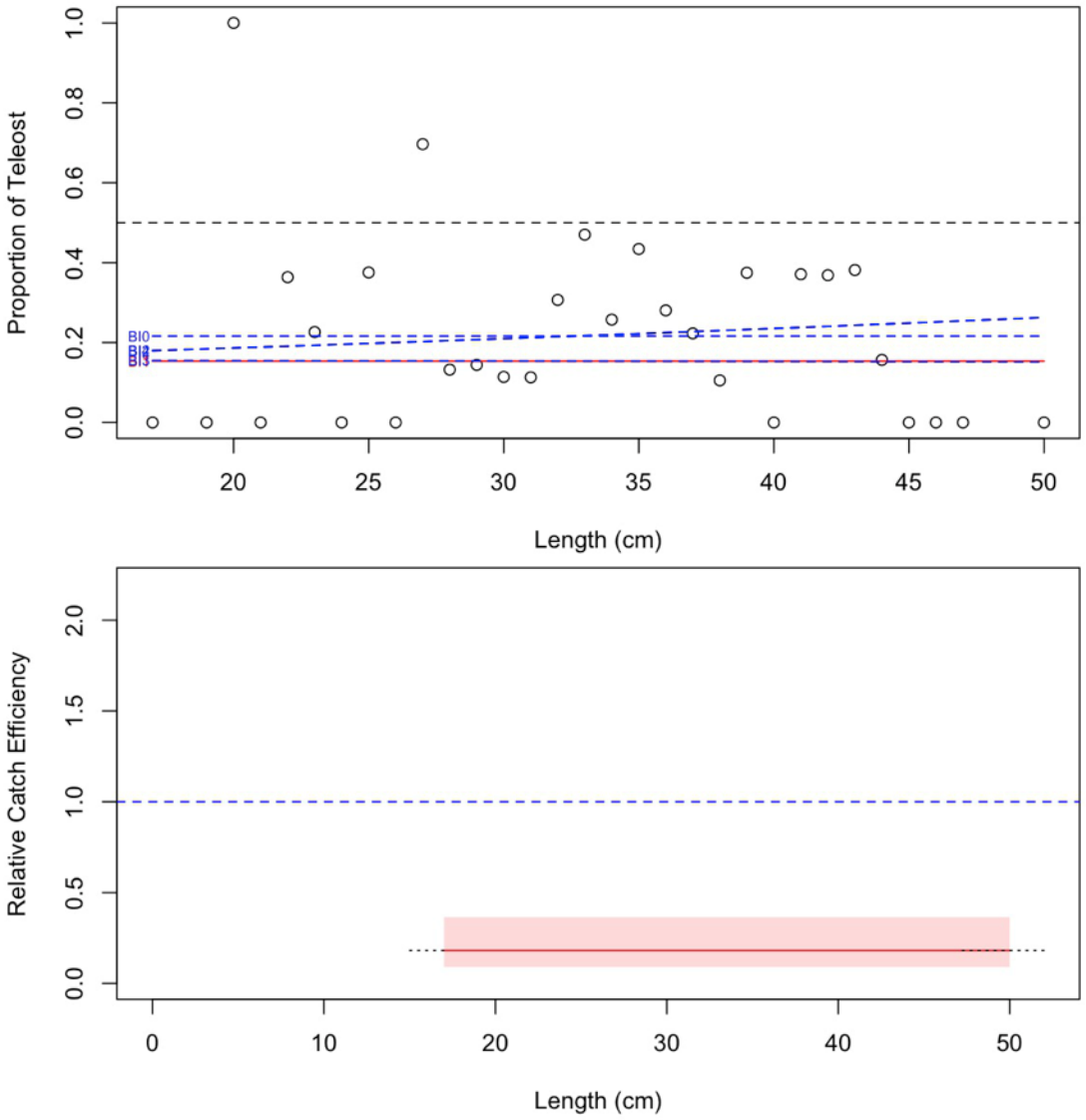

Figure 31b. Model fits and the selected length-based calibration for Hippoglossina oblonga (142).

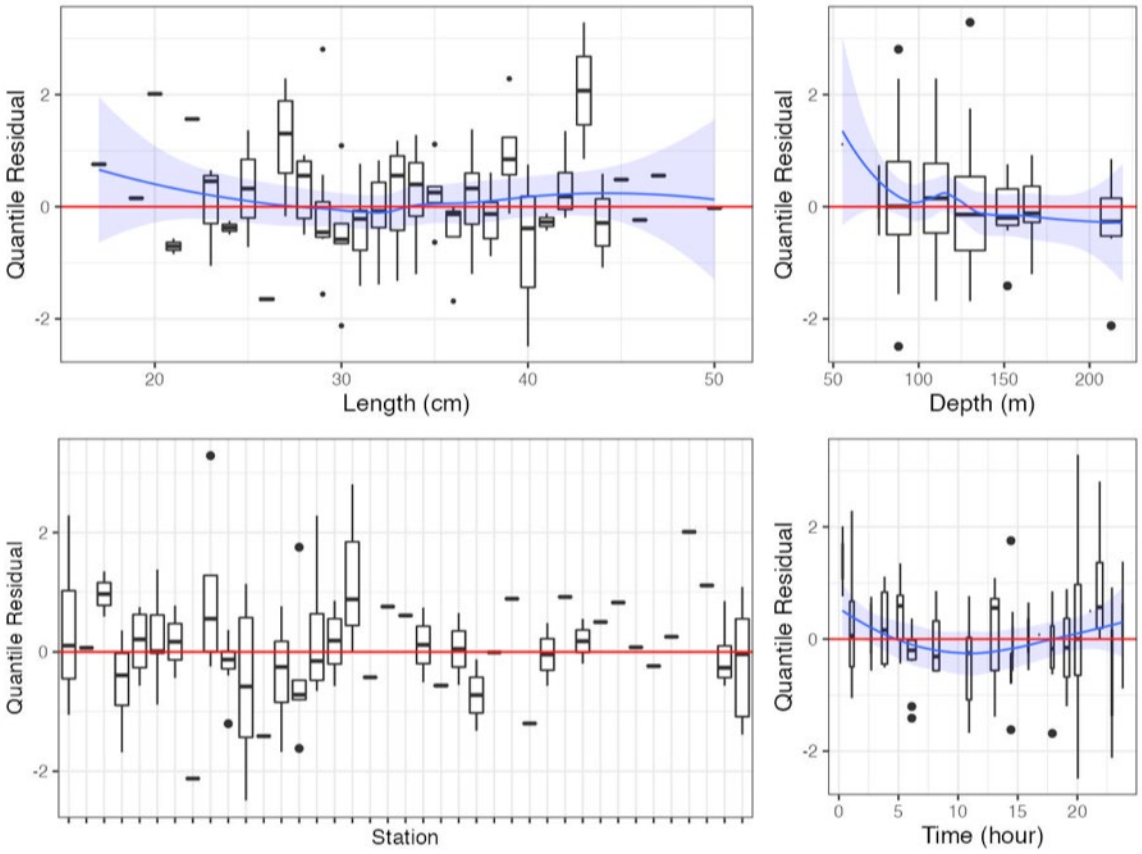

Figure 31c. Randomized and normalized quantile residuals for the selected model for Hippoglossina oblonga (142).

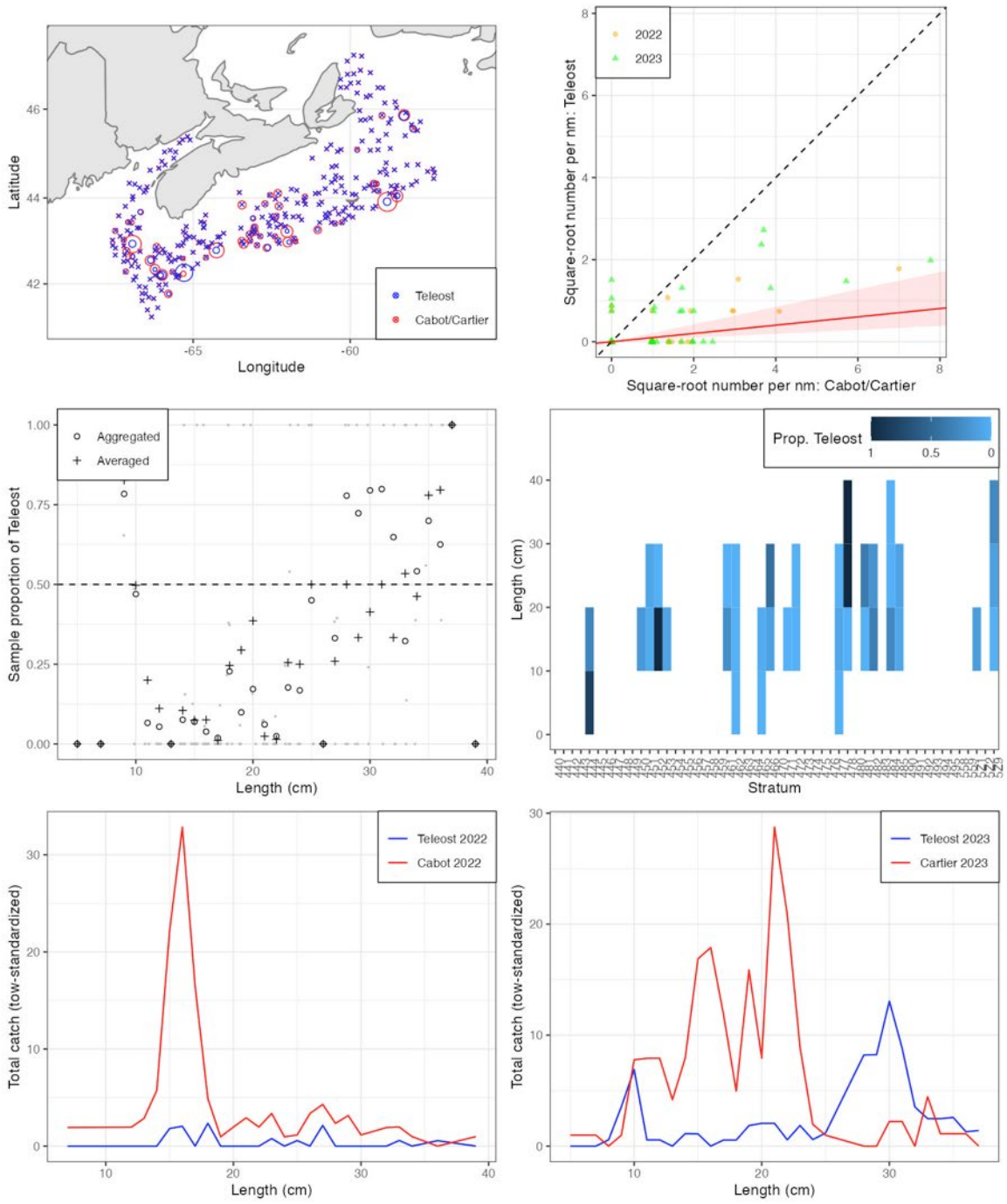

Figure 32a. Visualisation of comparative fishing data and size-aggregated model fit for Argentina silus (160).

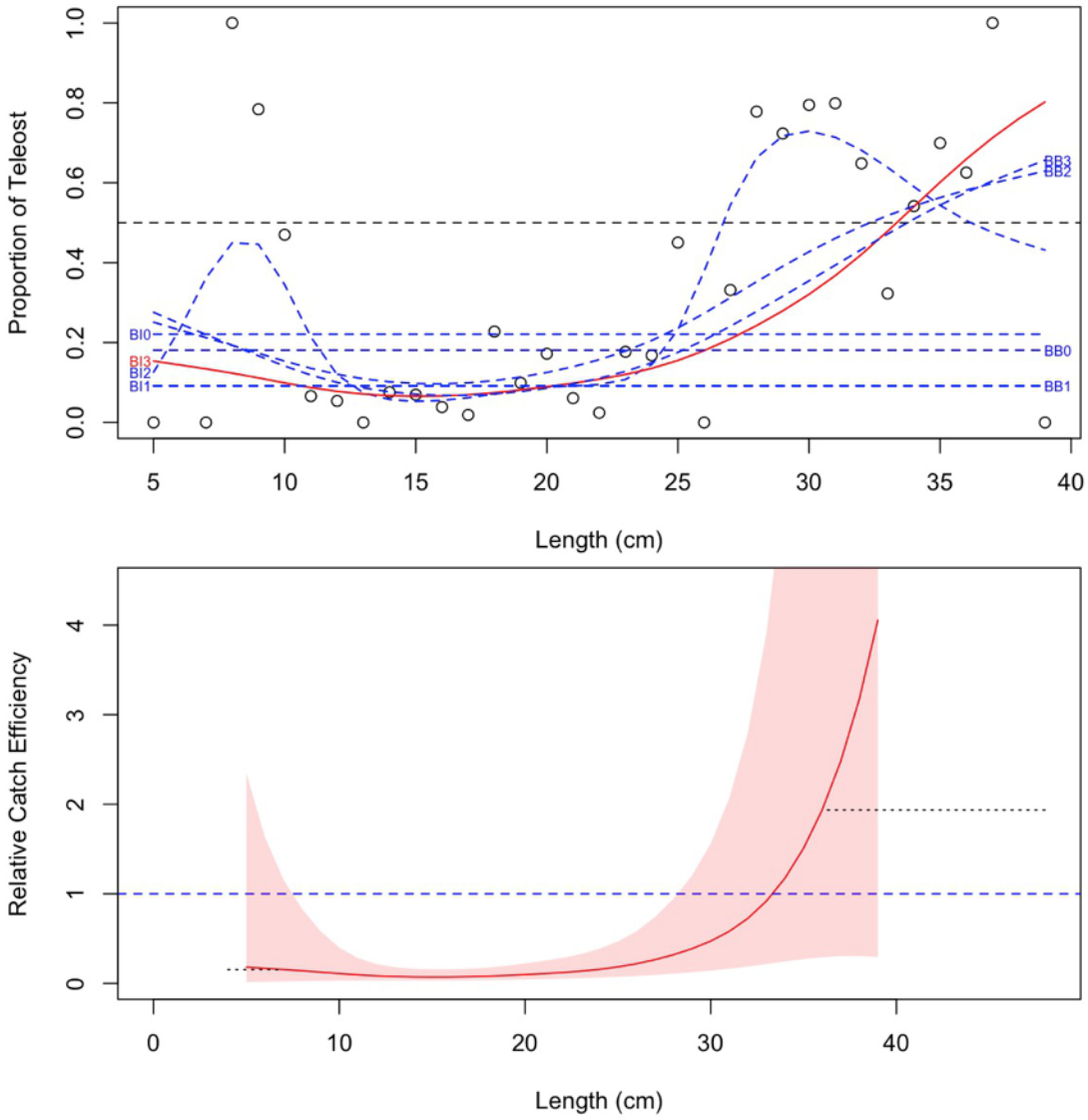

Figure 32b. Model fits and the selected length-based calibration for Argentina silus (160).

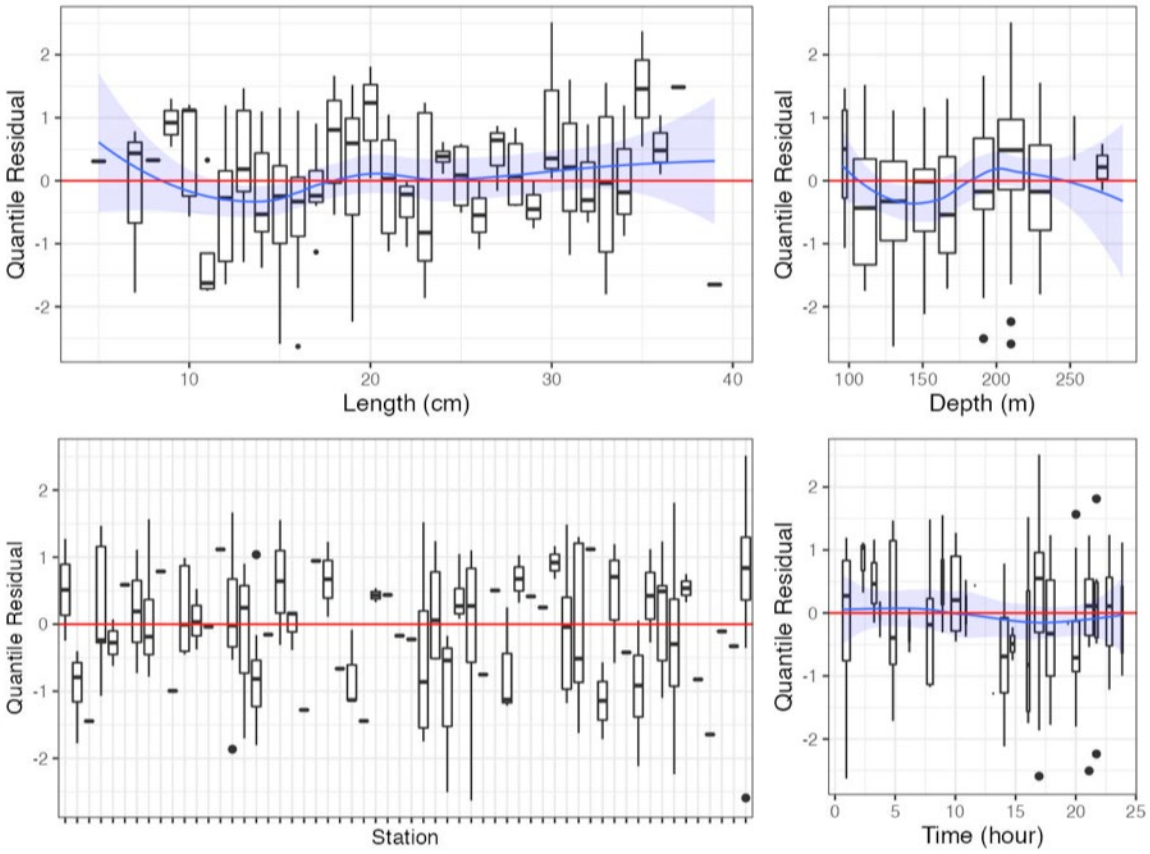

Figure 32c. Randomized and normalized quantile residuals for the selected model for Argentina silus (160).

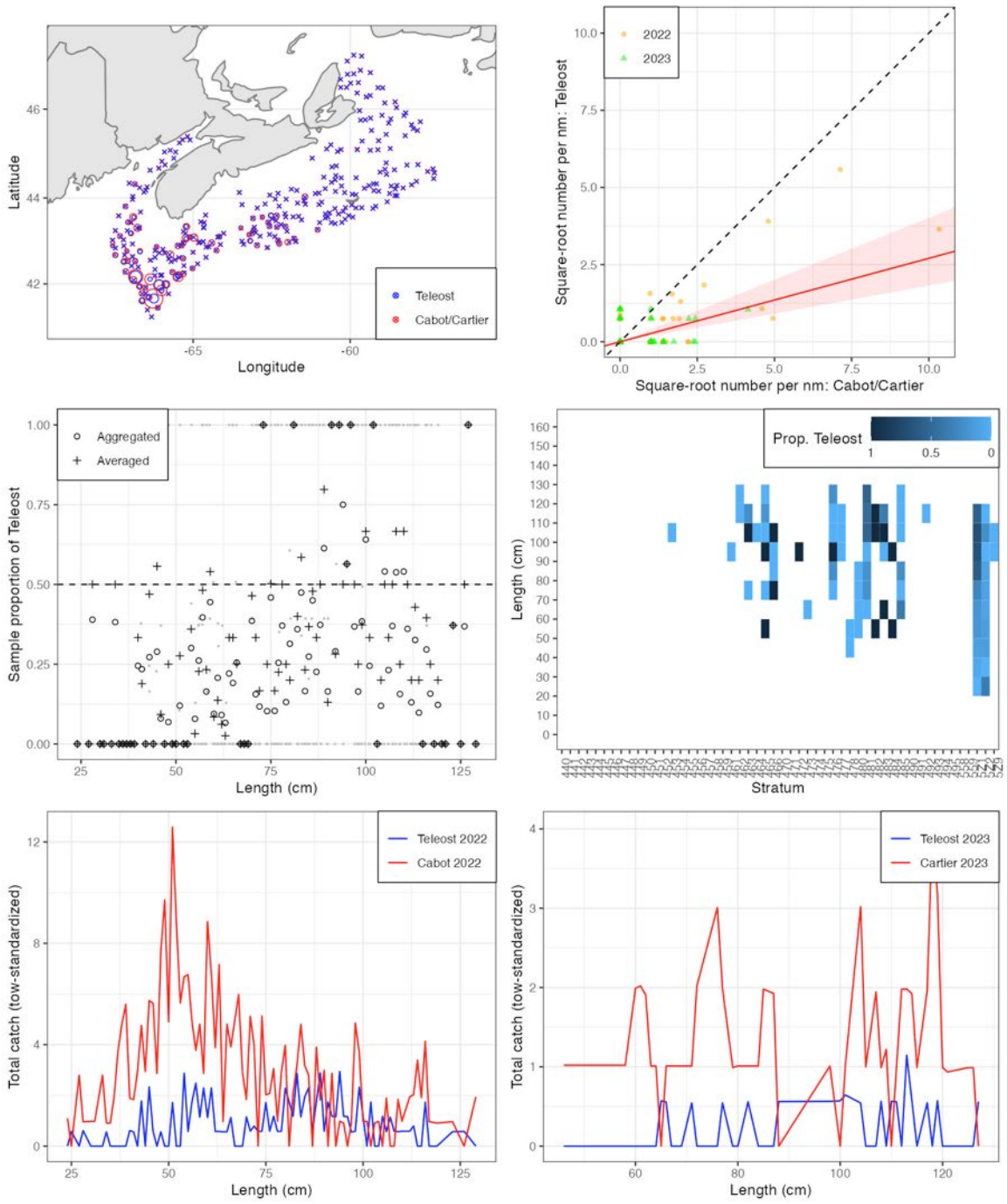

Figure 33a. Visualisation of comparative fishing data and size-aggregated model fit for Dipturus laevis (200).

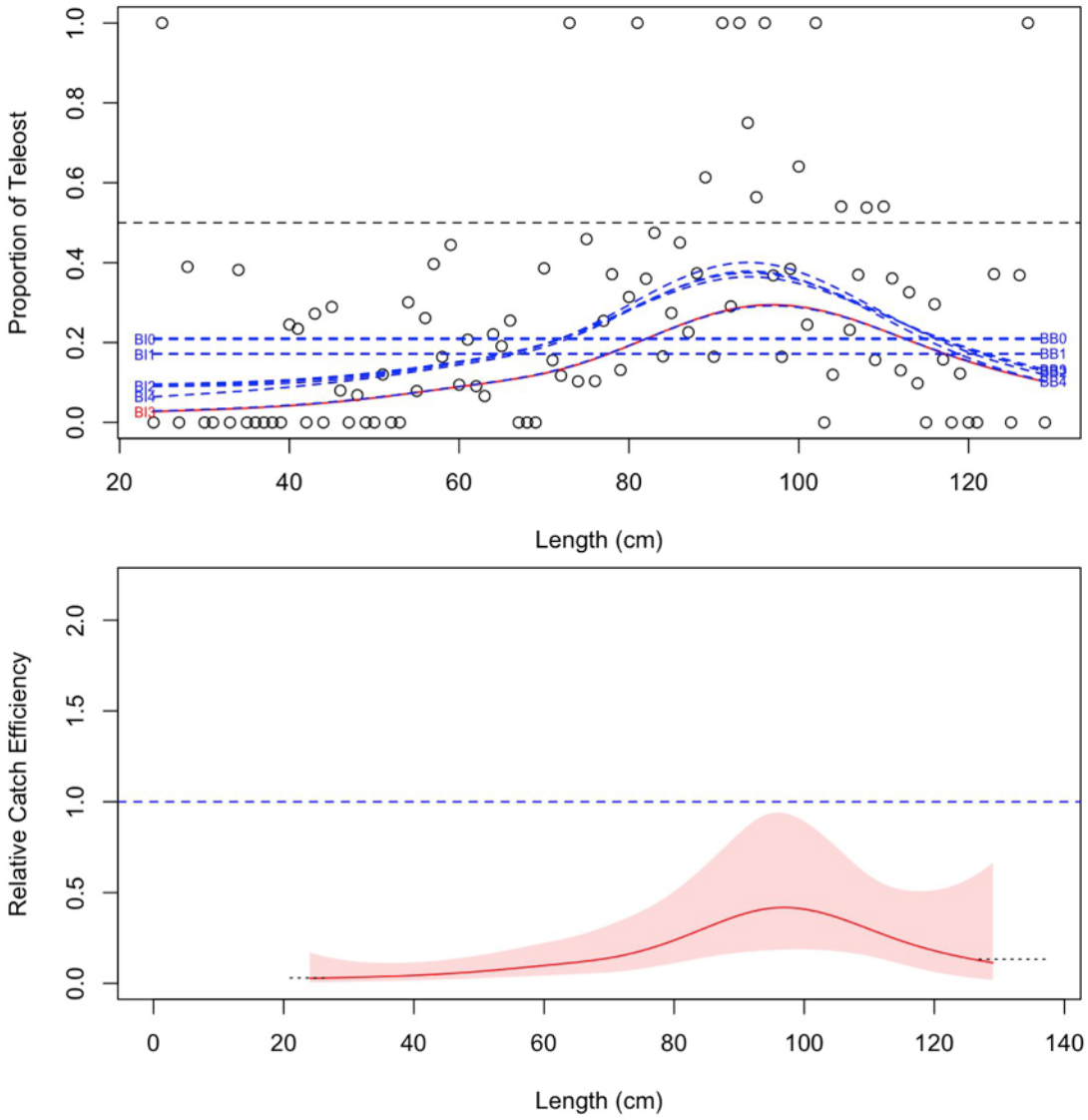

Figure 33b. Model fits and the selected length-based calibration for Dipturus laevis (200).

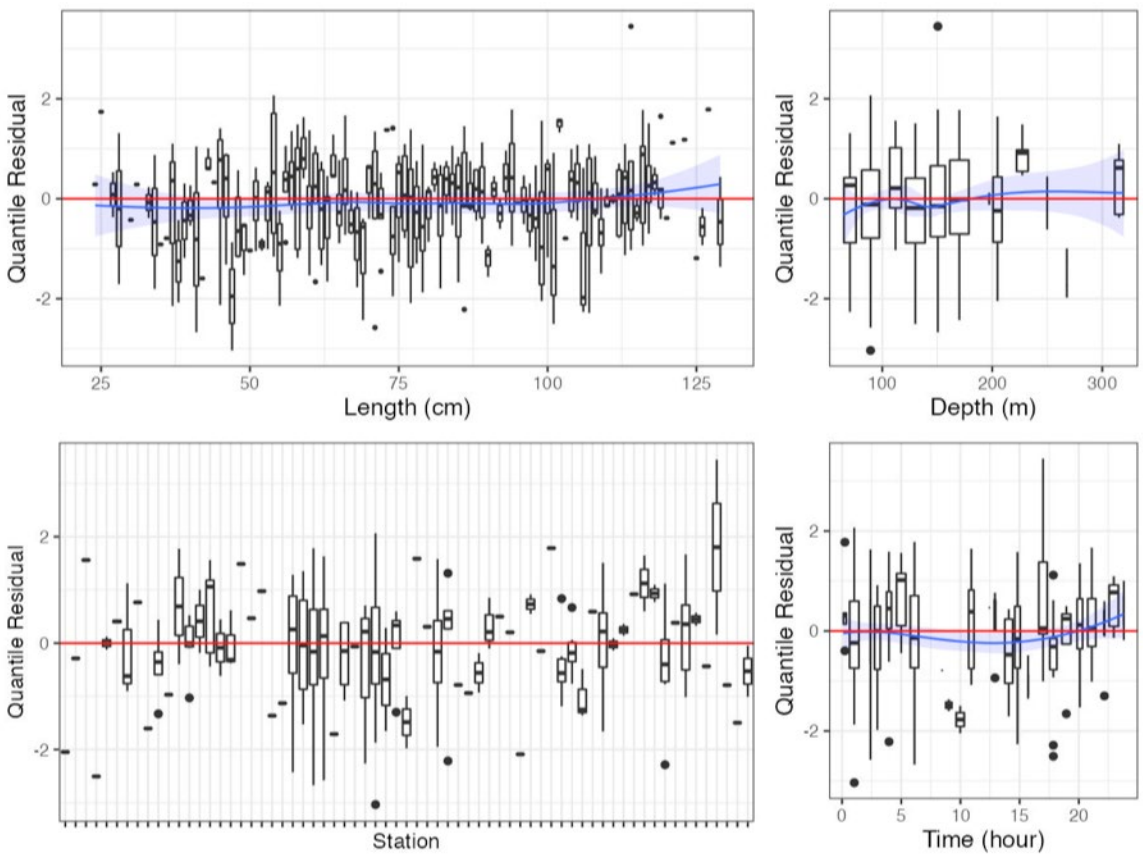

Figure 33c. Randomized and normalized quantile residuals for the selected model for Dipturus laevis (200).

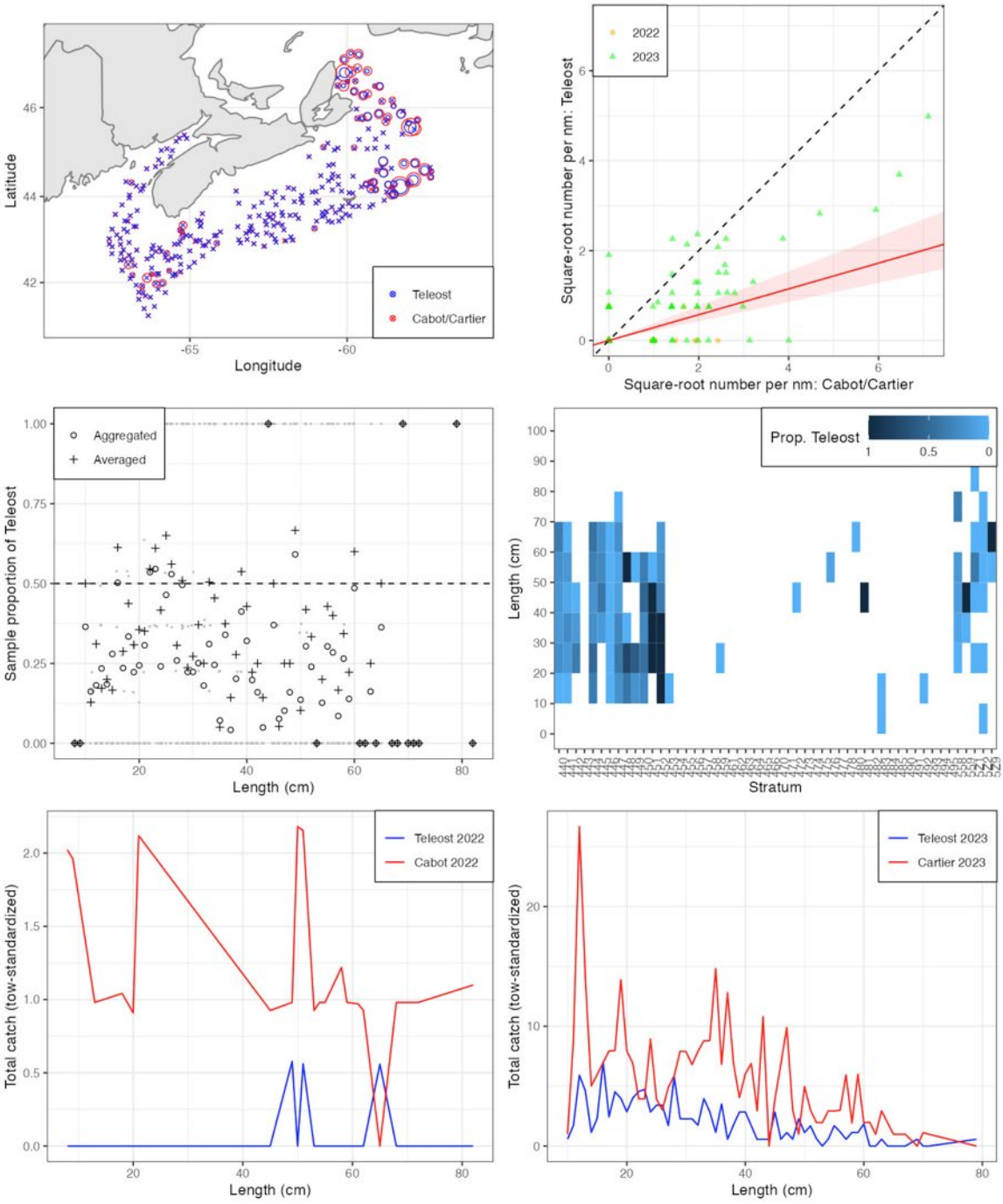

Figure 34a. Visualisation of comparative fishing data and size-aggregated model fit for Amblyraja radiata (201).

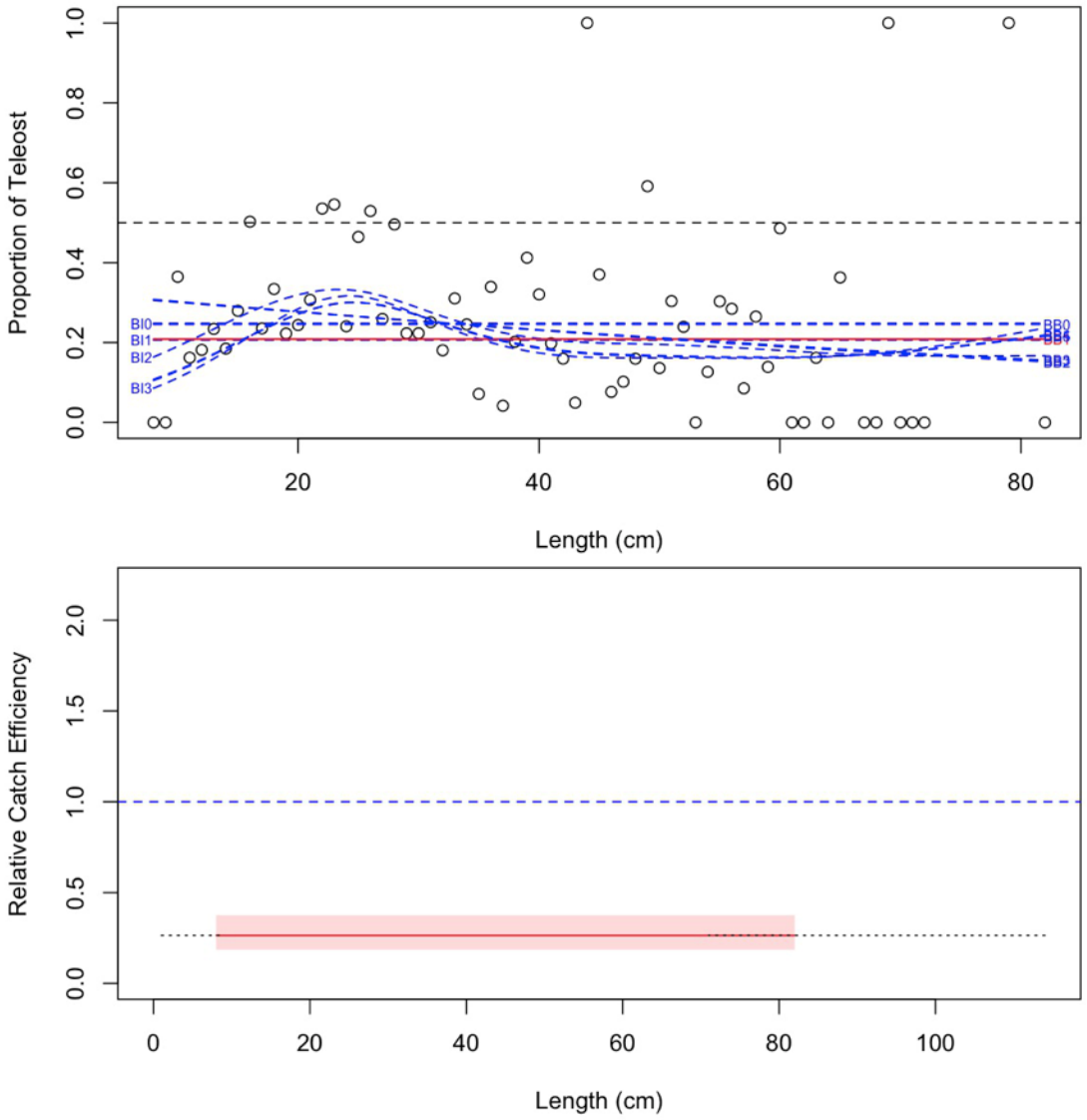

Figure 34b. Model fits and the selected length-based calibration for Amblyraja radiata (201).

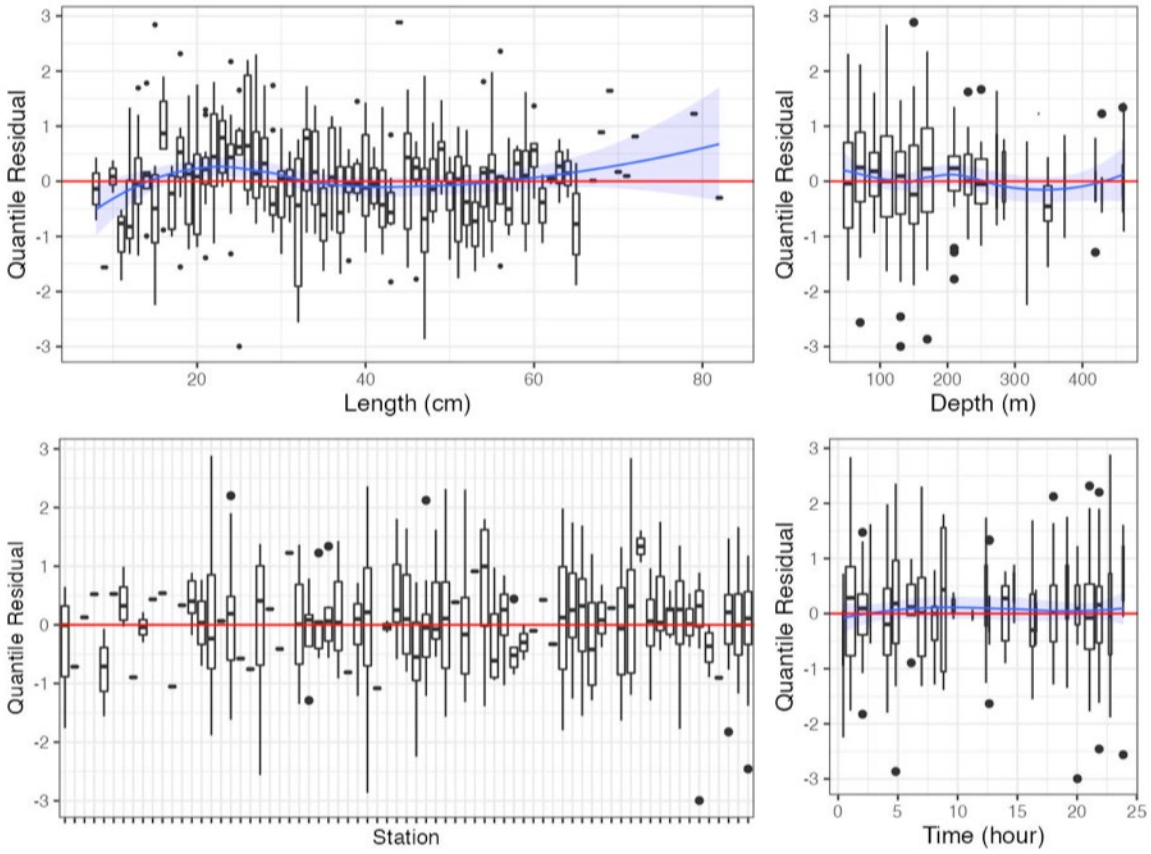

Figure 34c. Randomized and normalized quantile residuals for the selected model for Amblyraja radiata (201).

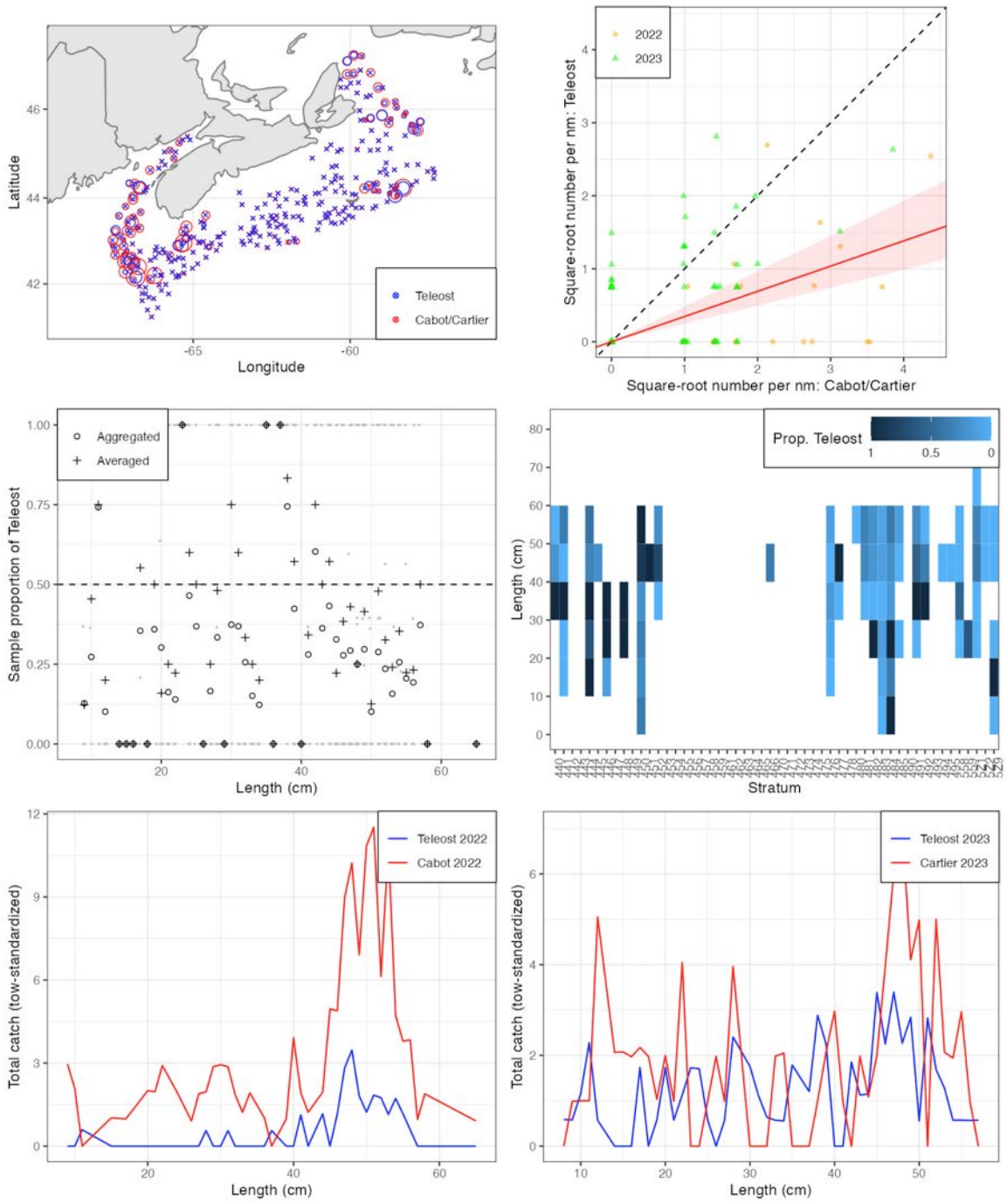

Figure 35a. Visualisation of comparative fishing data and size-aggregated model fit for Malacoraja senta (202).

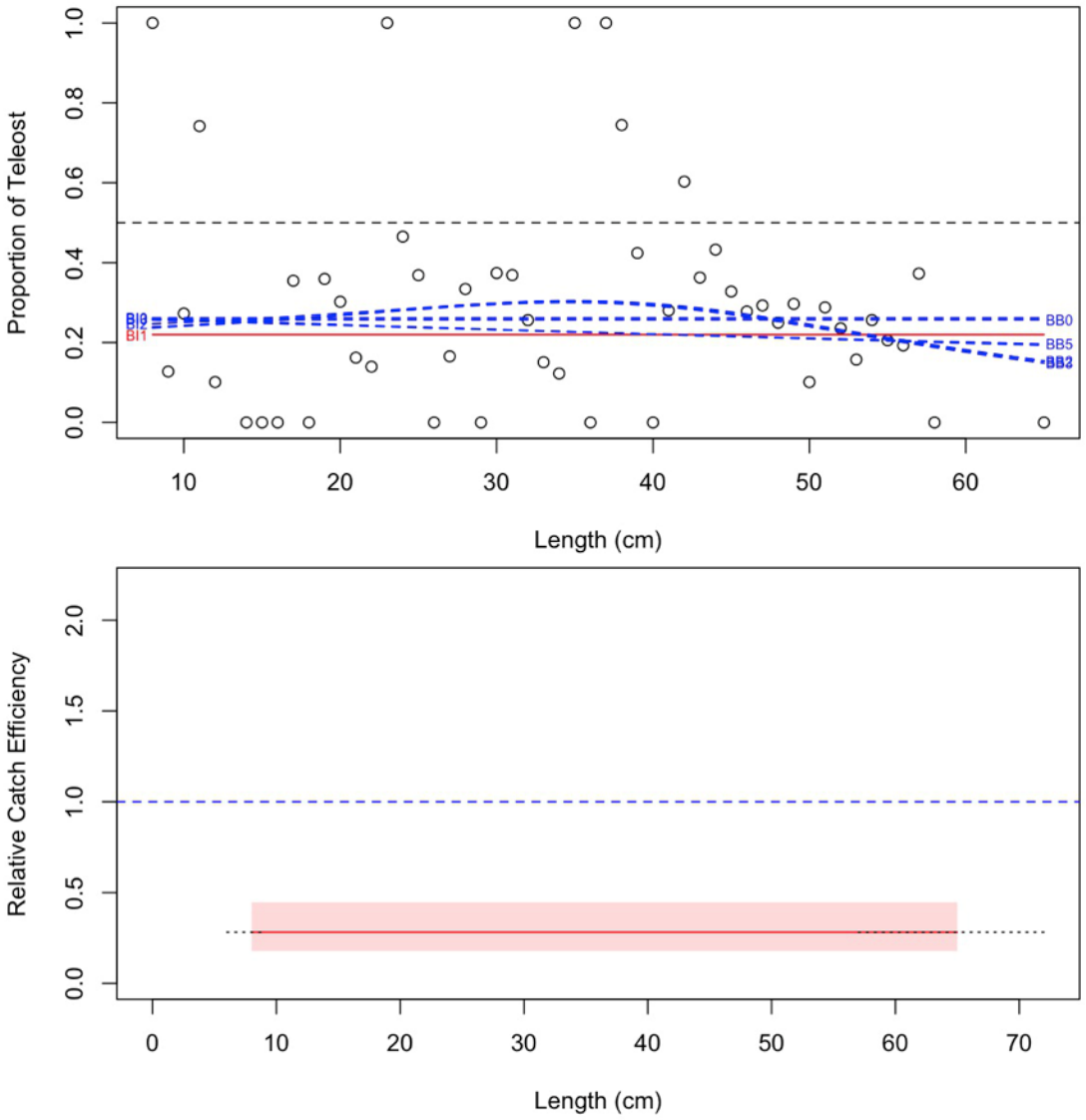

Figure 35b. Model fits and the selected length-based calibration for Malacoraja senta (202).

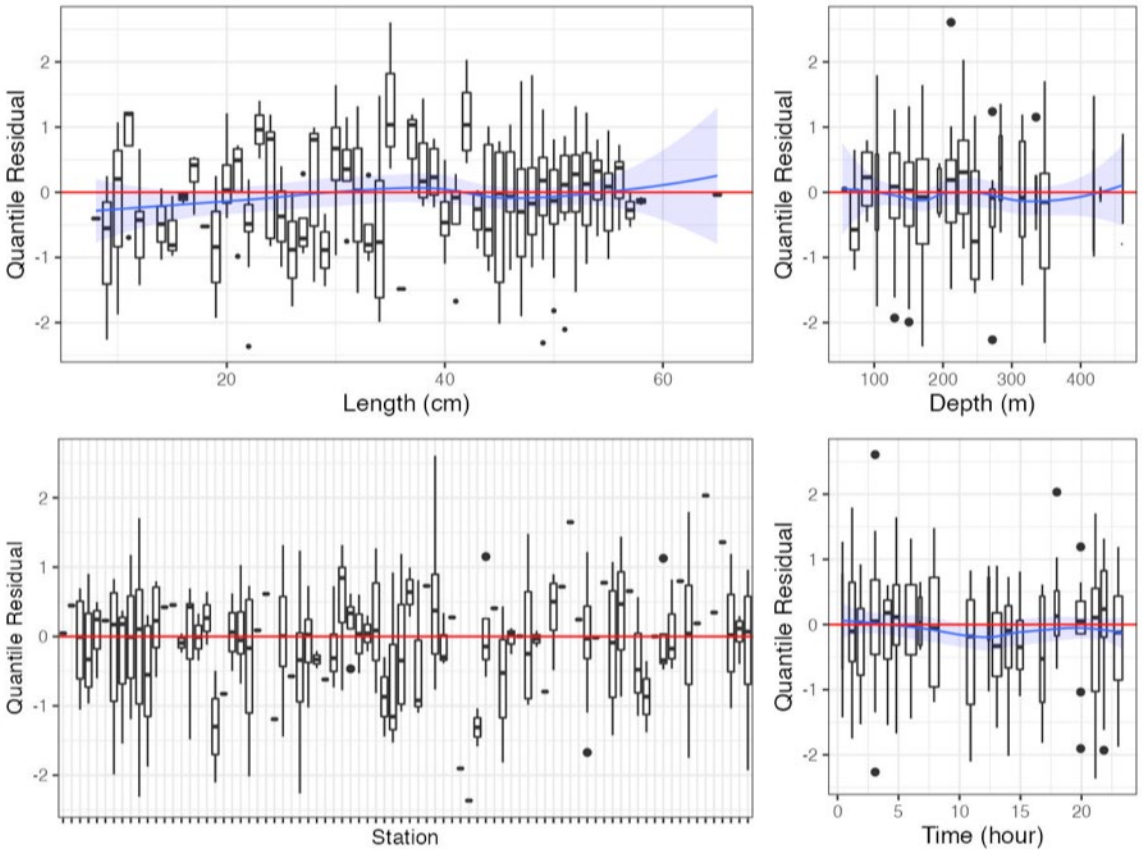

Figure 35c. Randomized and normalized quantile residuals for the selected model for Malacoraja senta (202).

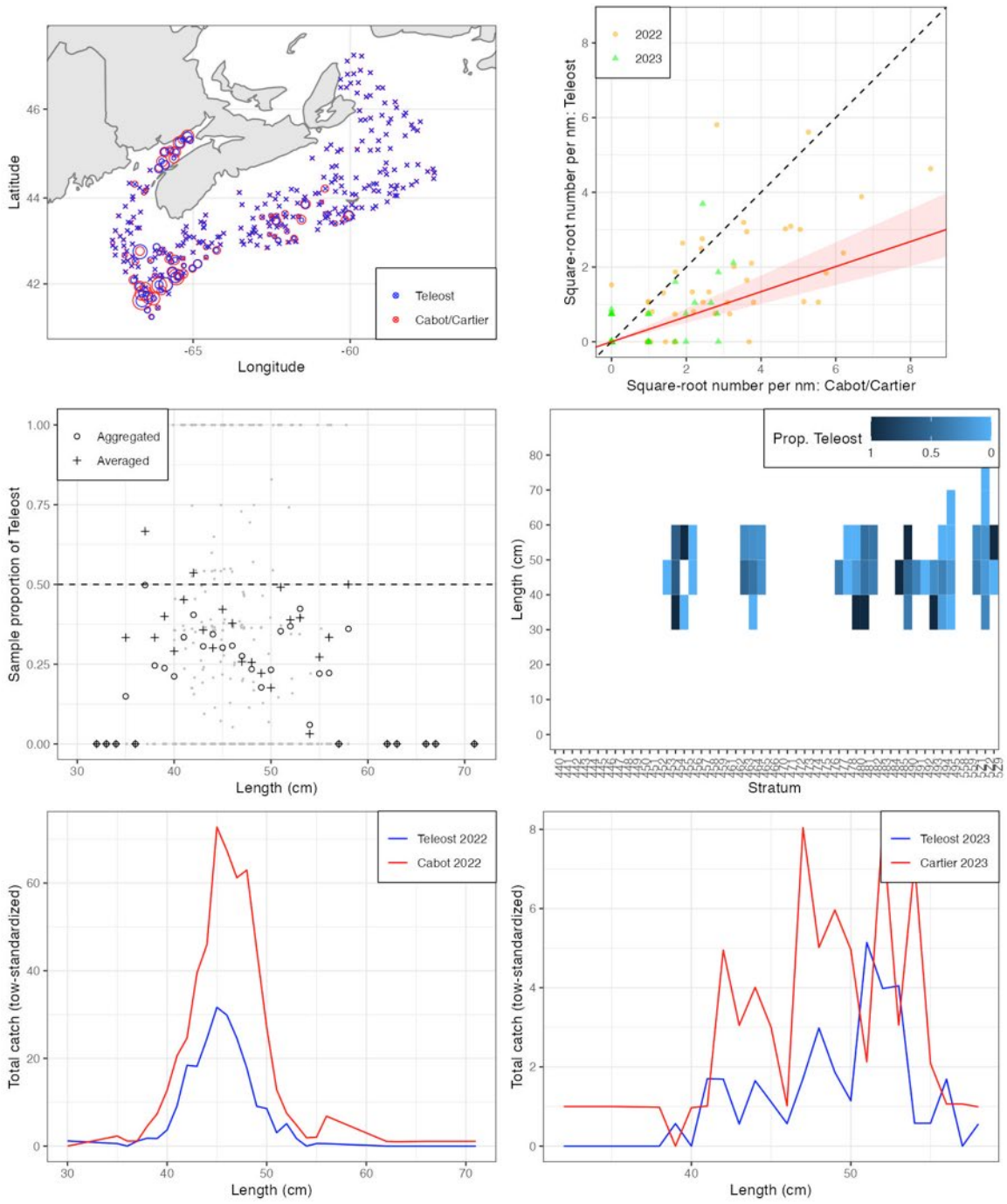

Figure 36a. Visualisation of comparative fishing data and size-aggregated model fit for Leucoraja erinacea (203).

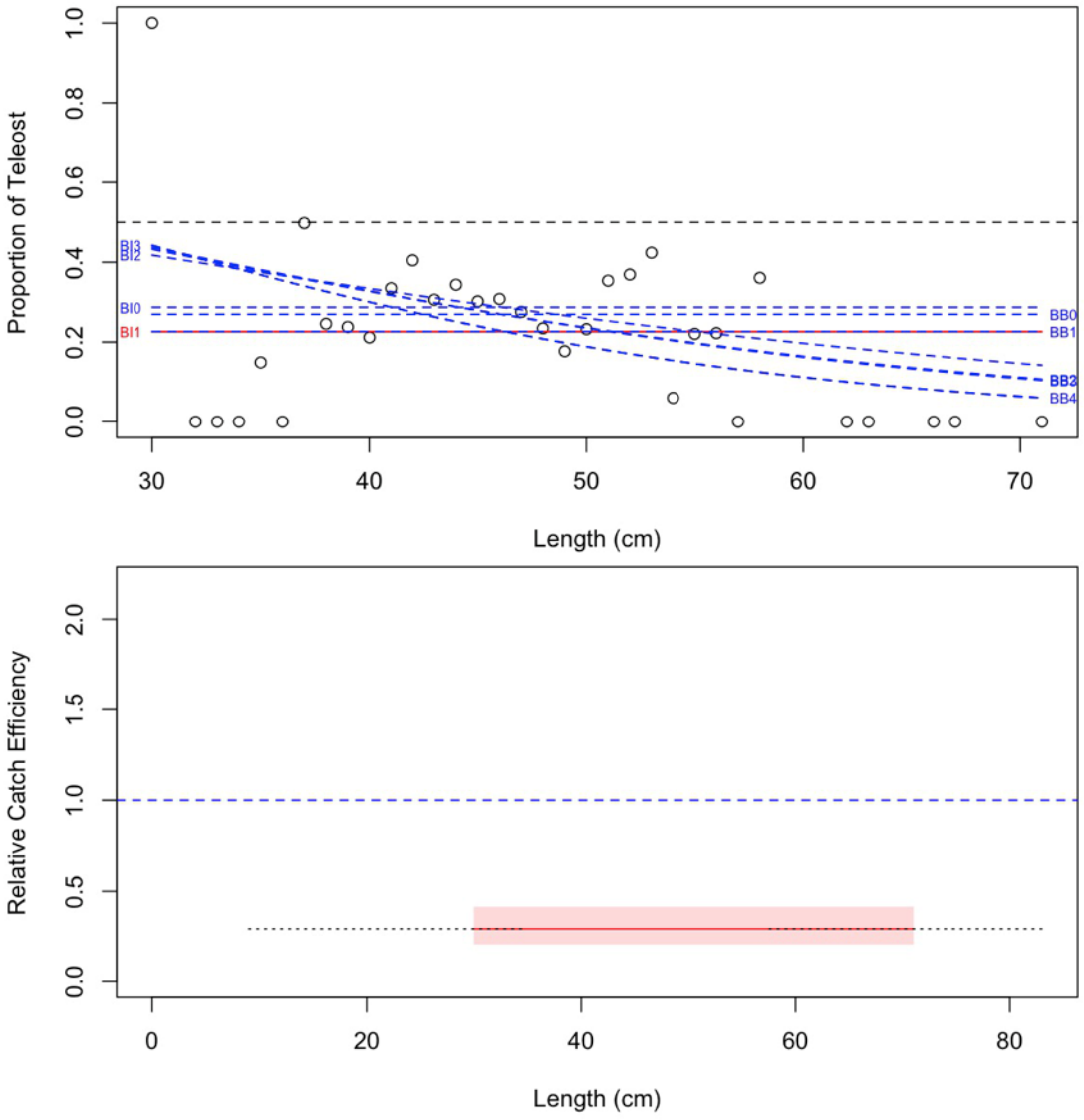

Figure 36b. Model fits and the selected length-based calibration for Leucoraja erinacea (203).

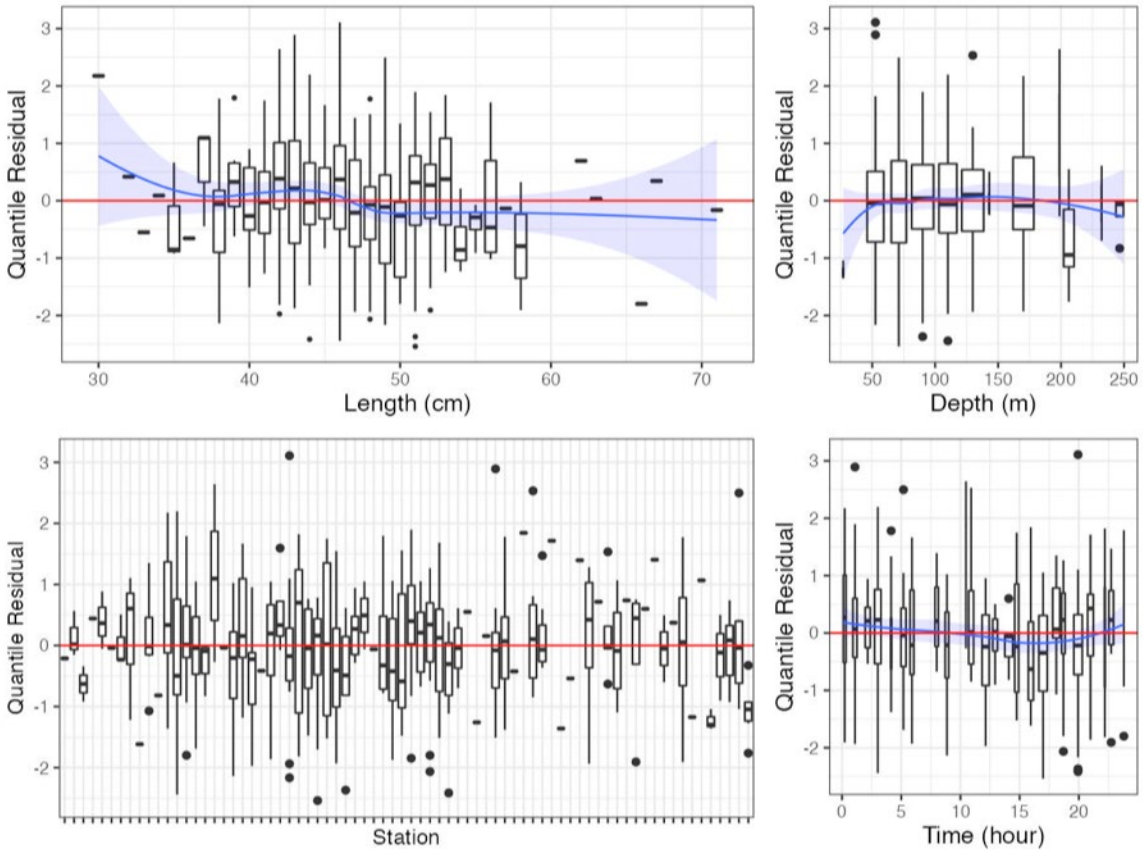

Figure 36c. Randomized and normalized quantile residuals for the selected model for Leucoraja erinacea (203).

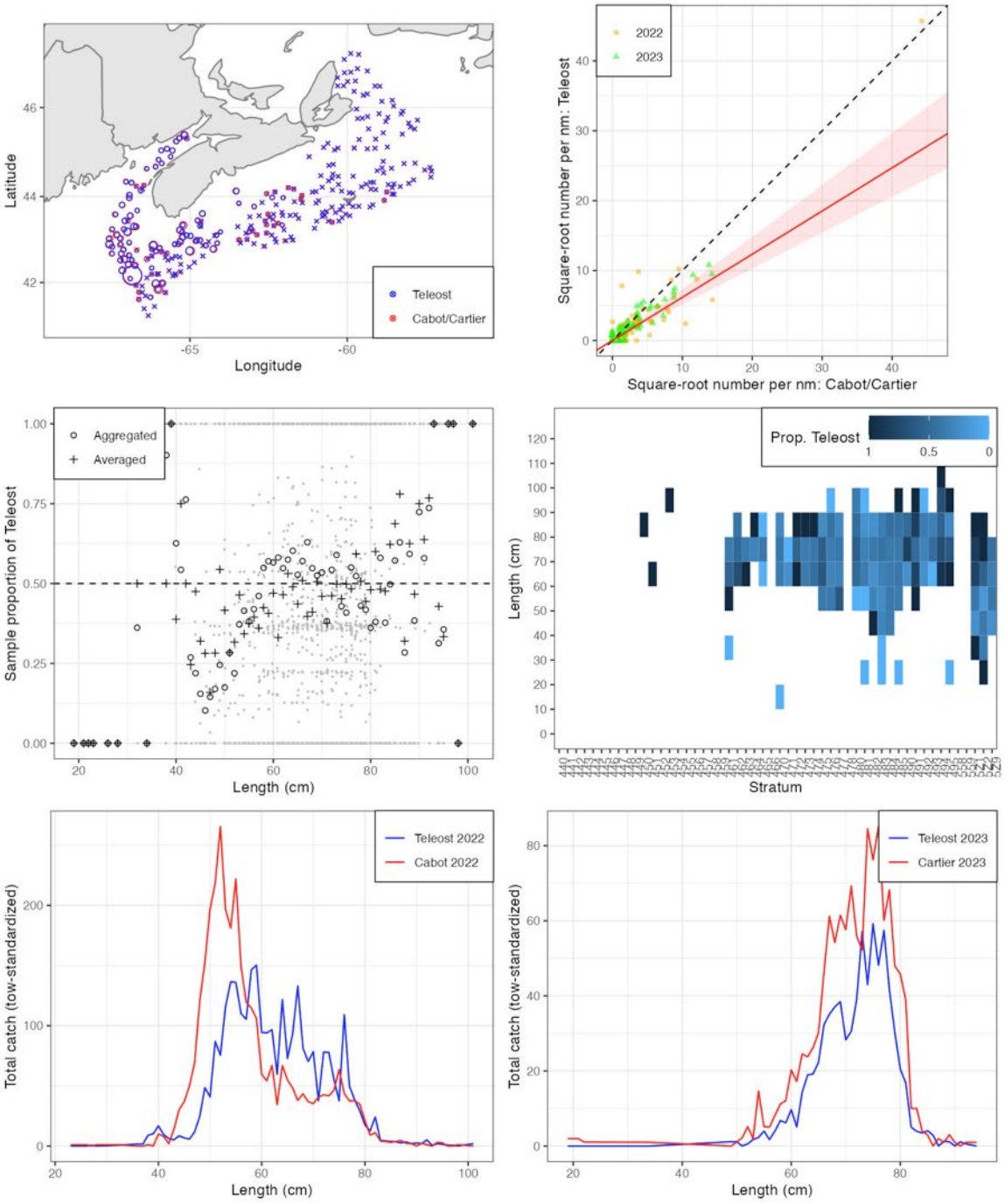

Figure 37a. Visualisation of comparative fishing data and size-aggregated model fit for Squalus acanthias (220).

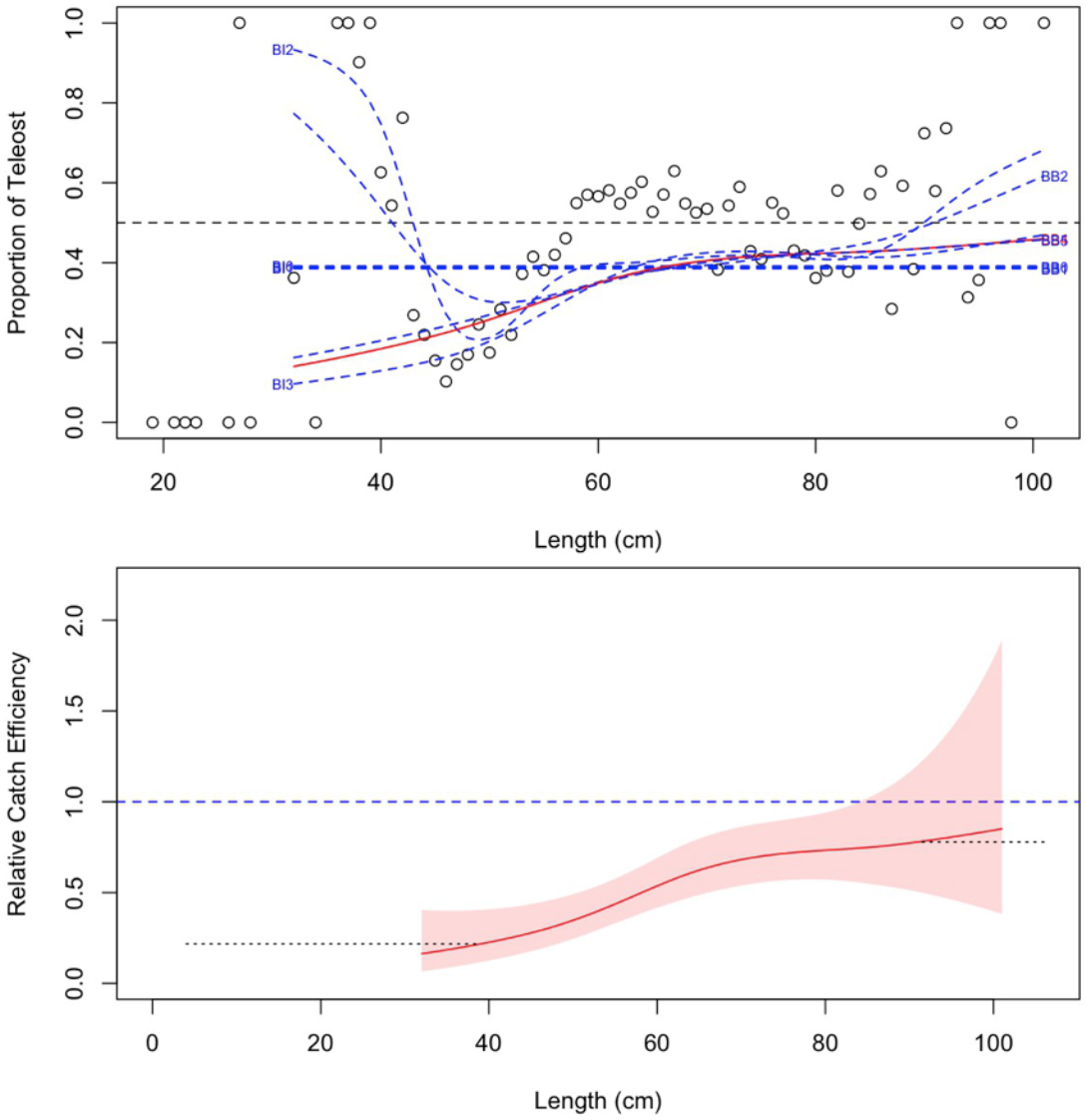

Figure 37b. Model fits and the selected length-based calibration for Squalus acanthias (220).

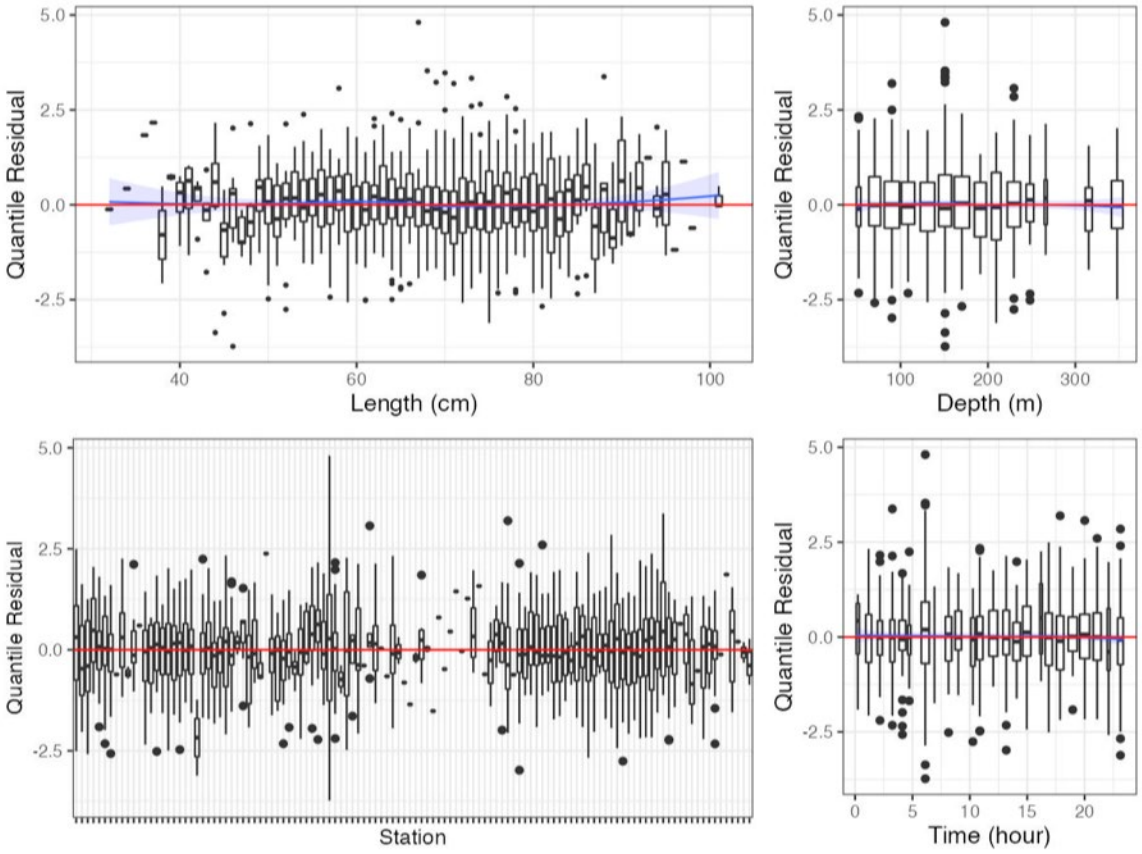

Figure 37c. Randomized and normalized quantile residuals for the selected model for Squalus acanthias (220).

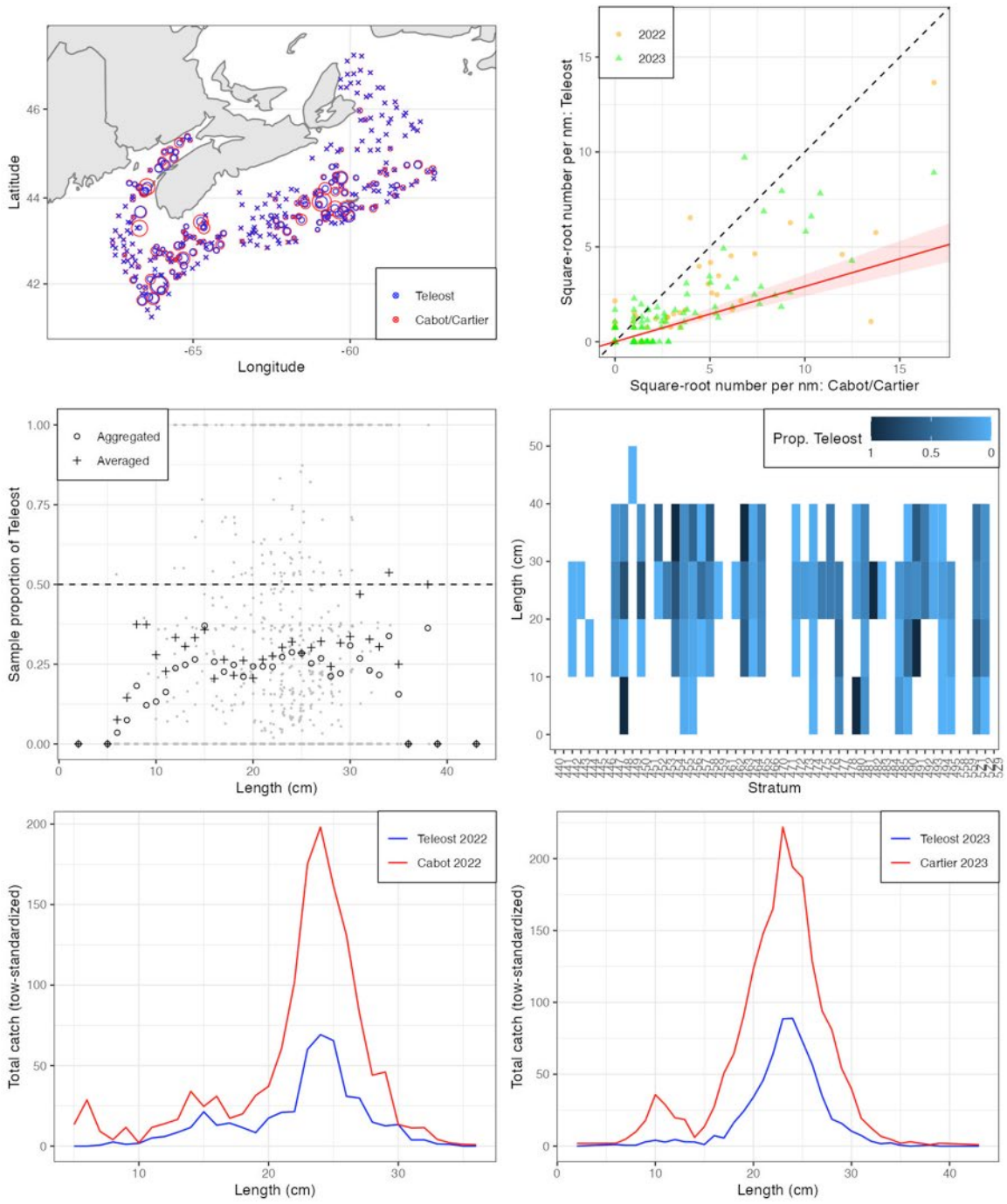

Figure 38a. Visualisation of comparative fishing data and size-aggregated model fit for Myoxocephalus octodecemspinosus (300).

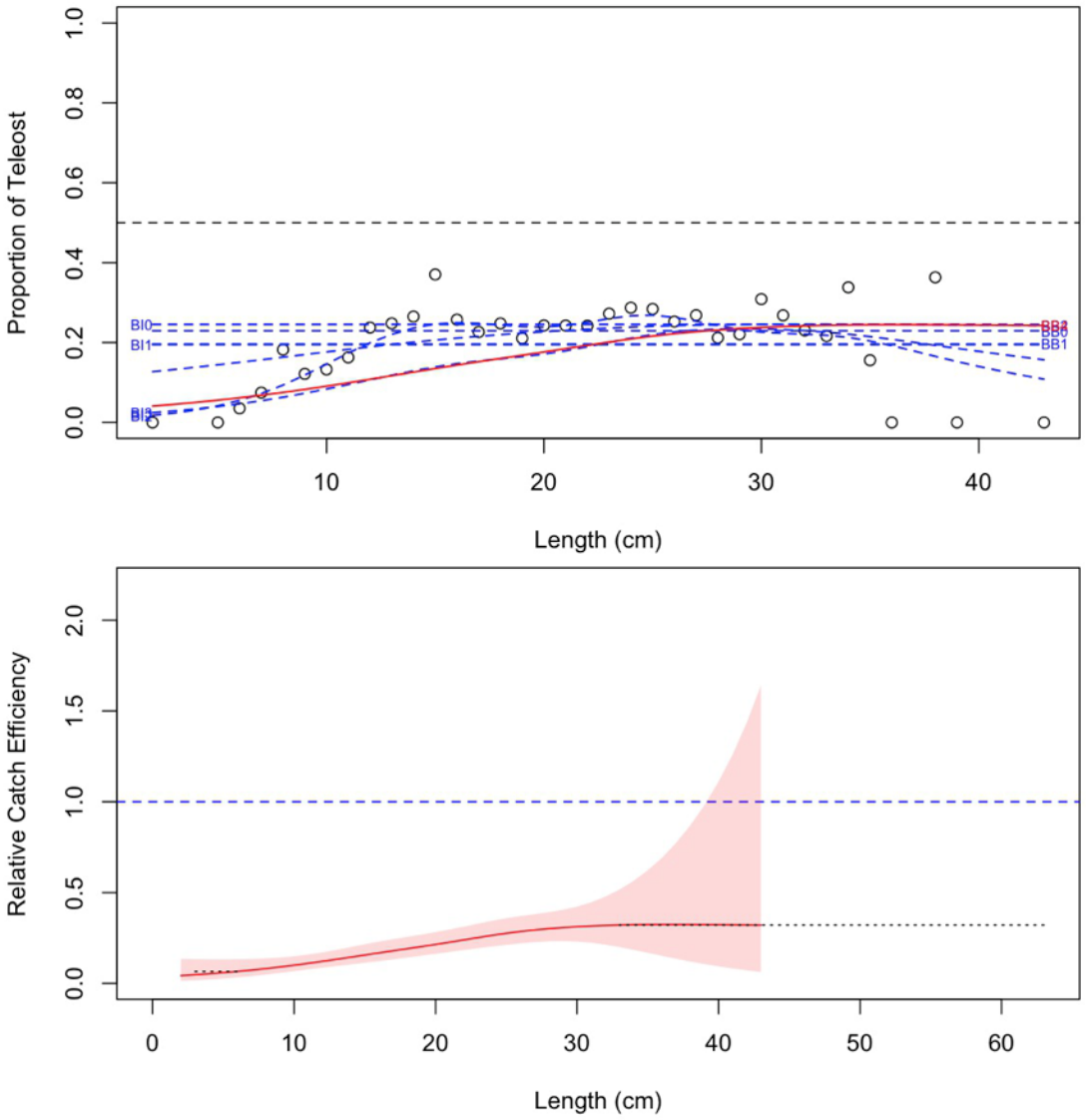

Figure 38b. Model fits and the selected length-based calibration for Myoxocephalus octodecemspinosus (300).

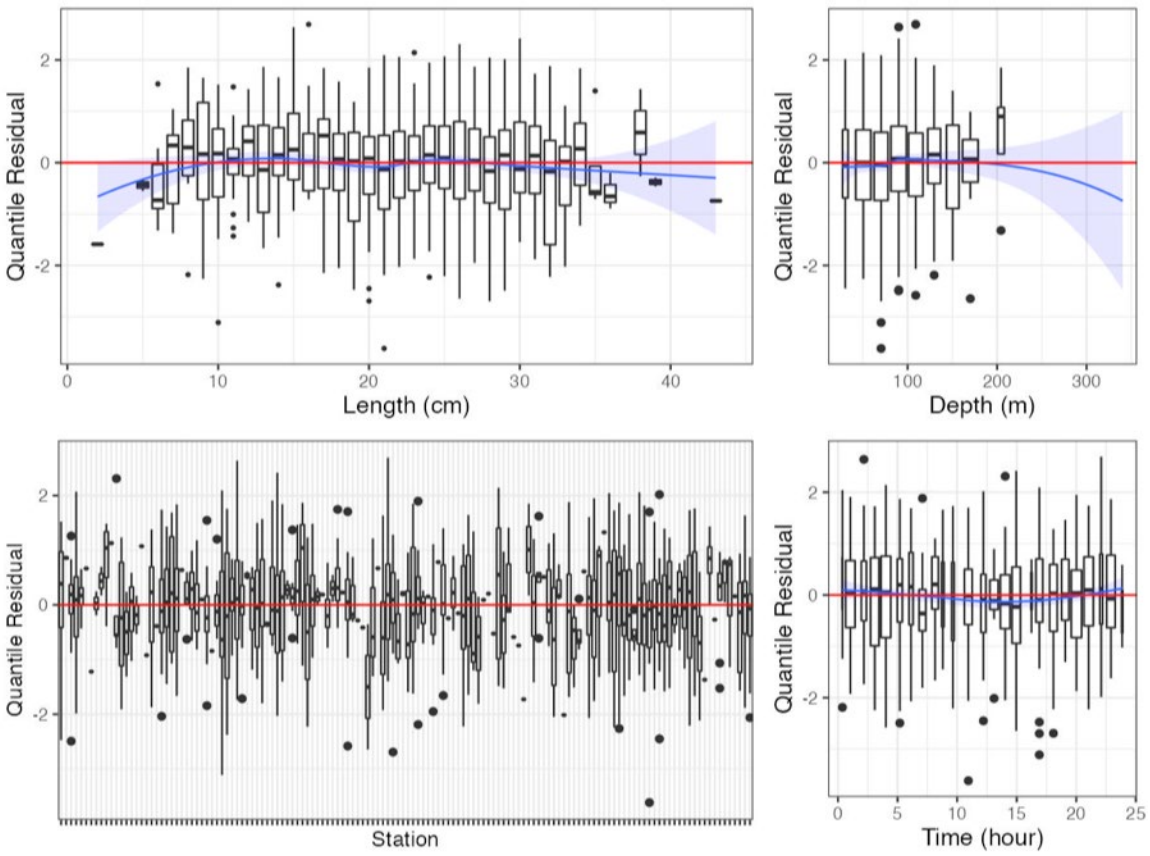

Figure 38c. Randomized and normalized quantile residuals for the selected model for Myoxocephalus octodecemspinosus (300).

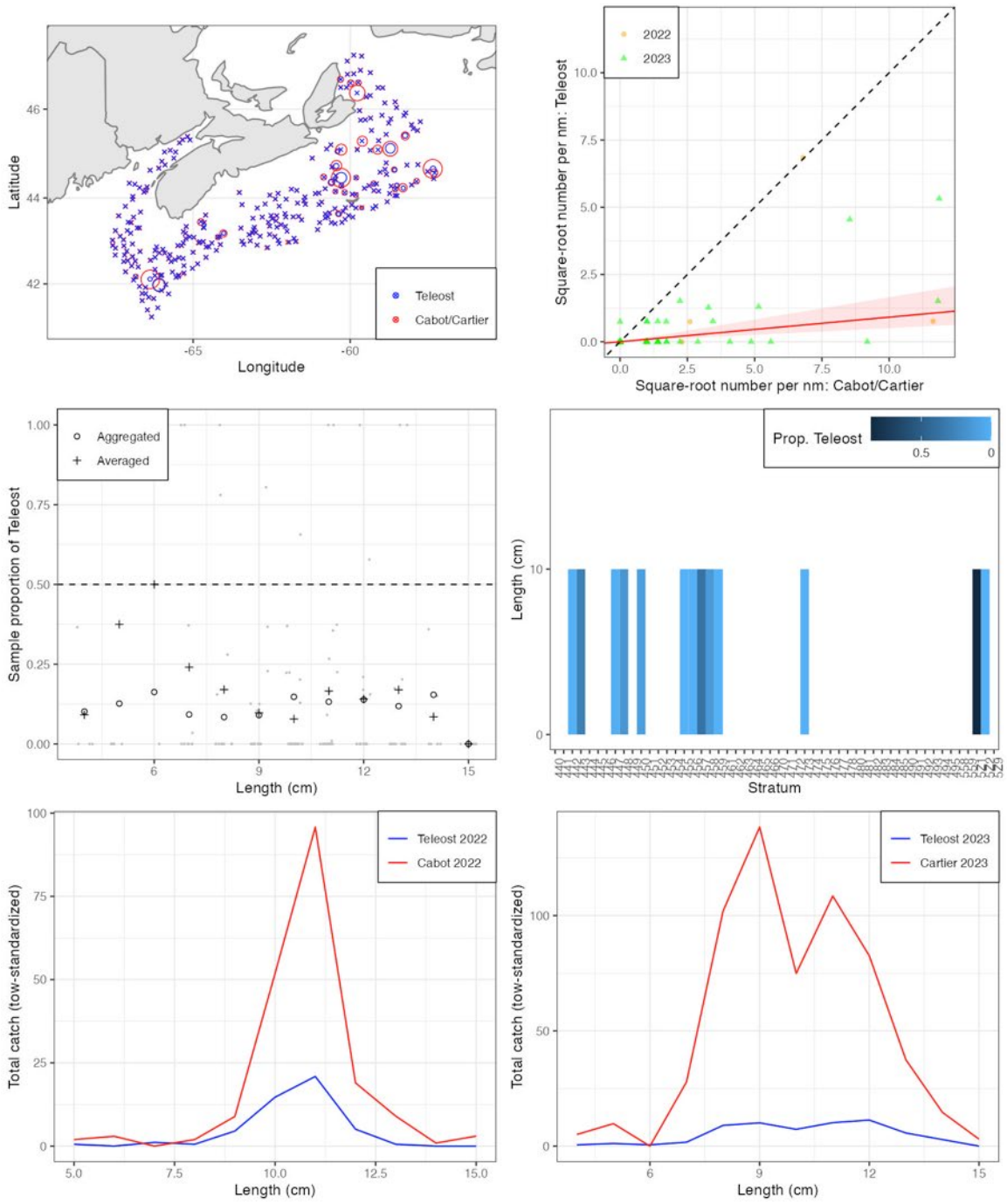

Figure 39a. Visualisation of comparative fishing data and size-aggregated model fit for Triglops murrayi (304).

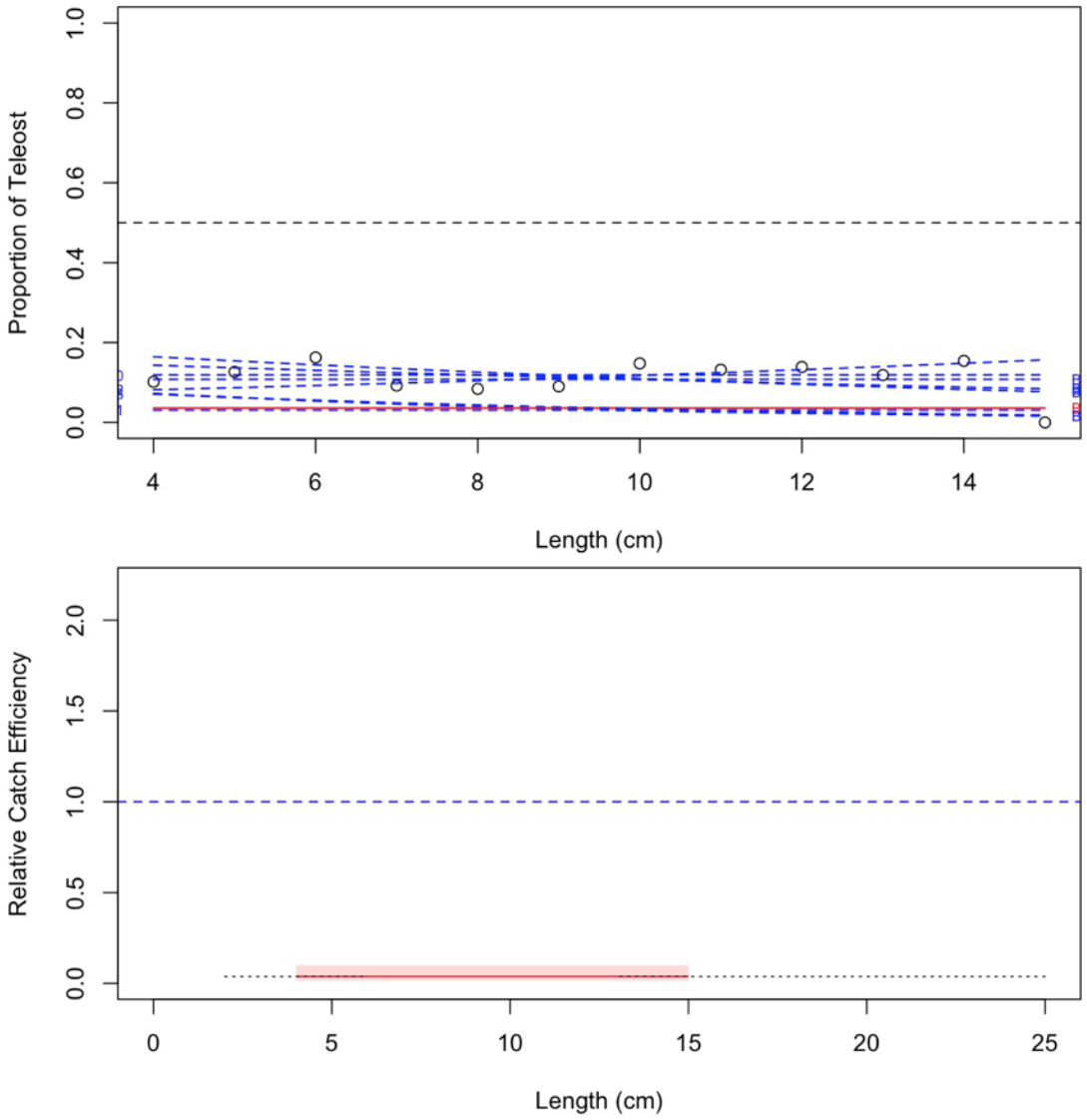

Figure 39b. Model fits and the selected length-based calibration for Triglops murrayi (304).

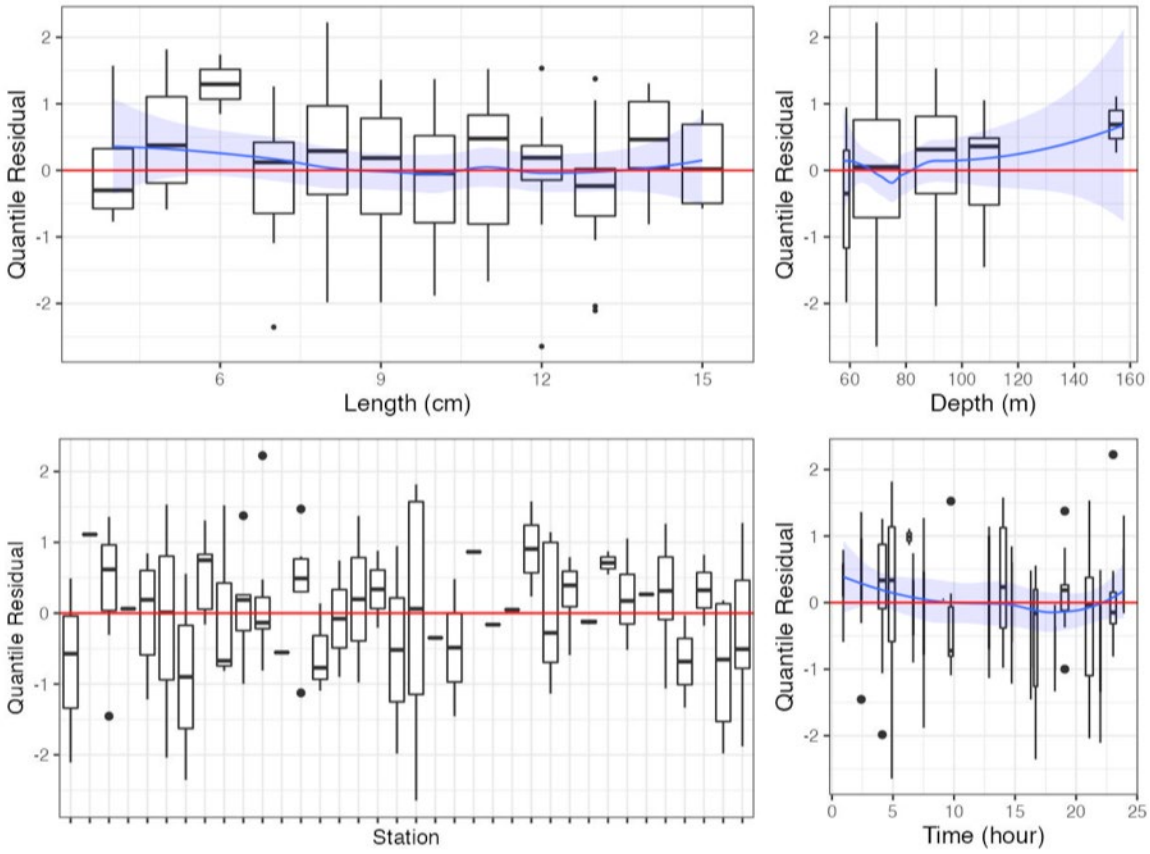

Figure 39c. Randomized and normalized quantile residuals for the selected model for Triglops murrayi (304).

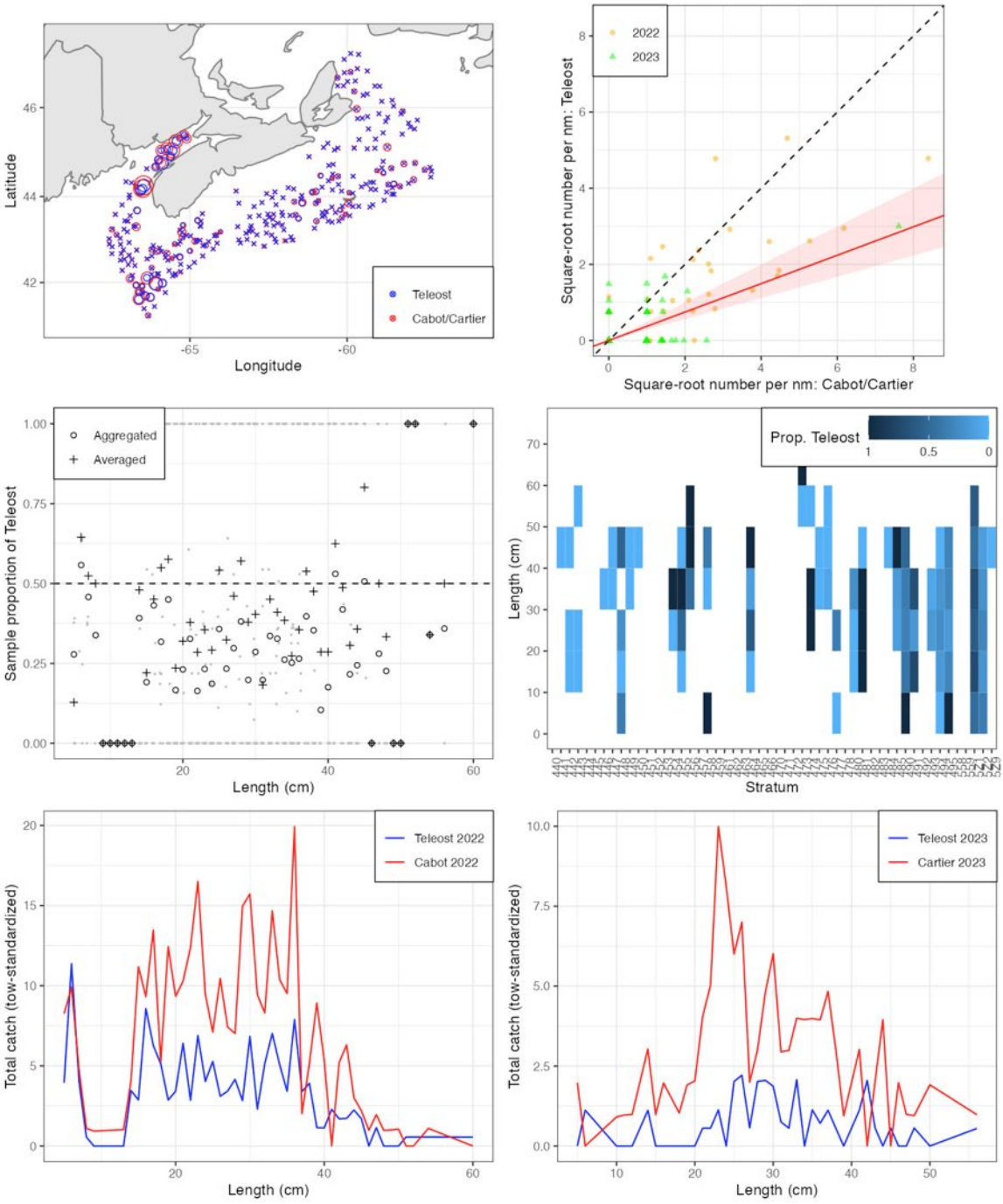

Figure 40a. Visualisation of comparative fishing data and size-aggregated model fit for Hemitripterus americanus (320).

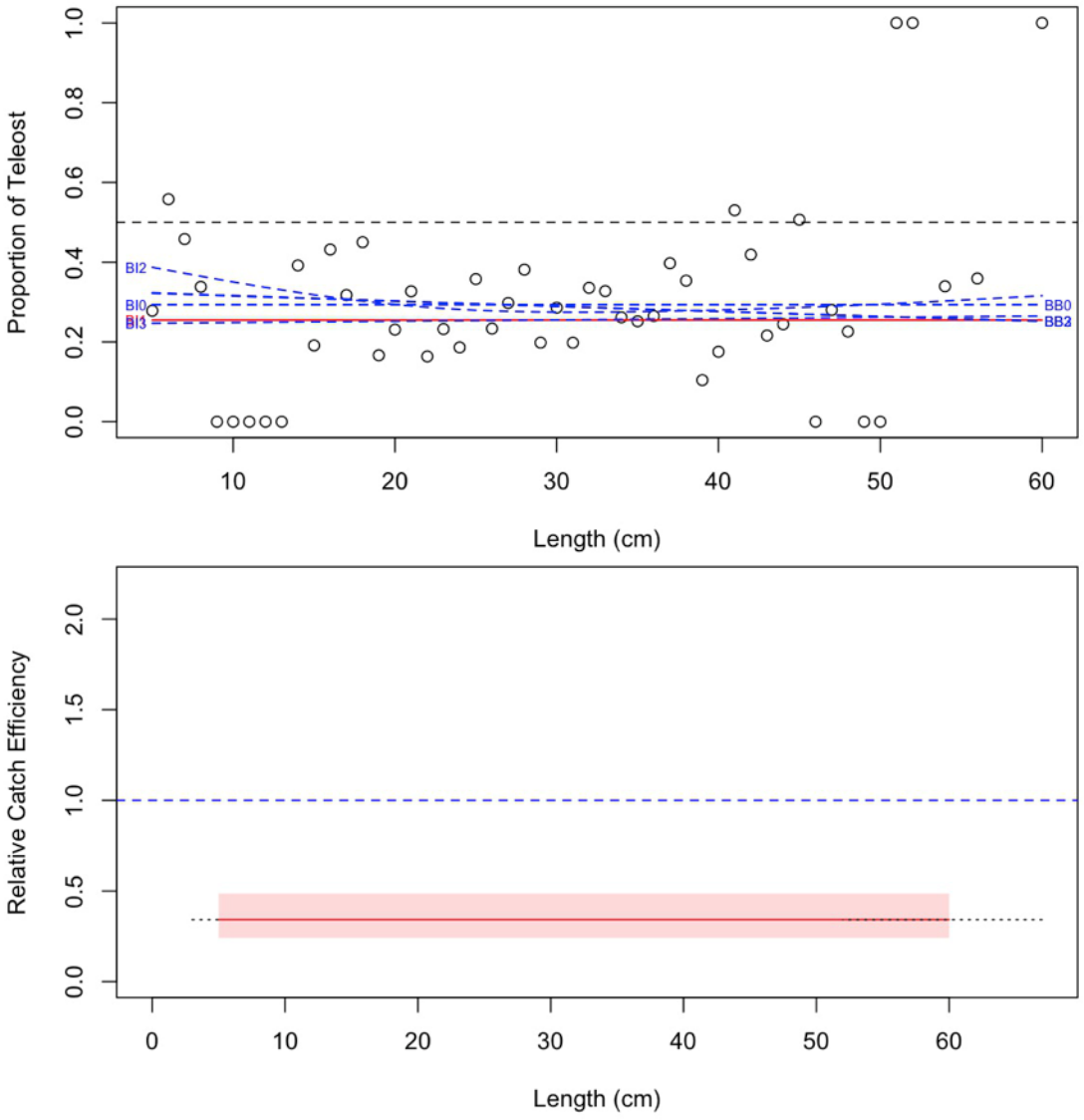

Figure 40b. Model fits and the selected length-based calibration for Hemitripterus americanus (320).

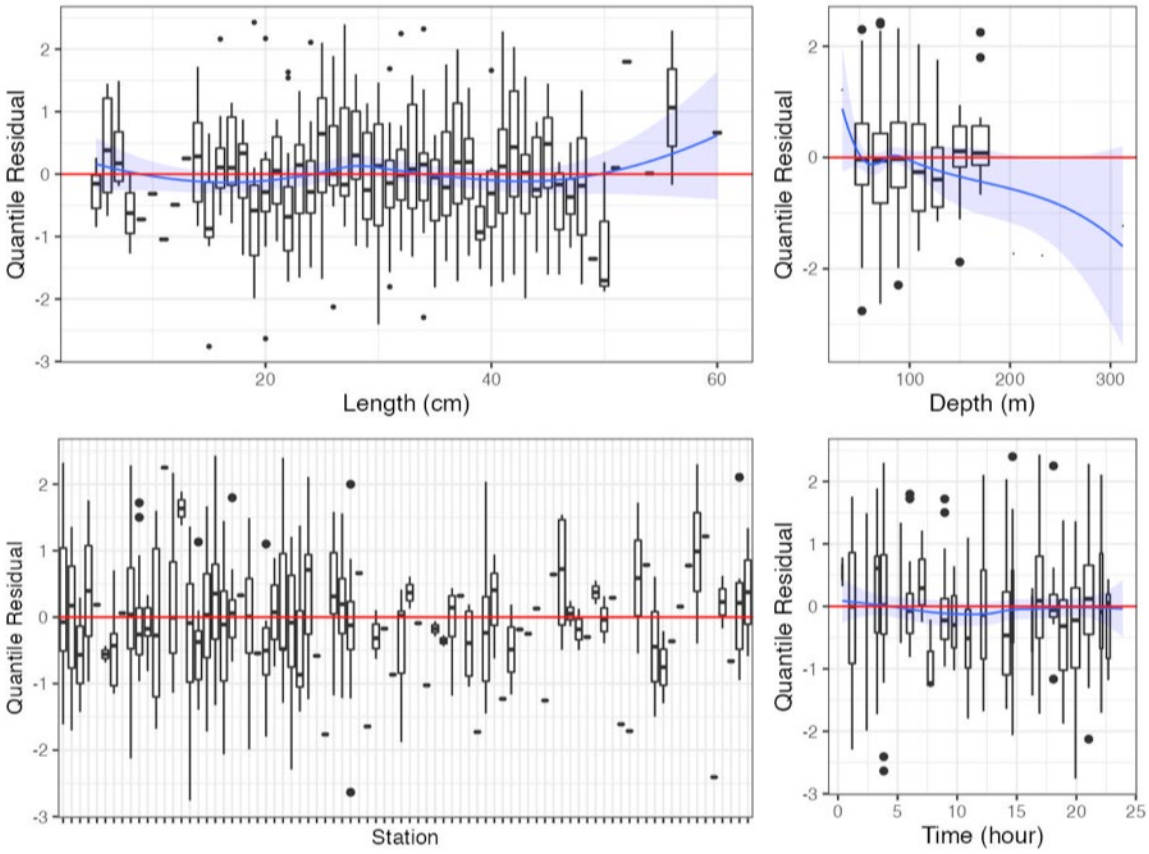

Figure 40c. Randomized and normalized quantile residuals for the selected model for Hemitripterus americanus (320).

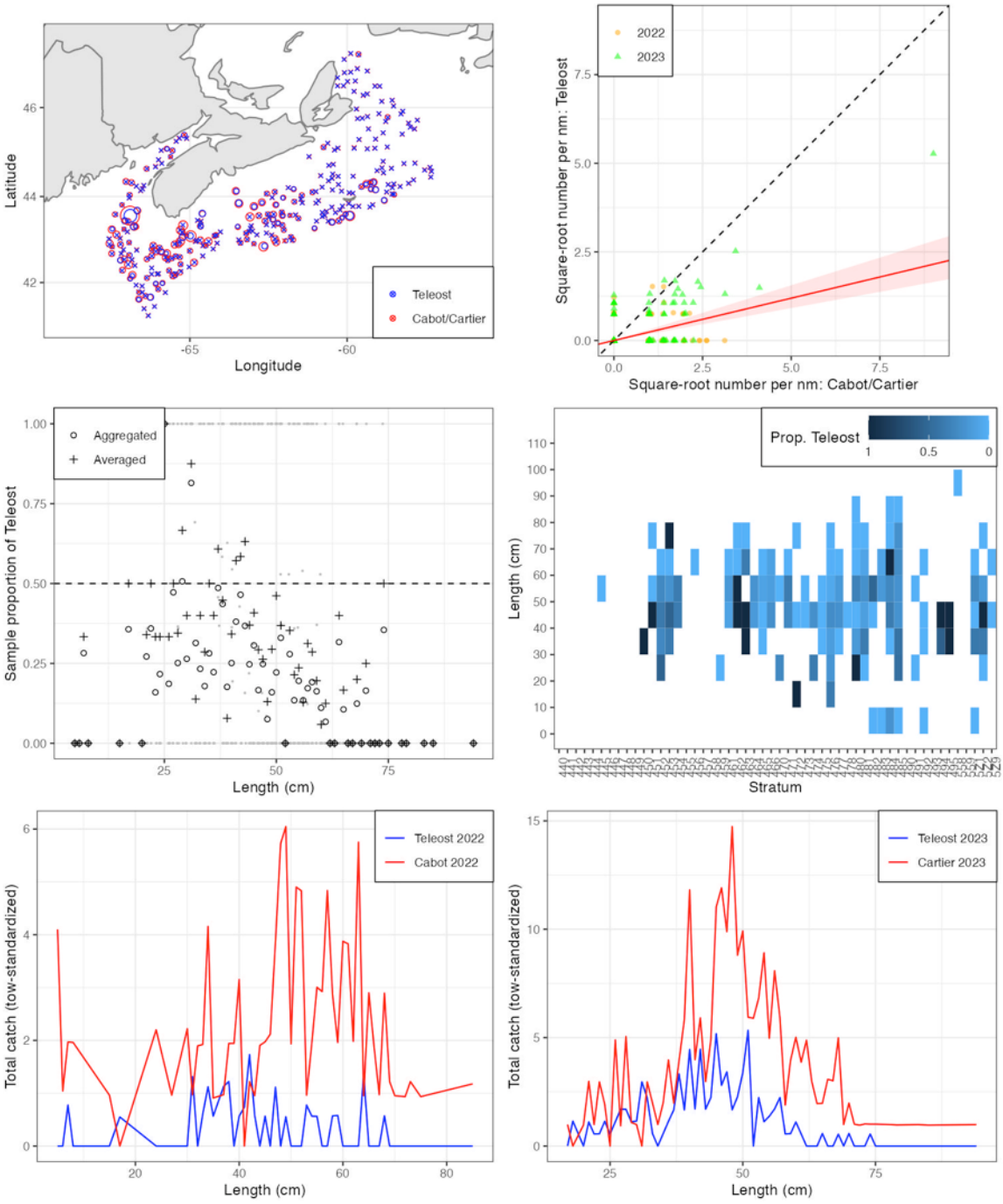

Figure 41a. Visualisation of comparative fishing data and size-aggregated model fit for Lophius americanus (400).

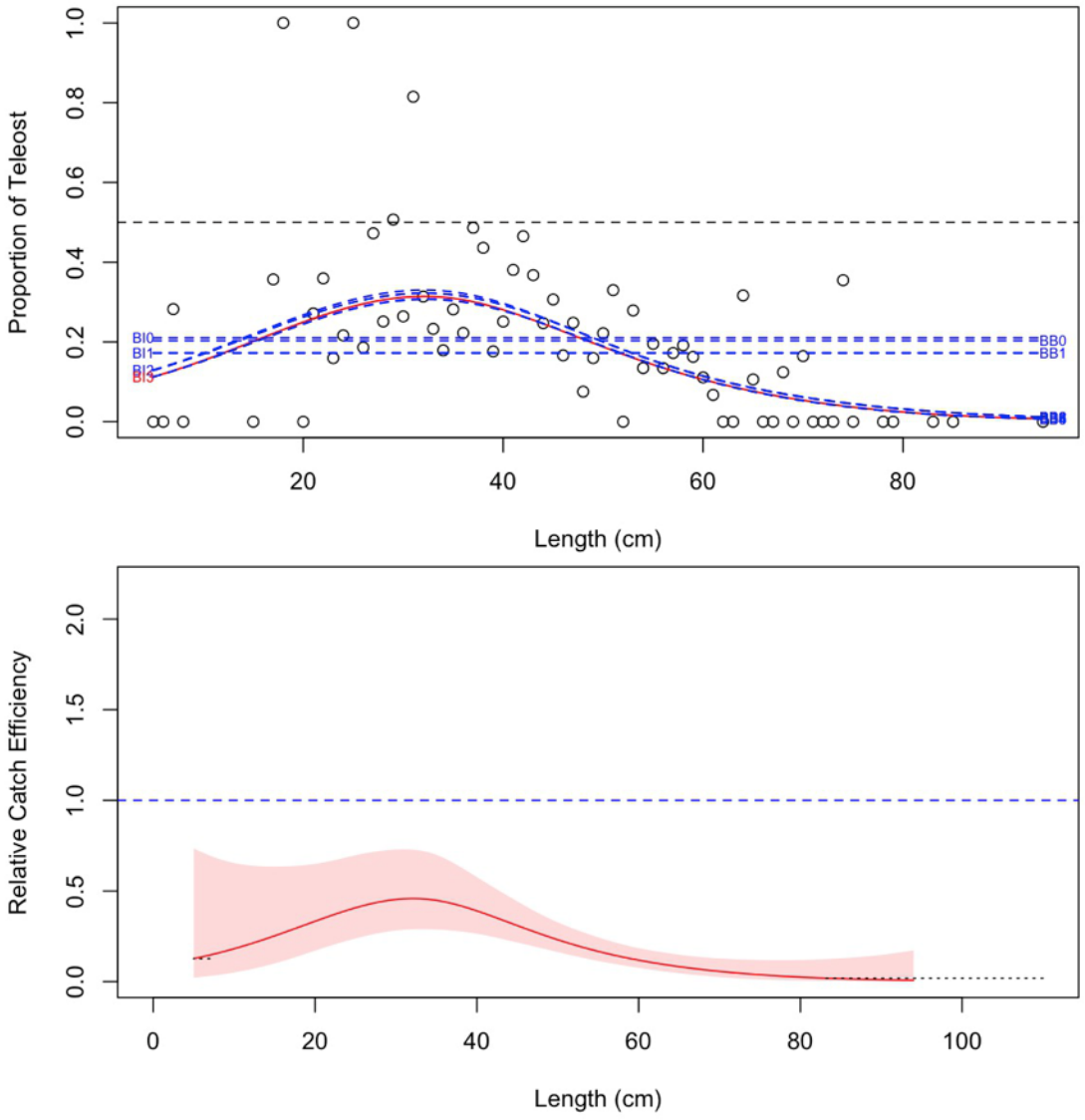

Figure 41b. Model fits and the selected length-based calibration for Lophius americanus (400).

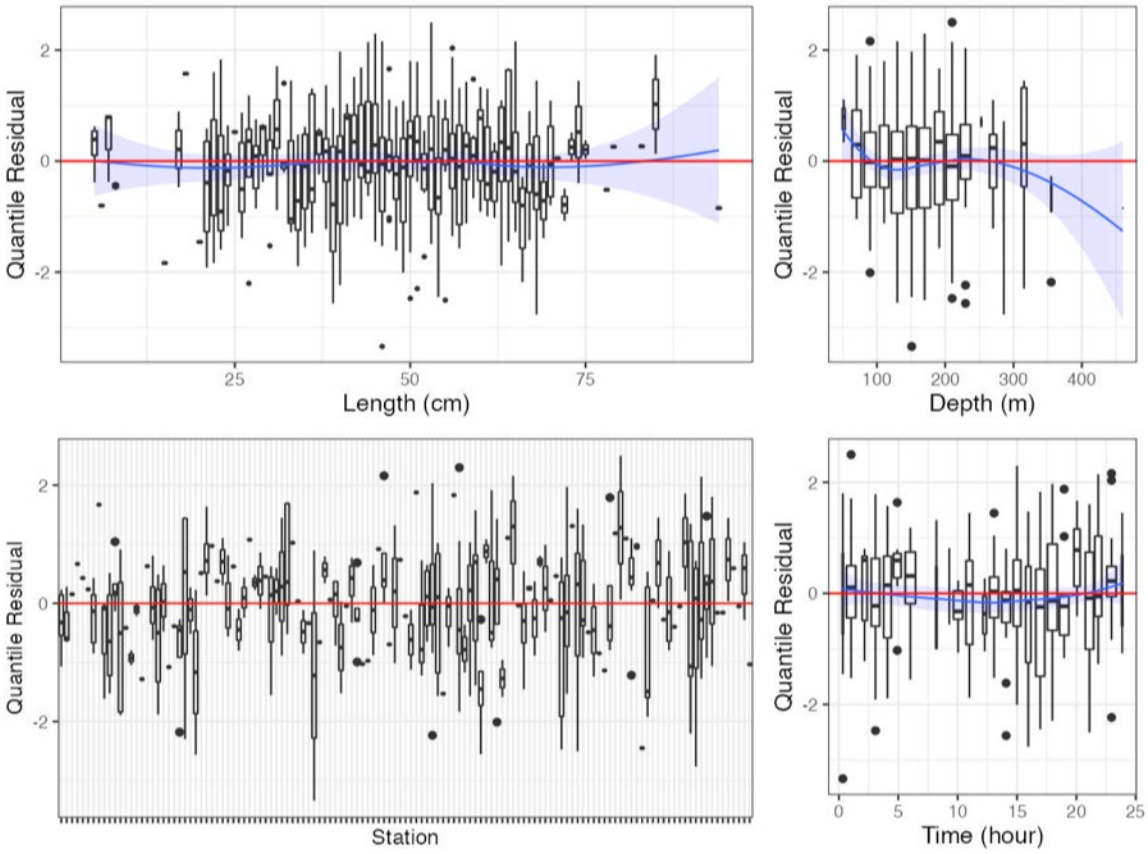

Figure 41c. Randomized and normalized quantile residuals for the selected model for Lophius americanus (400).

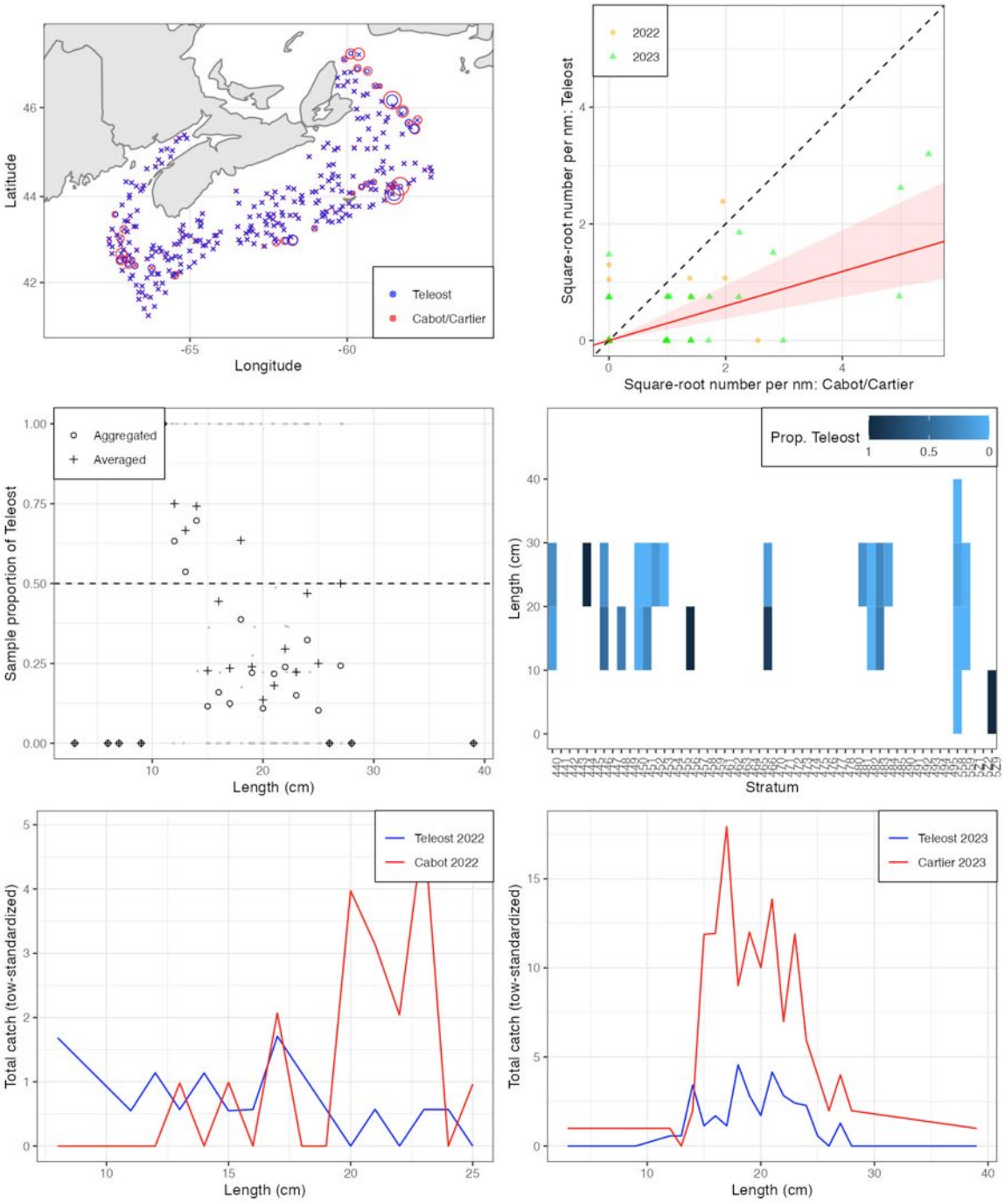

Figure 42a. Visualisation of comparative fishing data and size-aggregated model fit for Notolepis rissoi (712).

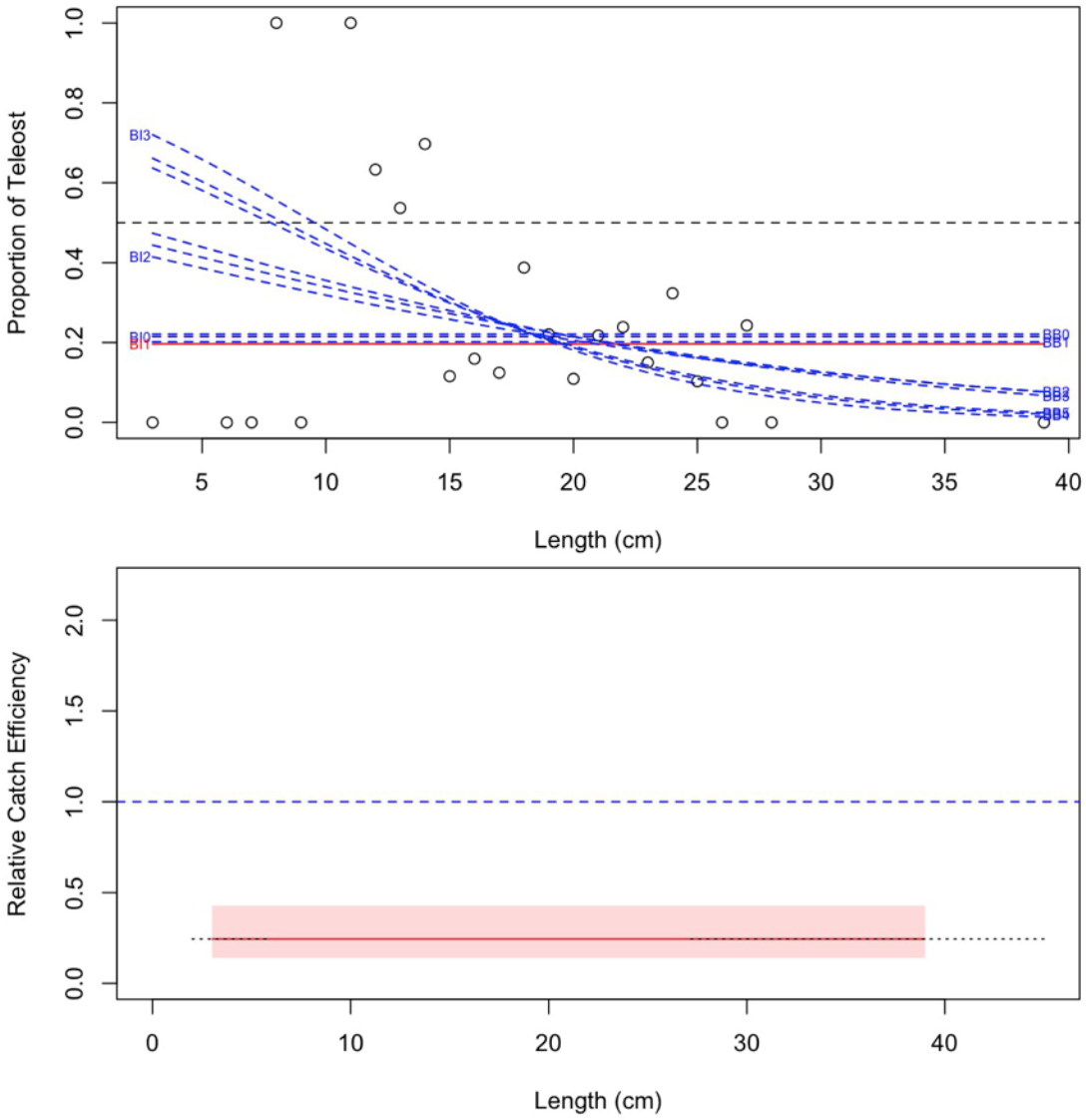

Figure 42b. Model fits and the selected length-based calibration for Notolepis rissoi (712).

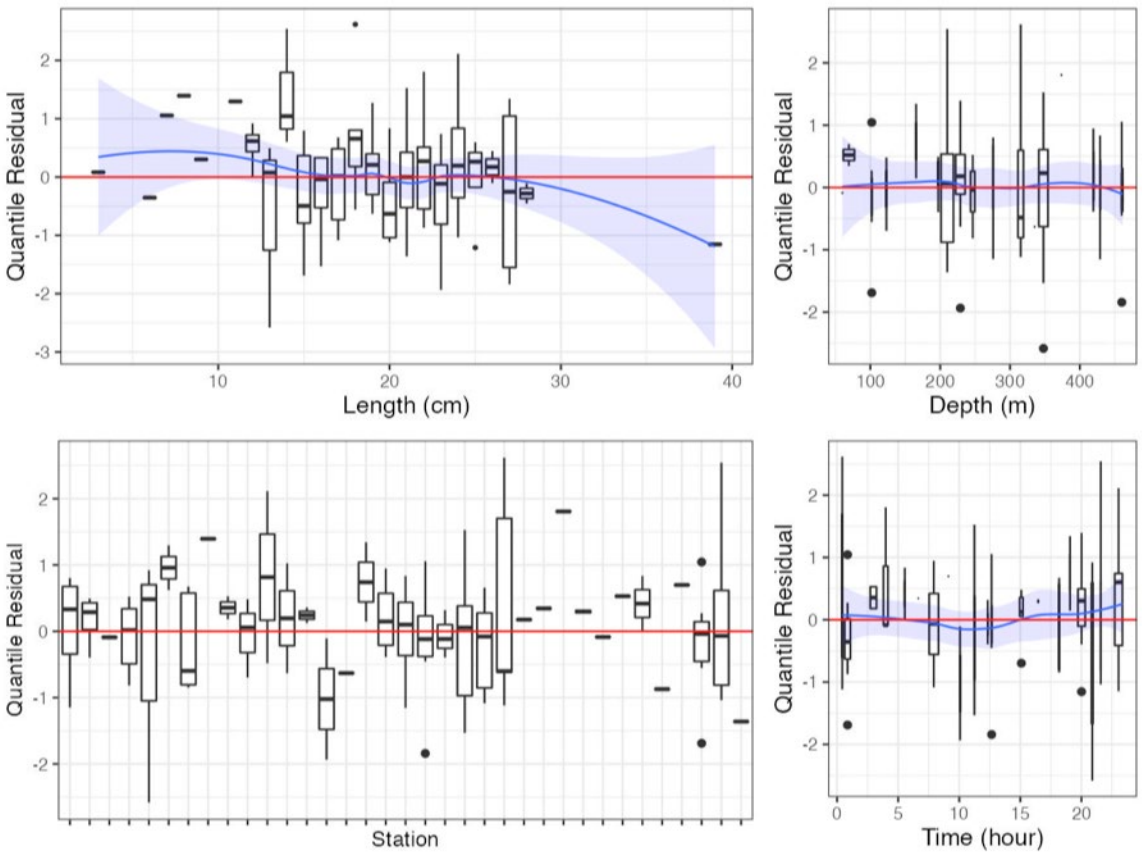

Figure 42c. Randomized and normalized quantile residuals for the selected model for Notolepis rissoi (712).

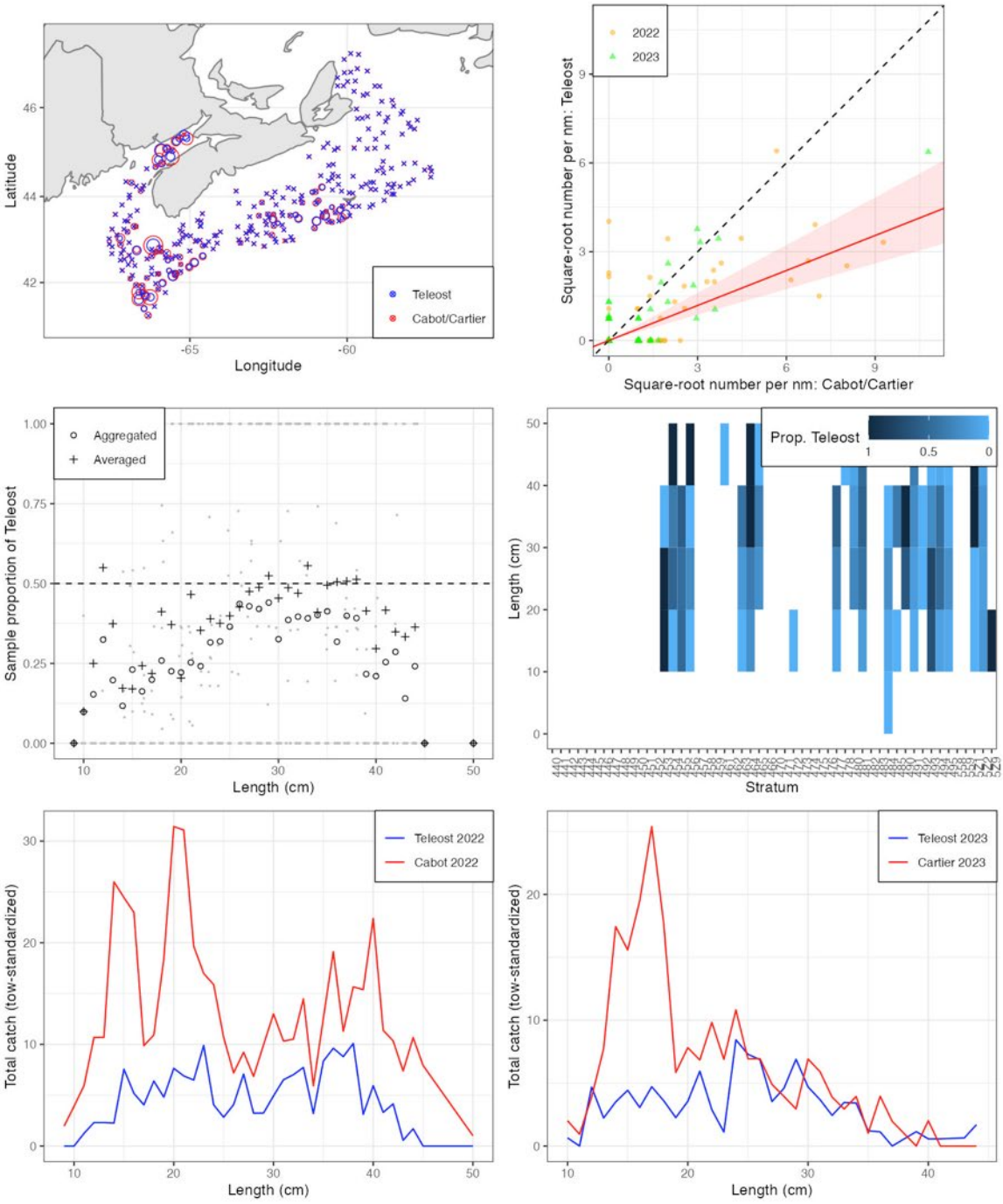

Figure 43a. Visualisation of comparative fishing data and size-aggregated model fit for Leucoraja sp. (1191).

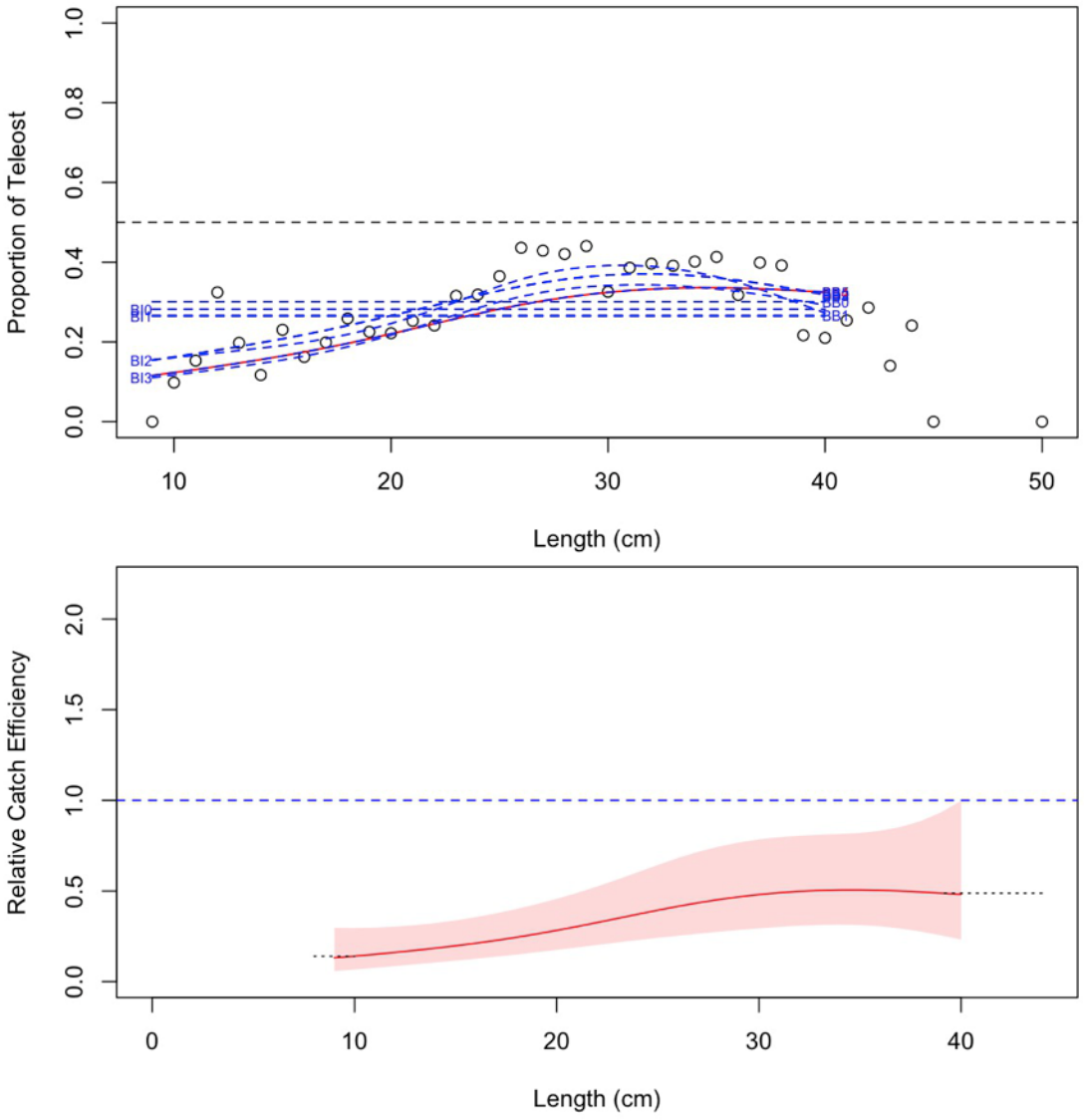

Figure 43b. Model fits and the selected length-based calibration for Leucoraja sp. (1191).

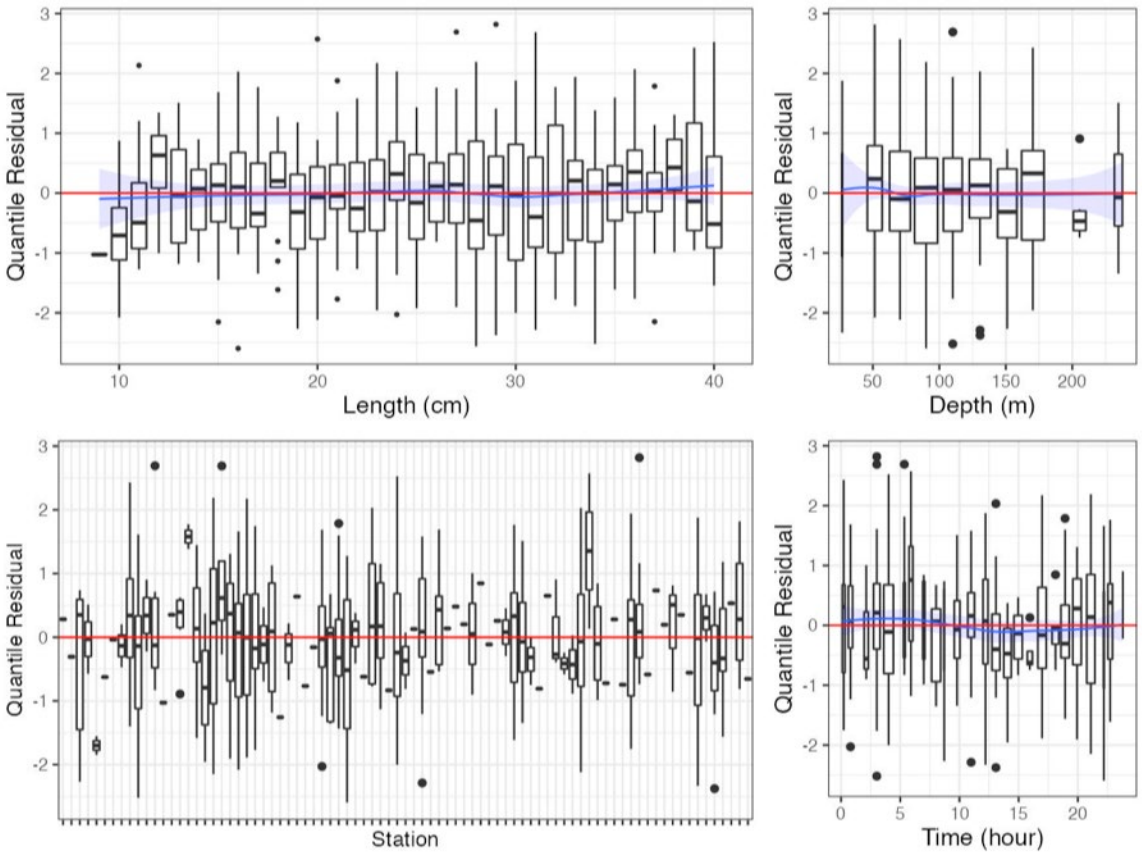

Figure 43c. Randomized and normalized quantile residuals for the selected model for Leucoraja sp. (1191).

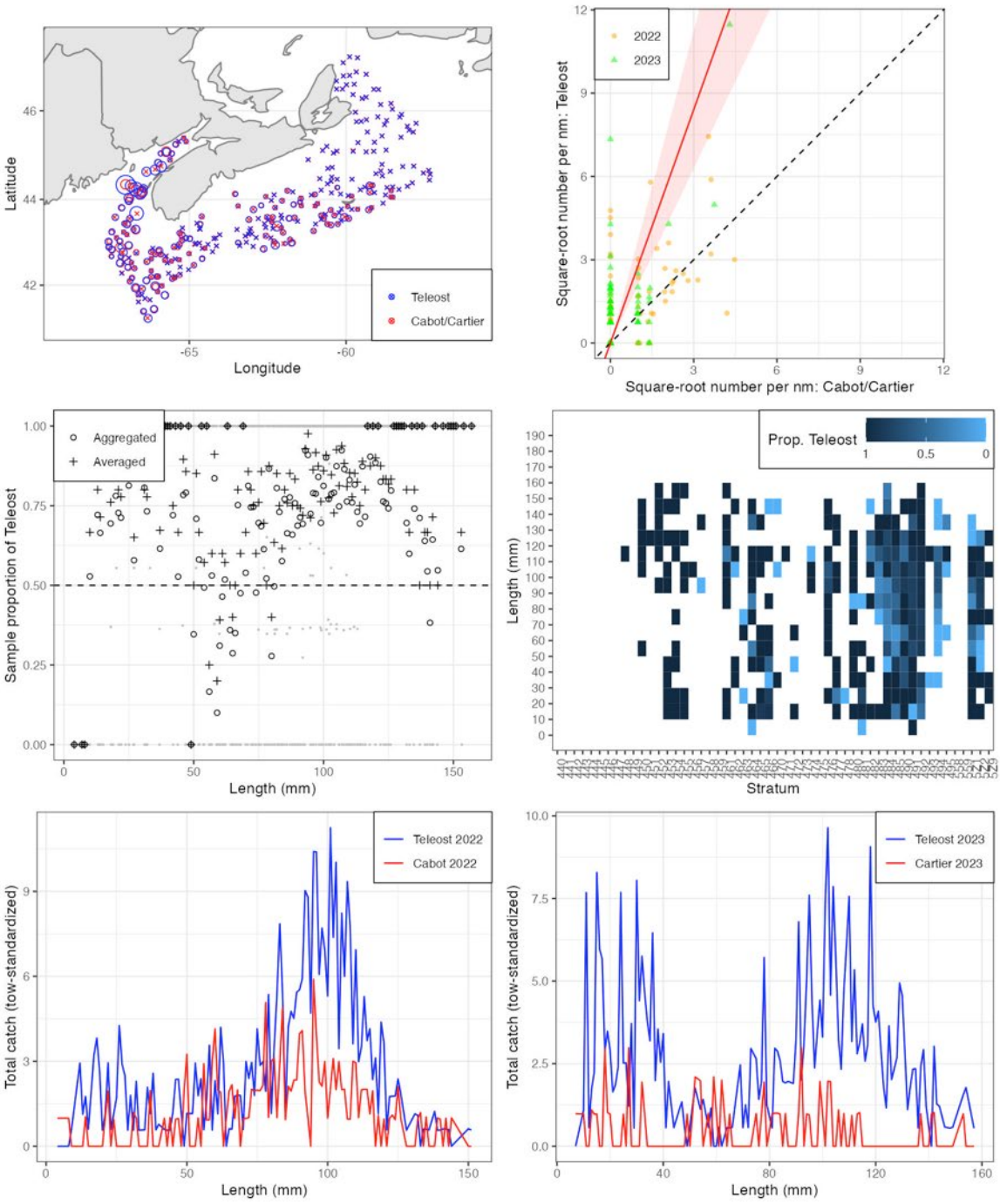

Figure 44a. Visualisation of comparative fishing data and size-aggregated model fit for Cancer borealis (2511).

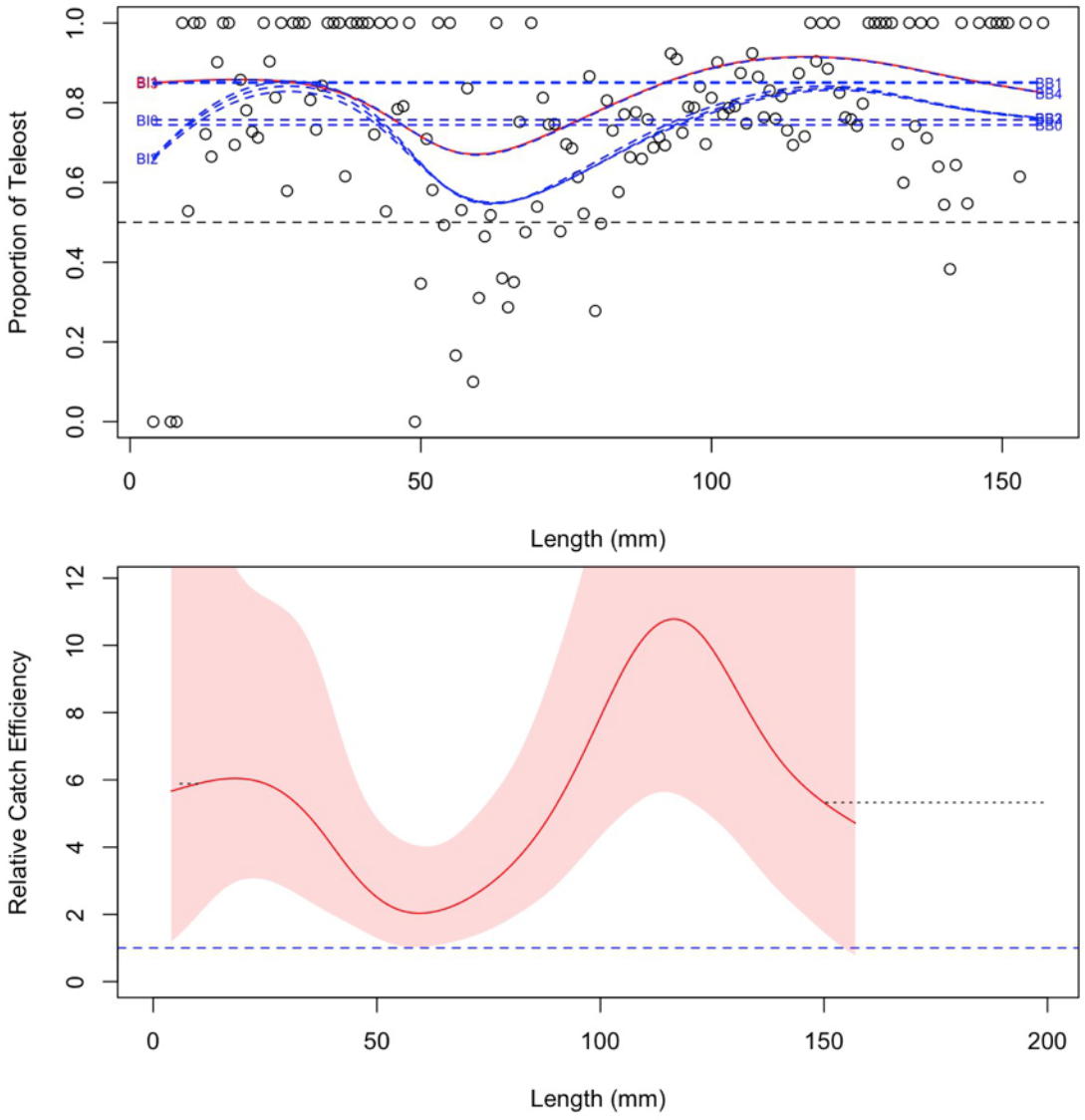

Figure 44b. Model fits and the selected length-based calibration for Cancer borealis (2511).

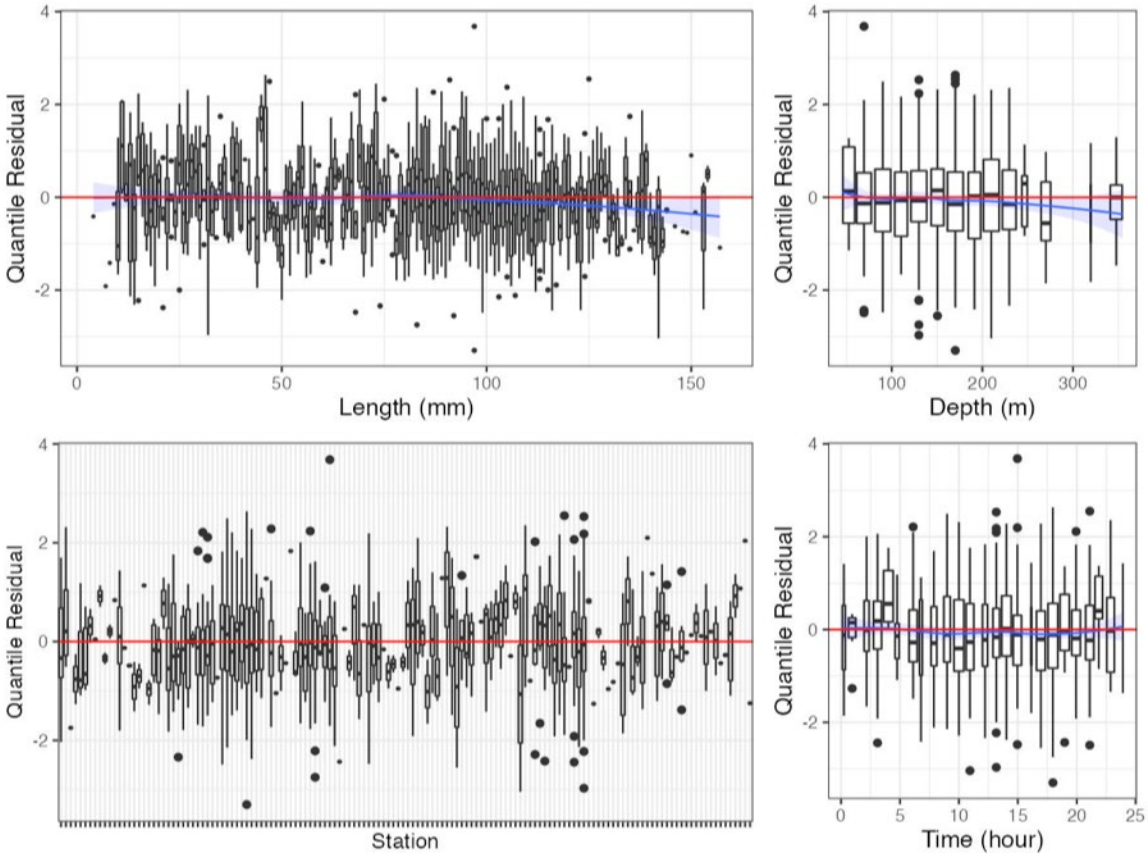

Figure 44c. Randomized and normalized quantile residuals for the selected model for Cancer borealis (2511).

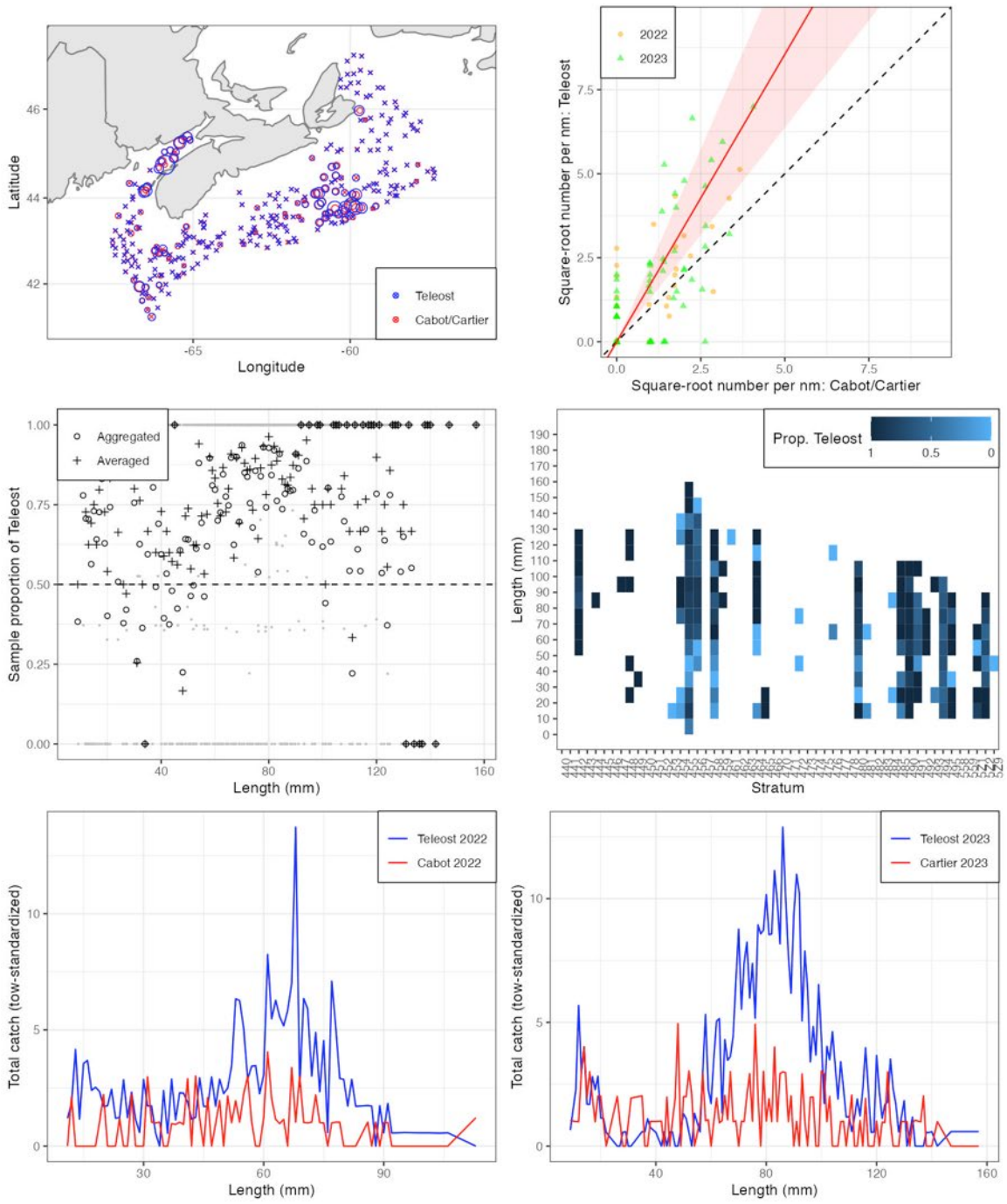

Figure 45a. Visualisation of comparative fishing data and size-aggregated model fit for Cancer irroratus (2513).

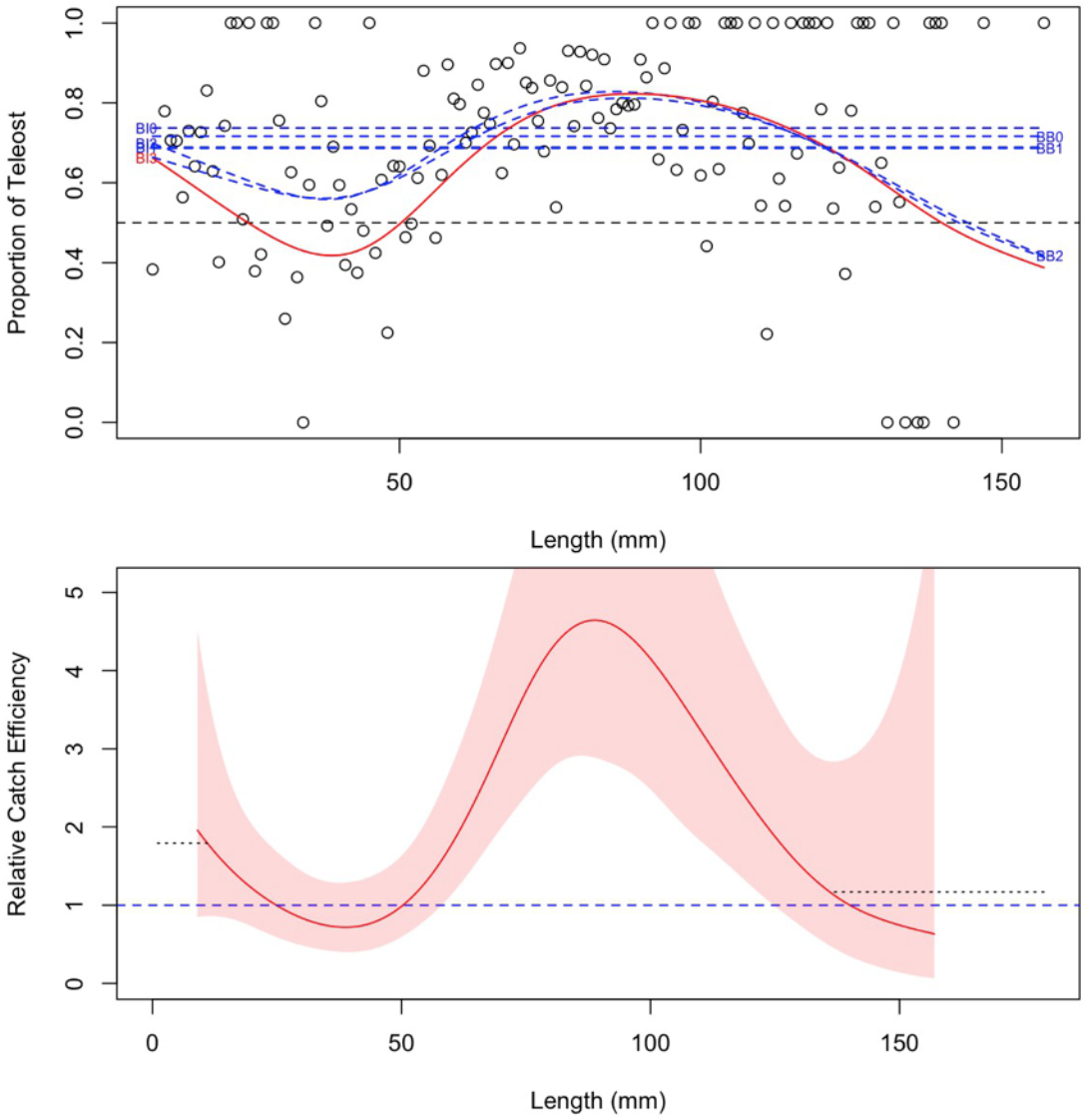

Figure 45b. Model fits and the selected length-based calibration for Cancer irroratus (2513).

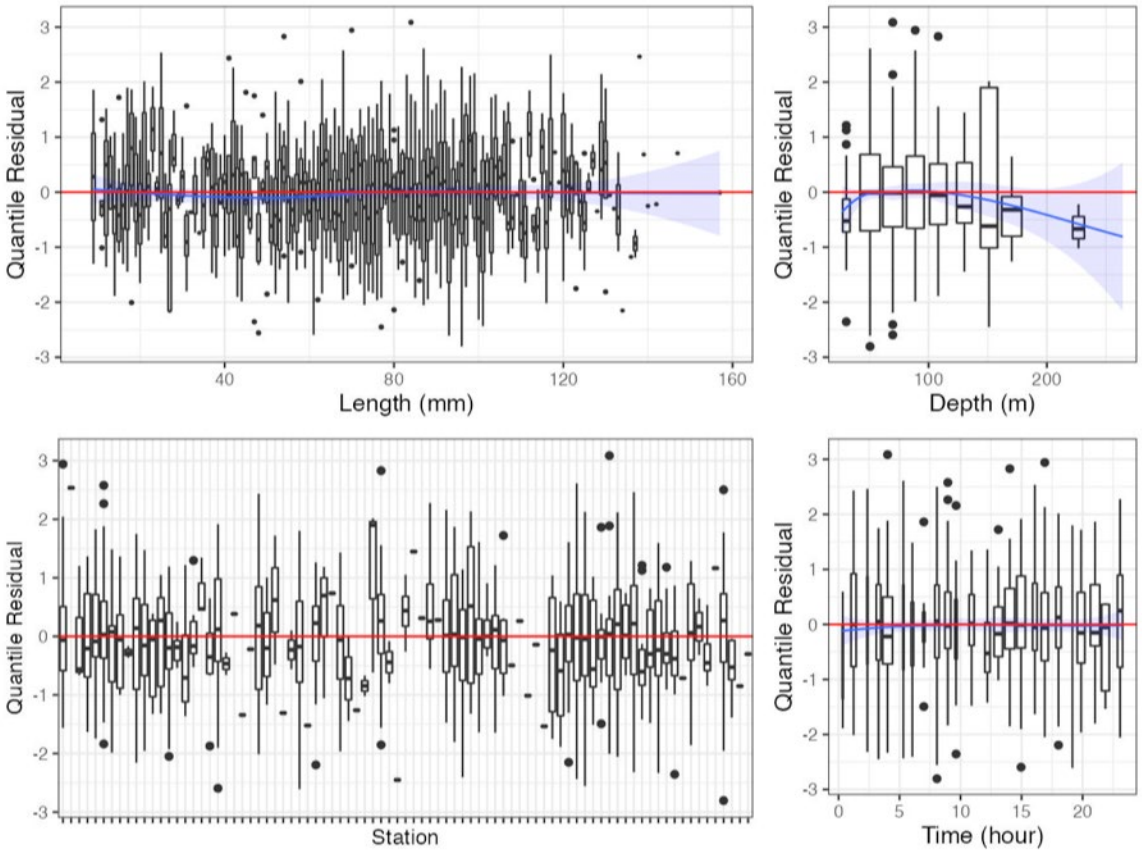

Figure 45c. Randomized and normalized quantile residuals for the selected model for Cancer irroratus (2513).

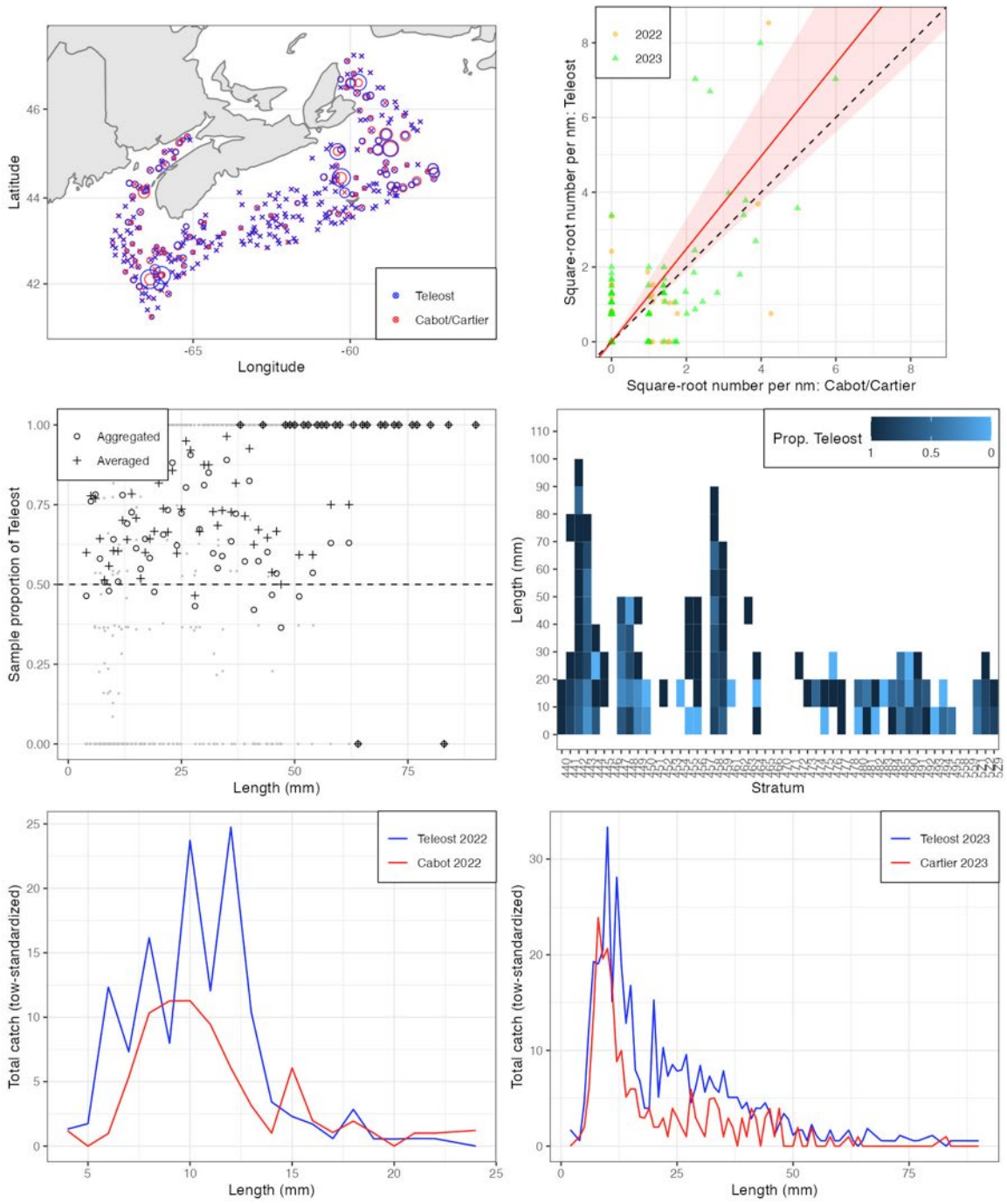

Figure 46a. Visualisation of comparative fishing data and size-aggregated model fit for Hyas sp. (2520).

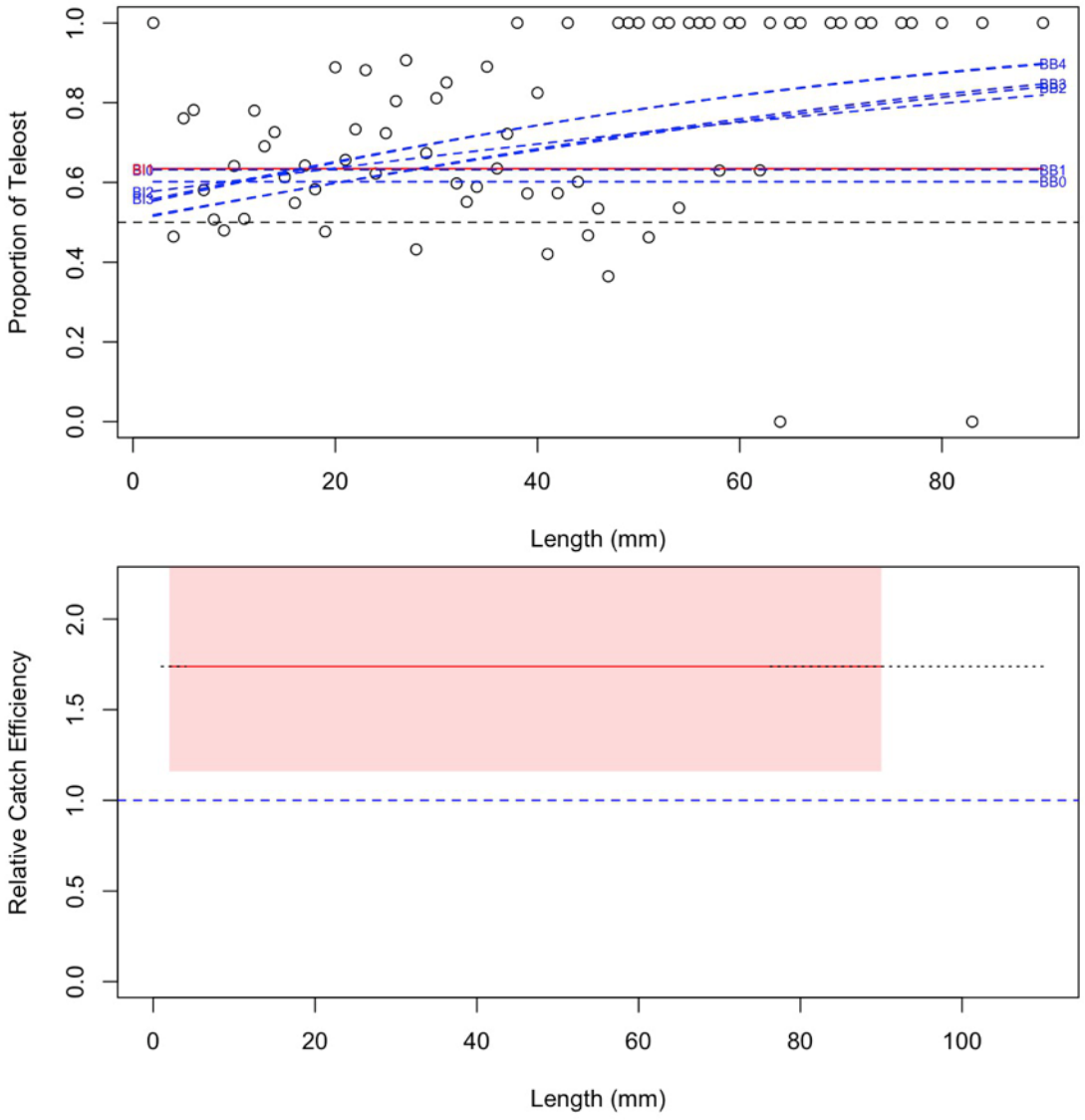

Figure 46b. Model fits and the selected length-based calibration for Hyas sp. (2520).

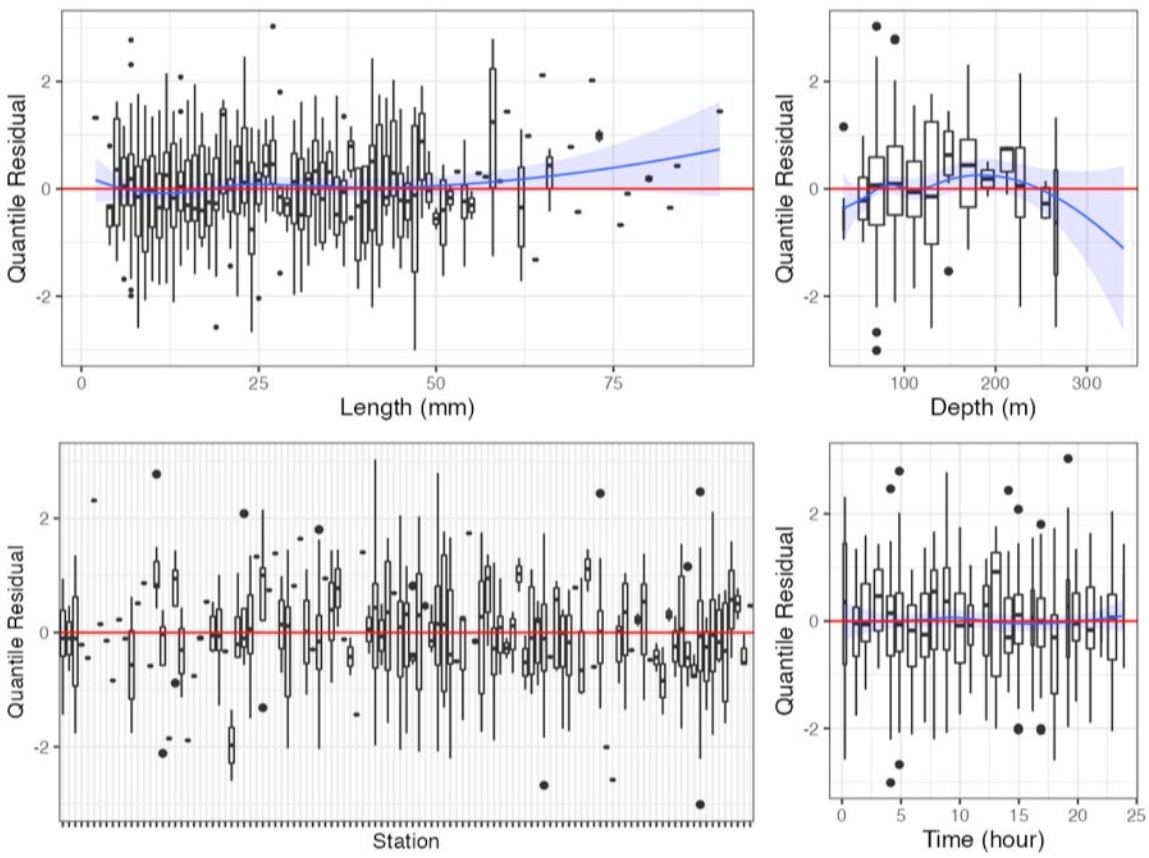

Figure 46c. Randomized and normalized quantile residuals for the selected model for Hyas sp. (2520).

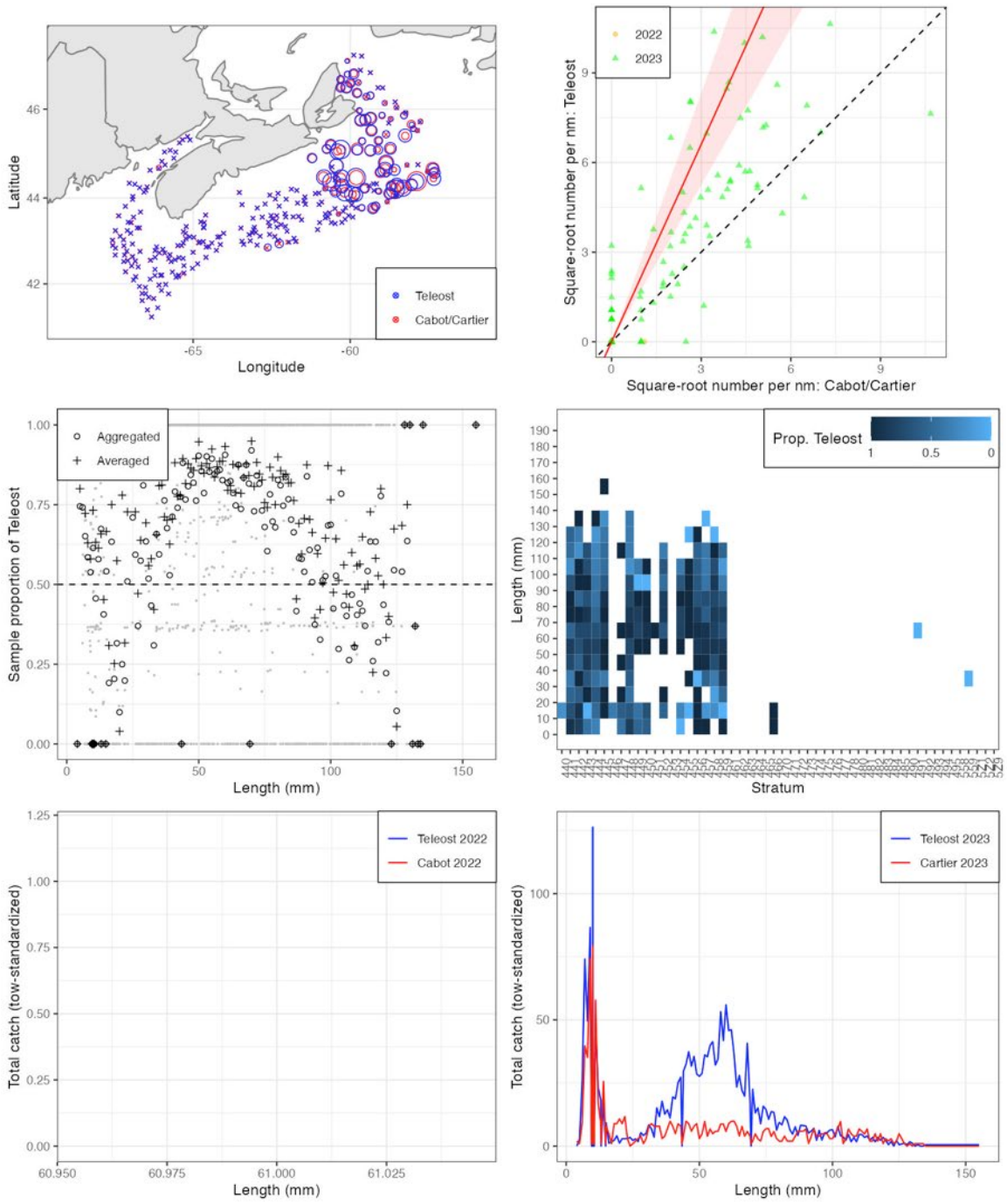

Figure 47a. Visualisation of comparative fishing data and size-aggregated model fit for Chionoecetes opilio (2526).

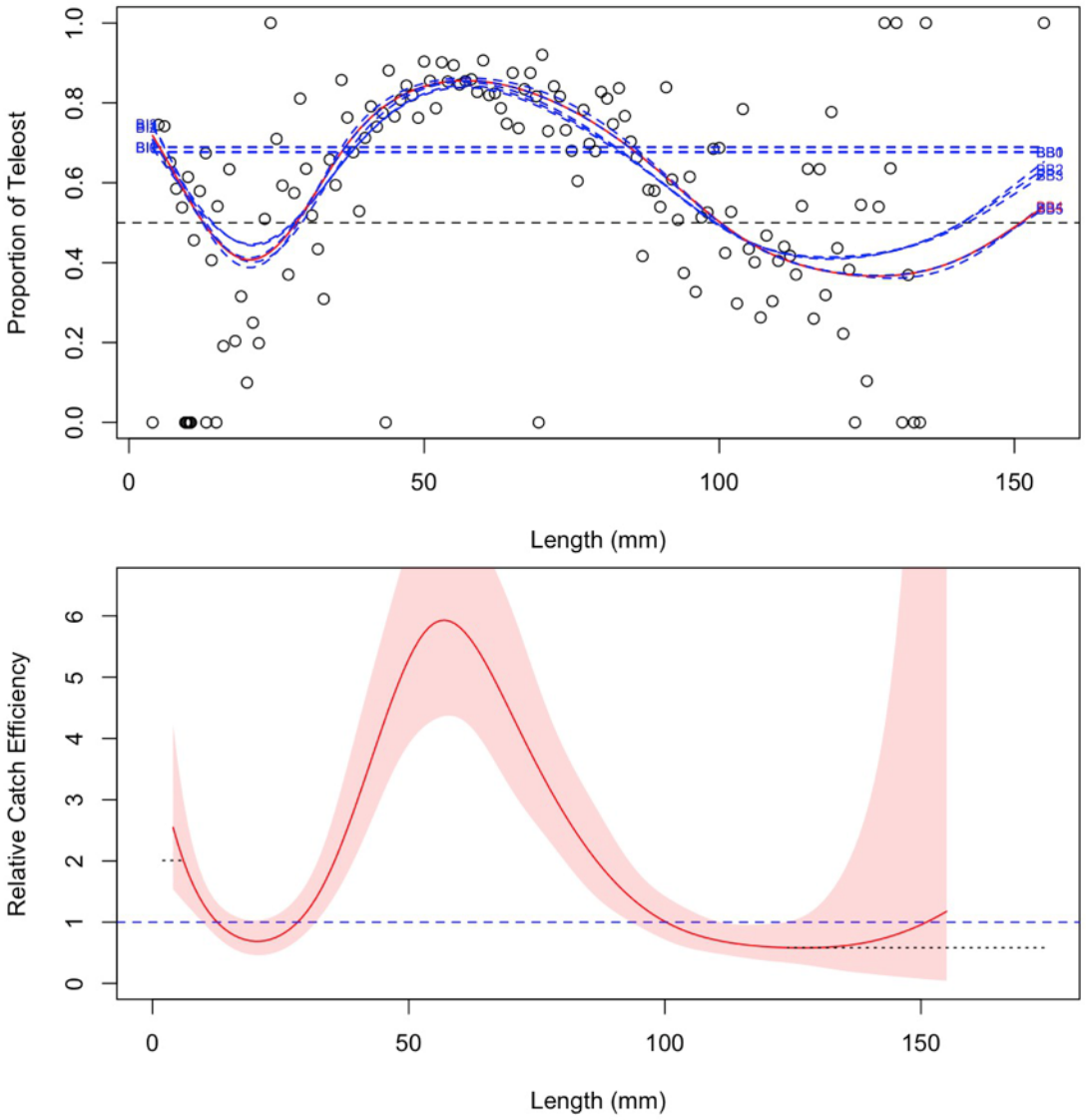

Figure 47b. Model fits and the selected length-based calibration for Chionoecetes opilio (2526).

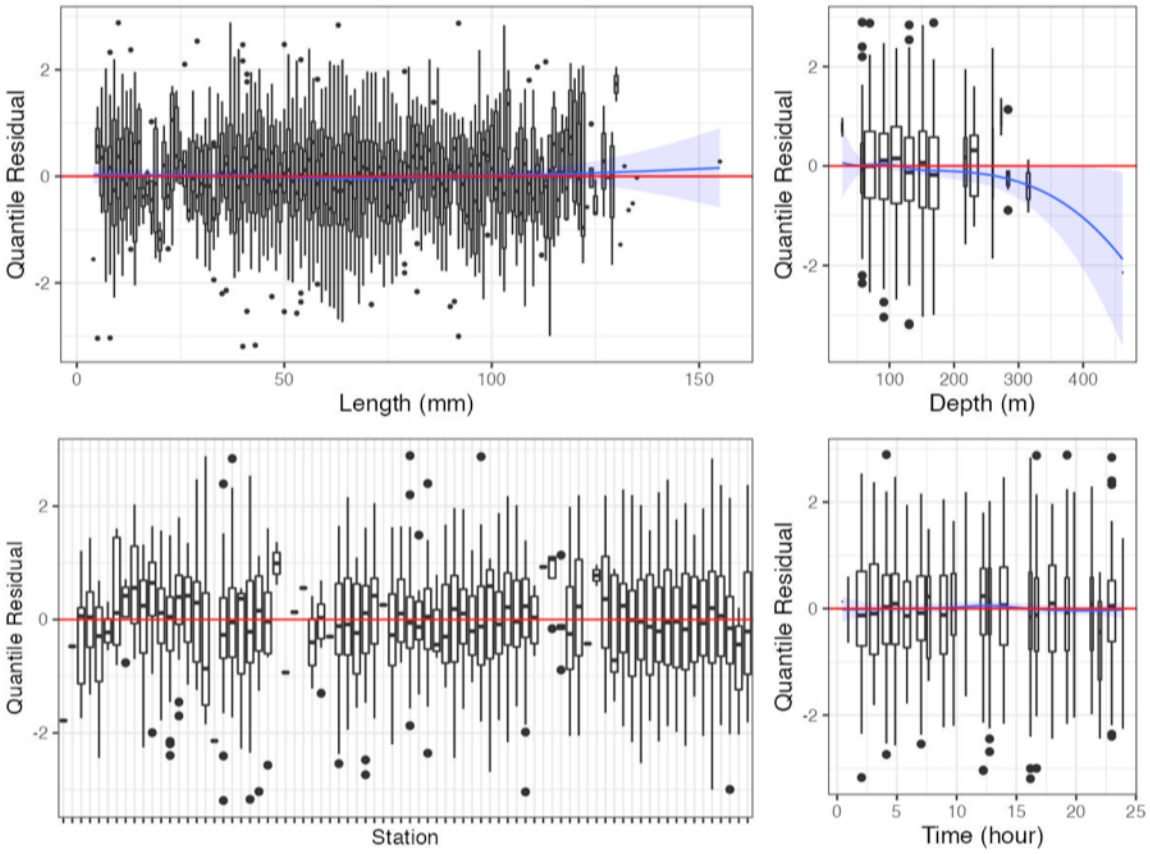

Figure 47c. Randomized and normalized quantile residuals for the selected model for Chionoecetes opilio (2526).

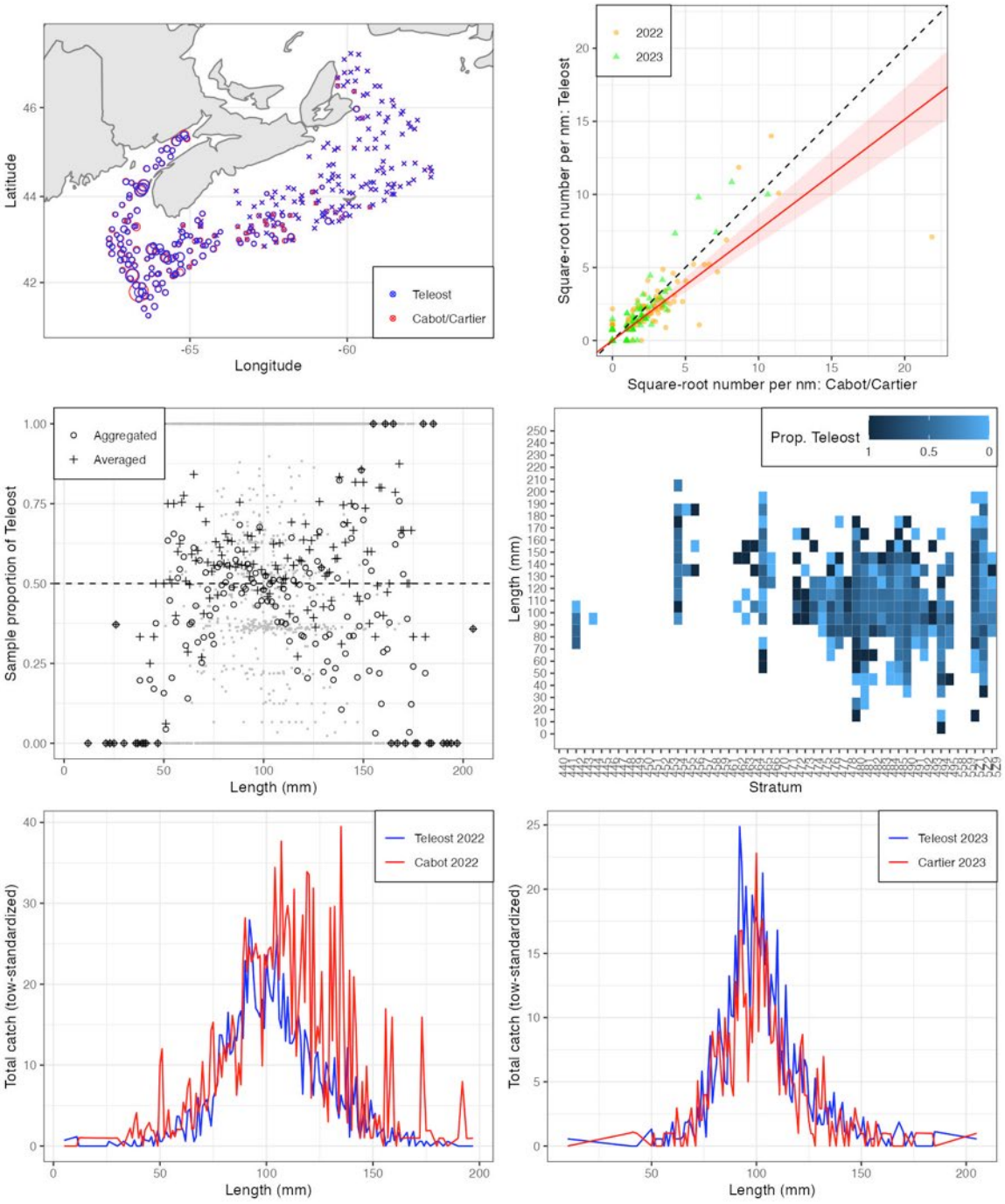

Figure 48a. Visualisation of comparative fishing data and size-aggregated model fit for Homarus americanus (2550).

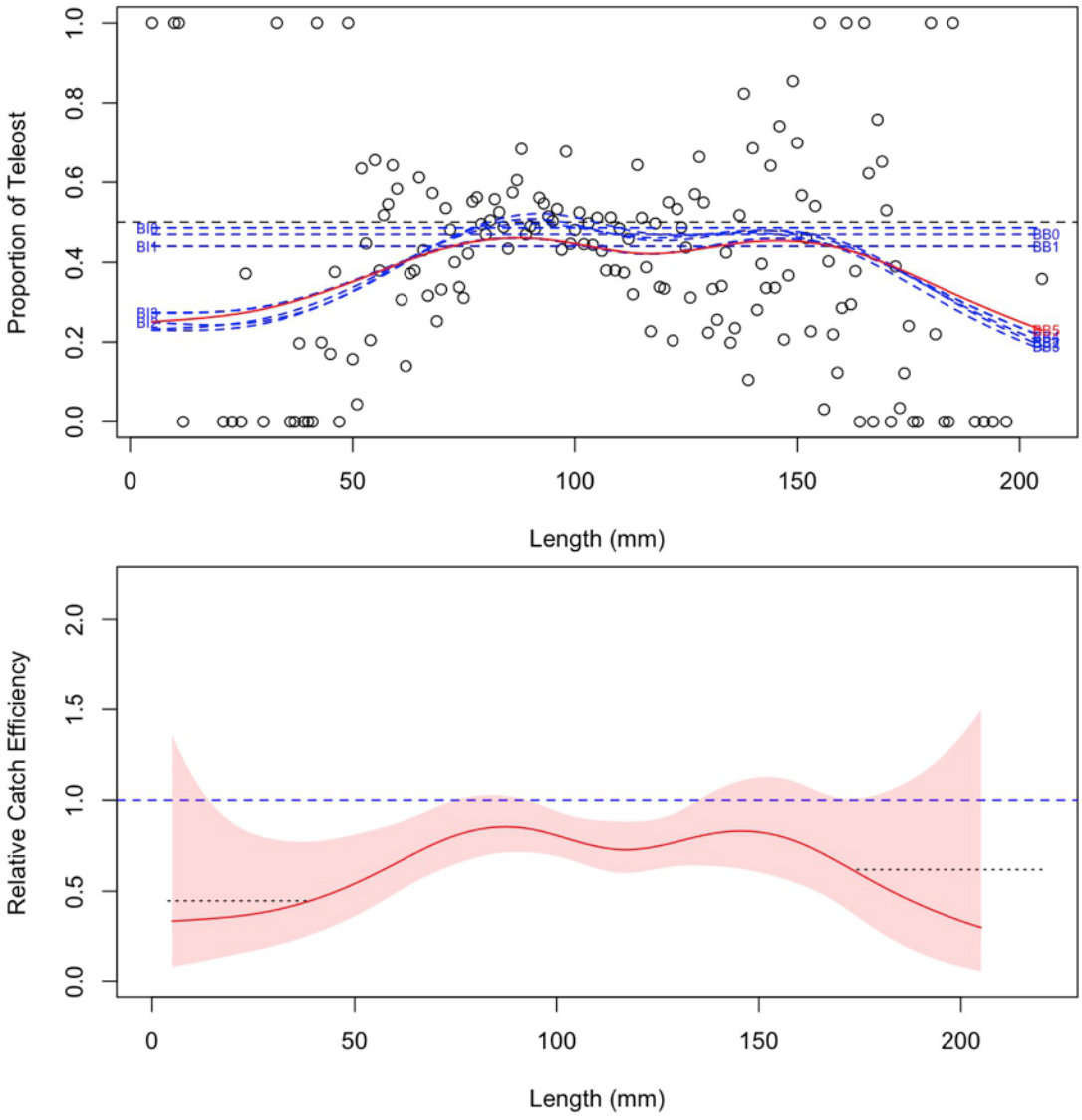

Figure 48b. Model fits and the selected length-based calibration for Homarus americanus (2550).

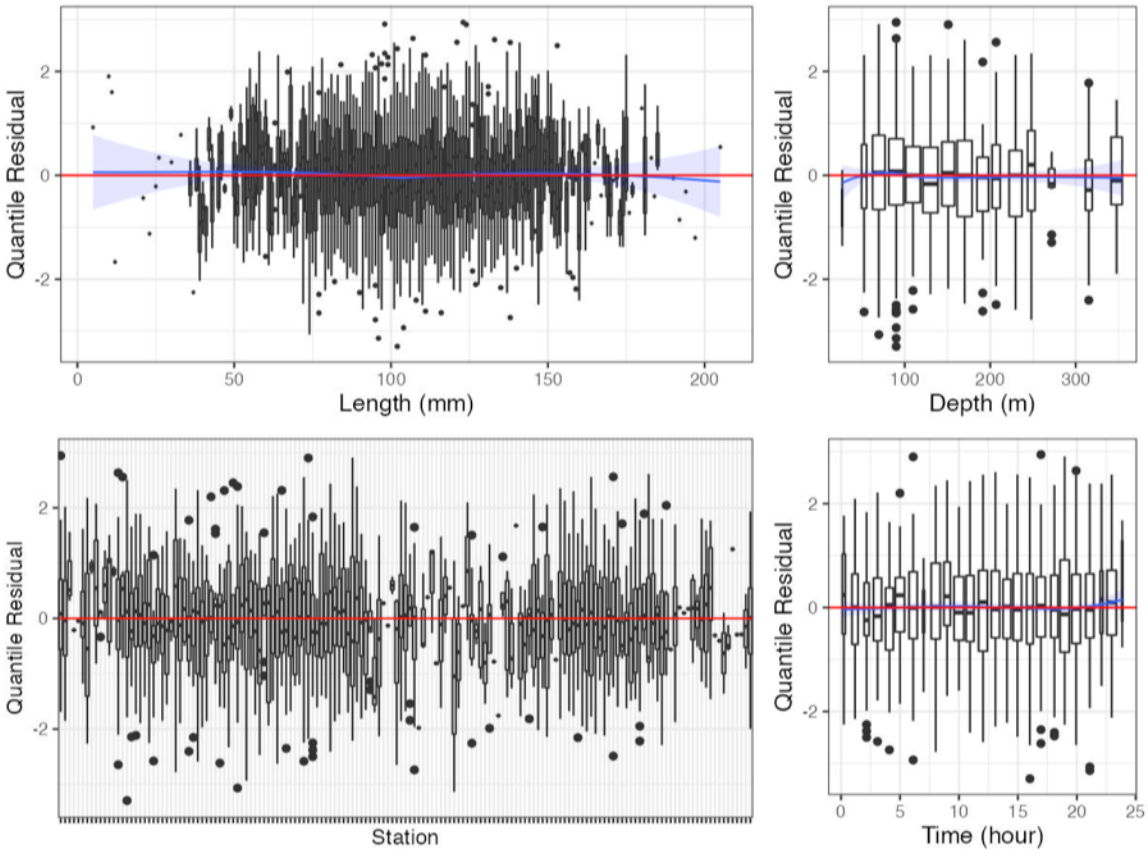

Figure 48c. Randomized and normalized quantile residuals for the selected model for Homarus americanus (2550).

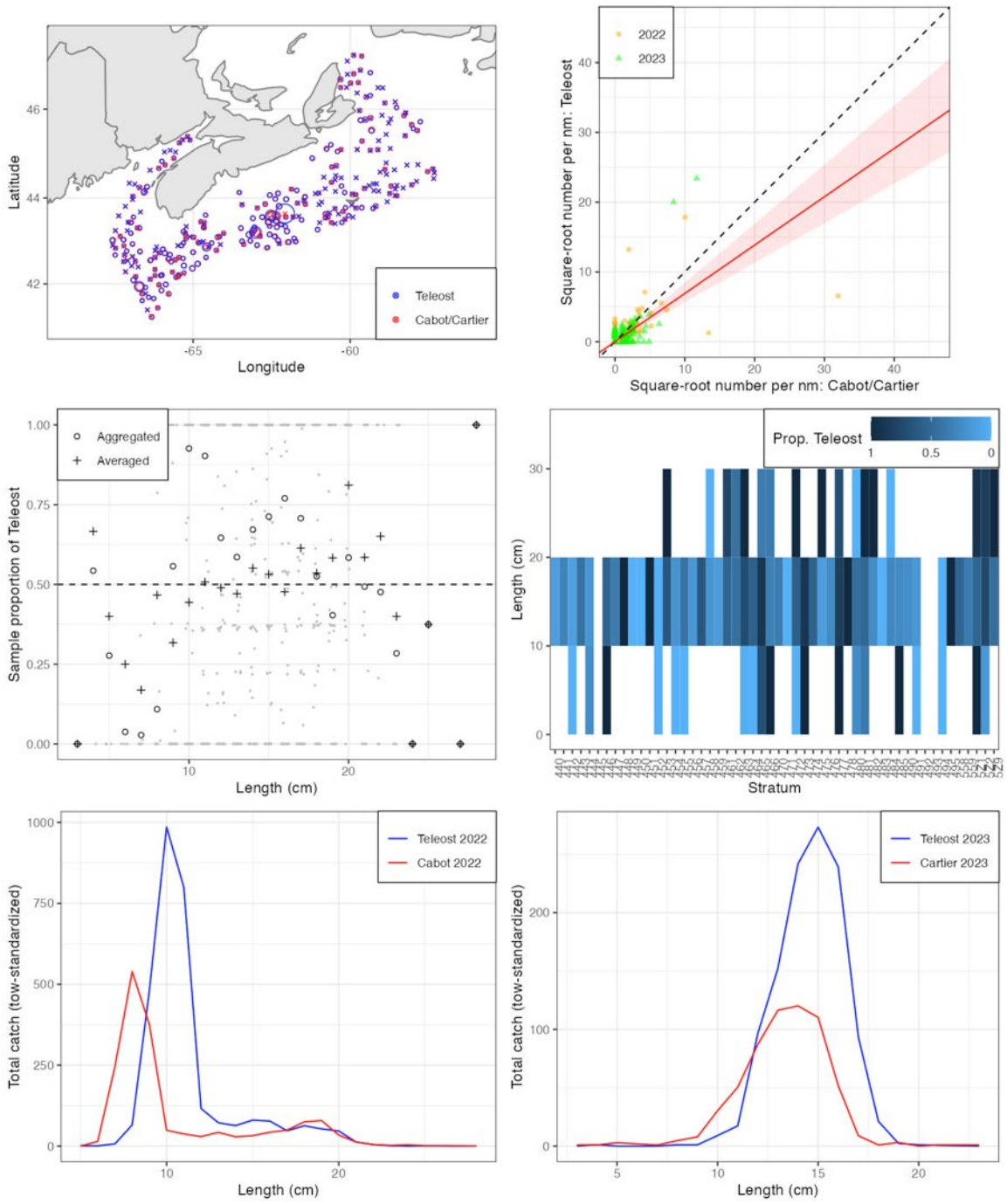

Figure 49a. Visualisation of comparative fishing data and size-aggregated model fit for Illex illecebrosus (4511).

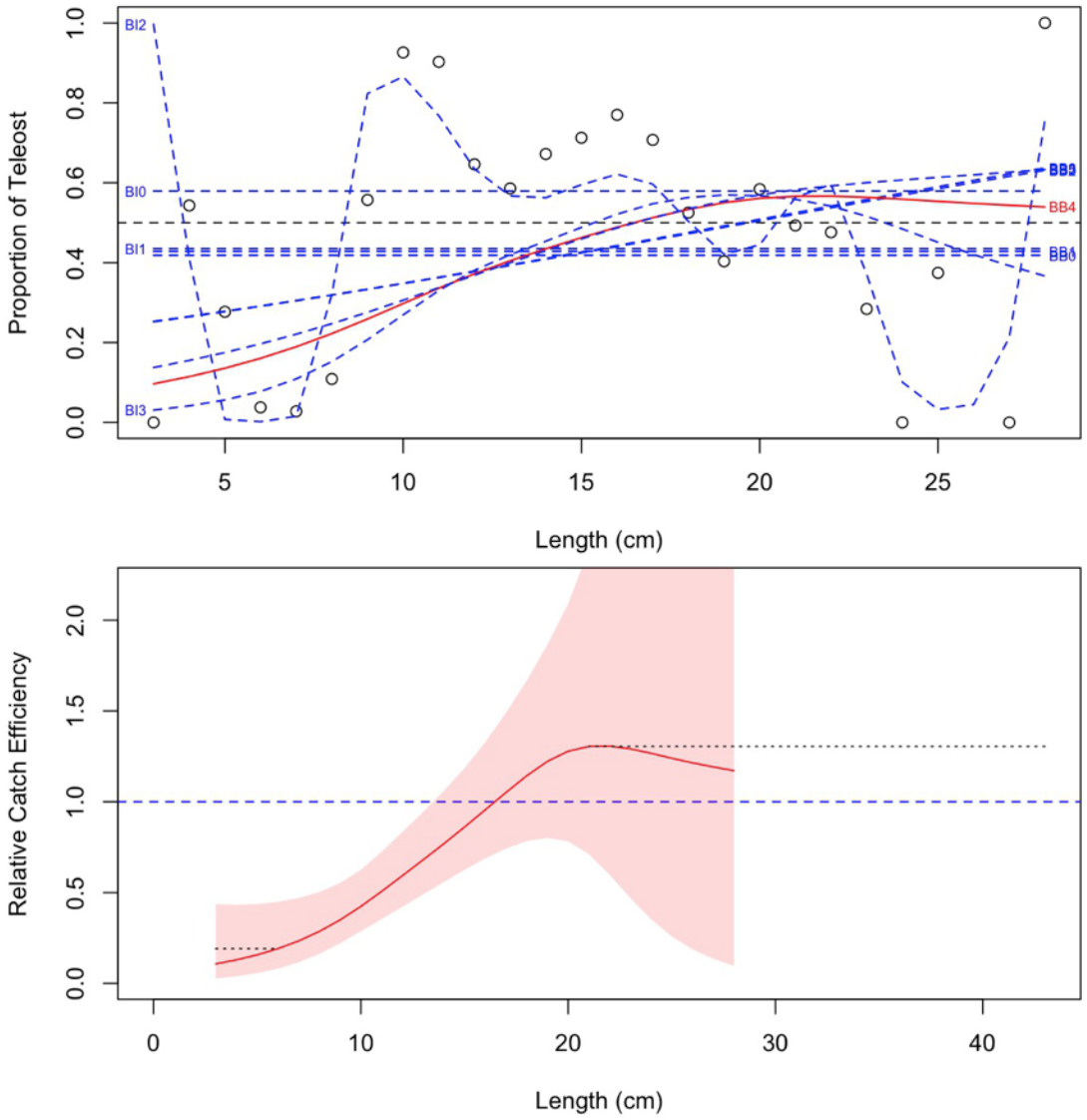

Figure 49b. Model fits and the selected length-based calibration for Illex illecebrosus (4511).

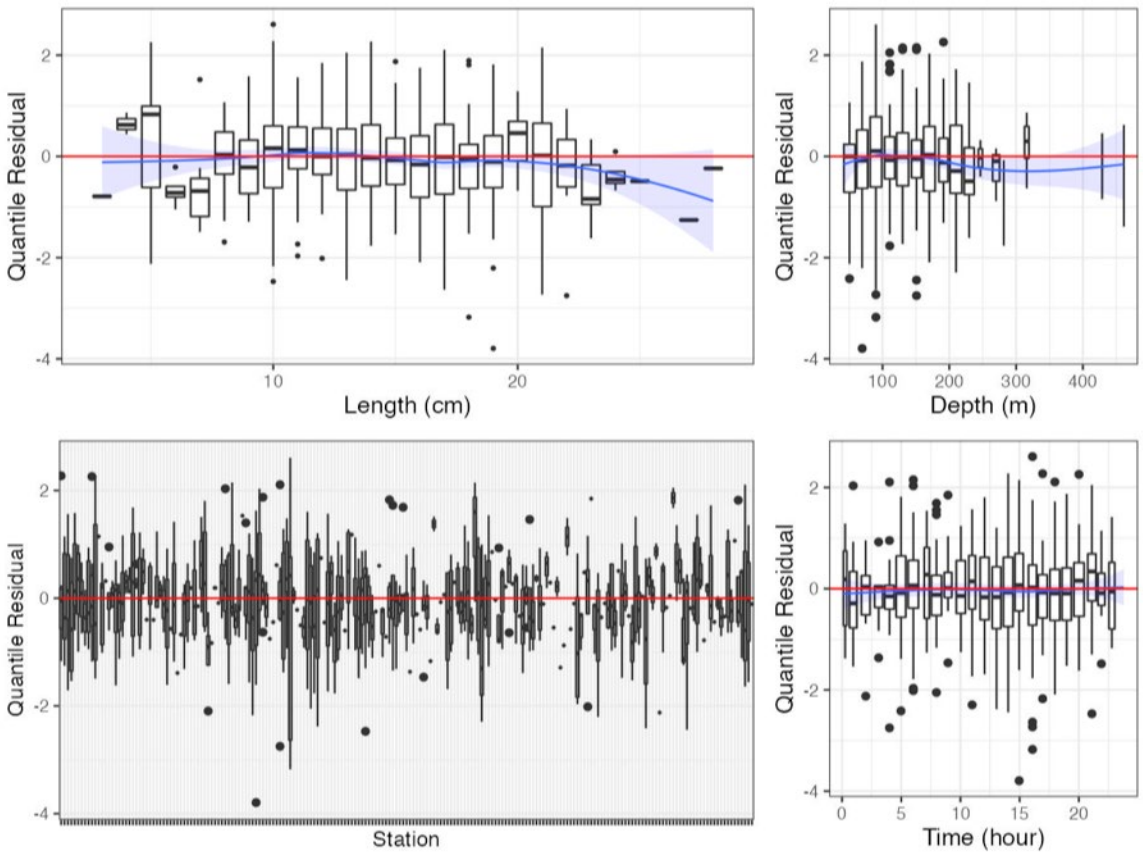

Figure 49c. Randomized and normalized quantile residuals for the selected model for Illex illecebrosus (4511).

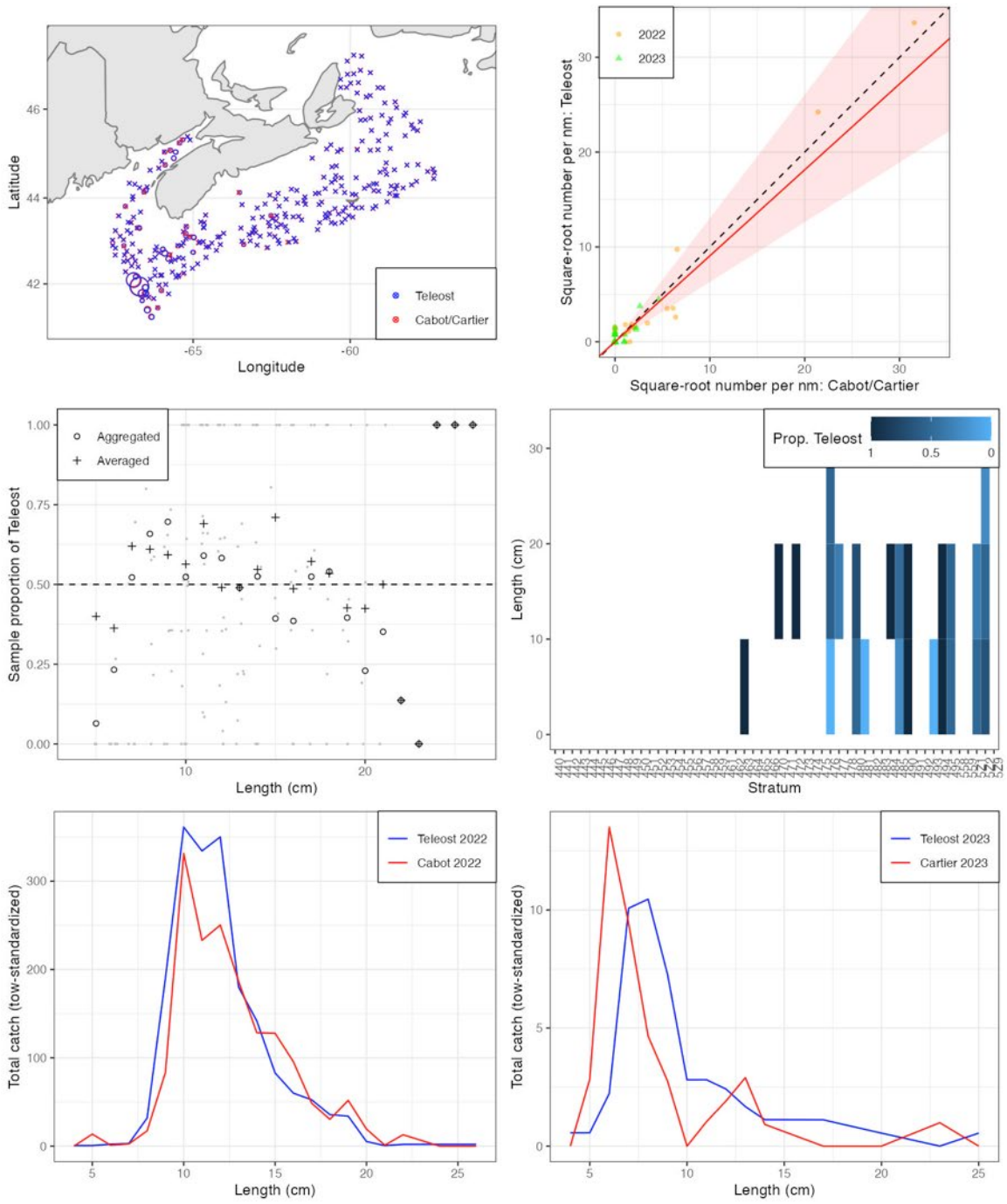

Figure 50a. Visualisation of comparative fishing data and size-aggregated model fit for Loligo pealeii (4512).

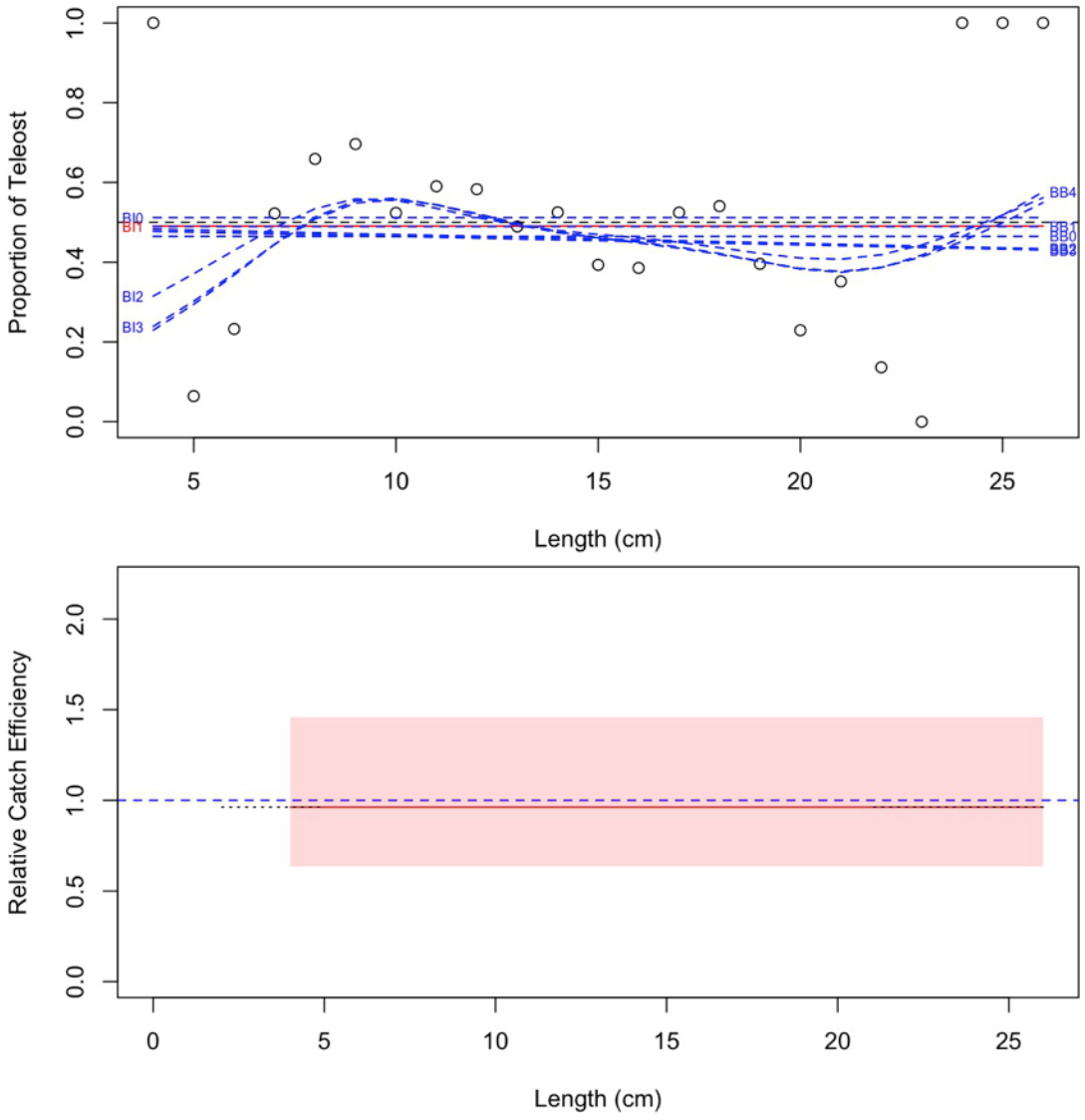

Figure 50b. Model fits and the selected length-based calibration for Loligo pealeii (4512).

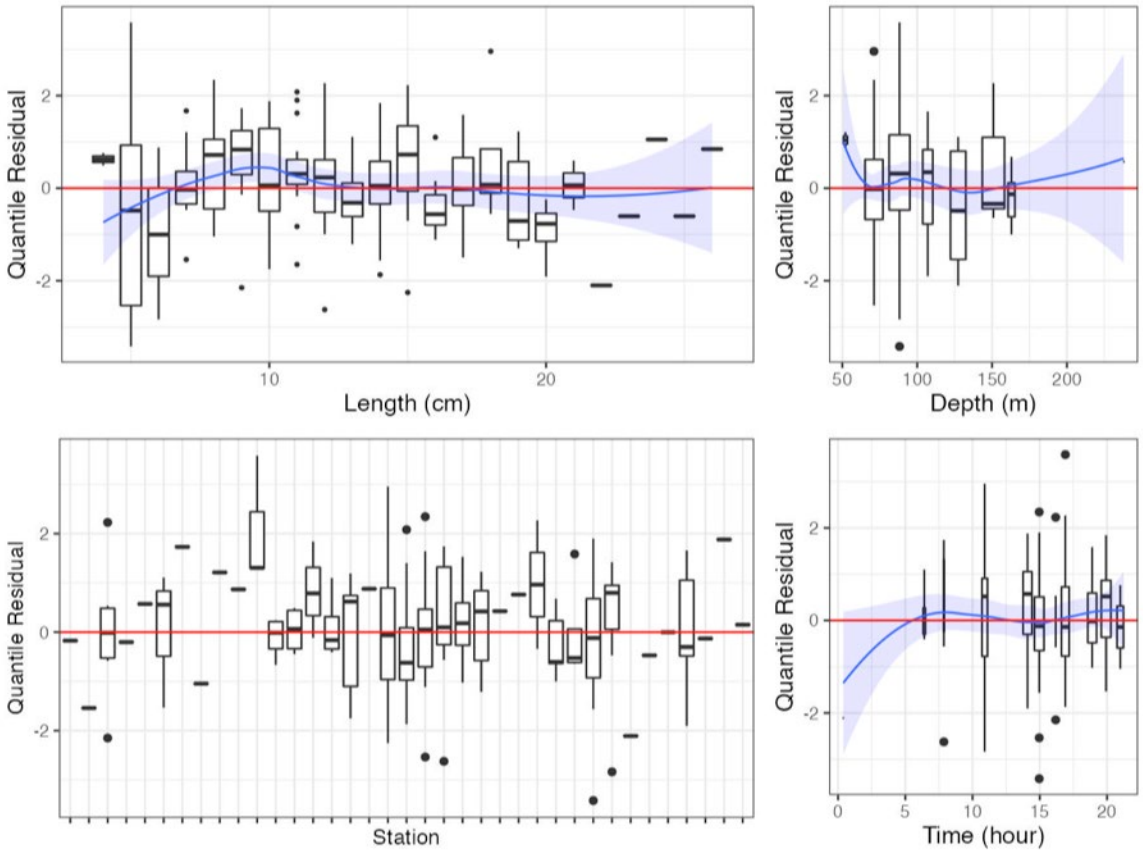

Figure 50c. Randomized and normalized quantile residuals for the selected model for Loligo pealeii (4512).

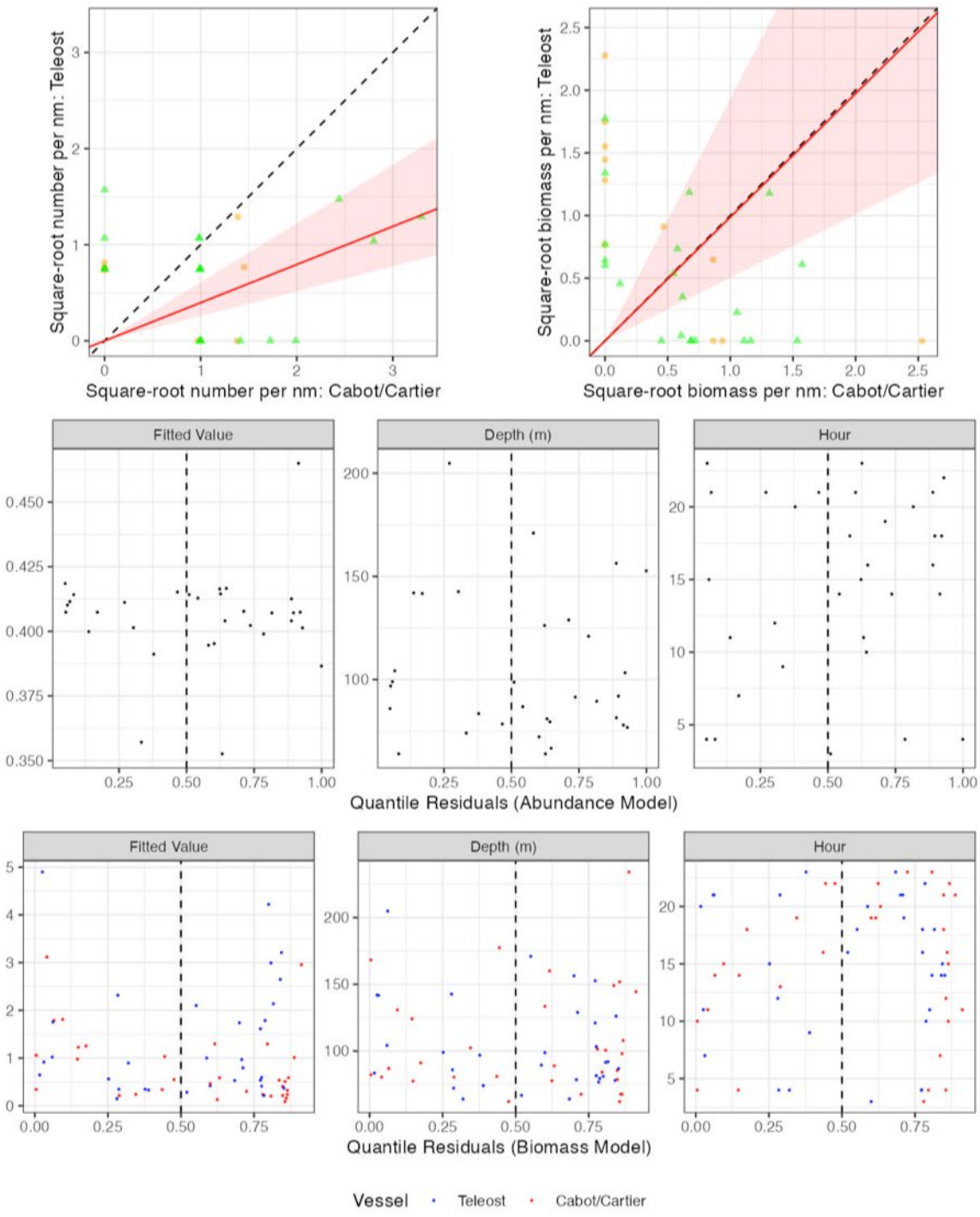

Figure 51. Visualisation of comparative fishing data, size-aggregated model predictions and residual diagnostics plots for Anarhichas lupus (50).

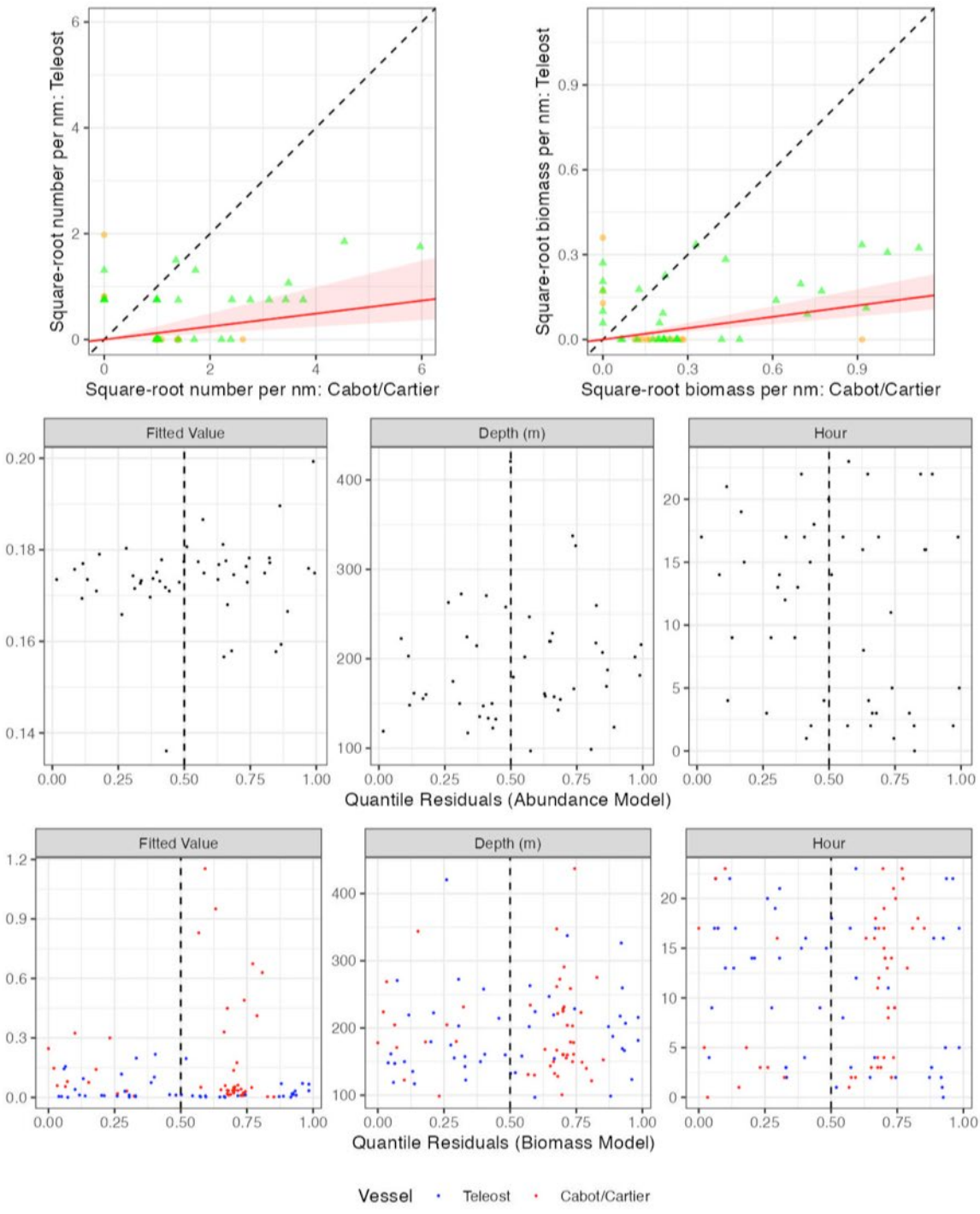

Figure 52. Visualisation of comparative fishing data, size-aggregated model predictions and residual diagnostics plots for Enchelyopus cimbrius (114).

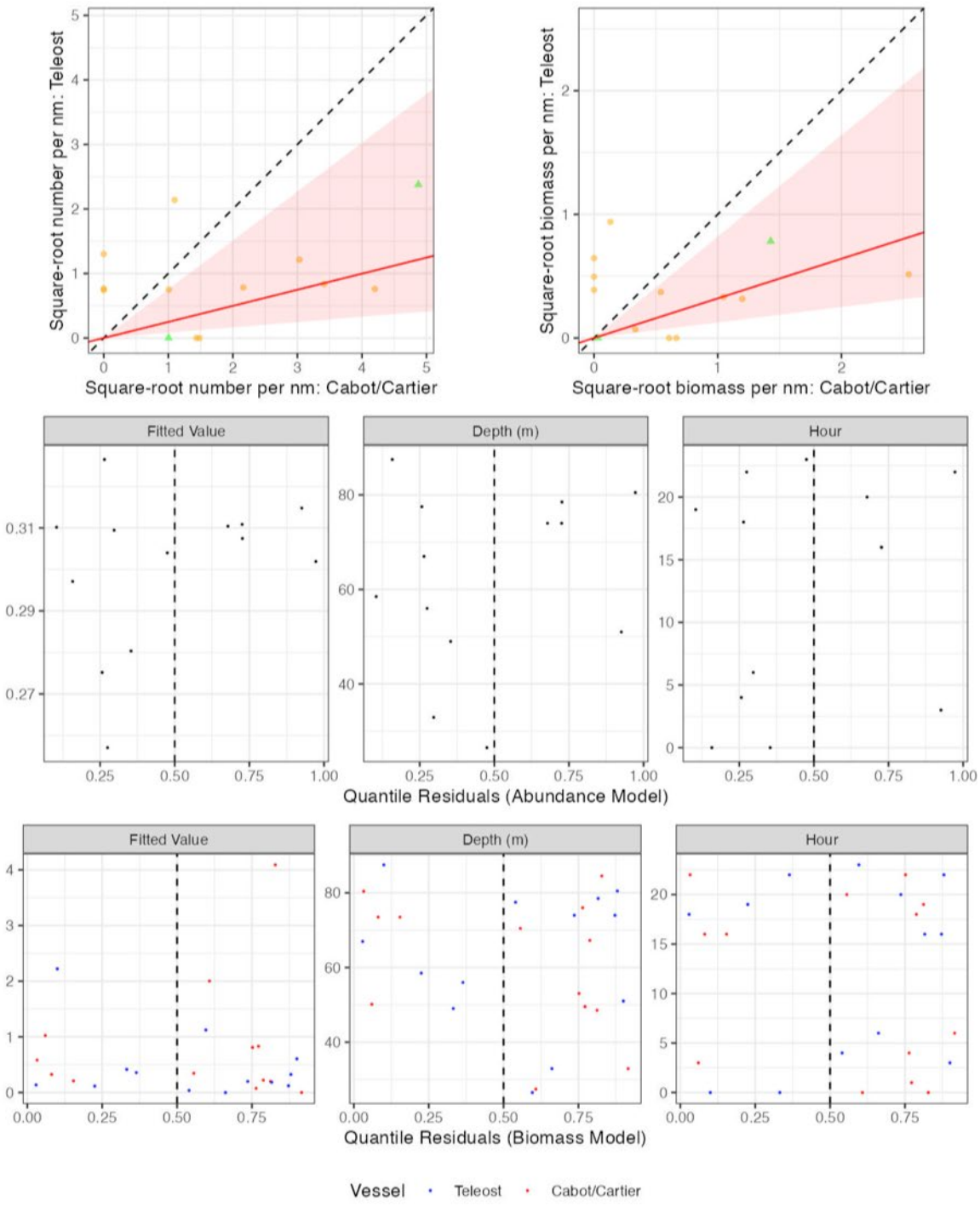

Figure 53. Visualisation of comparative fishing data, size-aggregated model predictions and residual diagnostics plots for Scophthalmus aquosus (143).

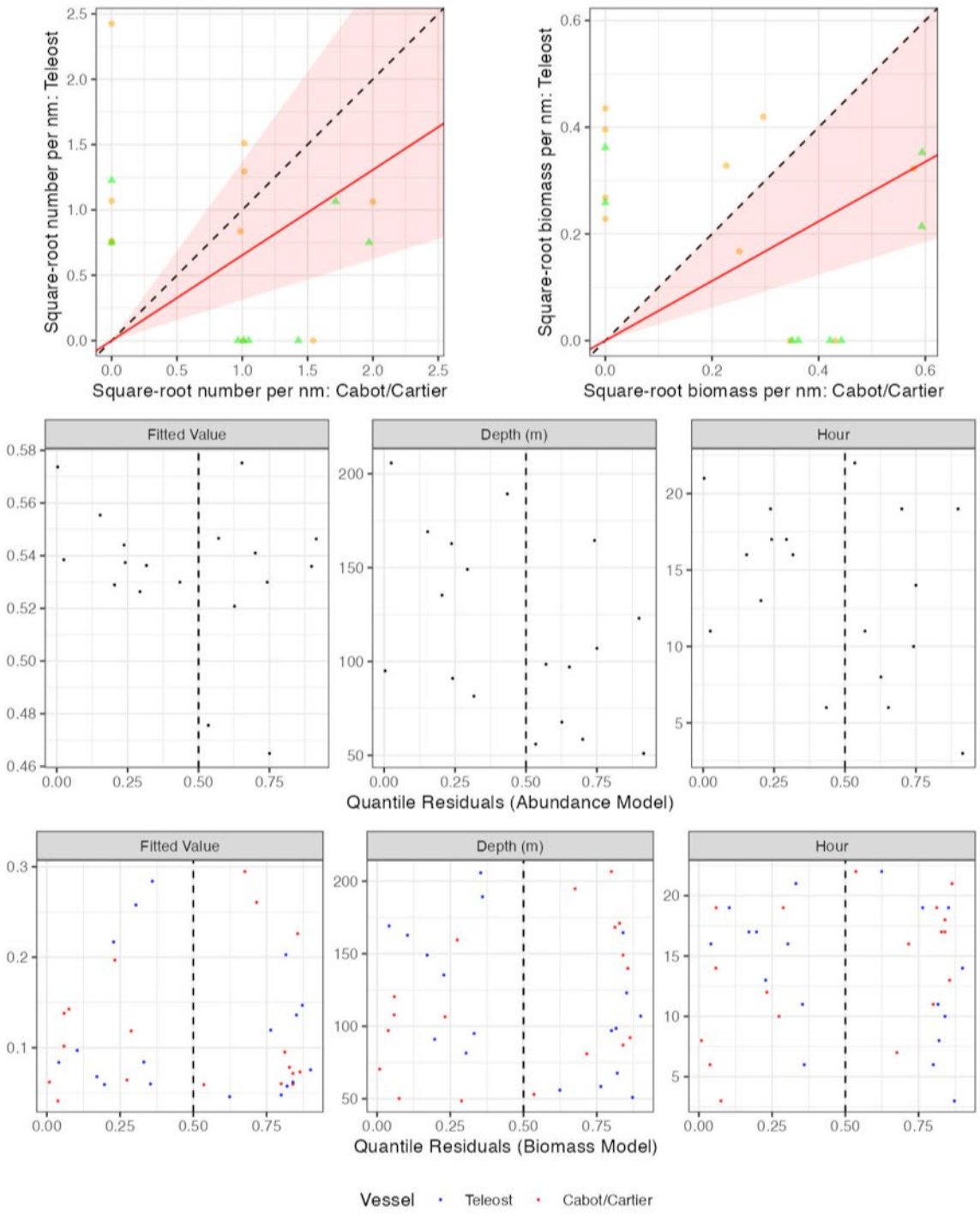

Figure 54. Visualisation of comparative fishing data, size-aggregated model predictions and residual diagnostics plots for Alosa aestivalis (165).

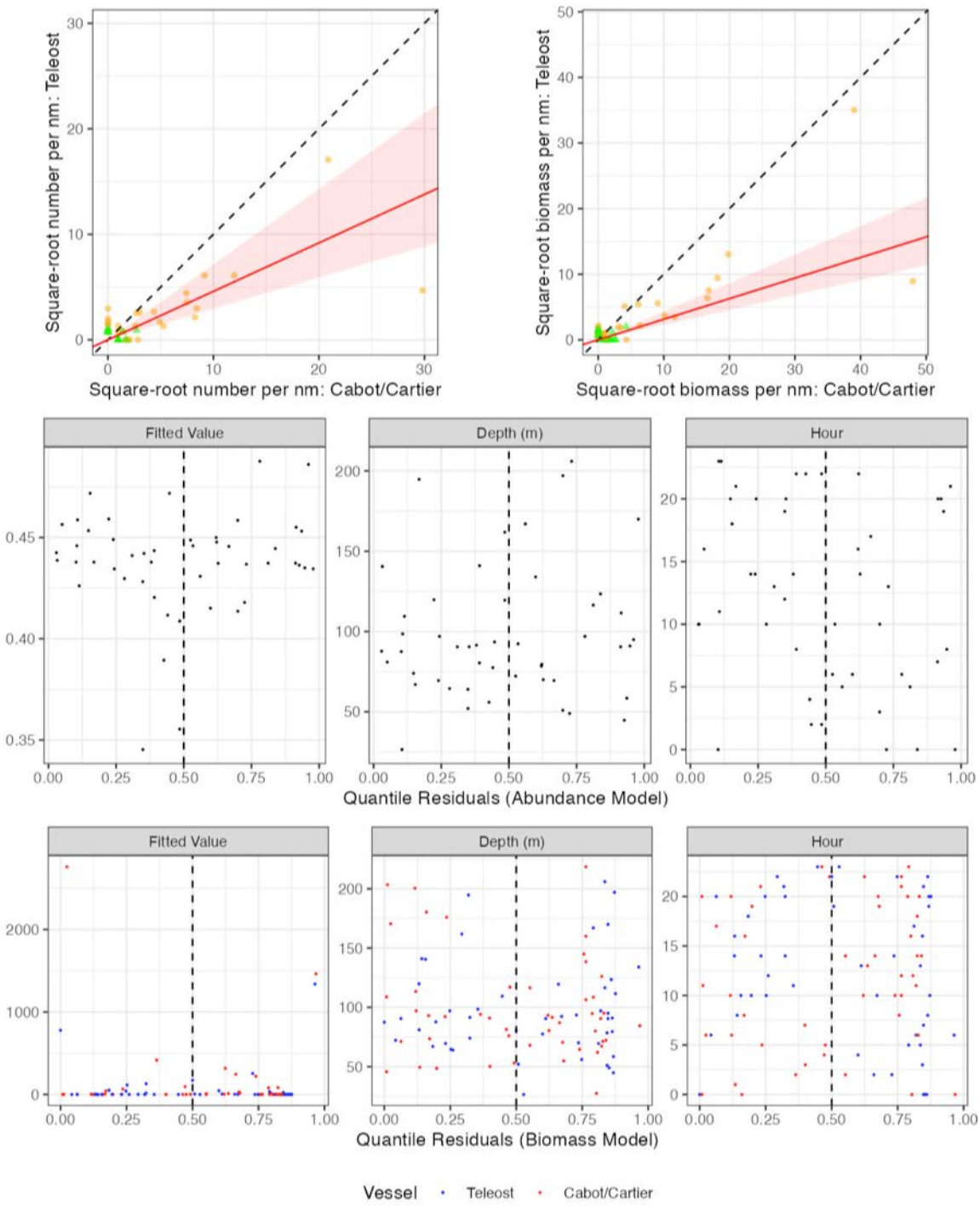

Figure 55. Visualisation of comparative fishing data, size-aggregated model predictions and residual diagnostics plots for Leucoraja ocellata (204).

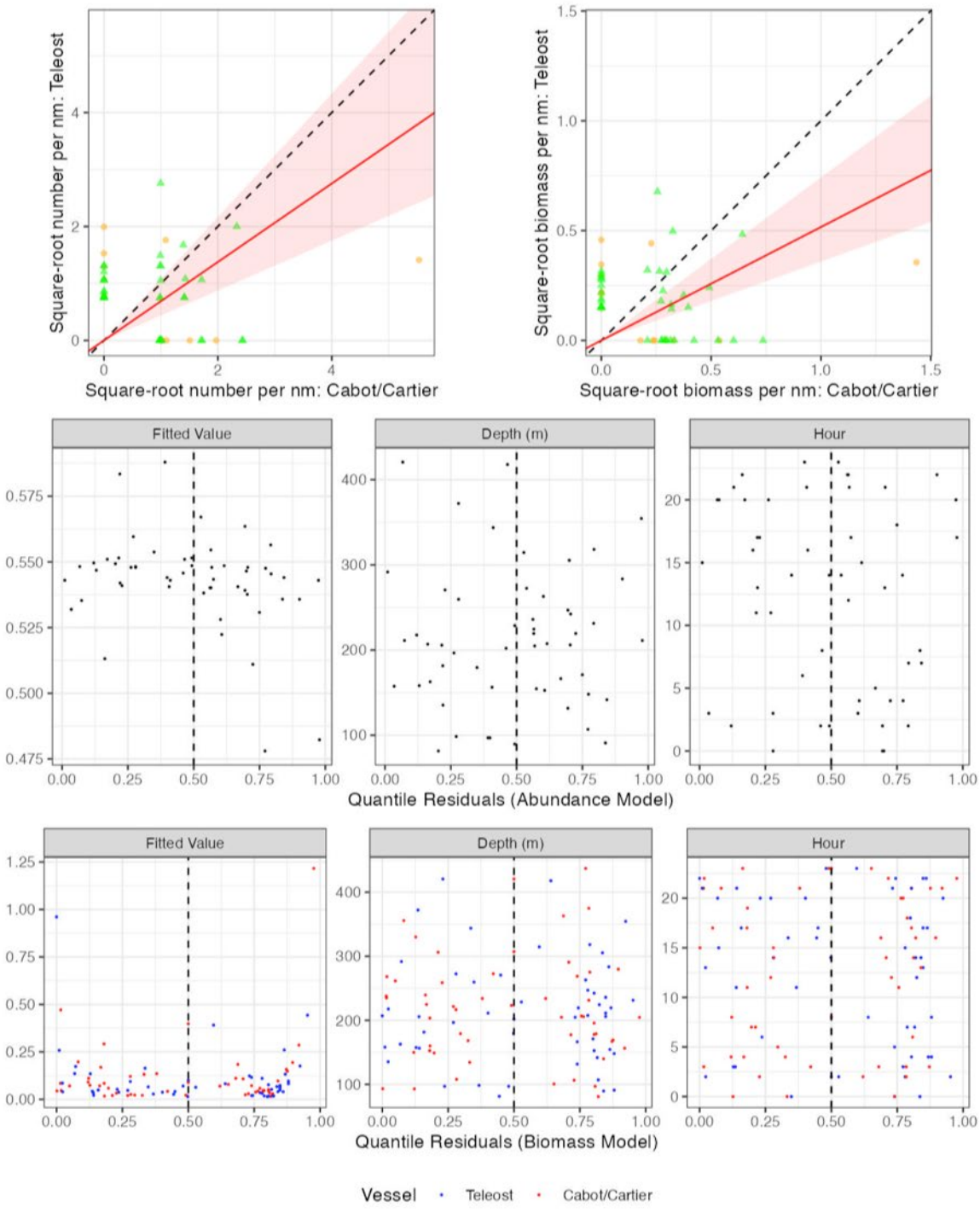

Figure 56. Visualisation of comparative fishing data, size-aggregated model predictions and residual diagnostics plots for Myxine glutinosa (241).

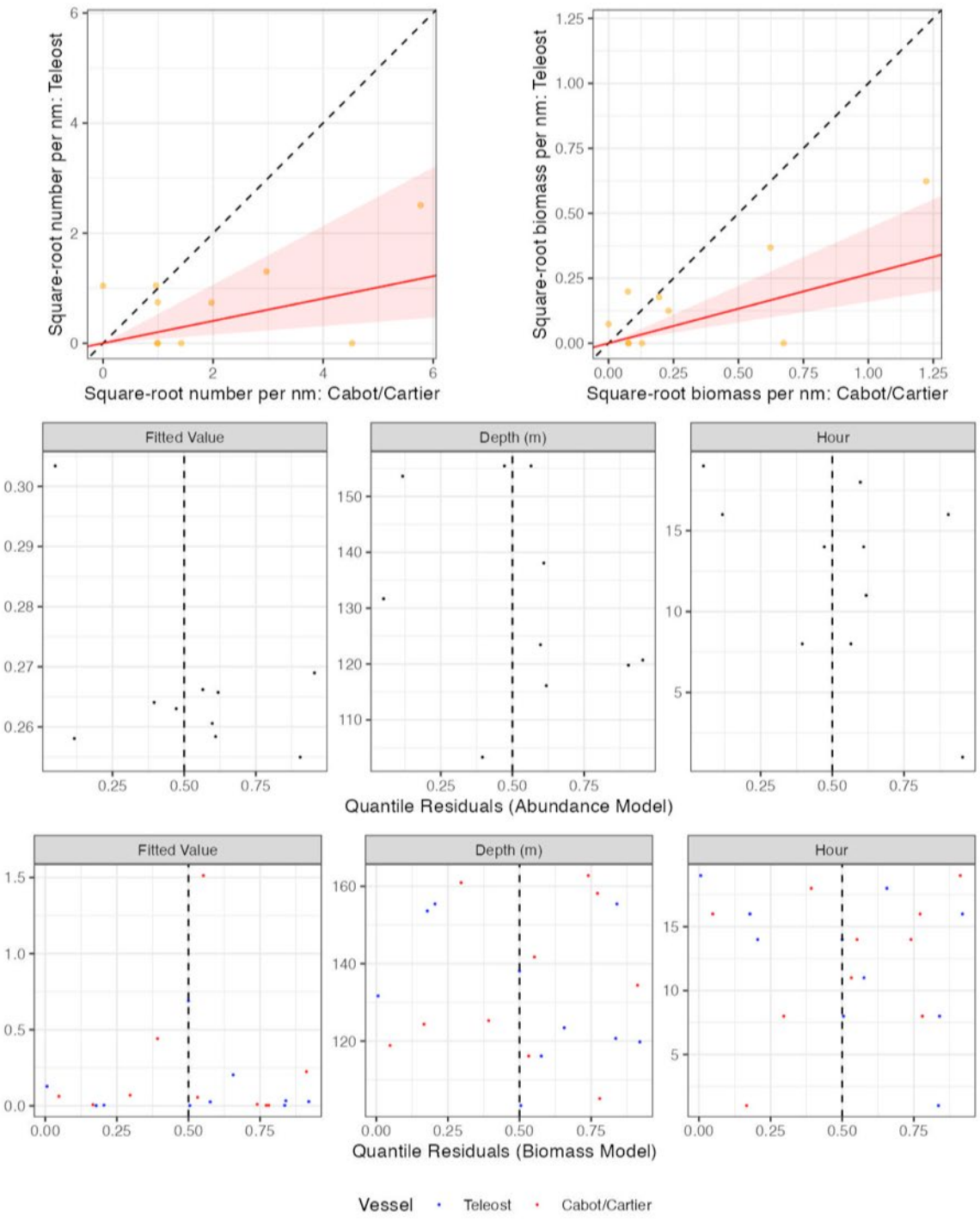

Figure 57. Visualisation of comparative fishing data, size-aggregated model predictions and residual diagnostics plots for Scorpaenidae. (280).

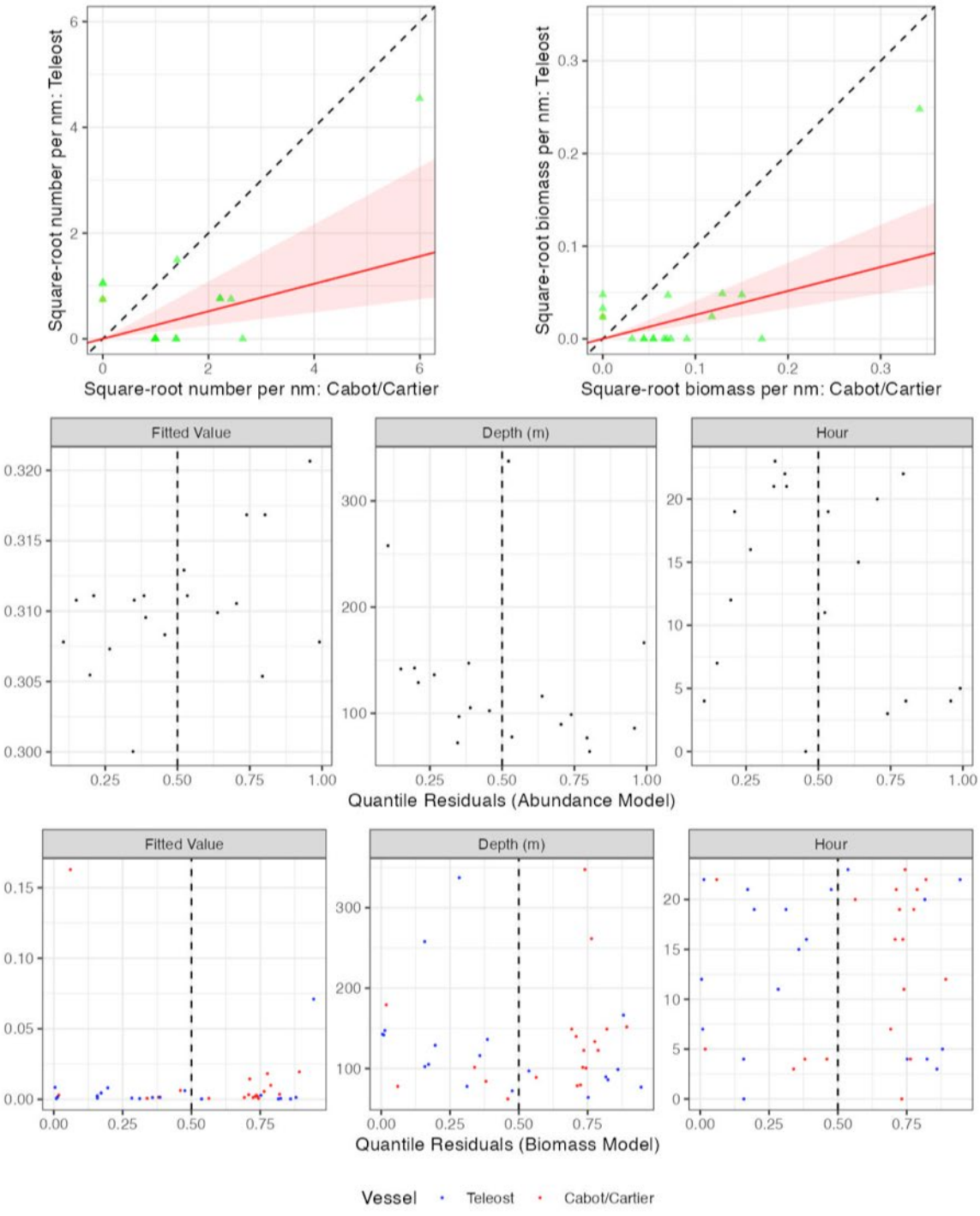

Figure 58. Visualisation of comparative fishing data, size-aggregated model predictions and residual diagnostics plots for Artediellus sp. (323).

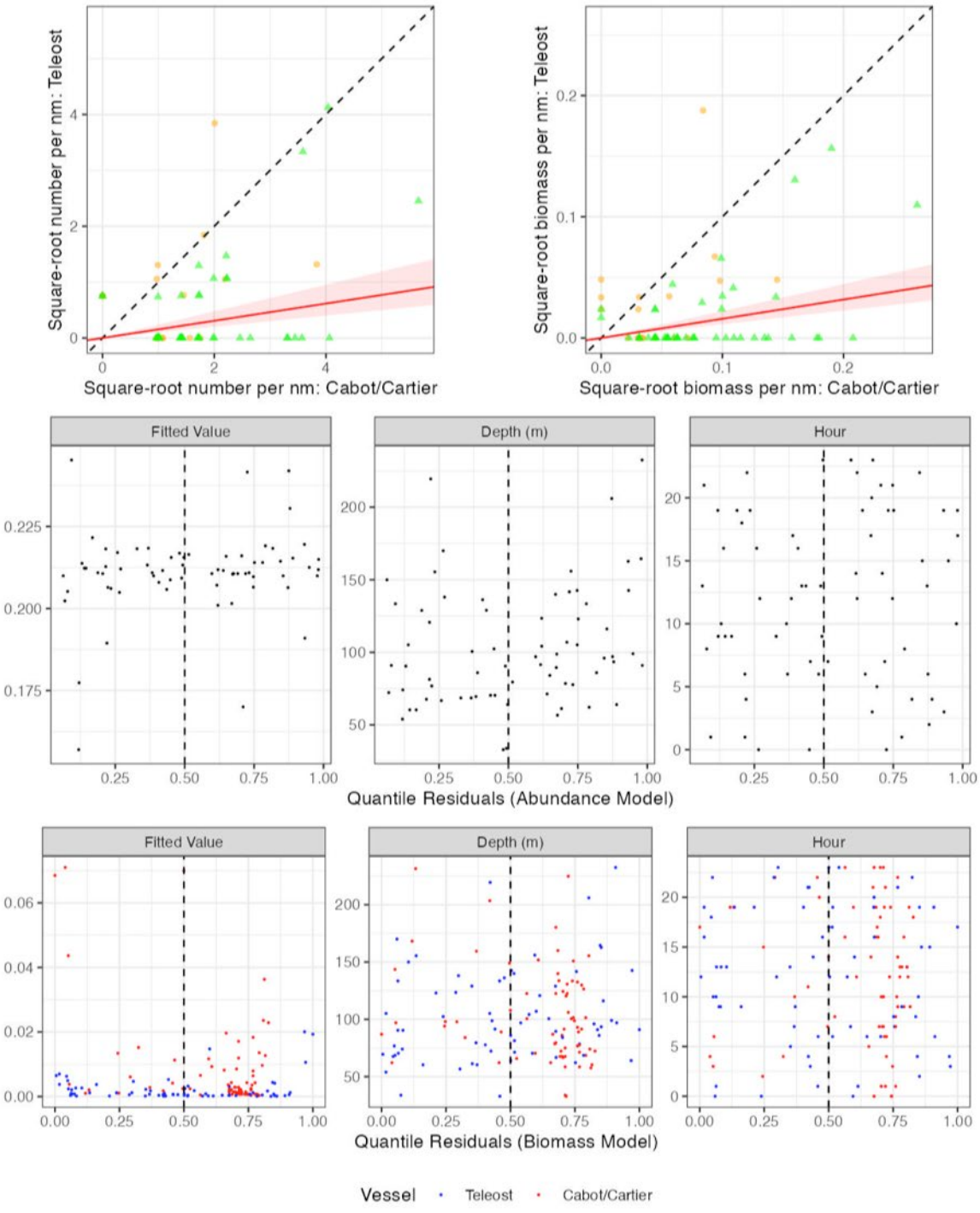

Figure 59. Visualisation of comparative fishing data, size-aggregated model predictions and residual diagnostics plots for Aspidophoroides monopterygius (340).

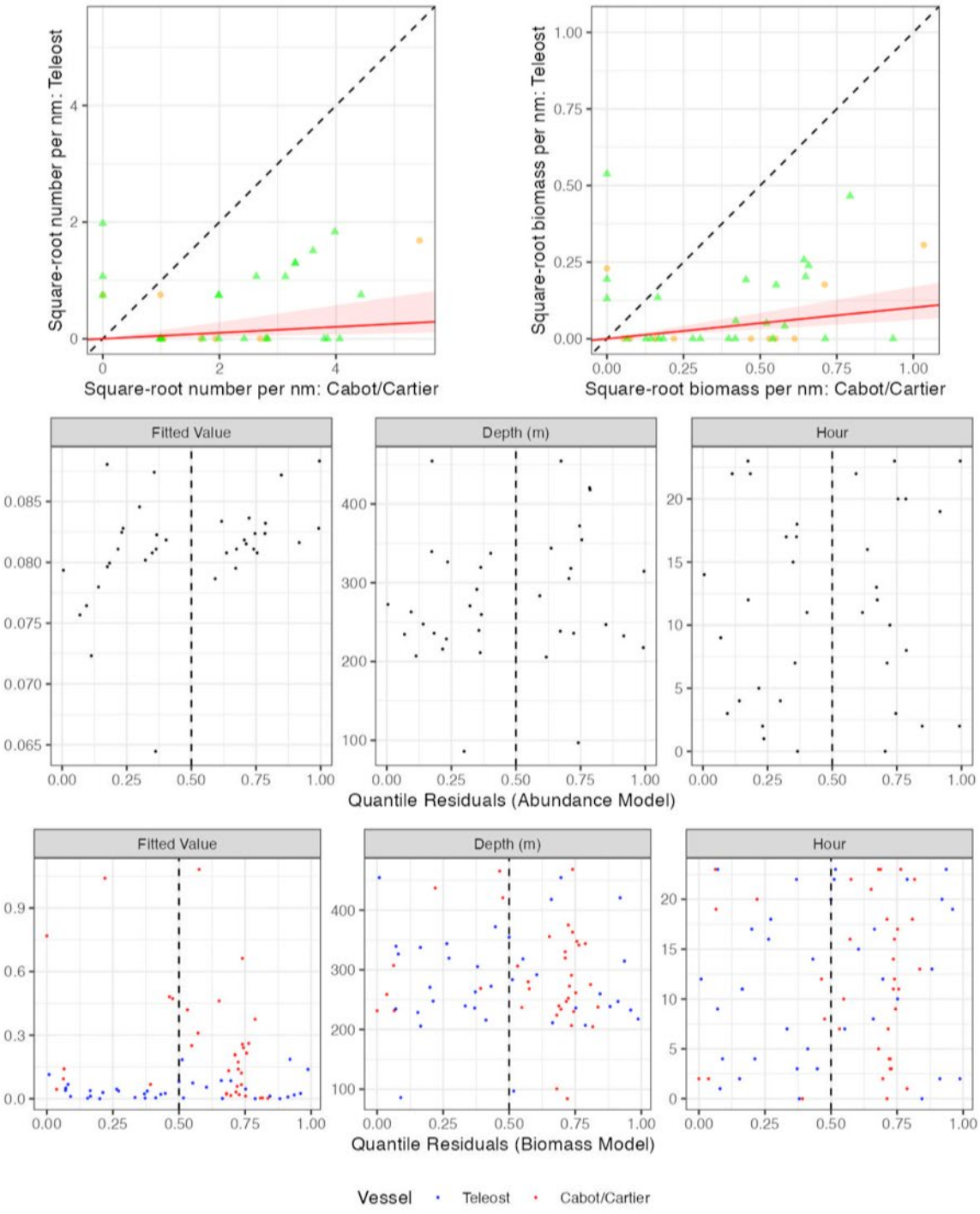

Figure 60. Visualisation of comparative fishing data, size-aggregated model predictions and residual diagnostics plots for Nezumia bairdii (410).

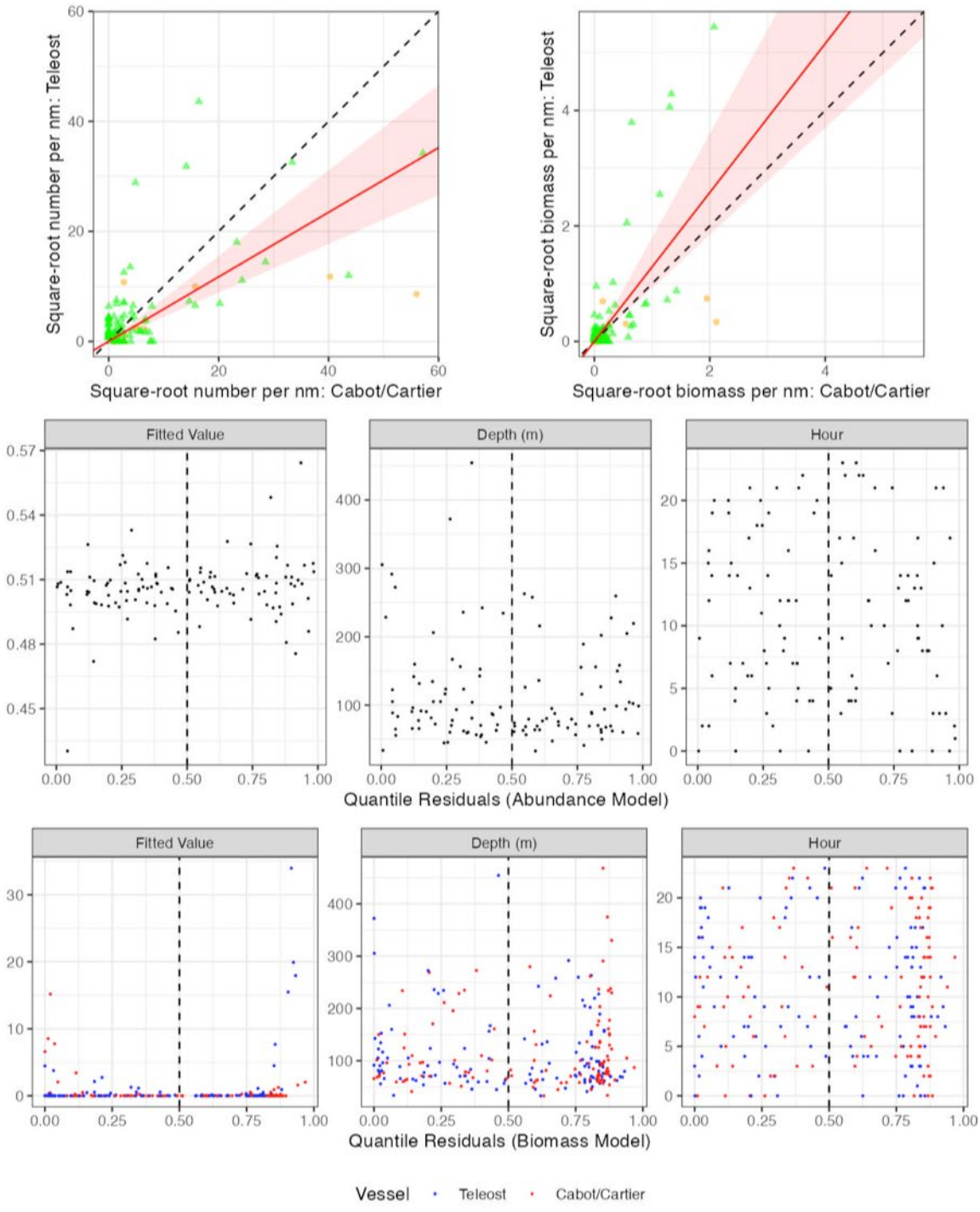

Figure 61. Visualisation of comparative fishing data, size-aggregated model predictions and residual diagnostics plots for Ammodytes dubius (610).

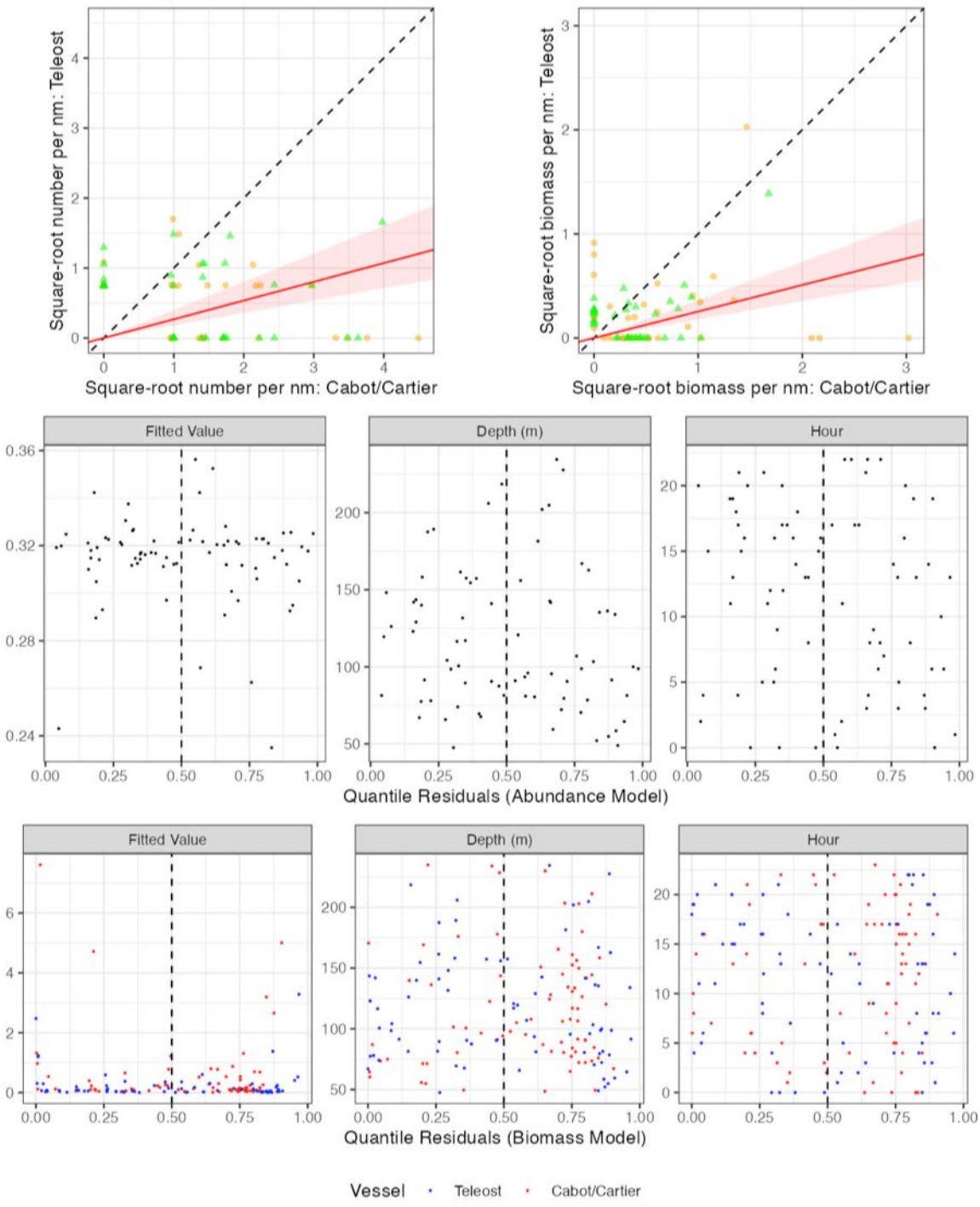

Figure 62. Visualisation of comparative fishing data, size-aggregated model predictions and residual diagnostics plots for Zoarces americanus (640).

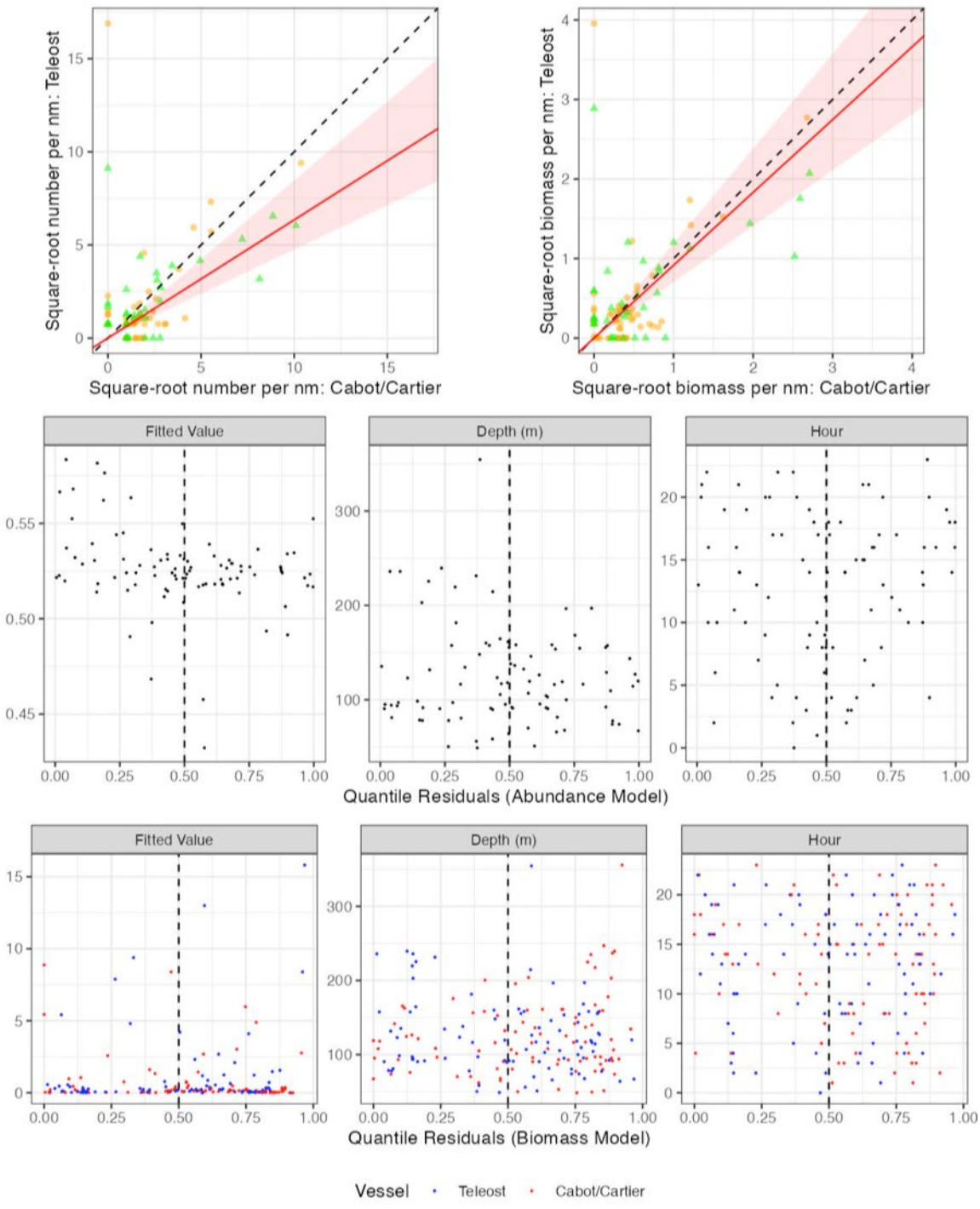

Figure 63. Visualisation of comparative fishing data, size-aggregated model predictions and residual diagnostics plots for Peprilus triacanthus (701).

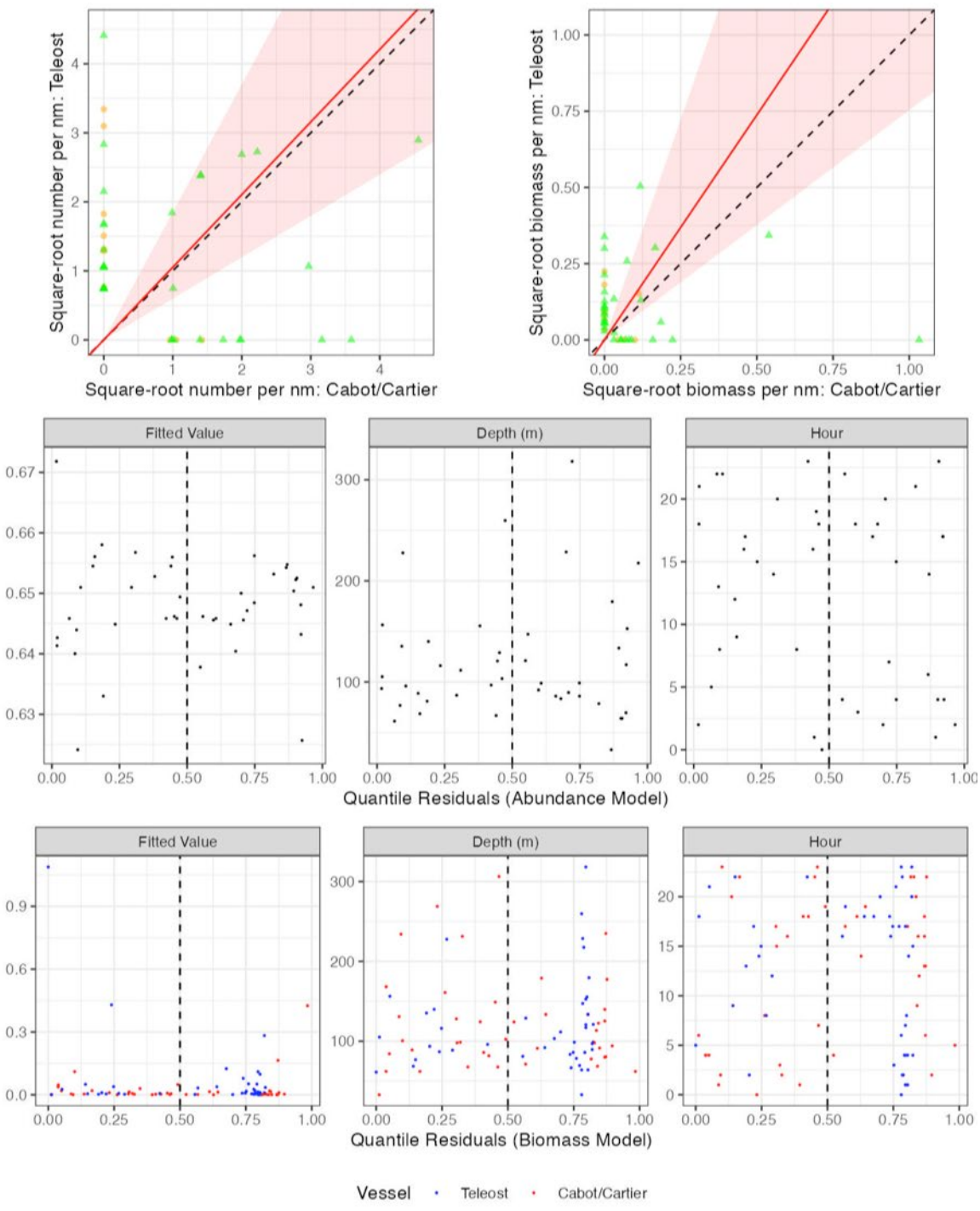

Figure 64. Visualisation of comparative fishing data, size-aggregated model predictions and residual diagnostics plots for Tunicata sp. (1810).

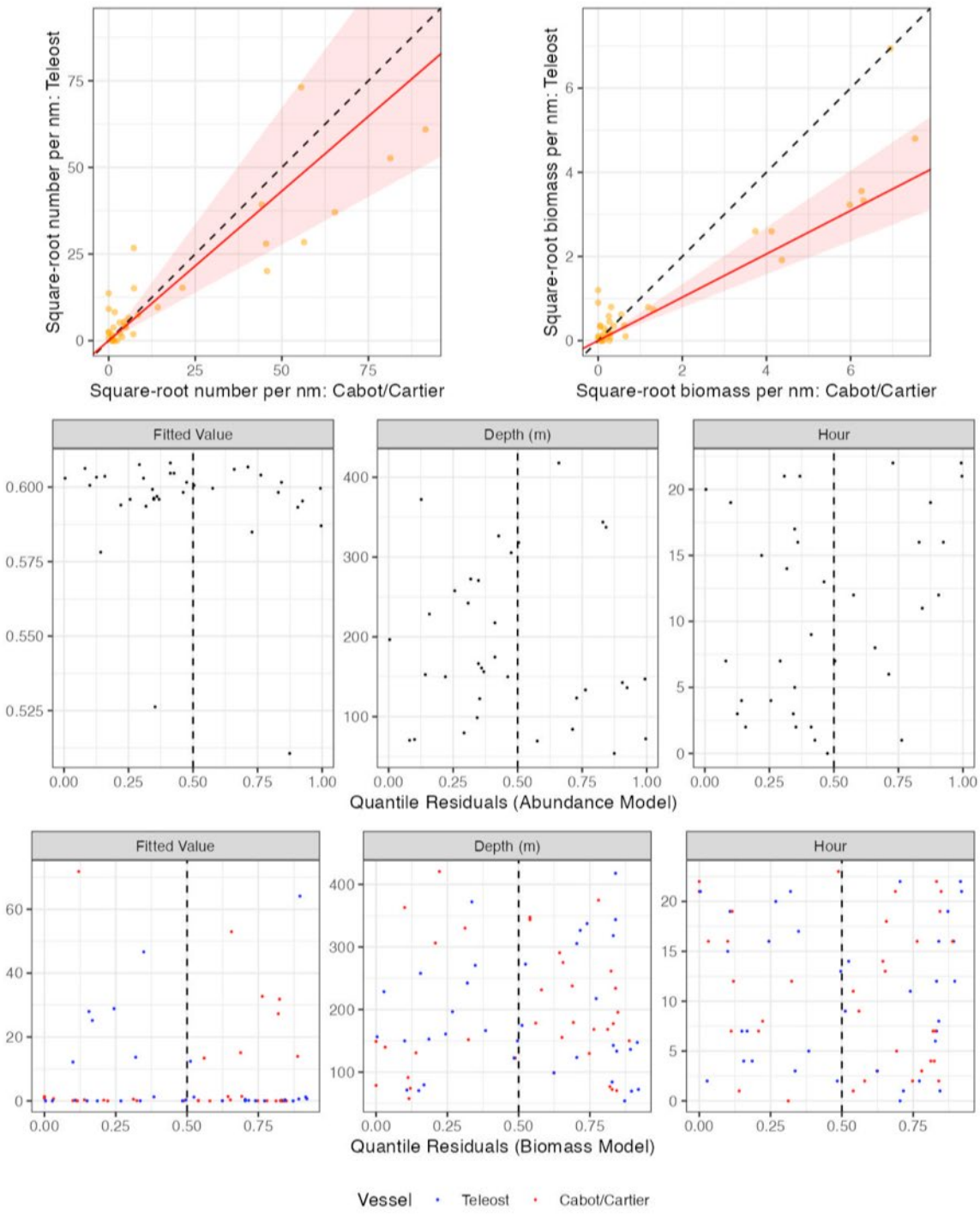

Figure 65. Visualisation of comparative fishing data, size-aggregated model predictions and residual diagnostics plots for Pandalus borealis (2211).

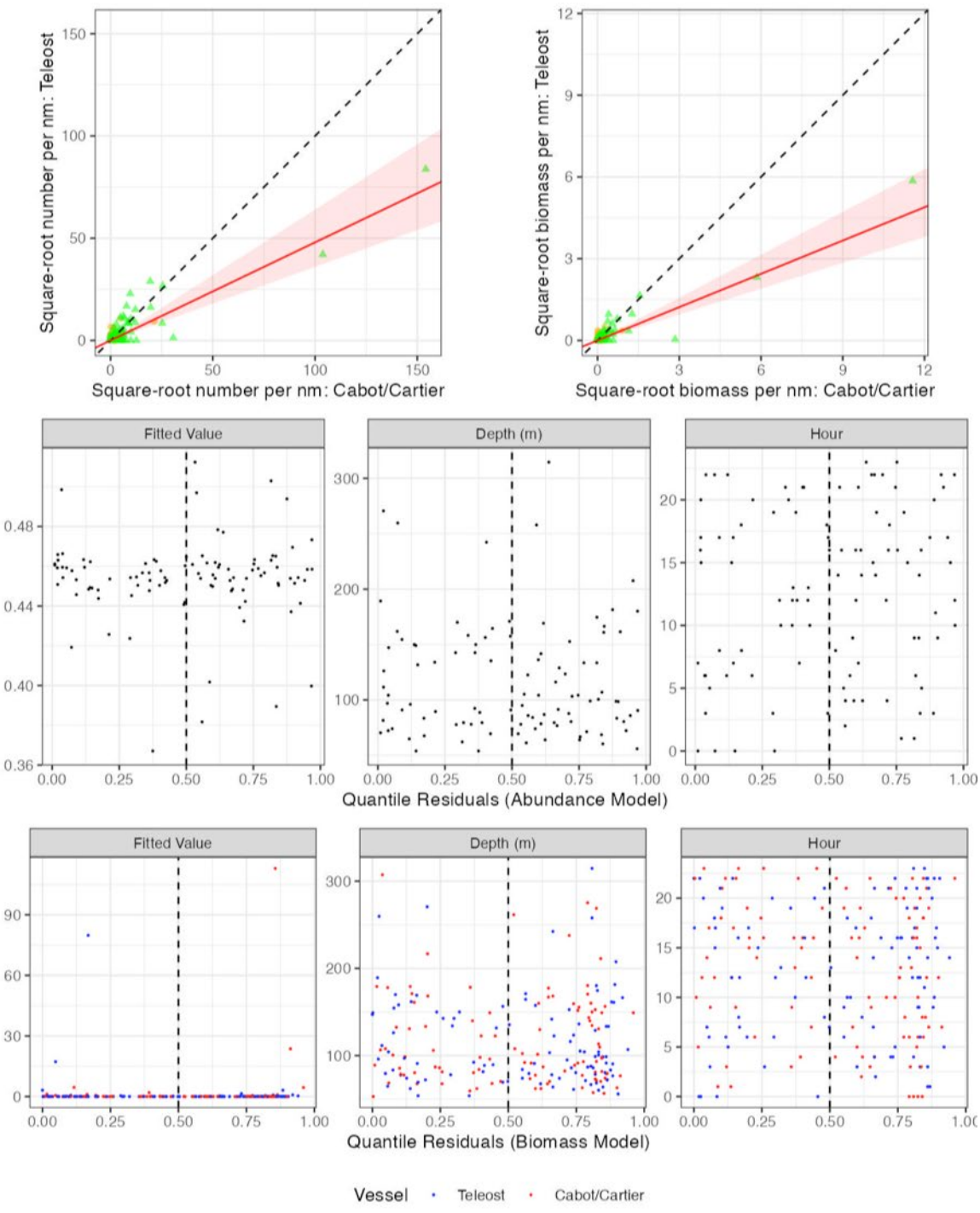

Figure 66. Visualisation of comparative fishing data, size-aggregated model predictions and residual diagnostics plots for Pandalus montagui (2212).

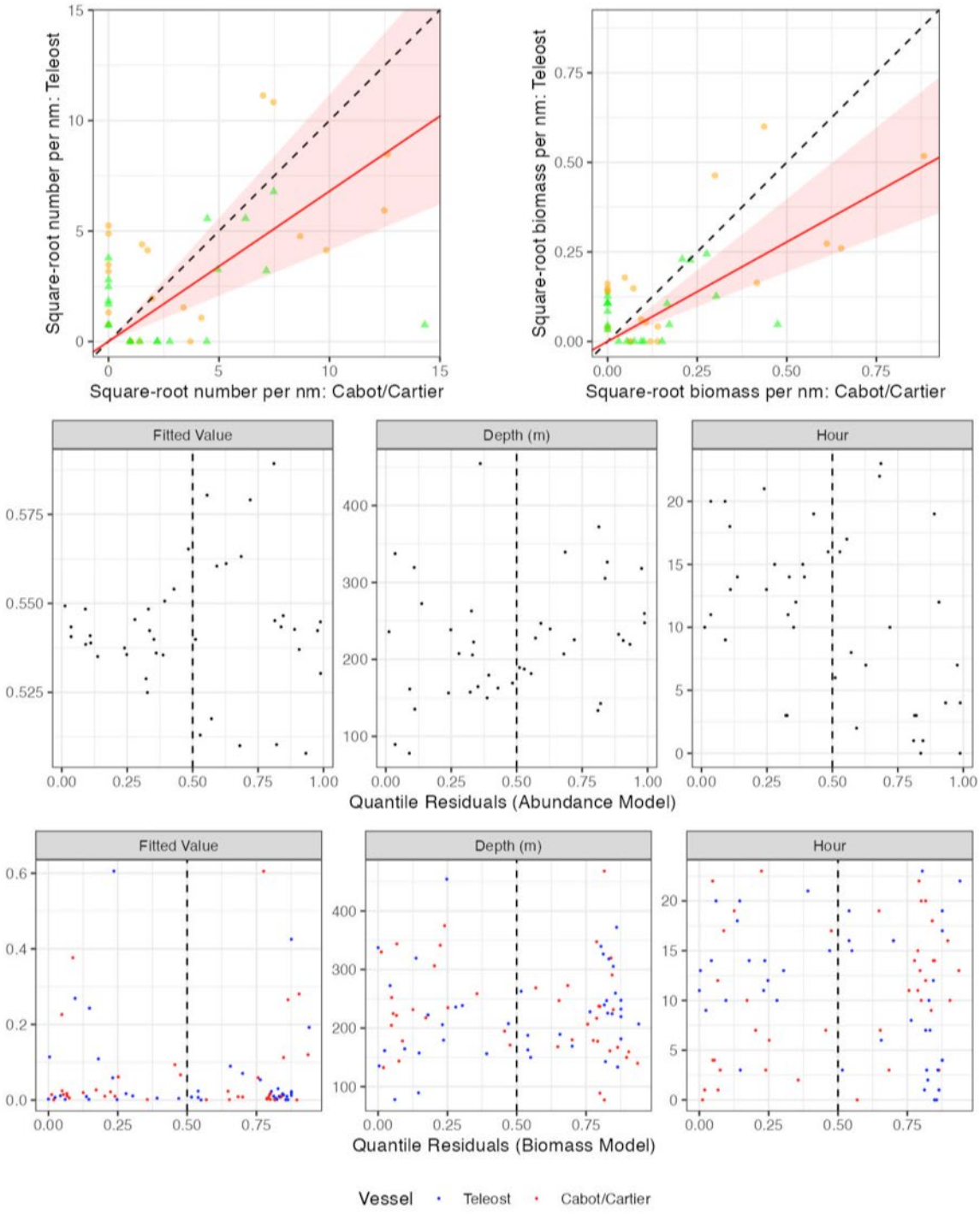

Figure 67. Visualisation of comparative fishing data, size-aggregated model predictions and residual diagnostics plots for Atlantopandalus propinqvus (2213).

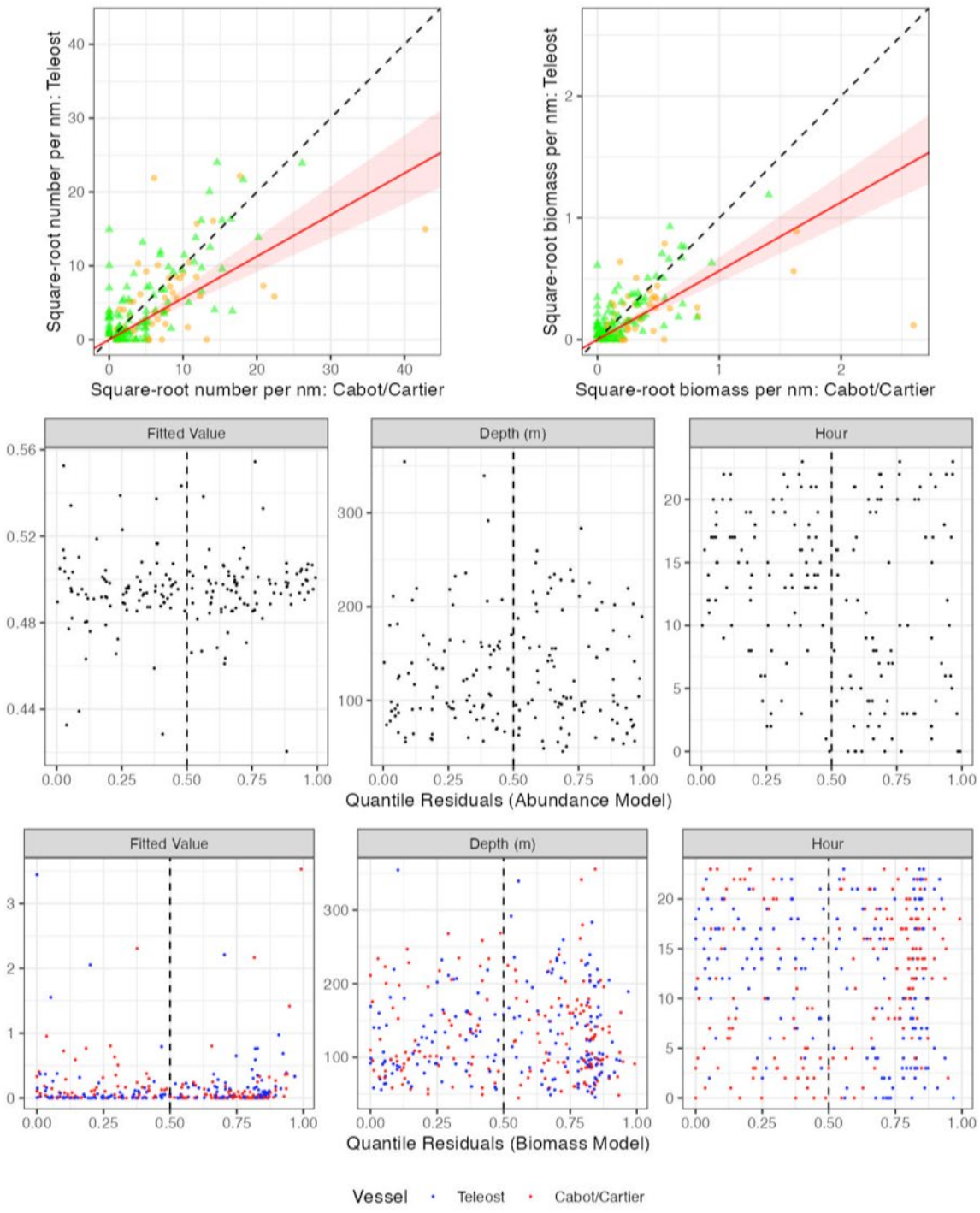

Figure 68. Visualisation of comparative fishing data, size-aggregated model predictions and residual diagnostics plots for Dichelopandalus leptocerus (2214).

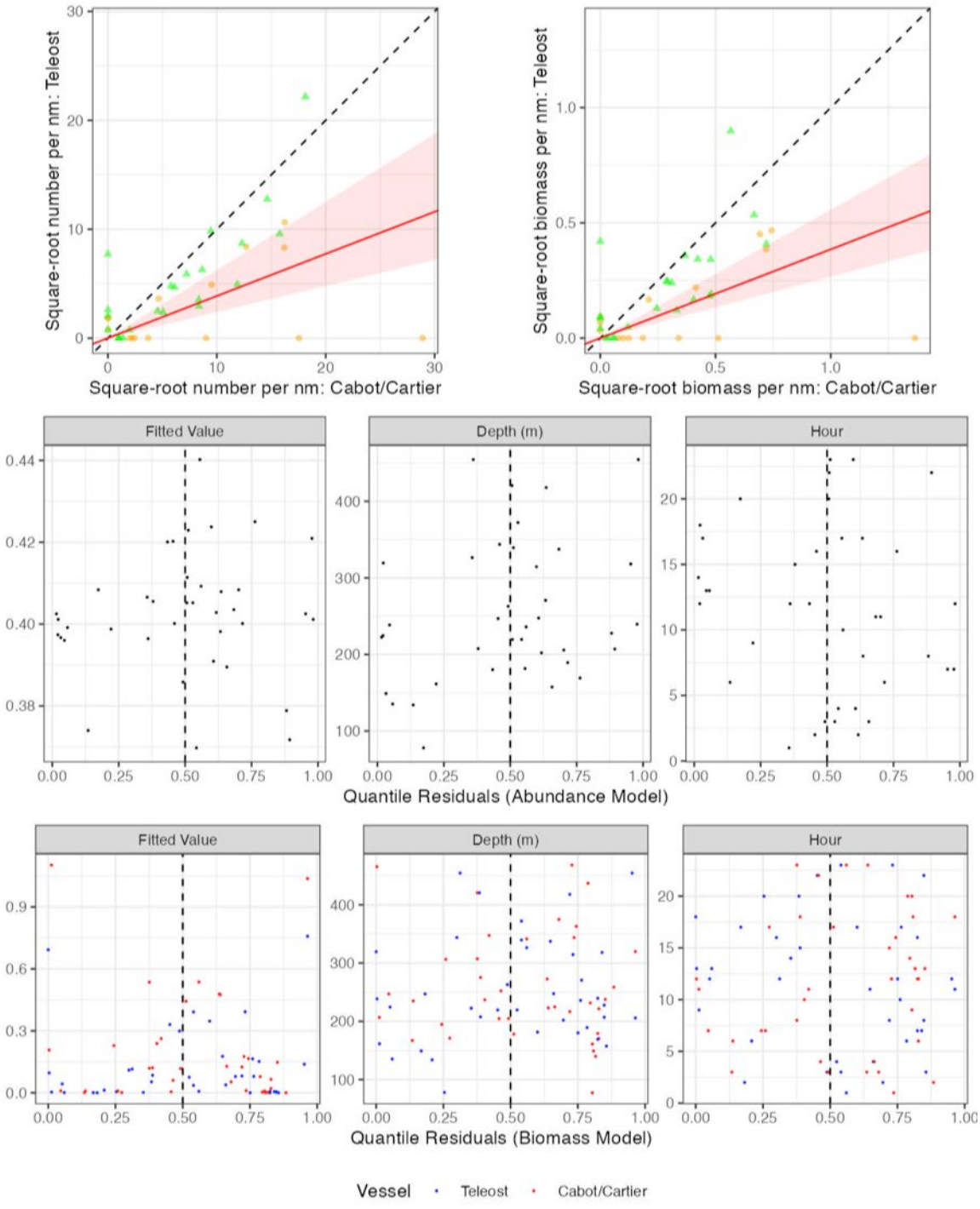

Figure 69. Visualisation of comparative fishing data, size-aggregated model predictions and residual diagnostics plots for Pasiphaea multidentata (2221).

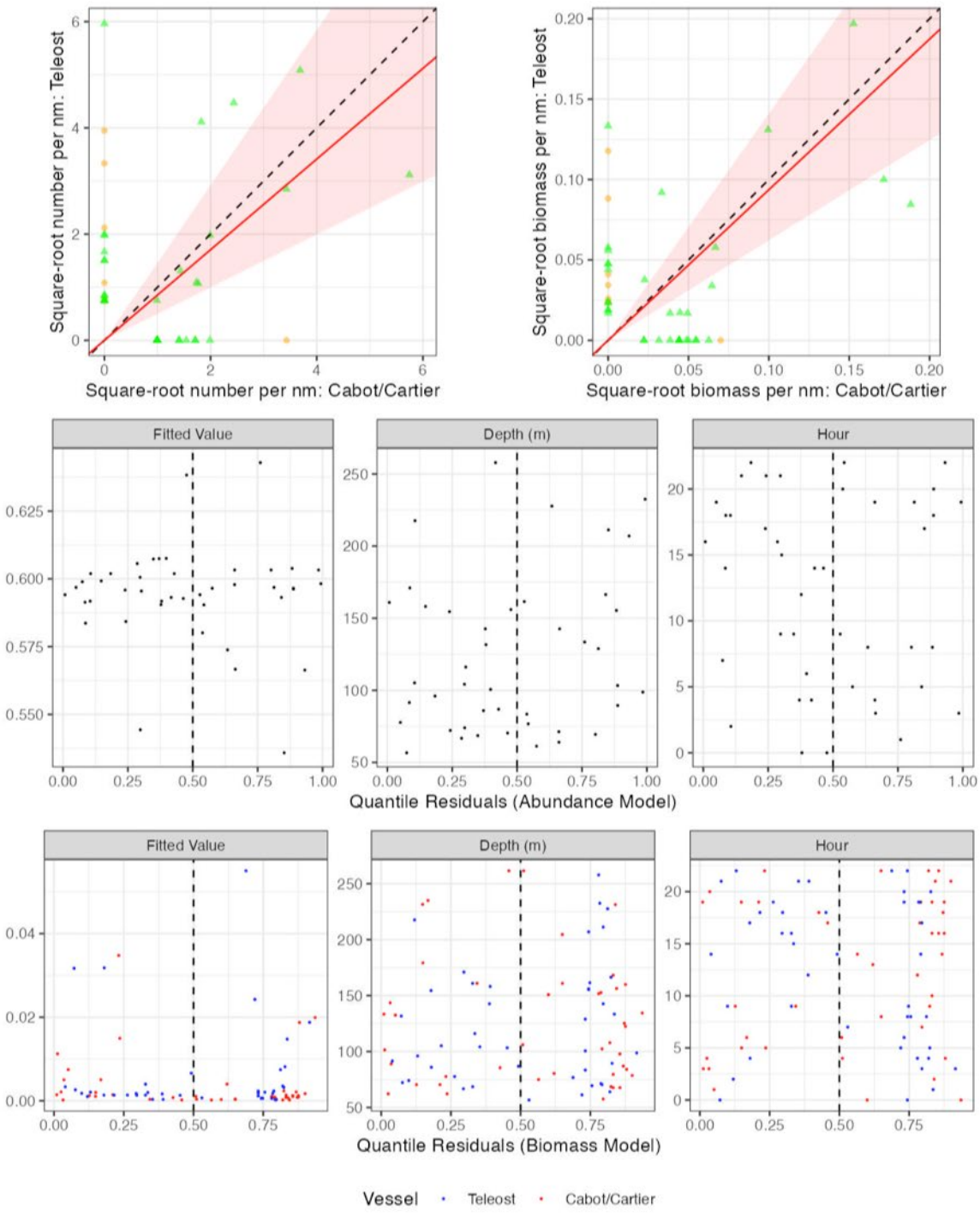

Figure 70. Visualisation of comparative fishing data, size-aggregated model predictions and residual diagnostics plots for Lebbeus polaris (2312).

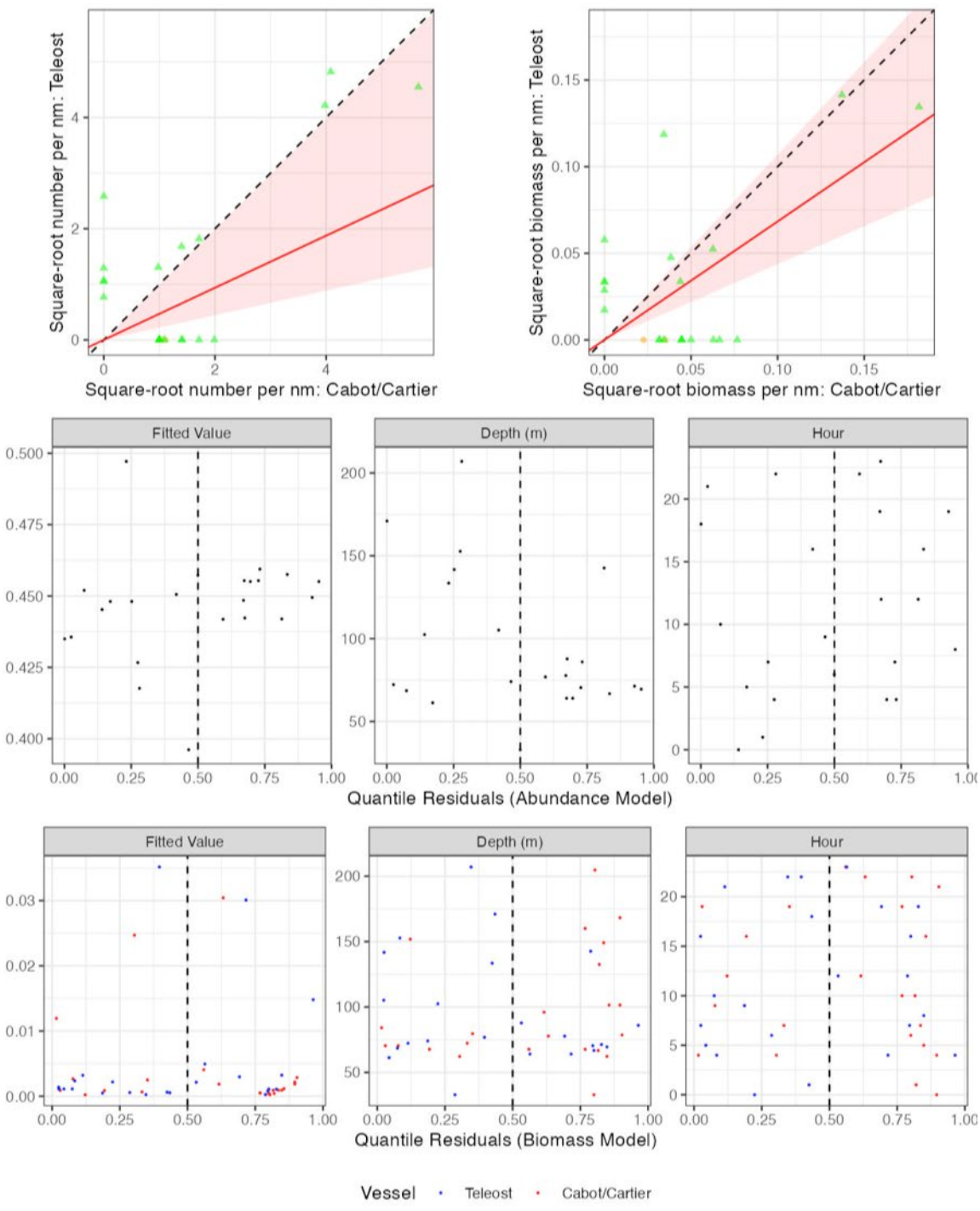

Figure 71. Visualisation of comparative fishing data, size-aggregated model predictions and residual diagnostics plots for Spirontocaris spinus (2316).

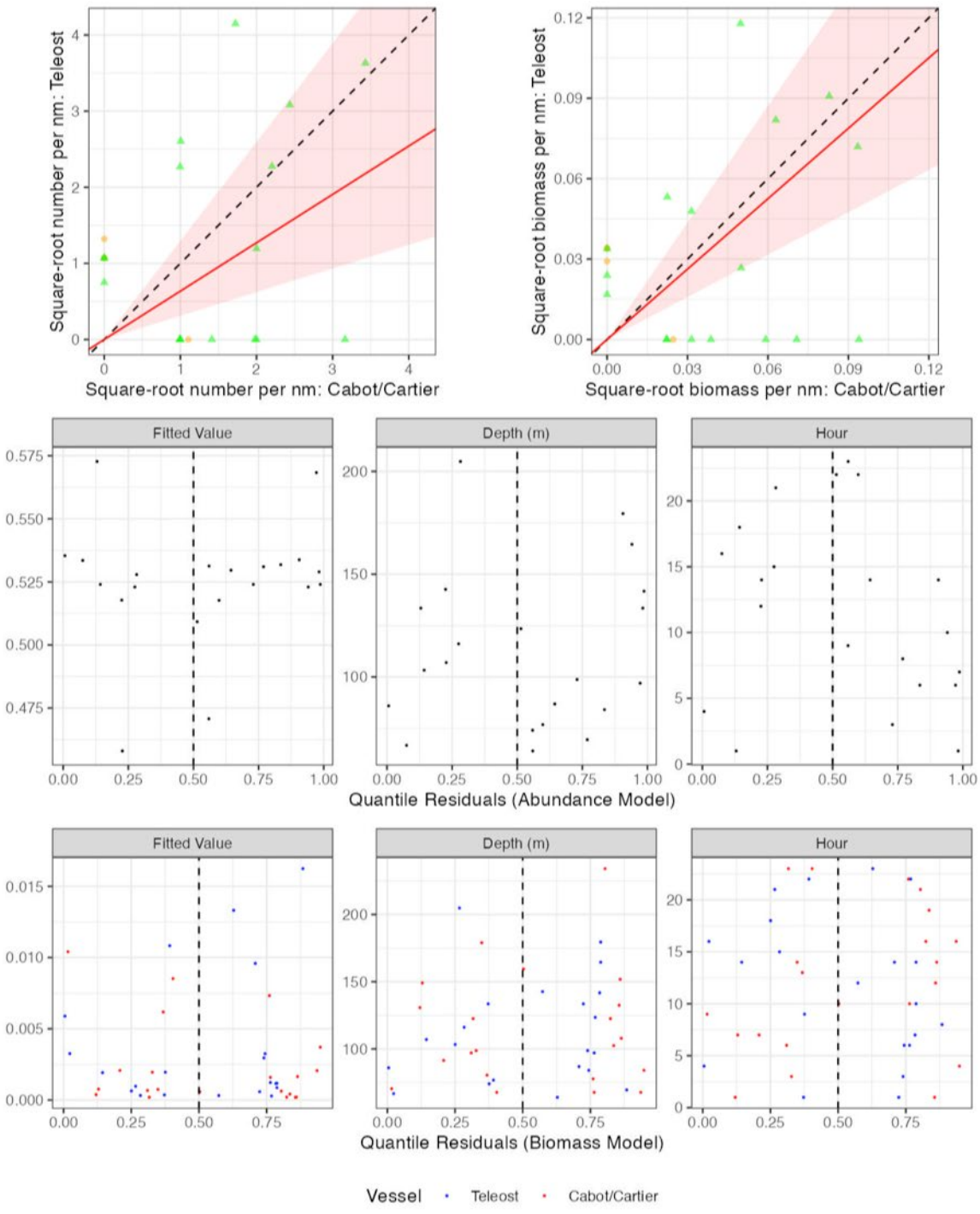

Figure 72. Visualisation of comparative fishing data, size-aggregated model predictions and residual diagnostics plots for Eualus fabricii (2332).

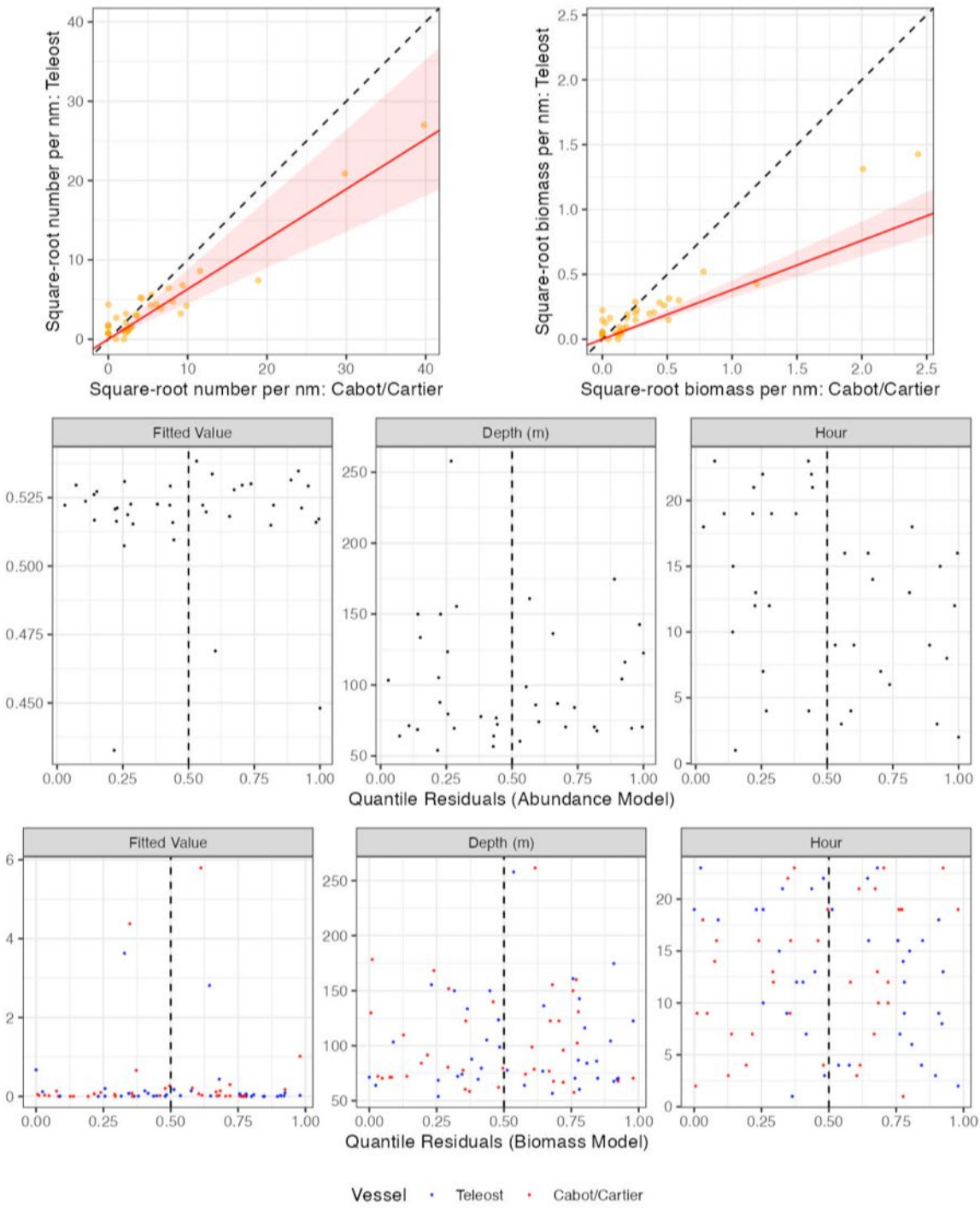

Figure 73. Visualisation of comparative fishing data, size-aggregated model predictions and residual diagnostics plots for Argis dentata (2411).

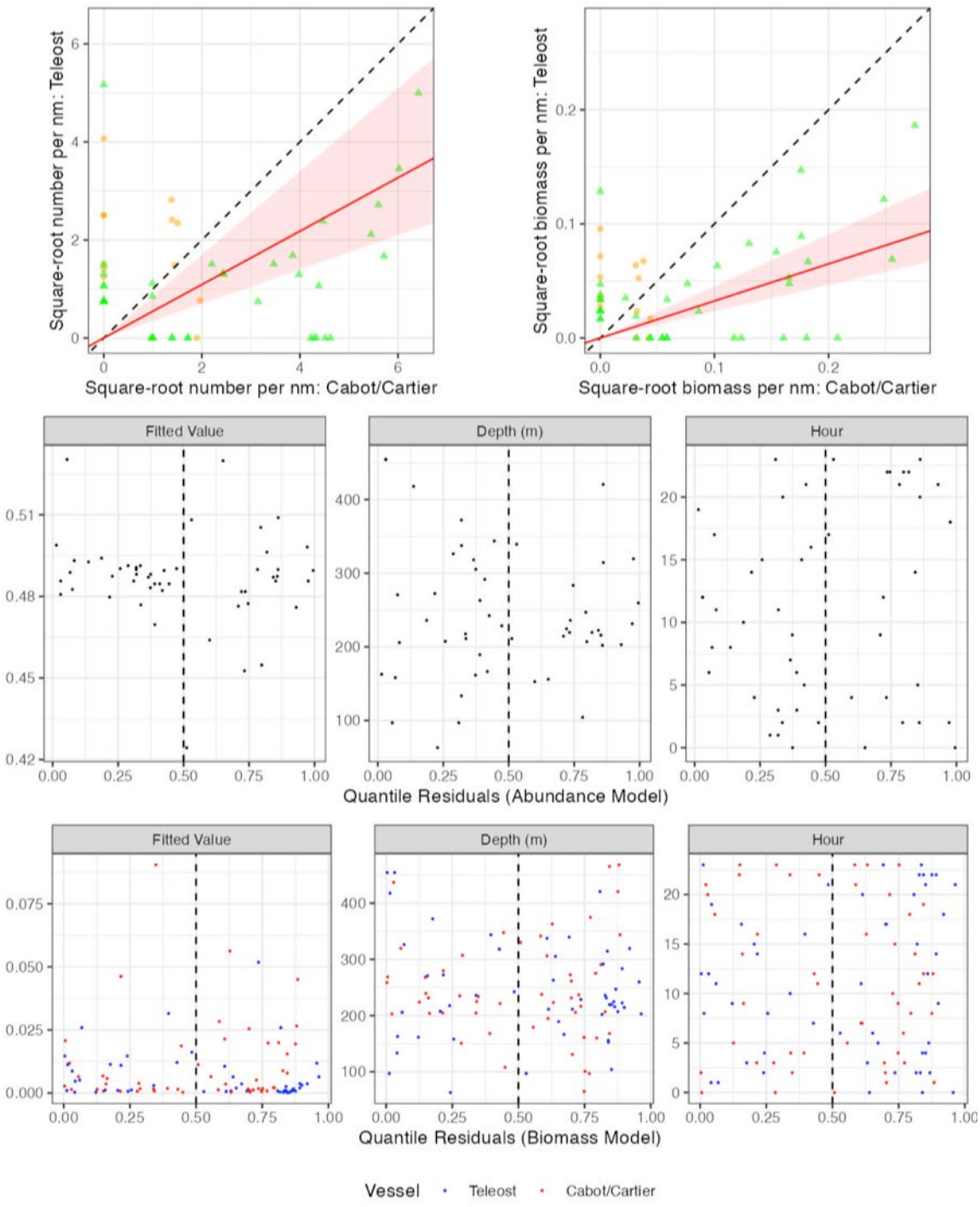

Figure 74. Visualisation of comparative fishing data, size-aggregated model predictions and residual diagnostics plots for Pontophilus norvegicus (2415).

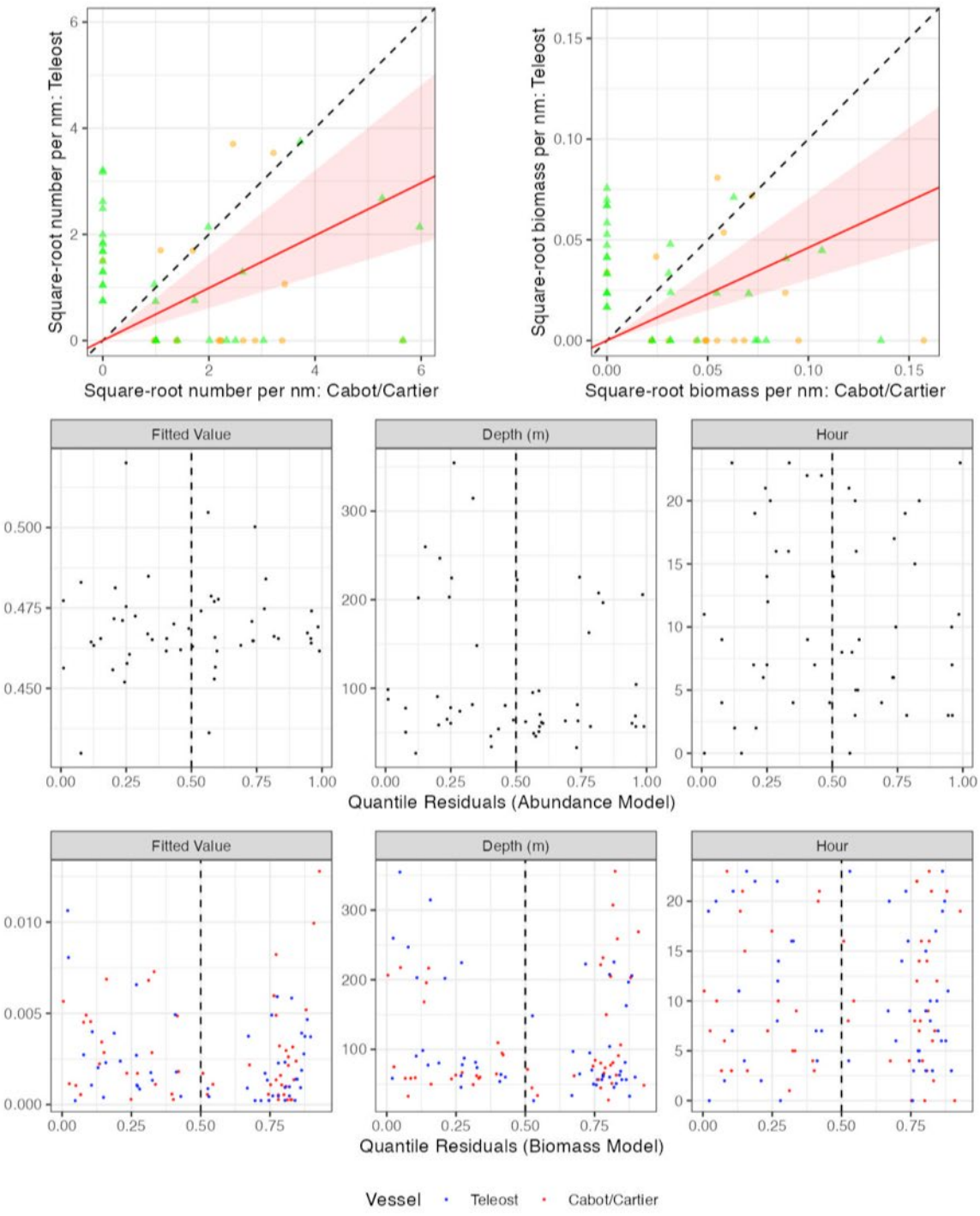

Figure 75. Visualisation of comparative fishing data, size-aggregated model predictions and residual diagnostics plots for Crangon septemspinosa (2417).

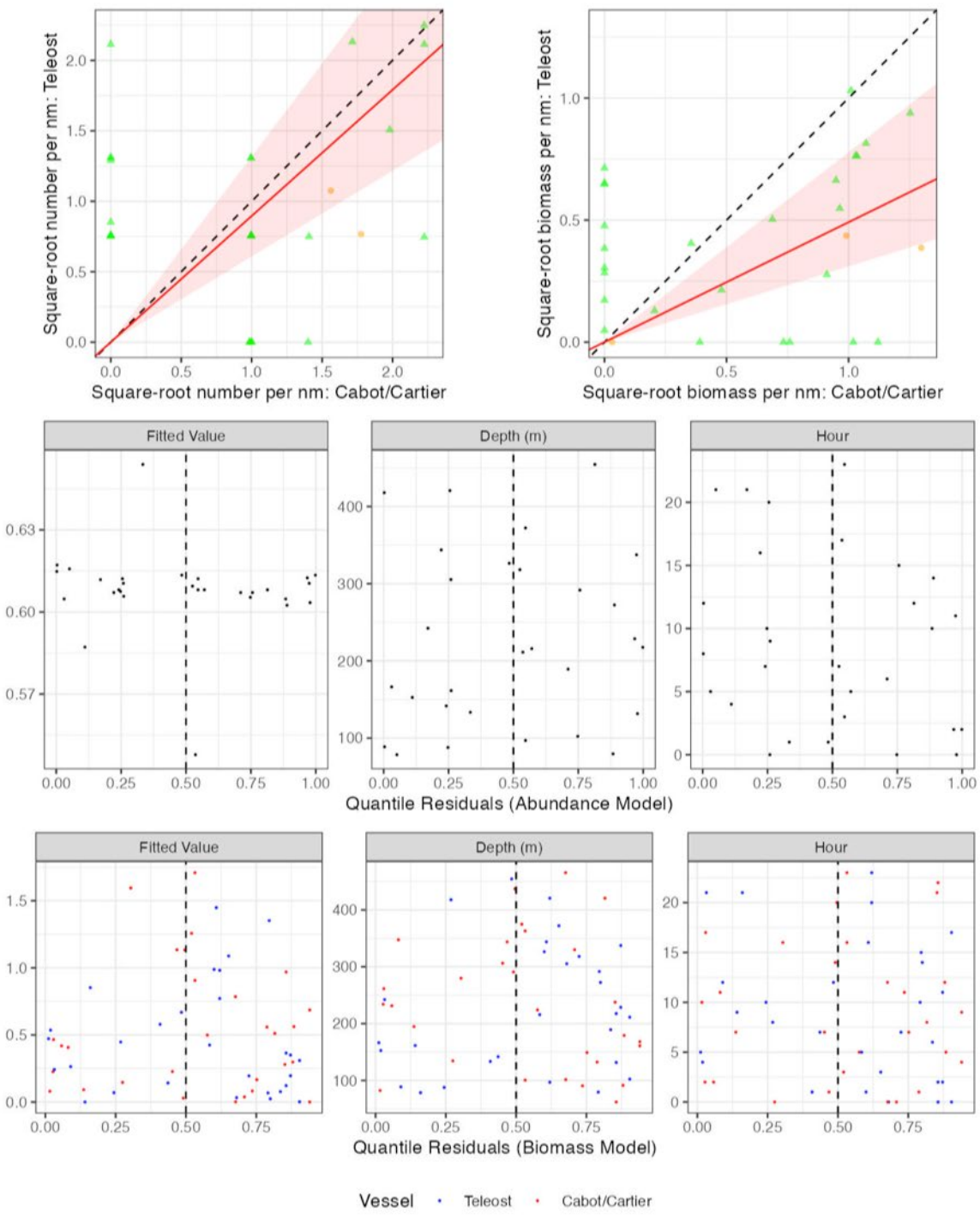

Figure 76. Visualisation of comparative fishing data, size-aggregated model predictions and residual diagnostics plots for Lithodes maja (2523).

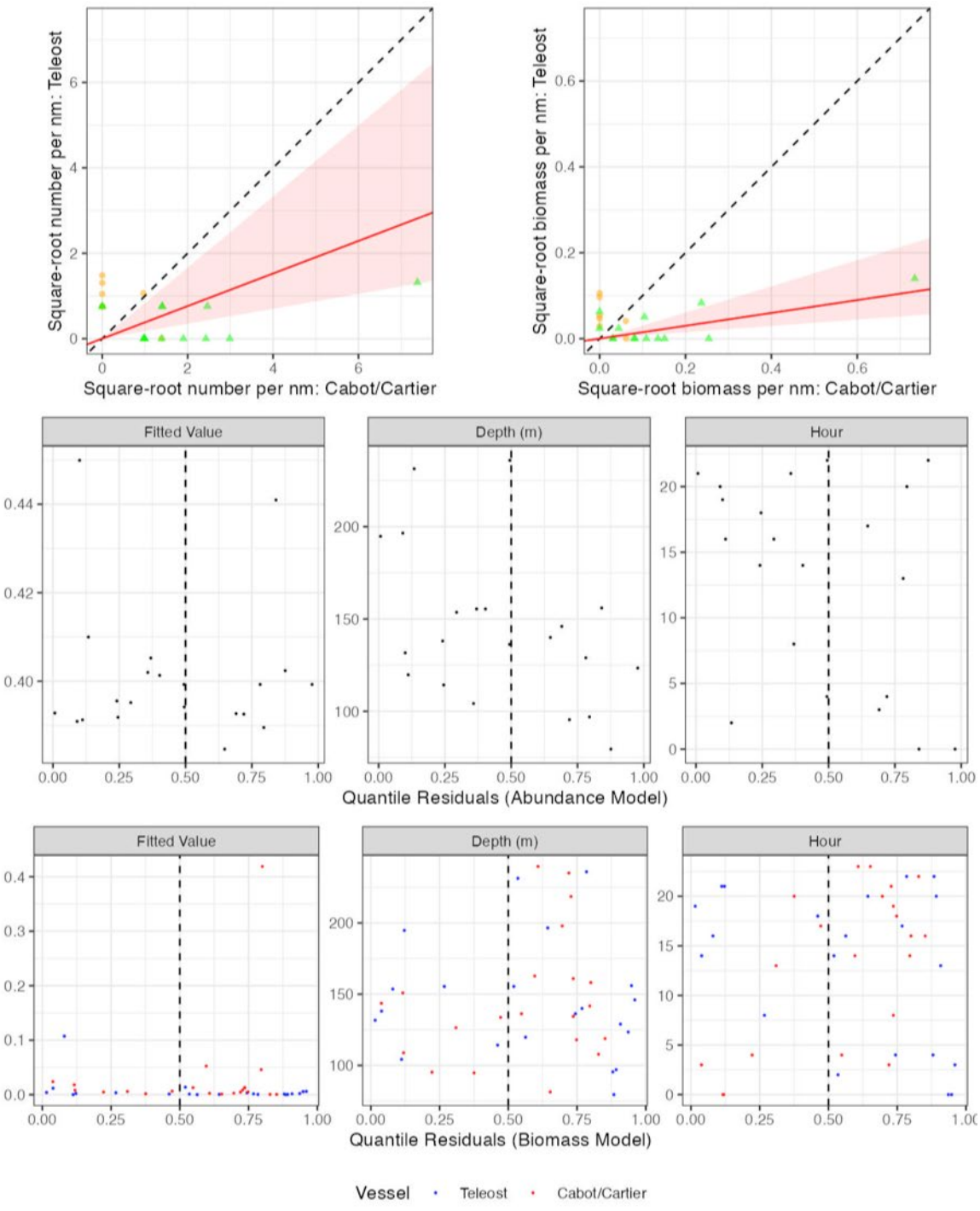

Figure 77. Visualisation of comparative fishing data, size-aggregated model predictions and residual diagnostics plots for Munida iris (2555).

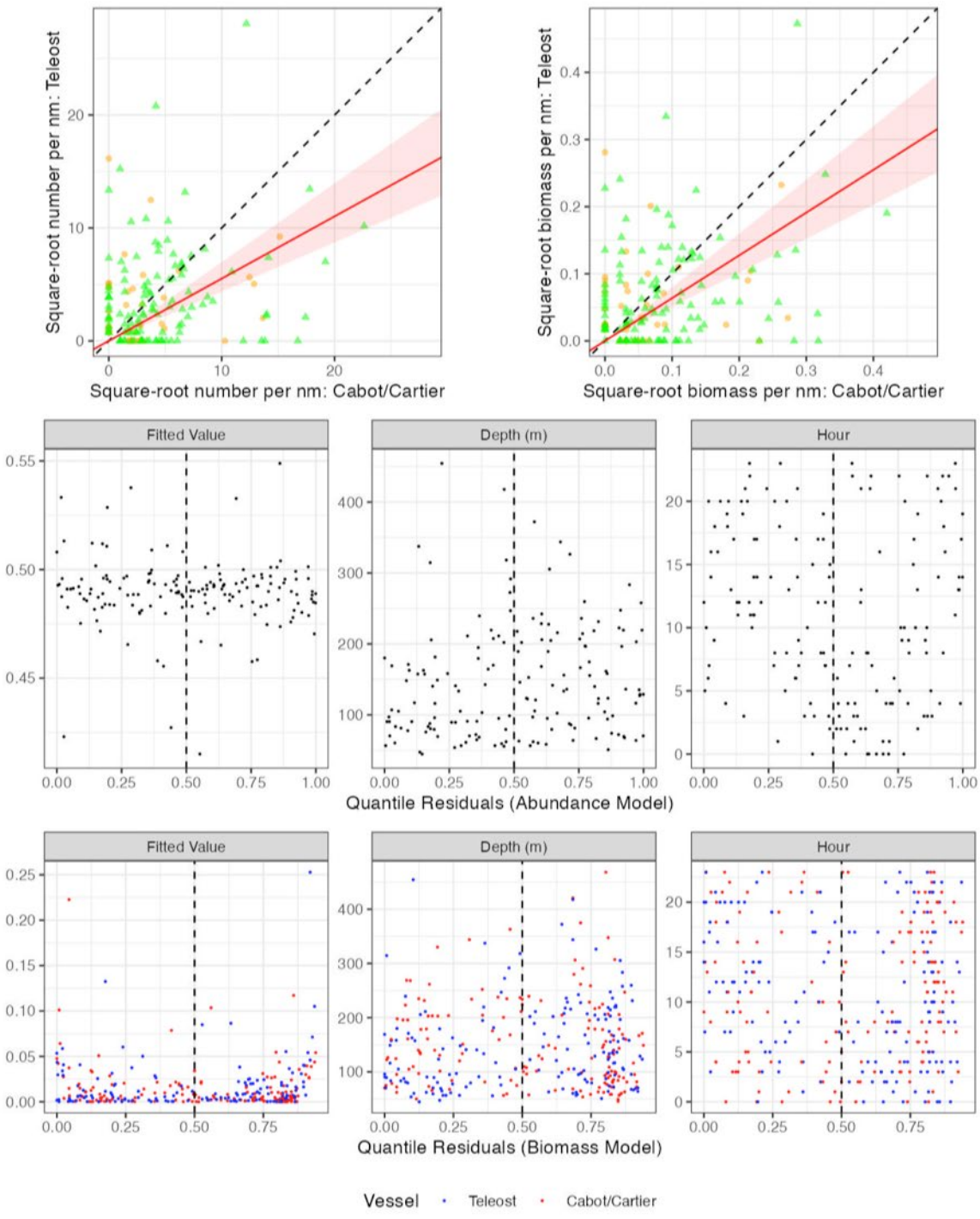

Figure 78. Visualisation of comparative fishing data, size-aggregated model predictions and residual diagnostics plots for Euphausiacea o. (2600).

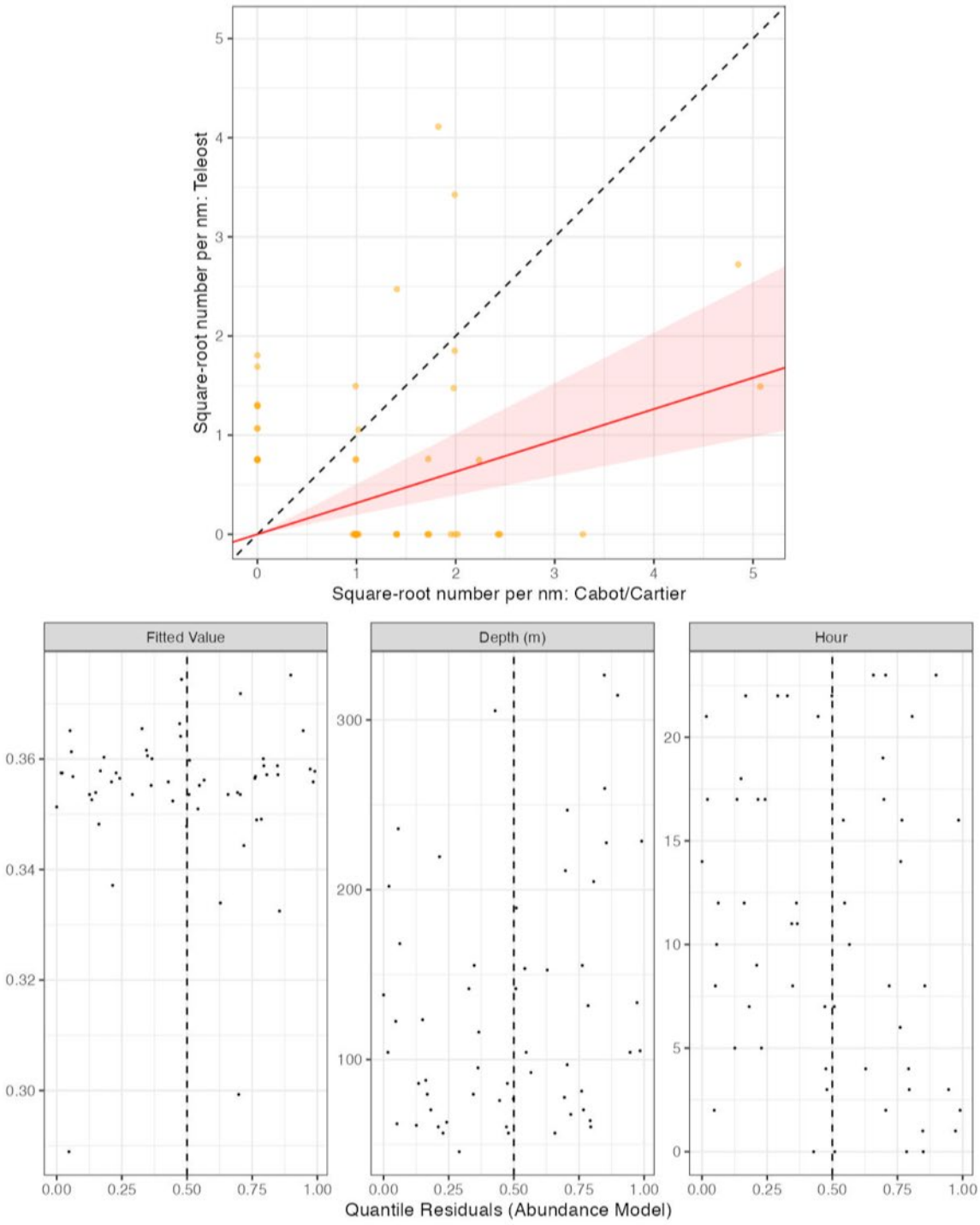

Figure 79. Visualisation of comparative fishing data, size-aggregated model predictions and residual diagnostics plots for Parathemisto sp. (2809).

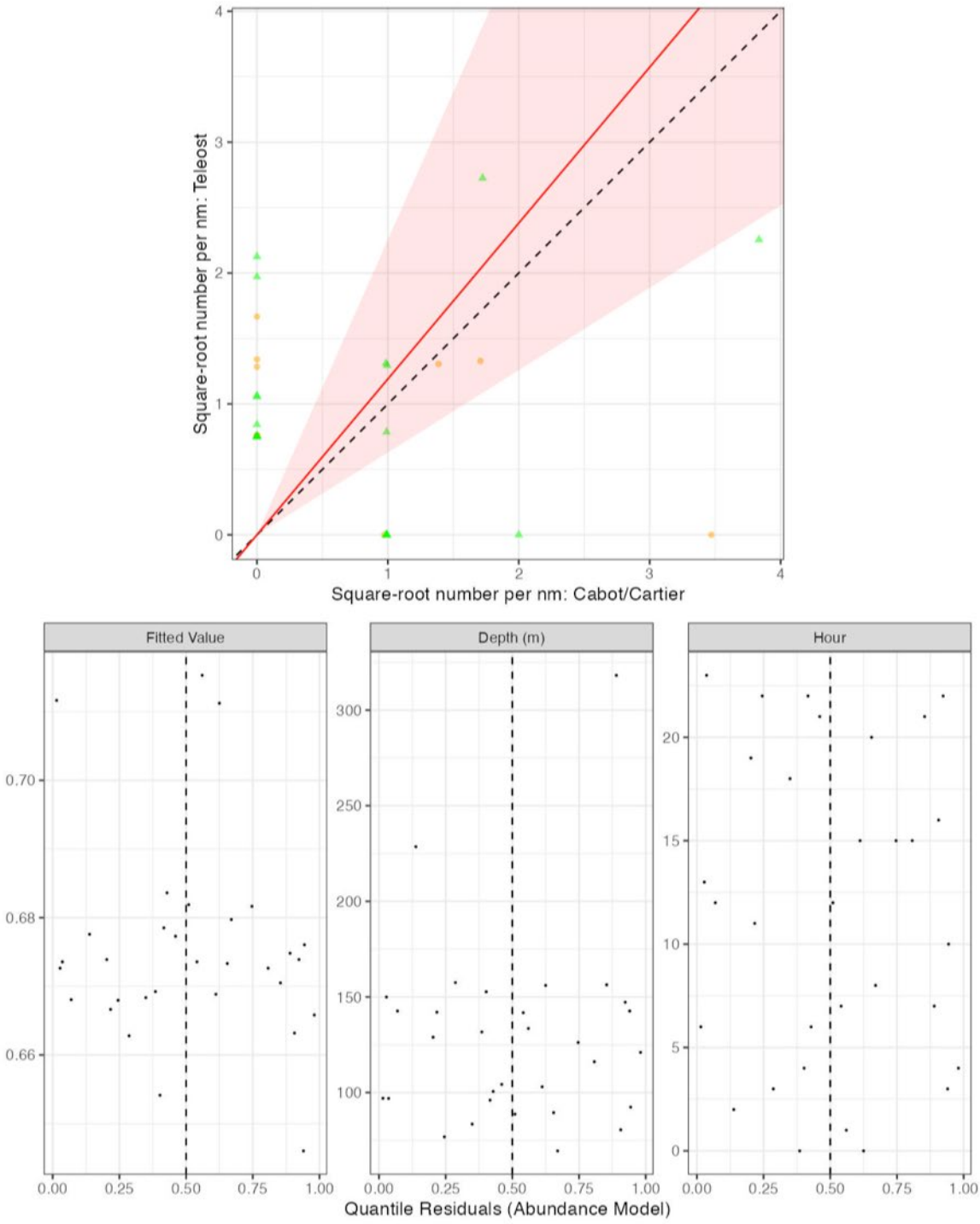

Figure 80. Visualisation of comparative fishing data, size-aggregated model predictions and residual diagnostics plots for Nymphon sp. (2893).

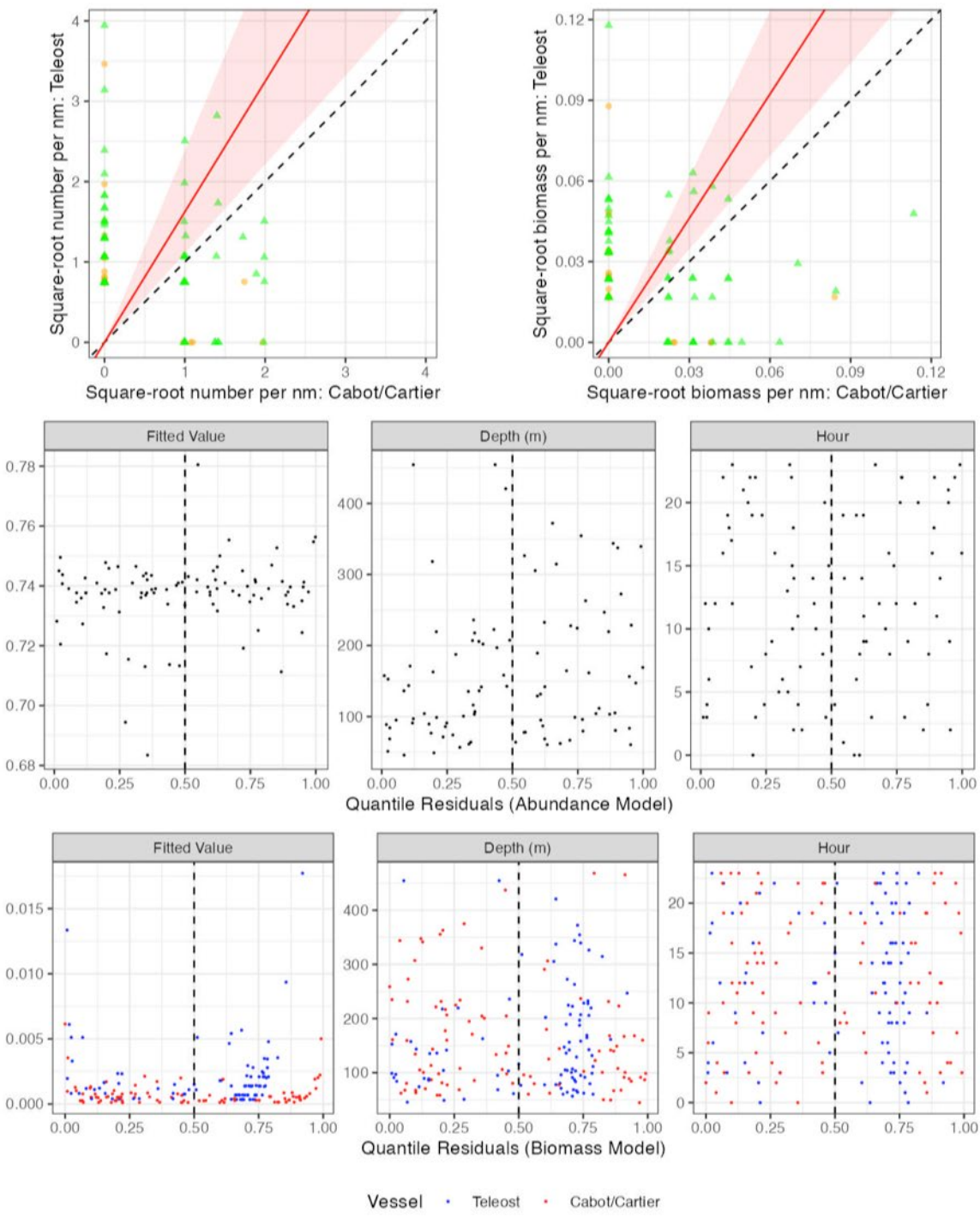

Figure 81. Visualisation of comparative fishing data, size-aggregated model predictions and residual diagnostics plots for Annelida p. (3000).

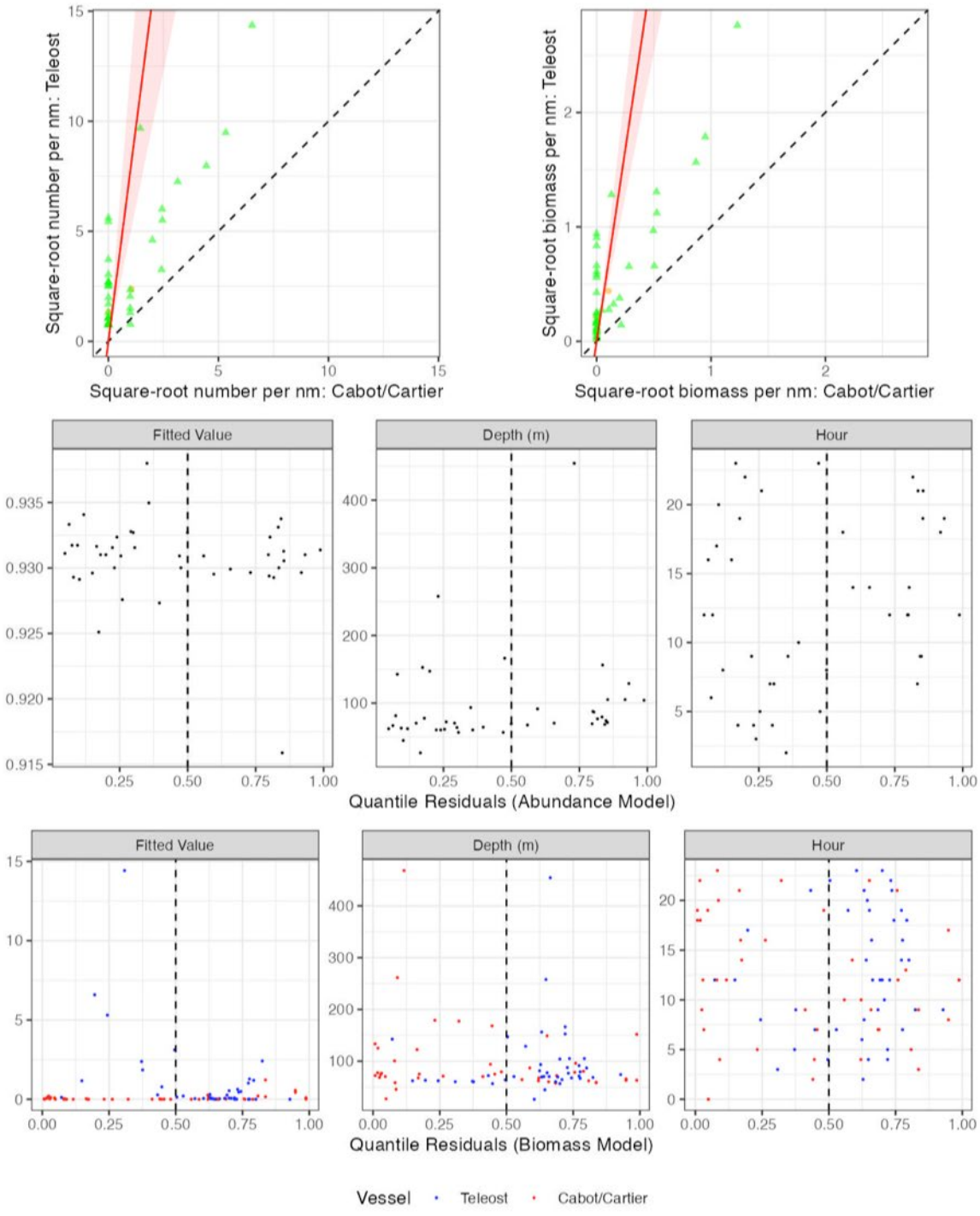

Figure 82. Visualisation of comparative fishing data, size-aggregated model predictions and residual diagnostics plots for Buccinum sp. (4210).

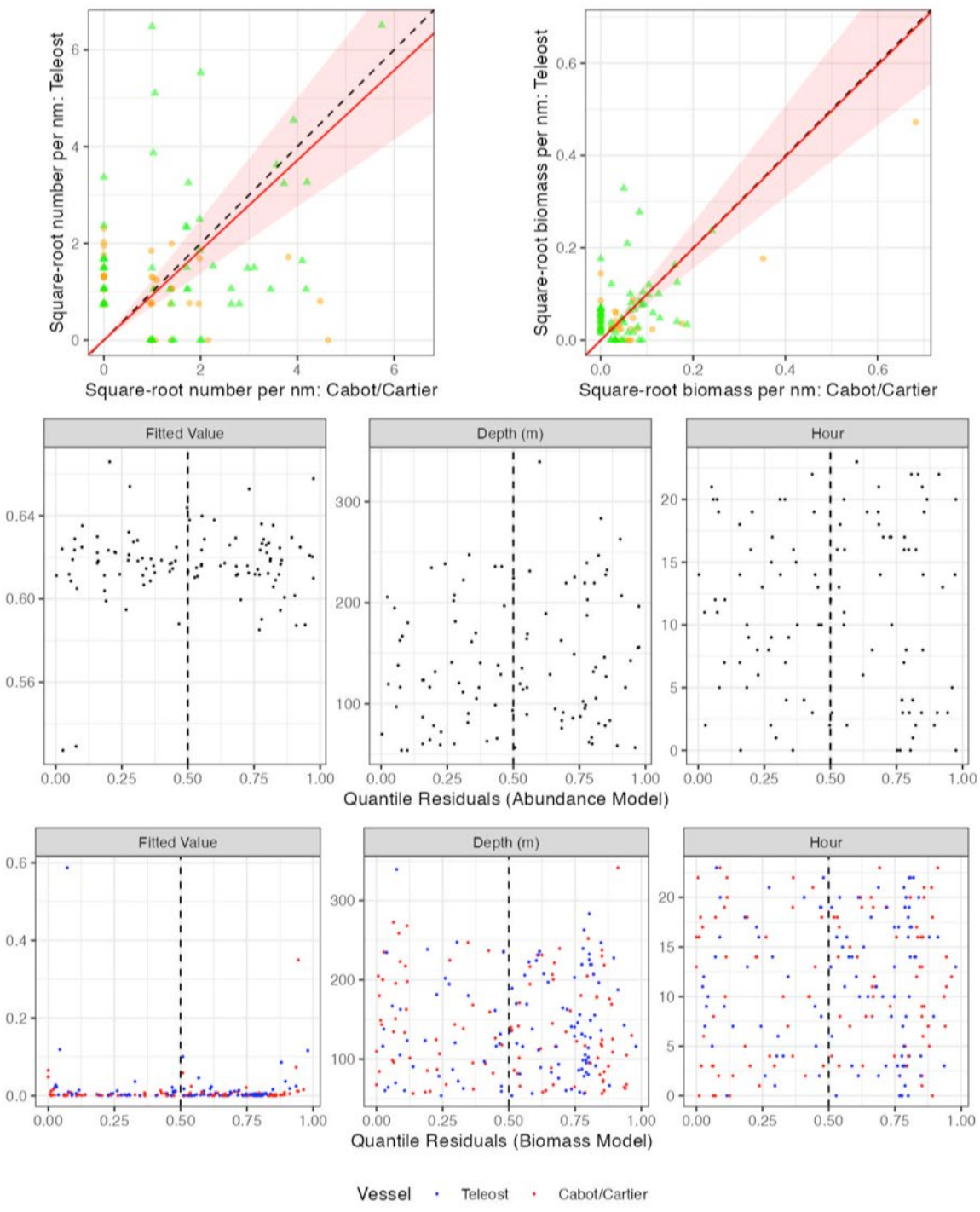

Figure 83. Visualisation of comparative fishing data, size-aggregated model predictions and residual diagnostics plots for Nudibranchia o. (4400).

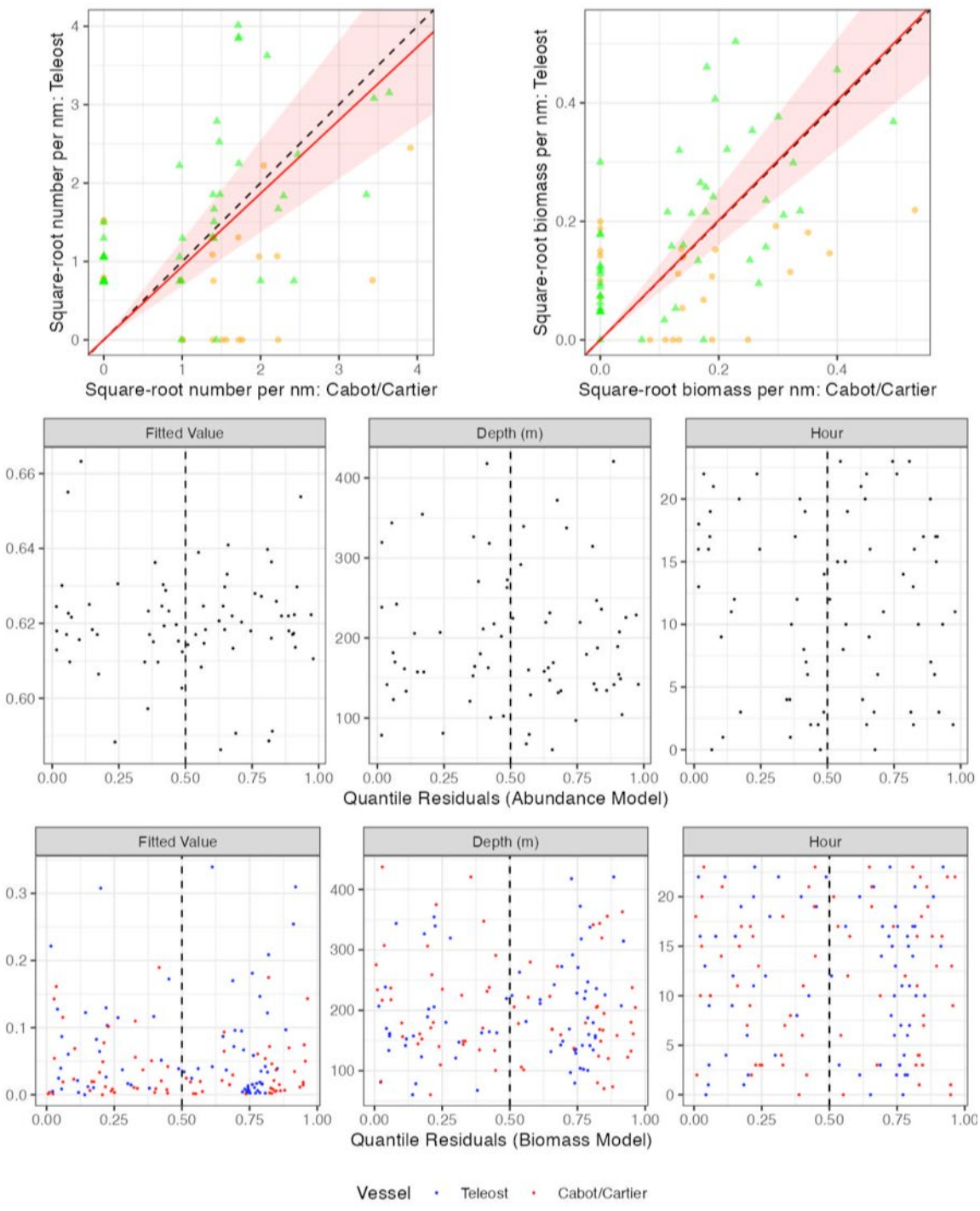

Figure 84. Visualisation of comparative fishing data, size-aggregated model predictions and residual diagnostics plots for Bathypolypus spp. (4508).

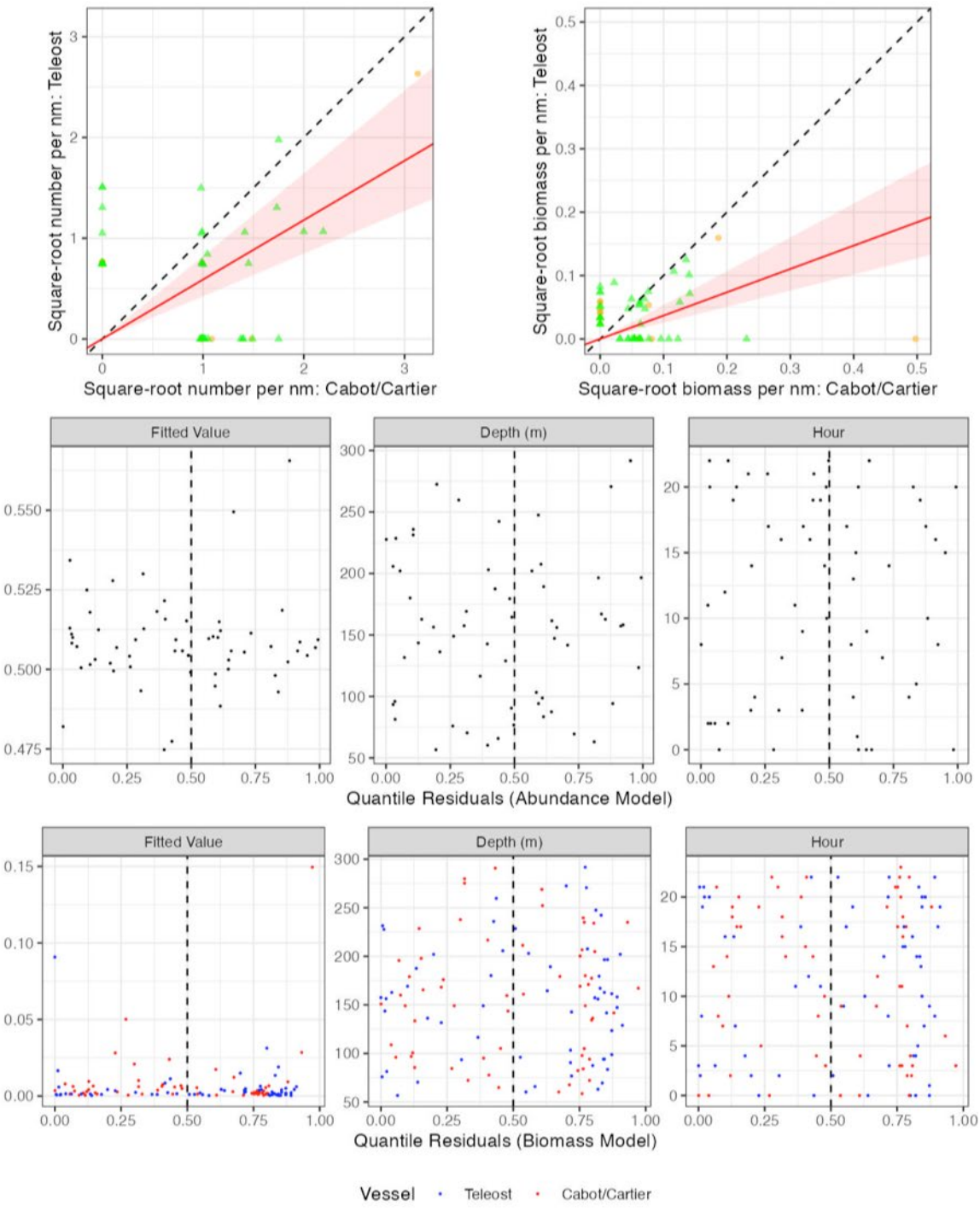

Figure 85. Visualisation of comparative fishing data, size-aggregated model predictions and residual diagnostics plots for Sepiolodae f. (4536).

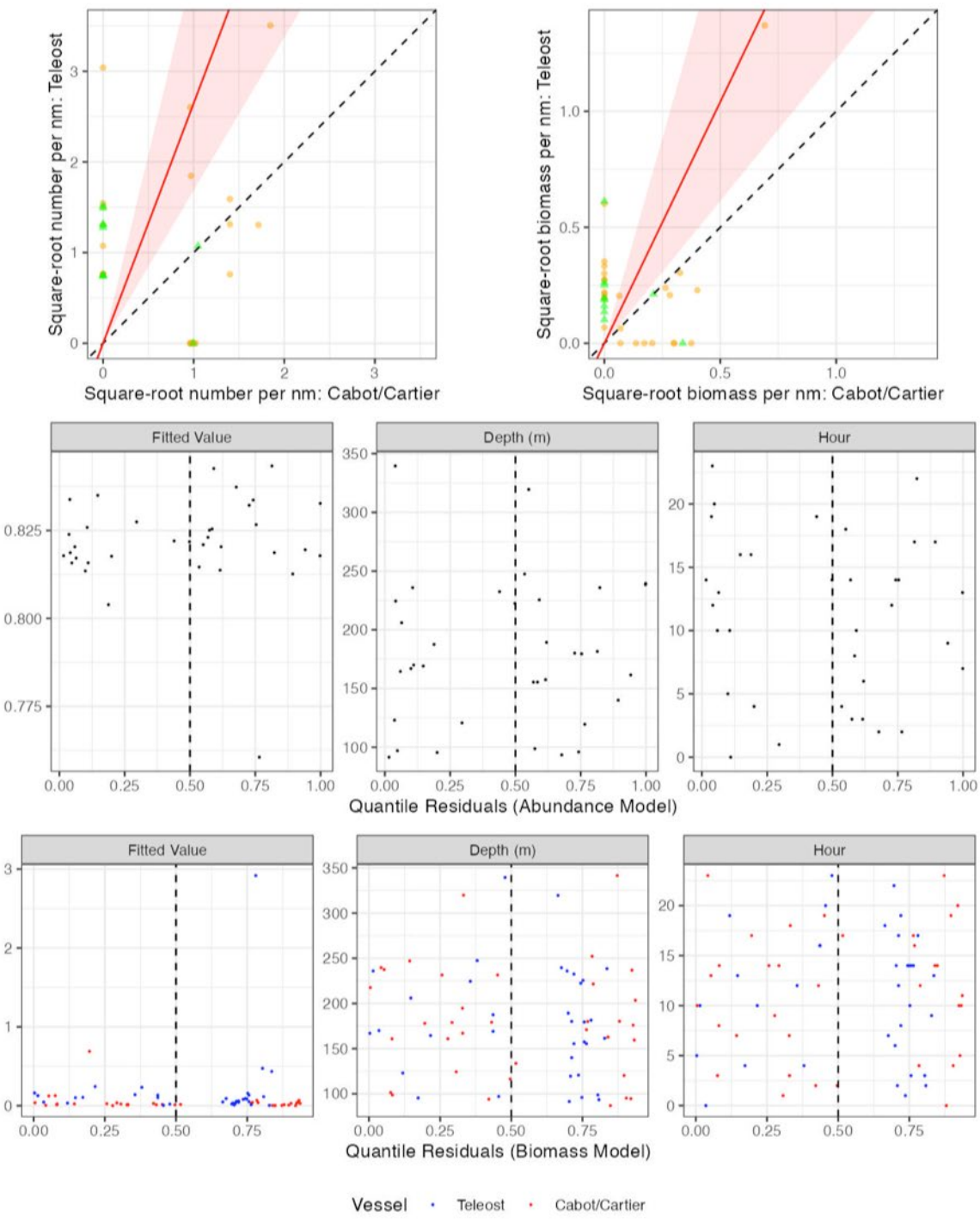

Figure 86. Visualisation of comparative fishing data, size-aggregated model predictions and residual diagnostics plots for Porania pulvilis (6102).

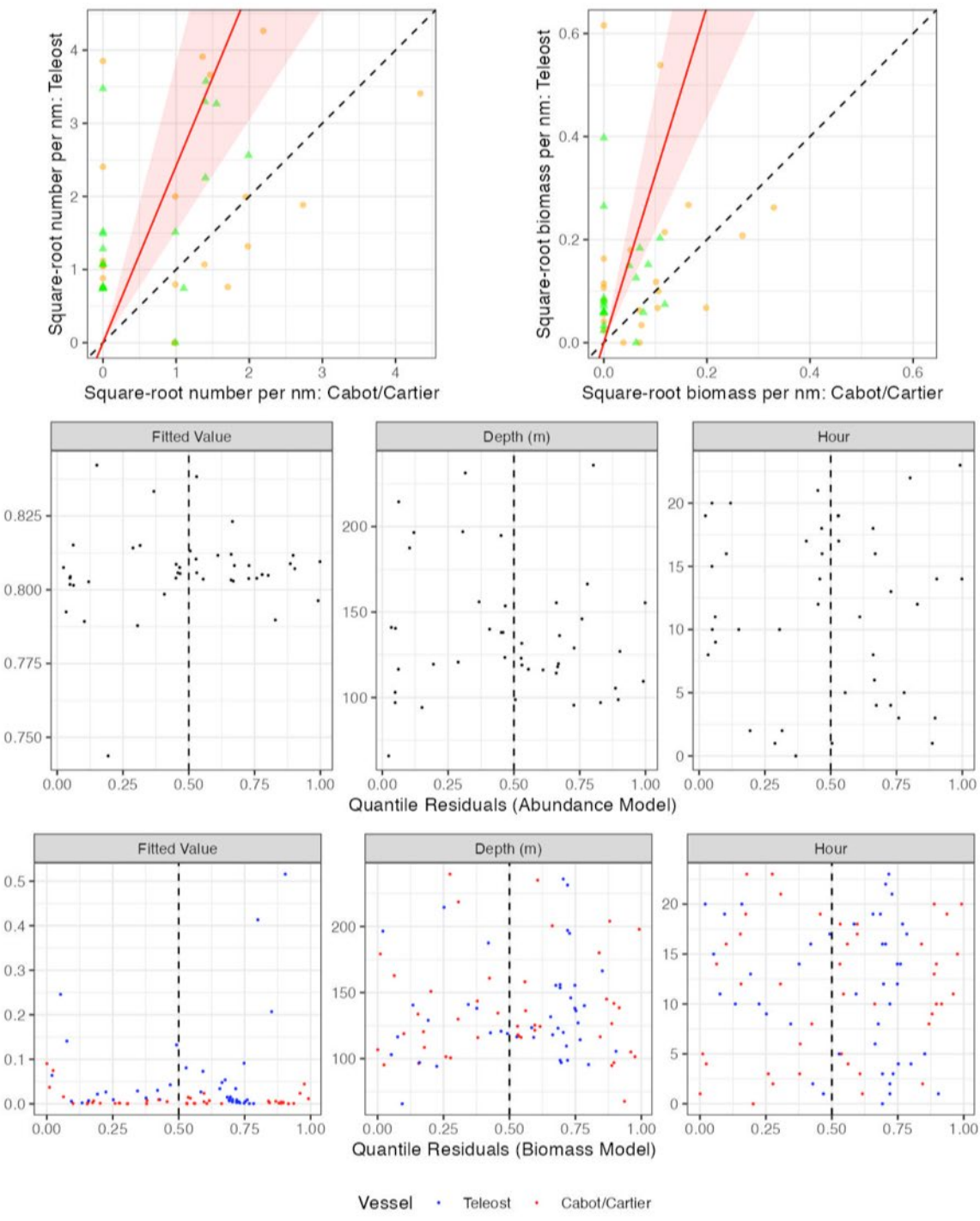

Figure 87. Visualisation of comparative fishing data, size-aggregated model predictions and residual diagnostics plots for Sclerasterias tanneri (6106).

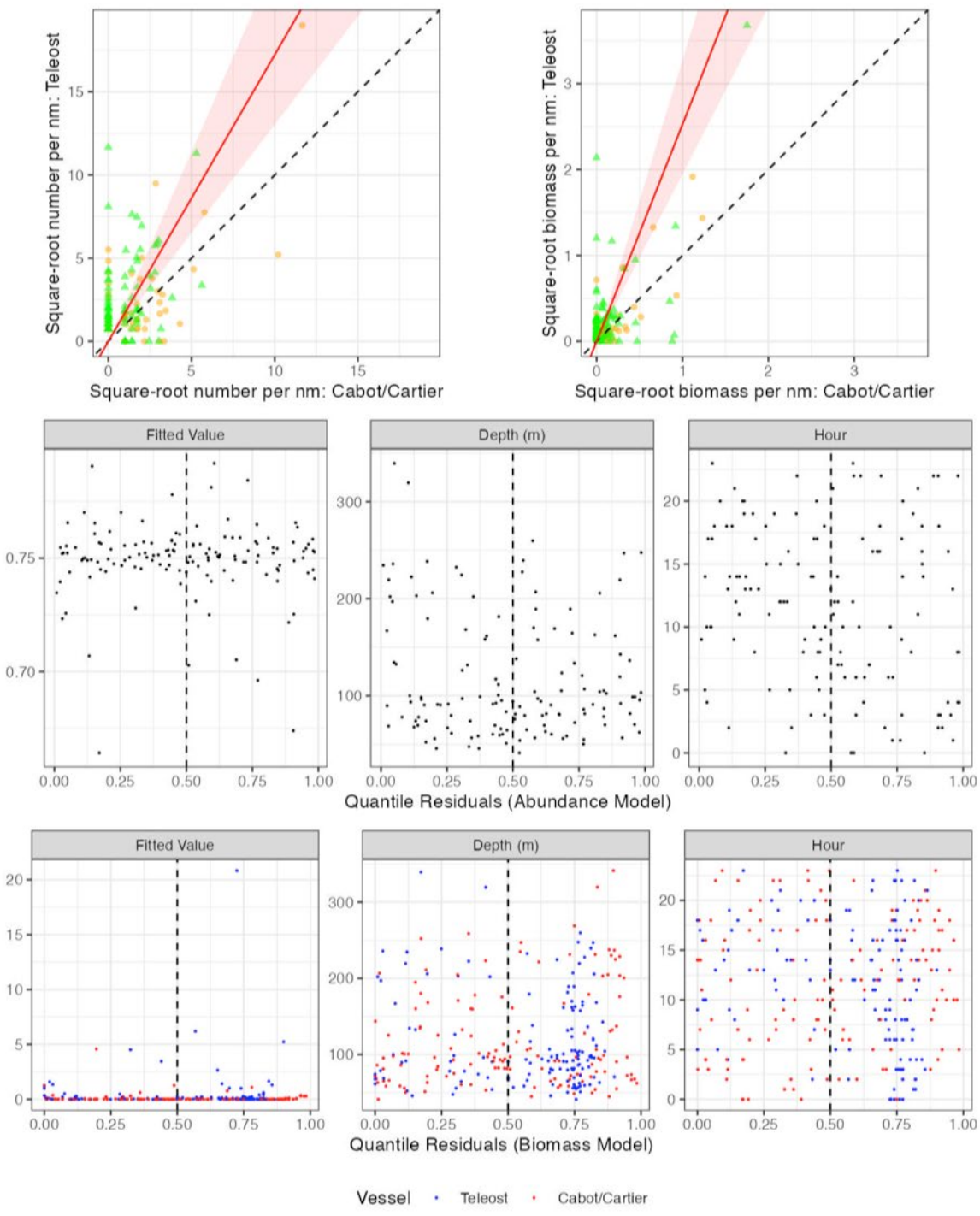

Figure 88. Visualisation of comparative fishing data, size-aggregated model predictions and residual diagnostics plots for Asterias rubens (6111).

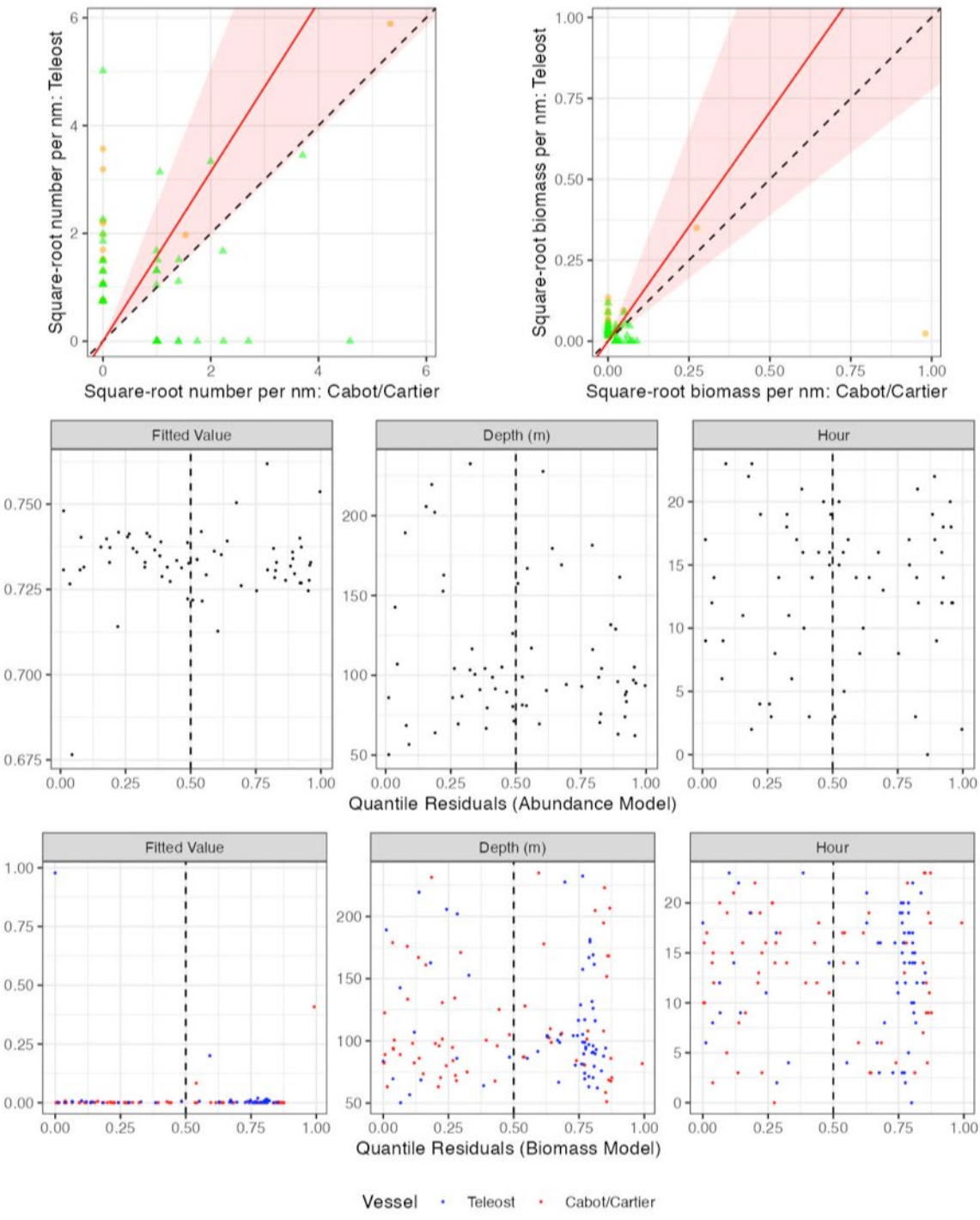

Figure 89. Visualisation of comparative fishing data, size-aggregated model predictions and residual diagnostics plots for Leptasterias sp. (6114).

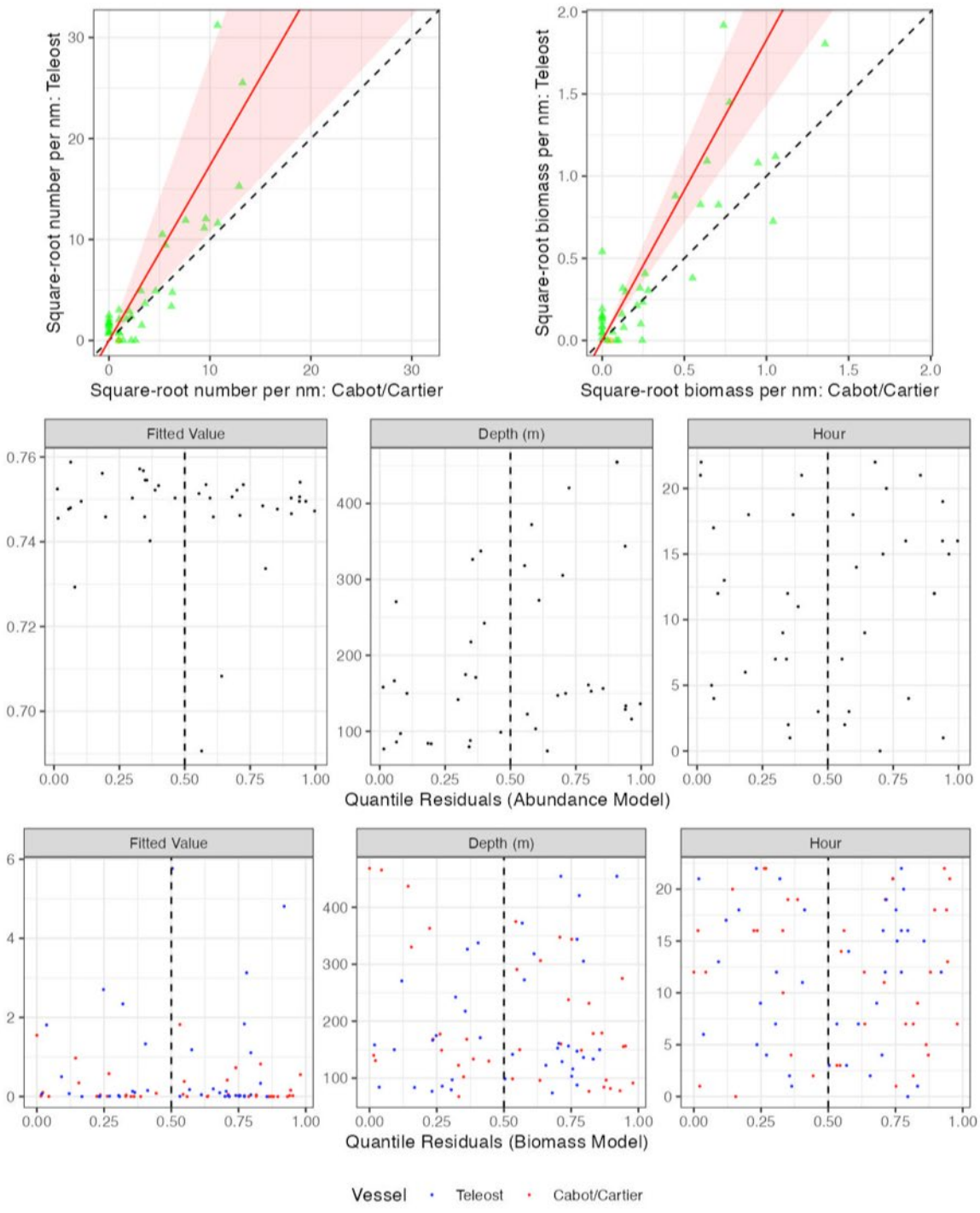

Figure 90. Visualisation of comparative fishing data, size-aggregated model predictions and residual diagnostics plots for Ctenodiscus crispatus (6115).

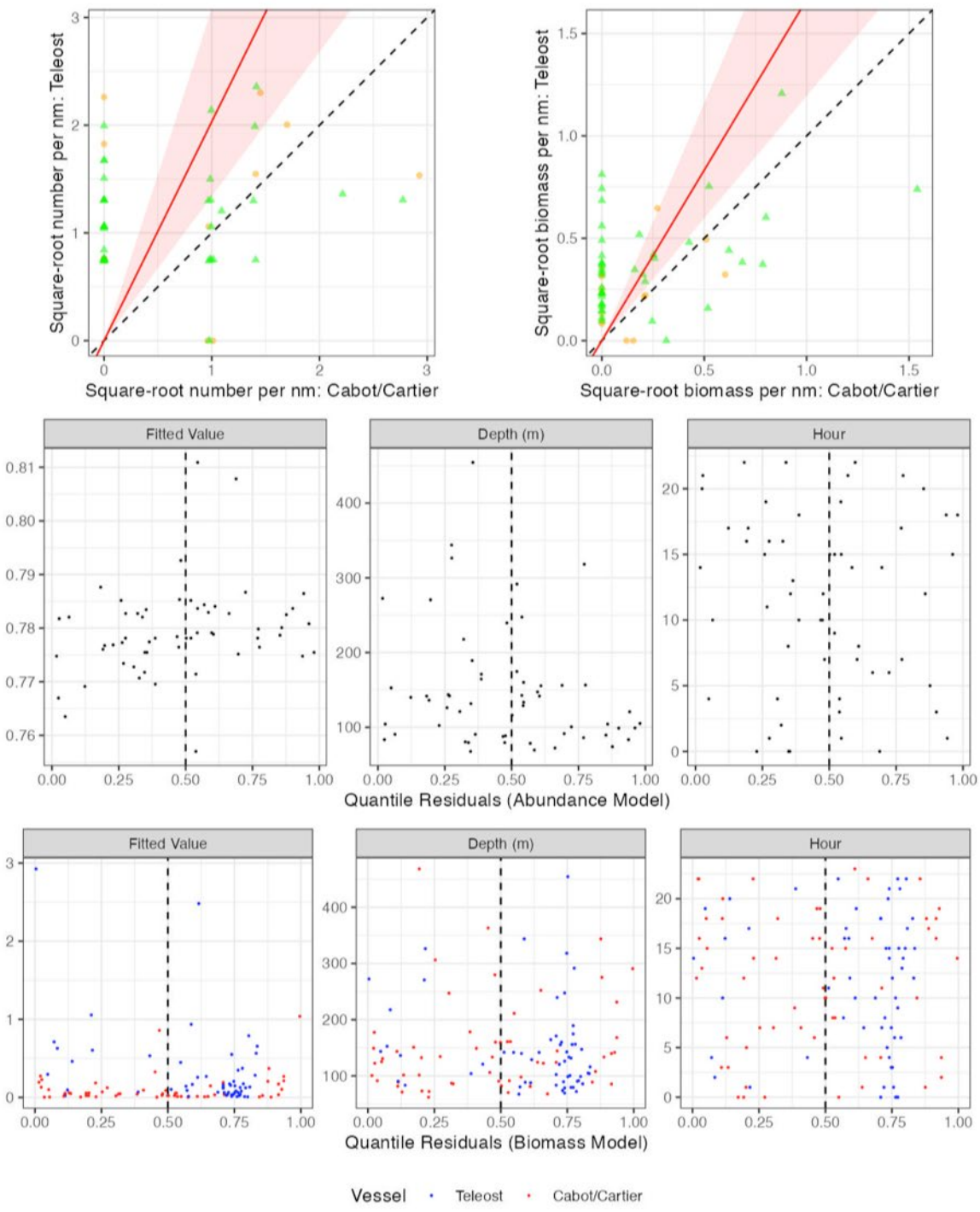

Figure 91. Visualisation of comparative fishing data, size-aggregated model predictions and residual diagnostics plots for Hippasteria phrygiana (6117).

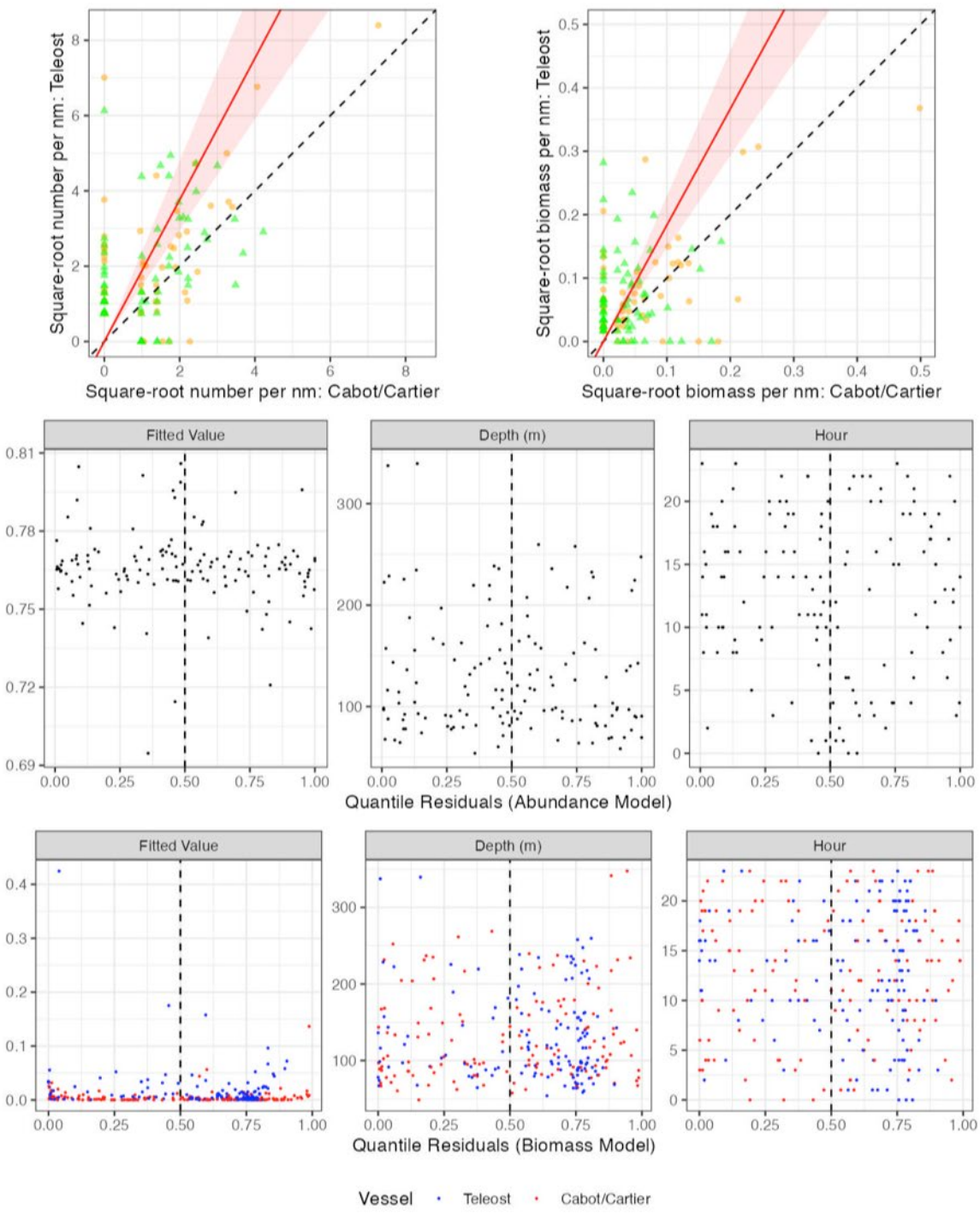

Figure 92. Visualisation of comparative fishing data, size-aggregated model predictions and residual diagnostics plots for Henricia sp. (6118).

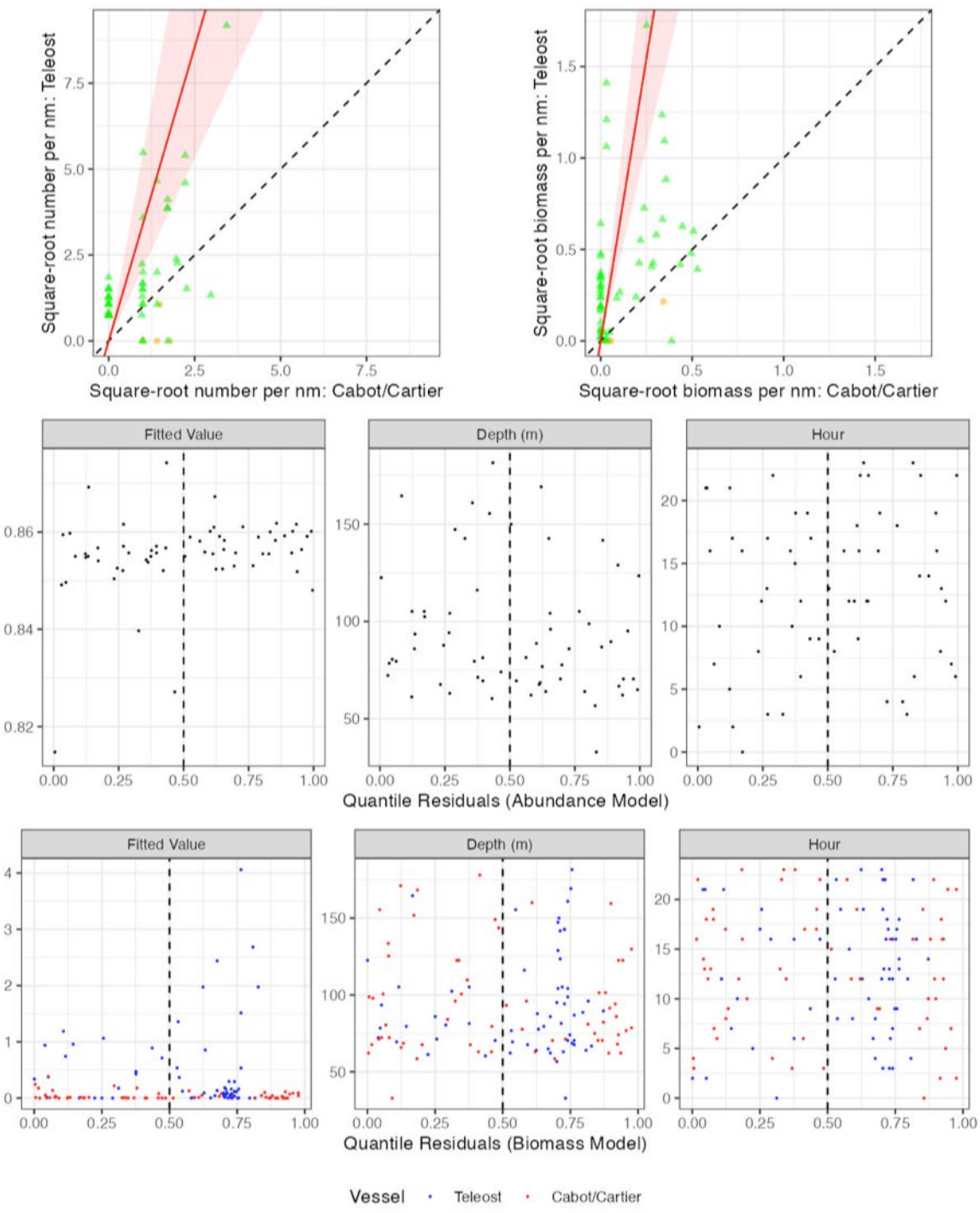

Figure 93. Visualisation of comparative fishing data, size-aggregated model predictions and residual diagnostics plots for Crossaster papposus (6123).

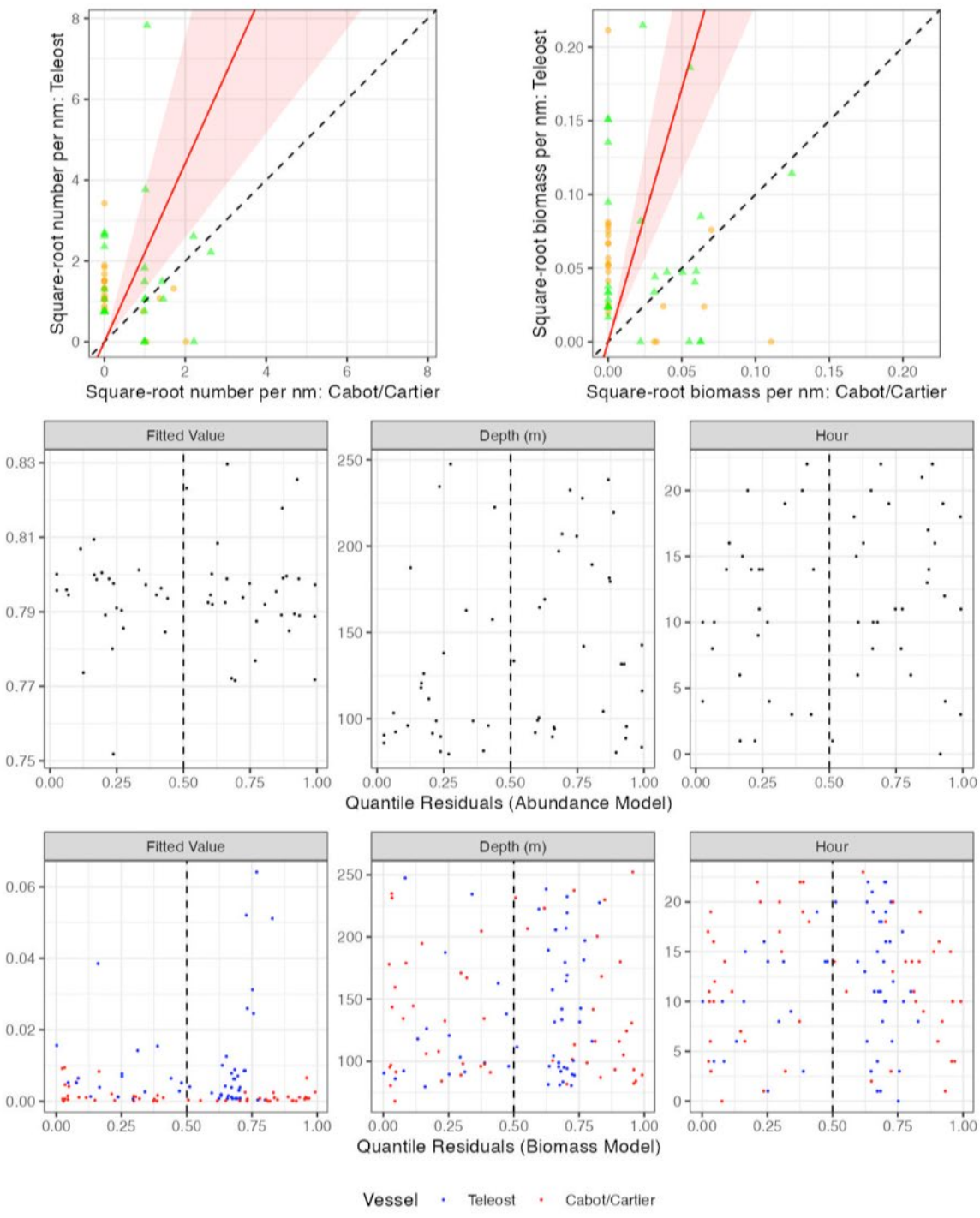

Figure 94. Visualisation of comparative fishing data, size-aggregated model predictions and residual diagnostics plots for Pteraster pulvillus (6126).

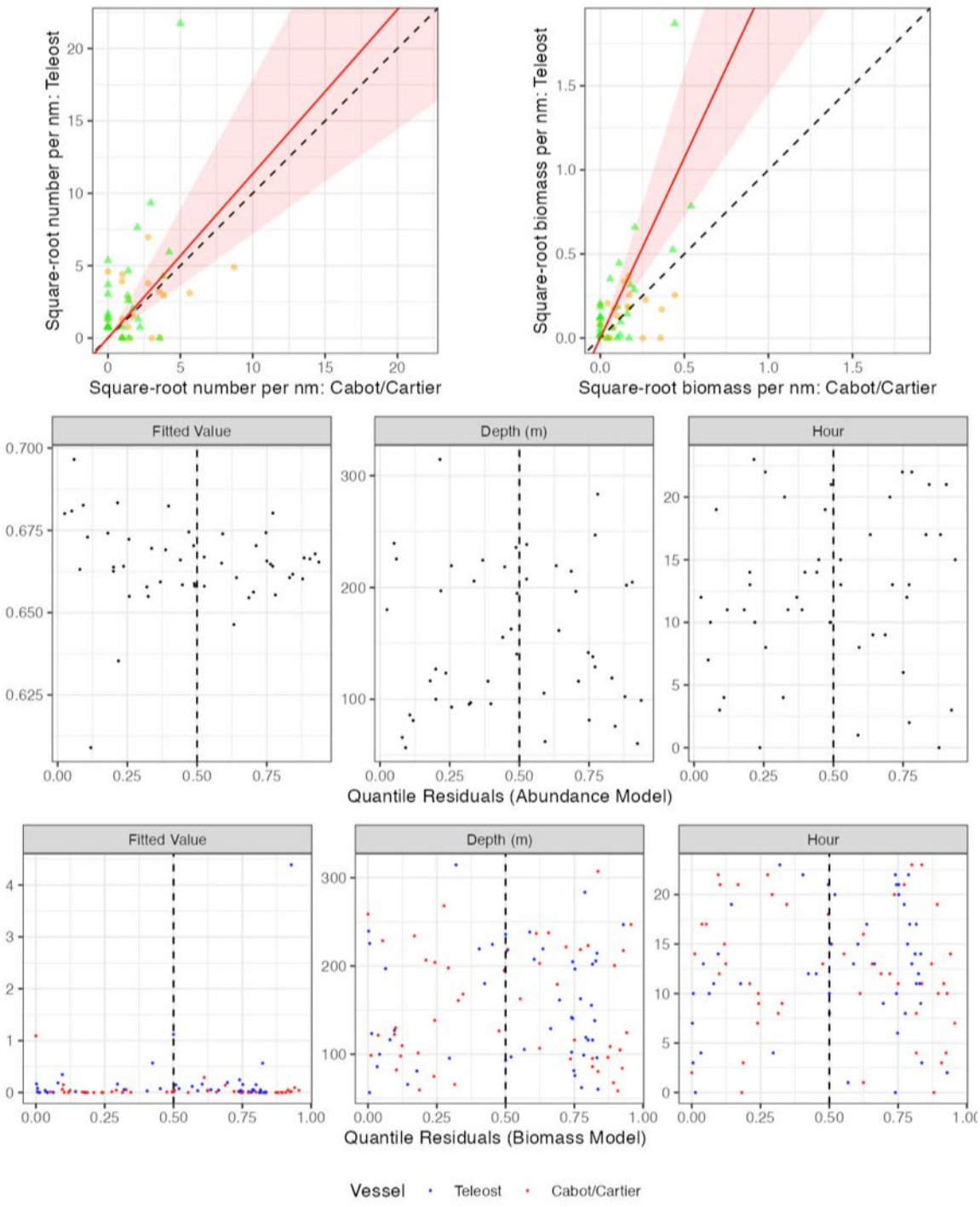

Figure 95. Visualisation of comparative fishing data, size-aggregated model predictions and residual diagnostics plots for Astropecten americanus (6136).

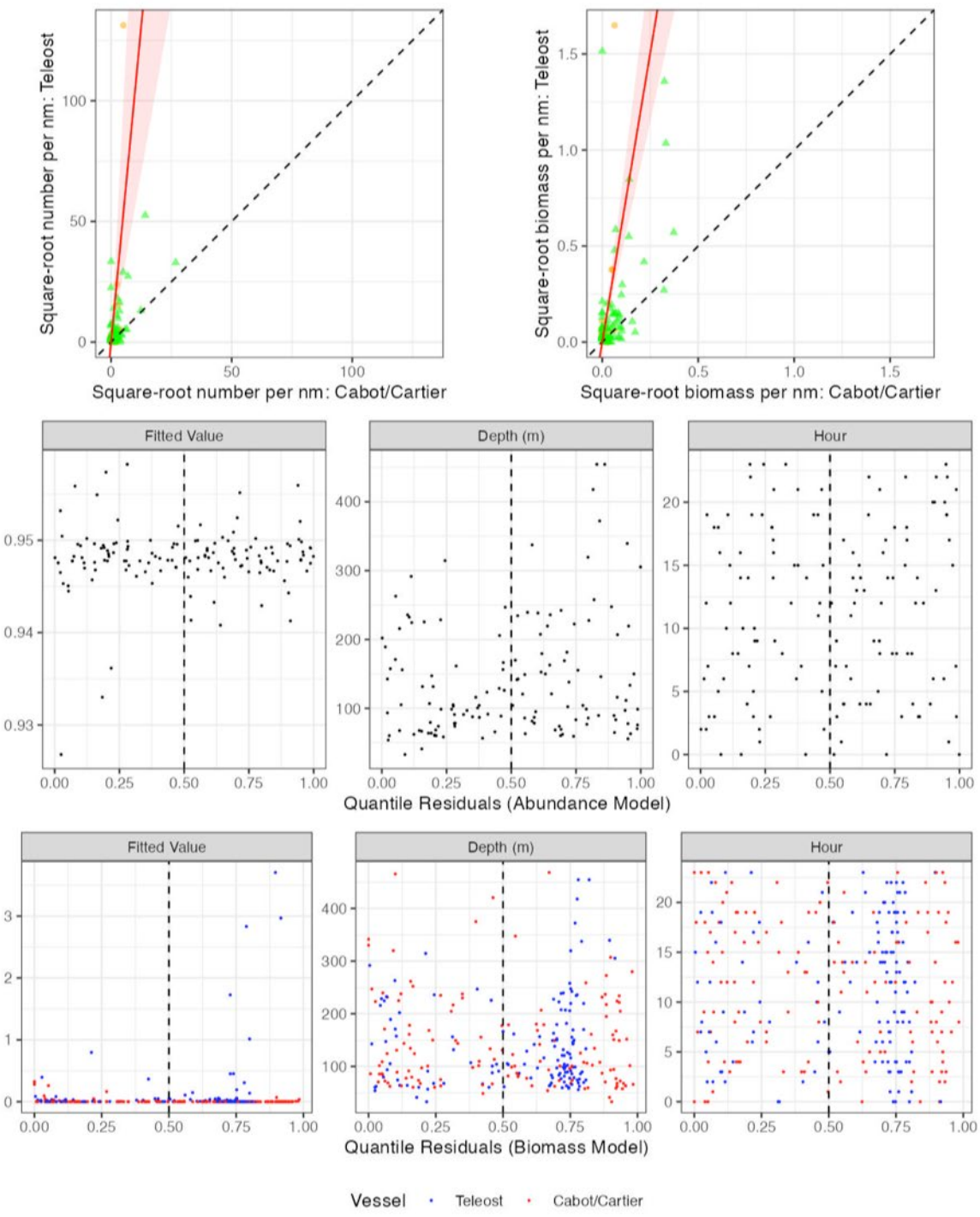

Figure 96. Visualisation of comparative fishing data, size-aggregated model predictions and residual diagnostics plots for Ophiuroidea s.c. (6200).

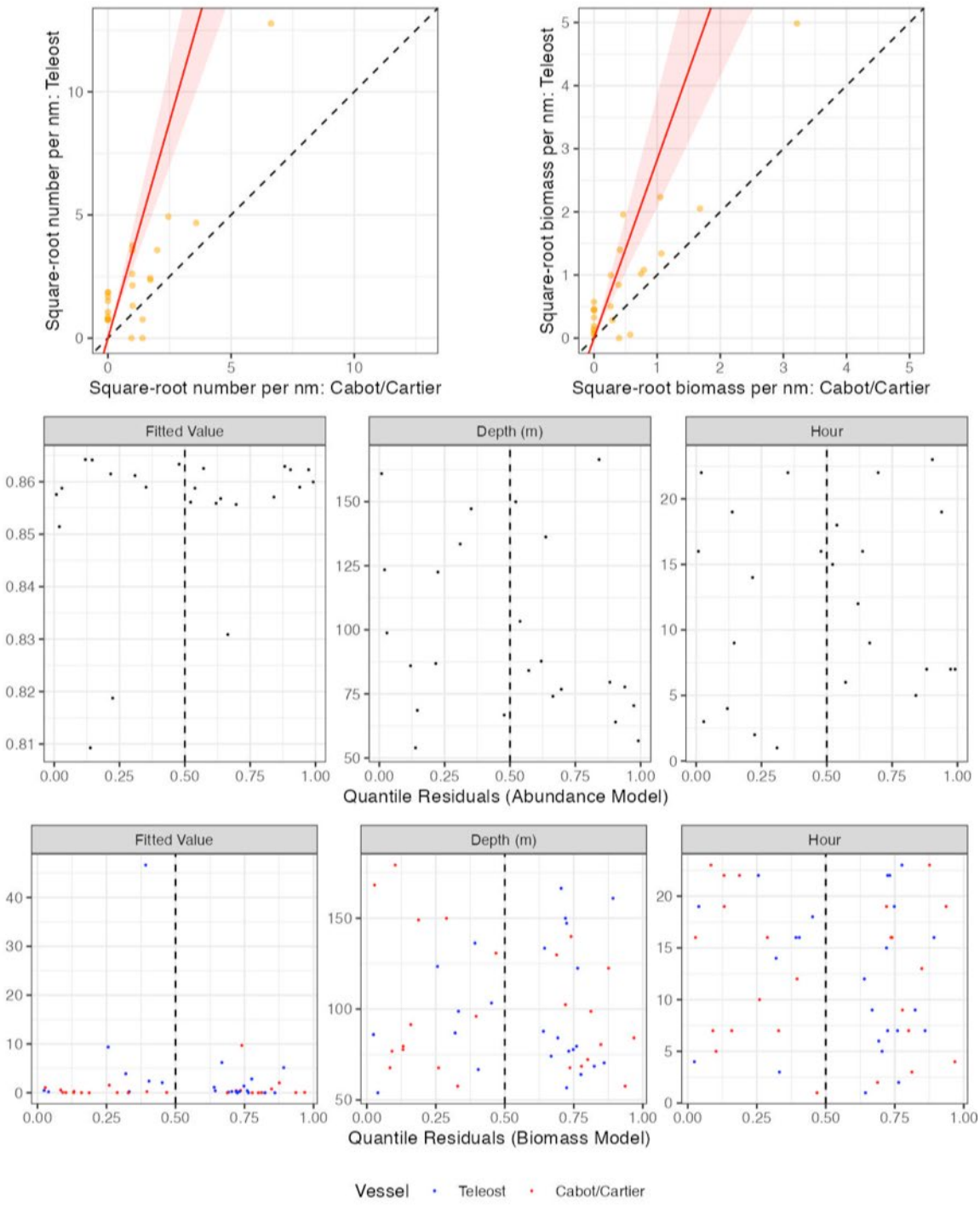

Figure 97. Visualisation of comparative fishing data, size-aggregated model predictions and residual diagnostics plots for Gorgonocephalidae,asteronychidae f. (6300).

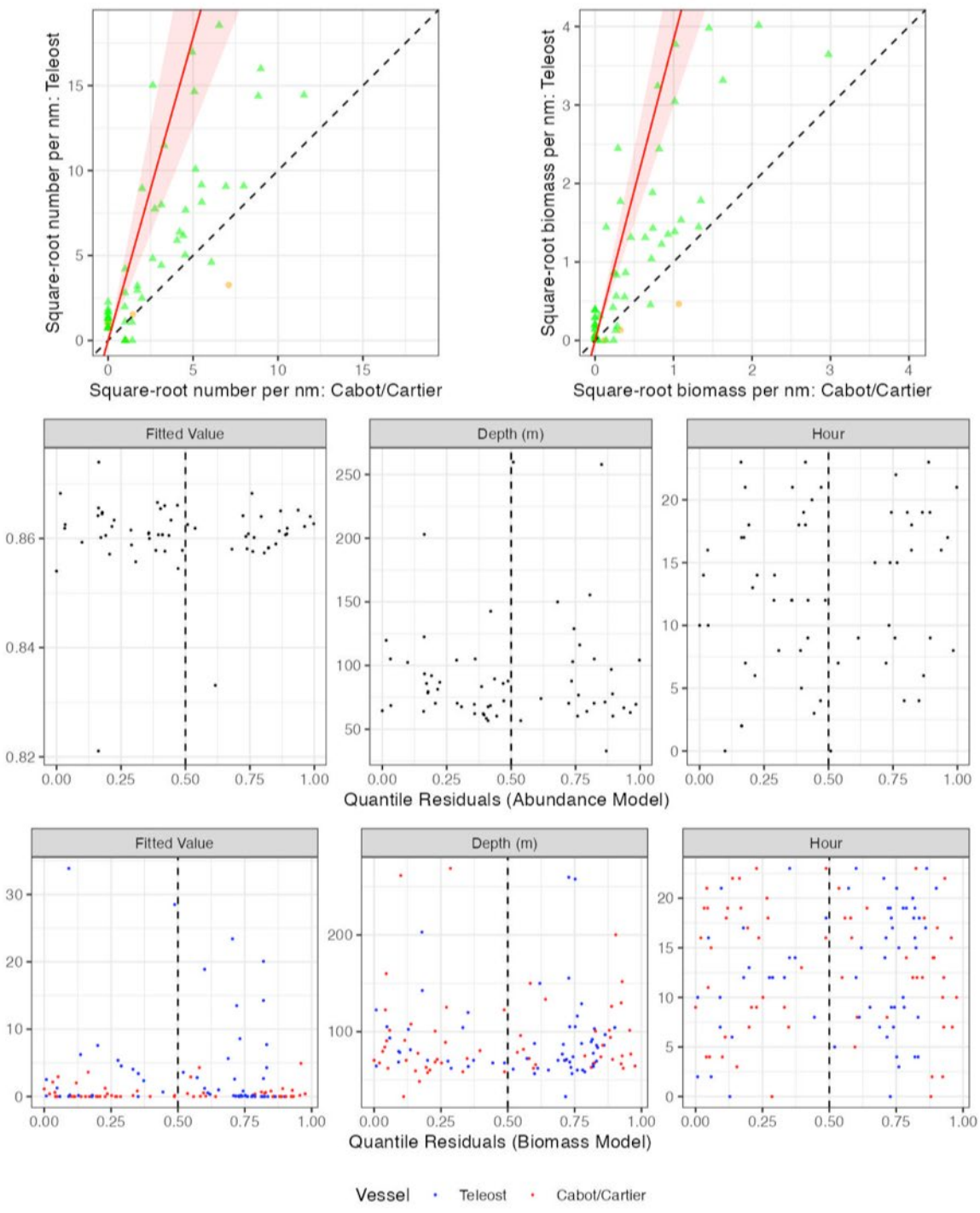

Figure 98. Visualisation of comparative fishing data, size-aggregated model predictions and residual diagnostics plots for Strongylocentrotus sp. (6400).

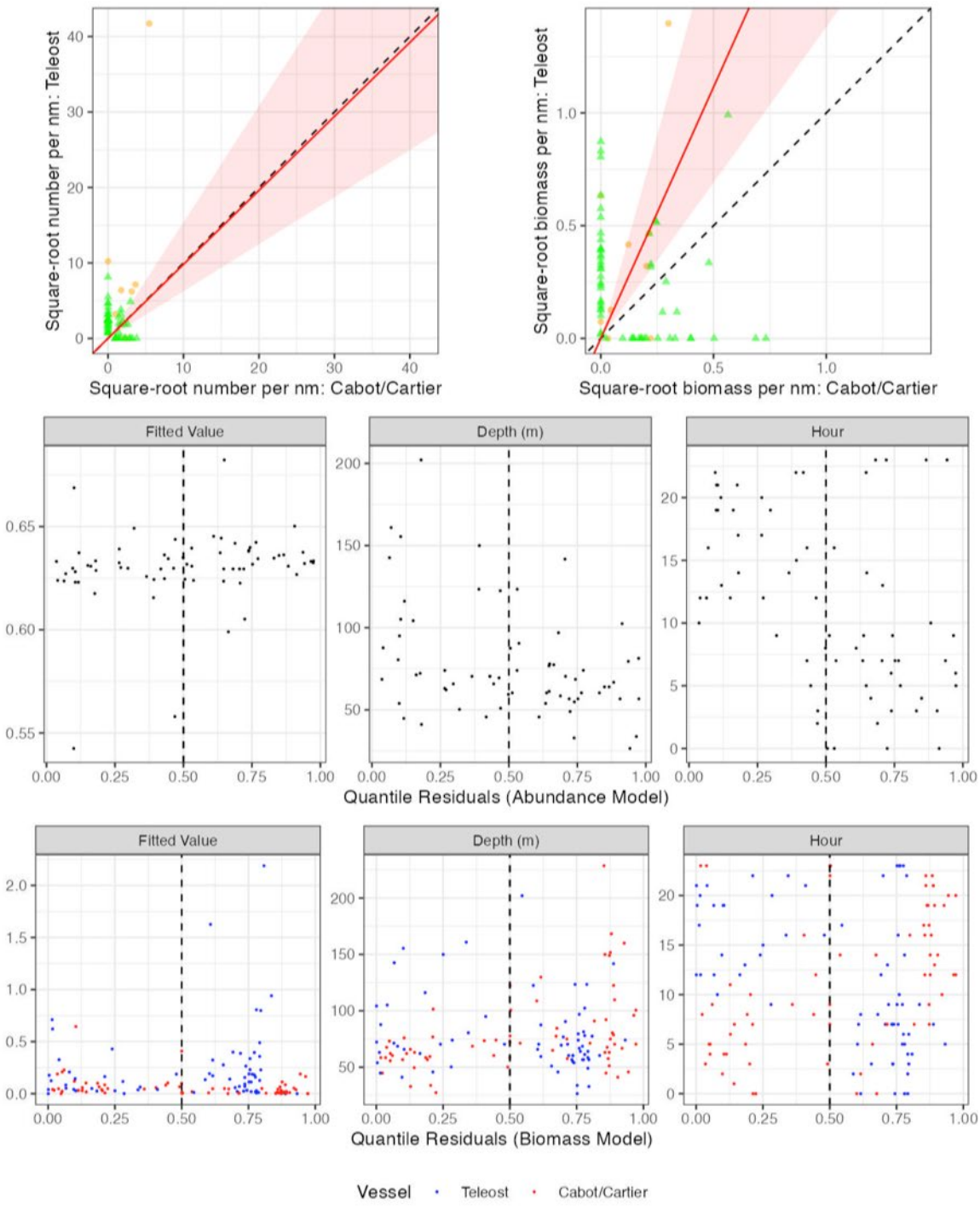

Figure 99. Visualisation of comparative fishing data, size-aggregated model predictions and residual diagnostics plots for Echinarachnius parma (6511).

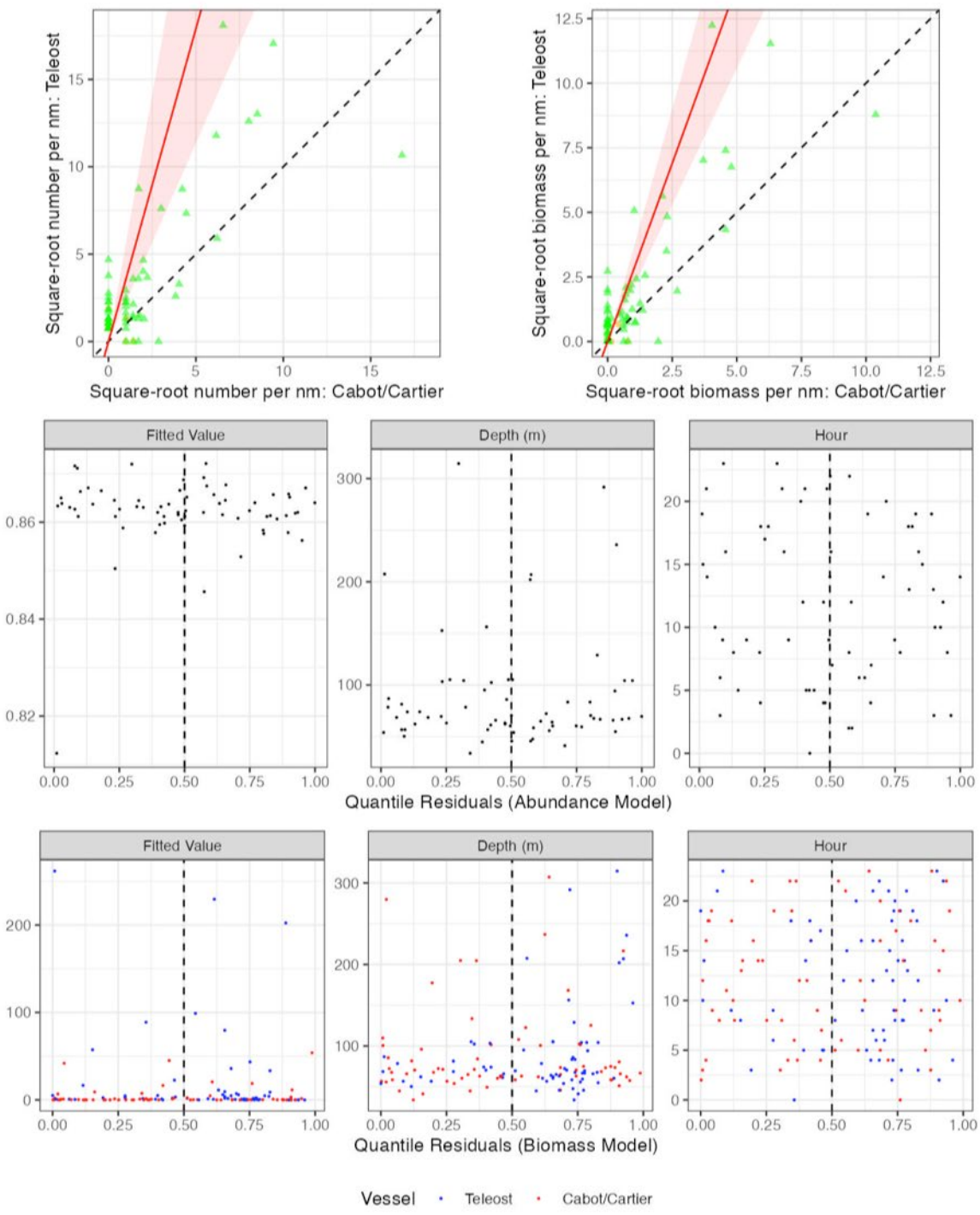

Figure 100. Visualisation of comparative fishing data, size-aggregated model predictions and residual diagnostics plots for Holothuroidea c. (6600).

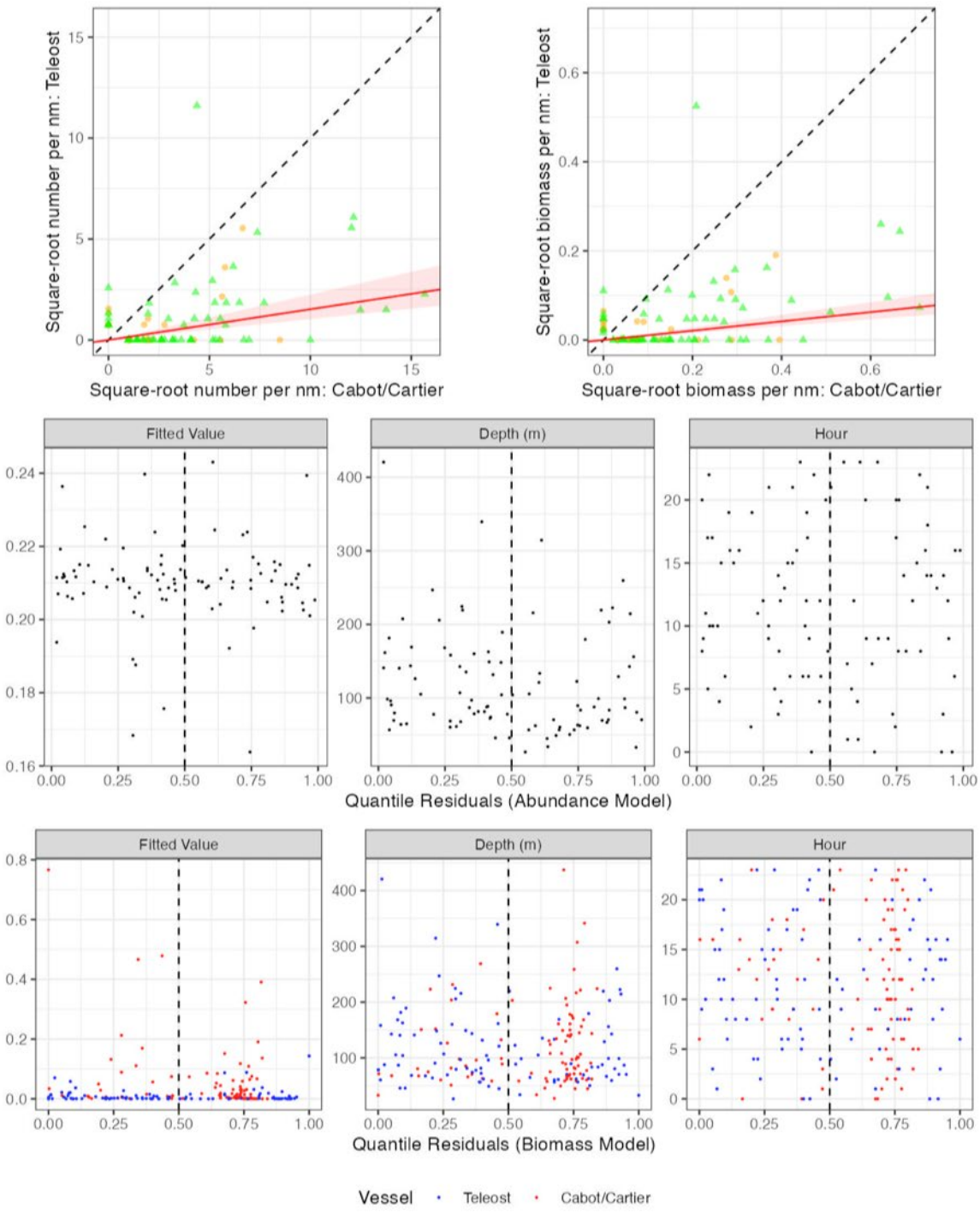

Figure 101. Visualisation of comparative fishing data, size-aggregated model predictions and residual diagnostics plots for Ctenophora p. (8100).

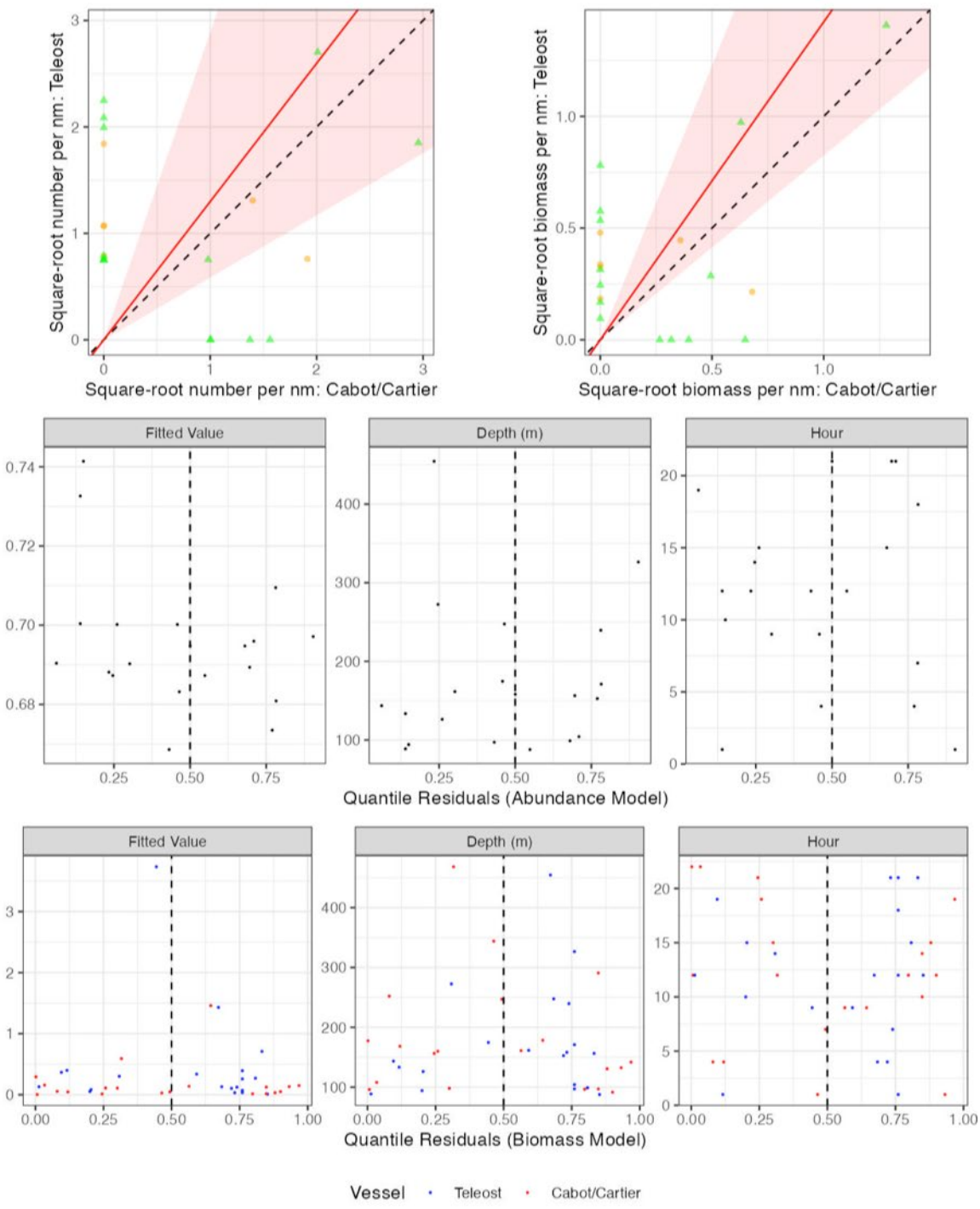

Figure 102. Visualisation of comparative fishing data, size-aggregated model predictions and residual diagnostics plots for Actinostola spp. (8216).

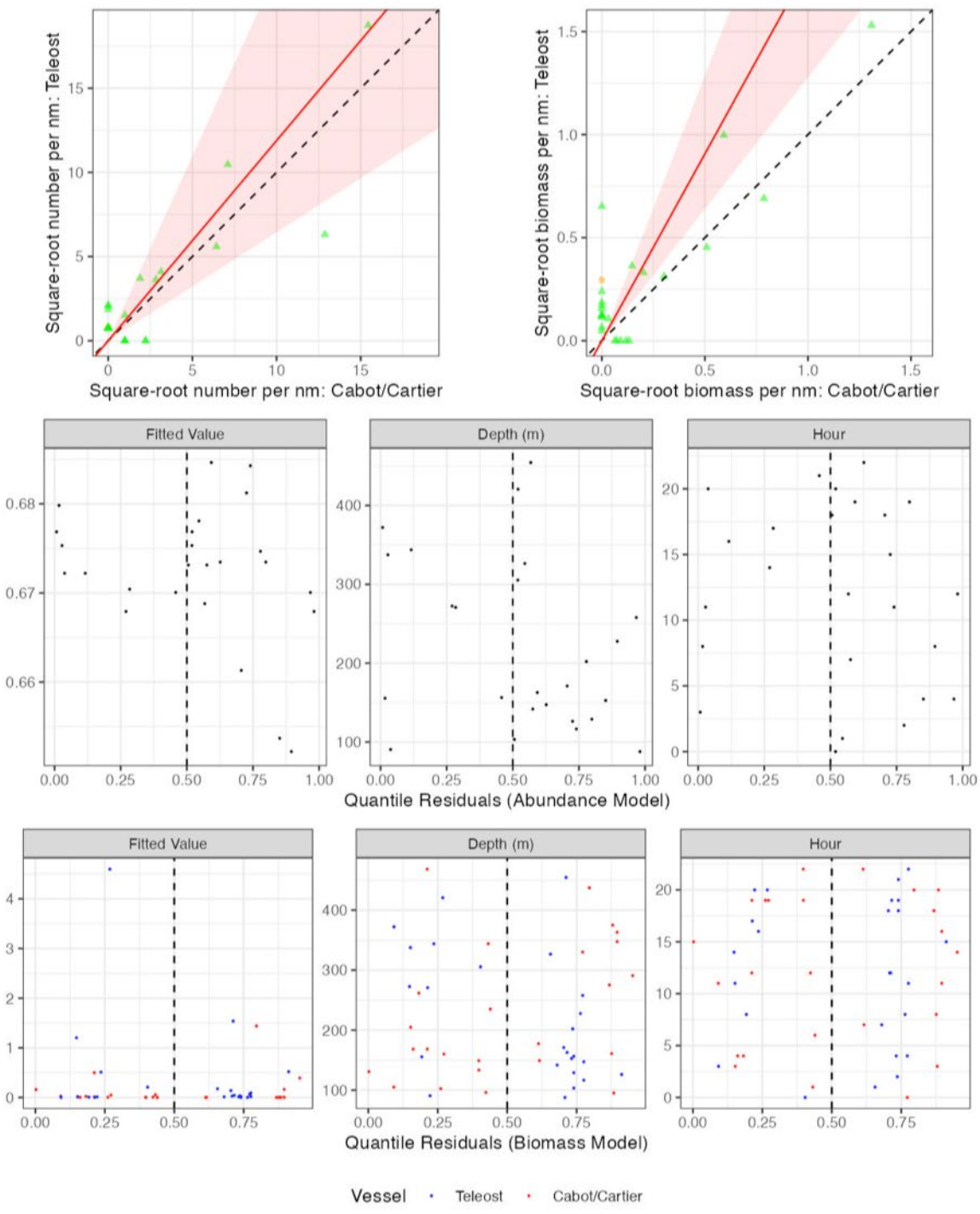

Figure 103. Visualisation of comparative fishing data, size-aggregated model predictions and residual diagnostics plots for Hormathia sp. (8316).

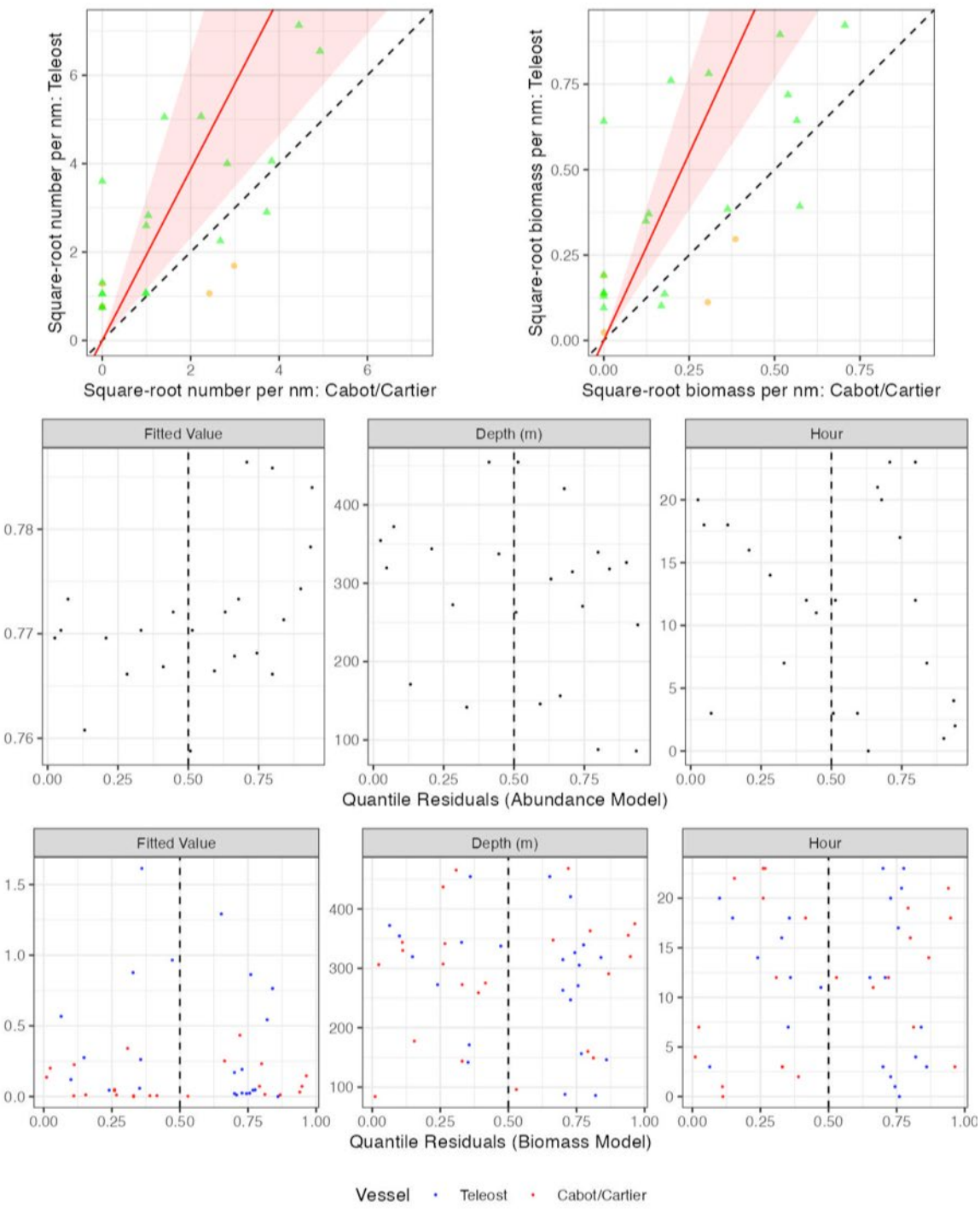

Figure 104. Visualisation of comparative fishing data, size-aggregated model predictions and residual diagnostics plots for Psilaster andromeda (8347).

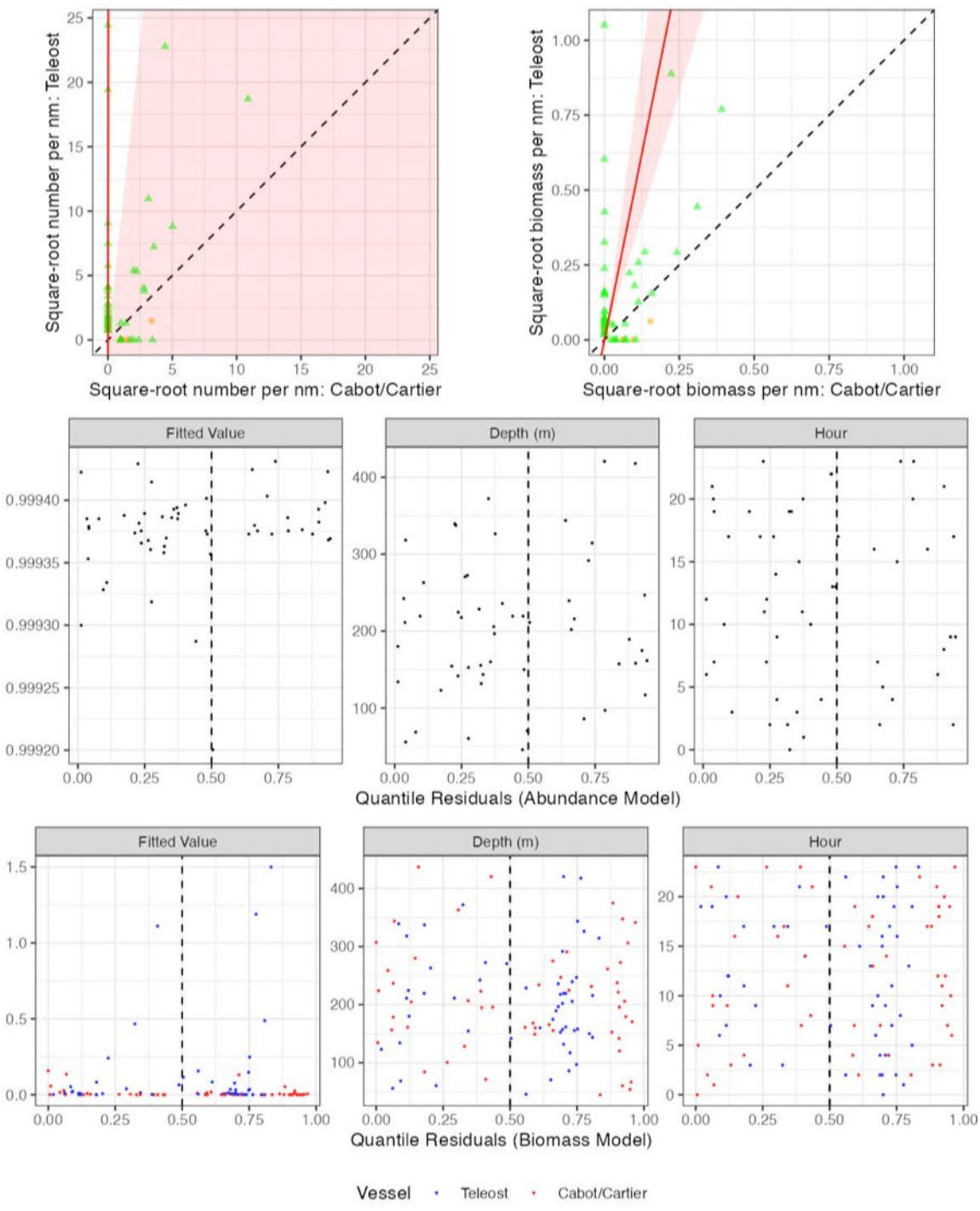

Figure 105. Visualisation of comparative fishing data, size-aggregated model predictions and residual diagnostics plots for Pennatula aculeata (8367).

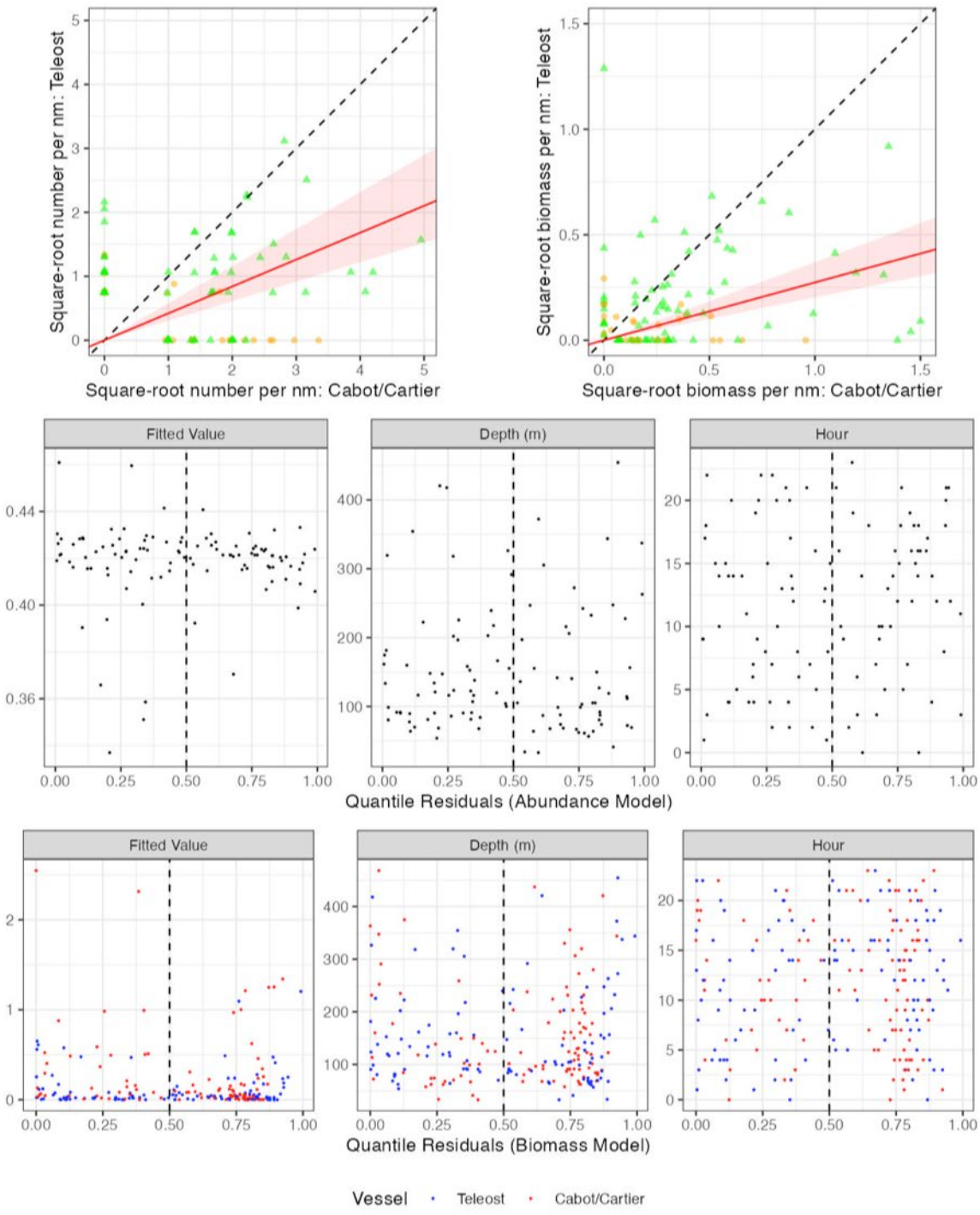

Figure 106. Visualisation of comparative fishing data, size-aggregated model predictions and residual diagnostics plots for Scyphozoa c. (8500).

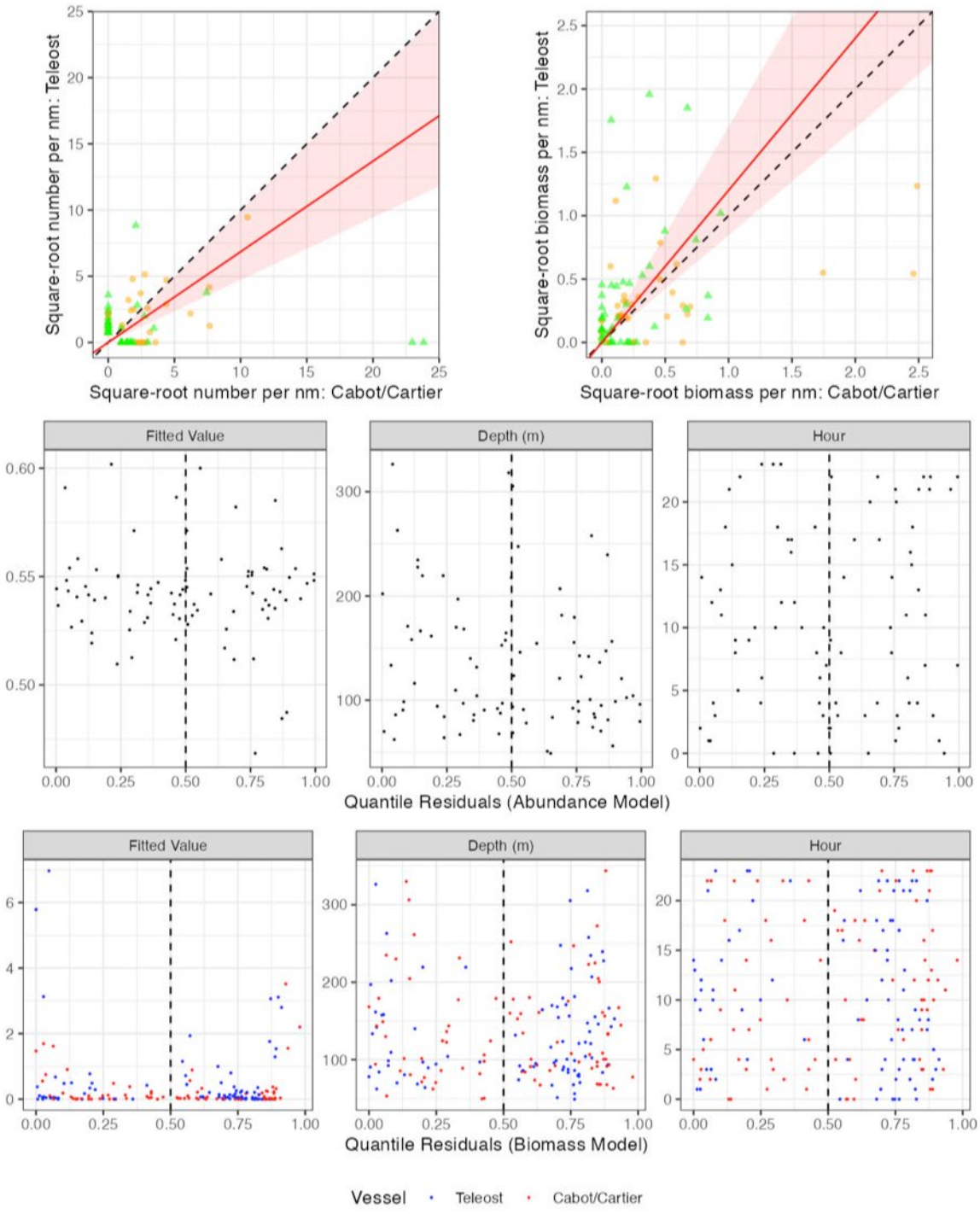

Figure 107. Visualisation of comparative fishing data, size-aggregated model predictions and residual diagnostics plots for Porifera p. (8600).

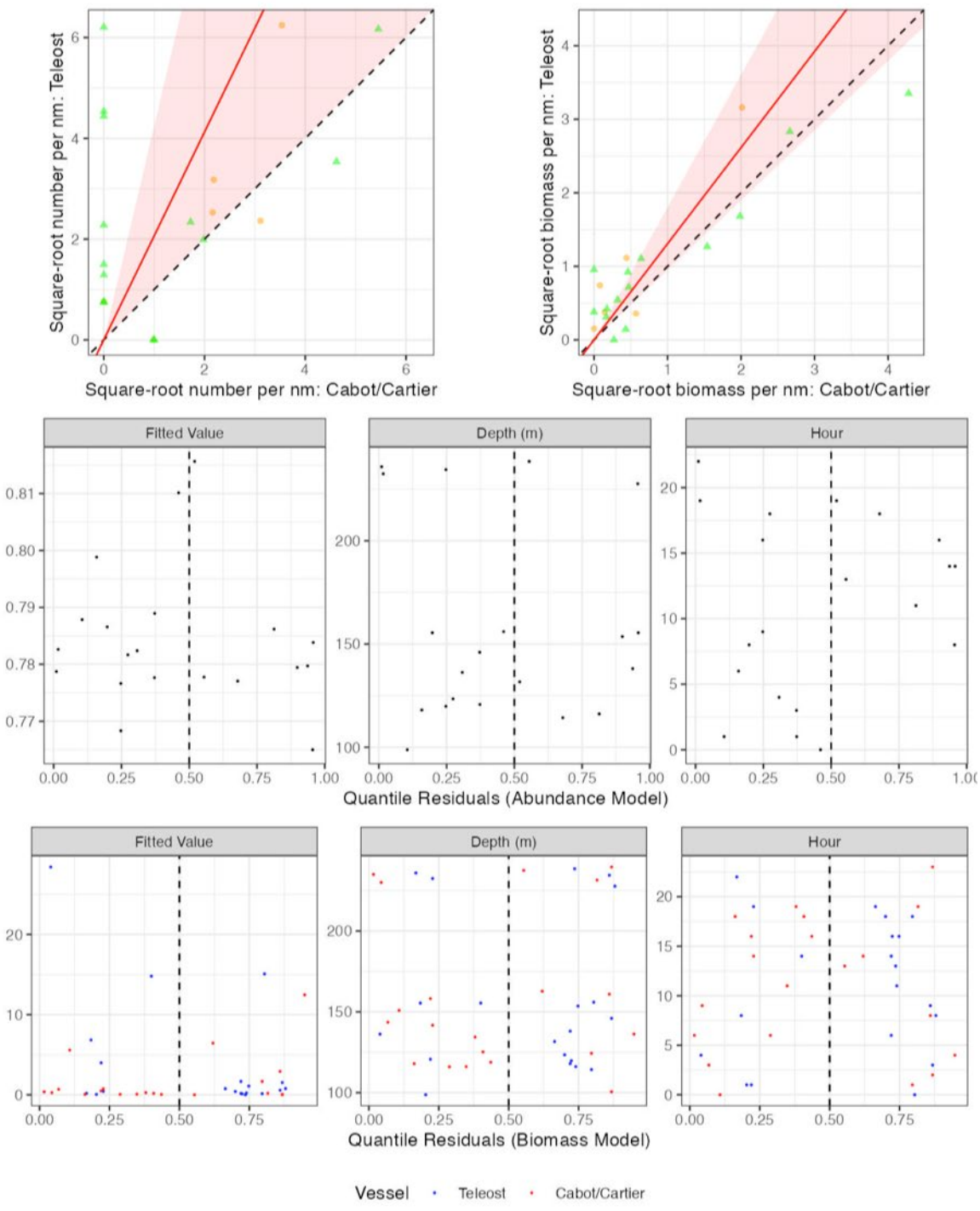

Figure 108. Visualisation of comparative fishing data, size-aggregated model predictions and residual diagnostics plots for Vazella pourtalesi (8601).

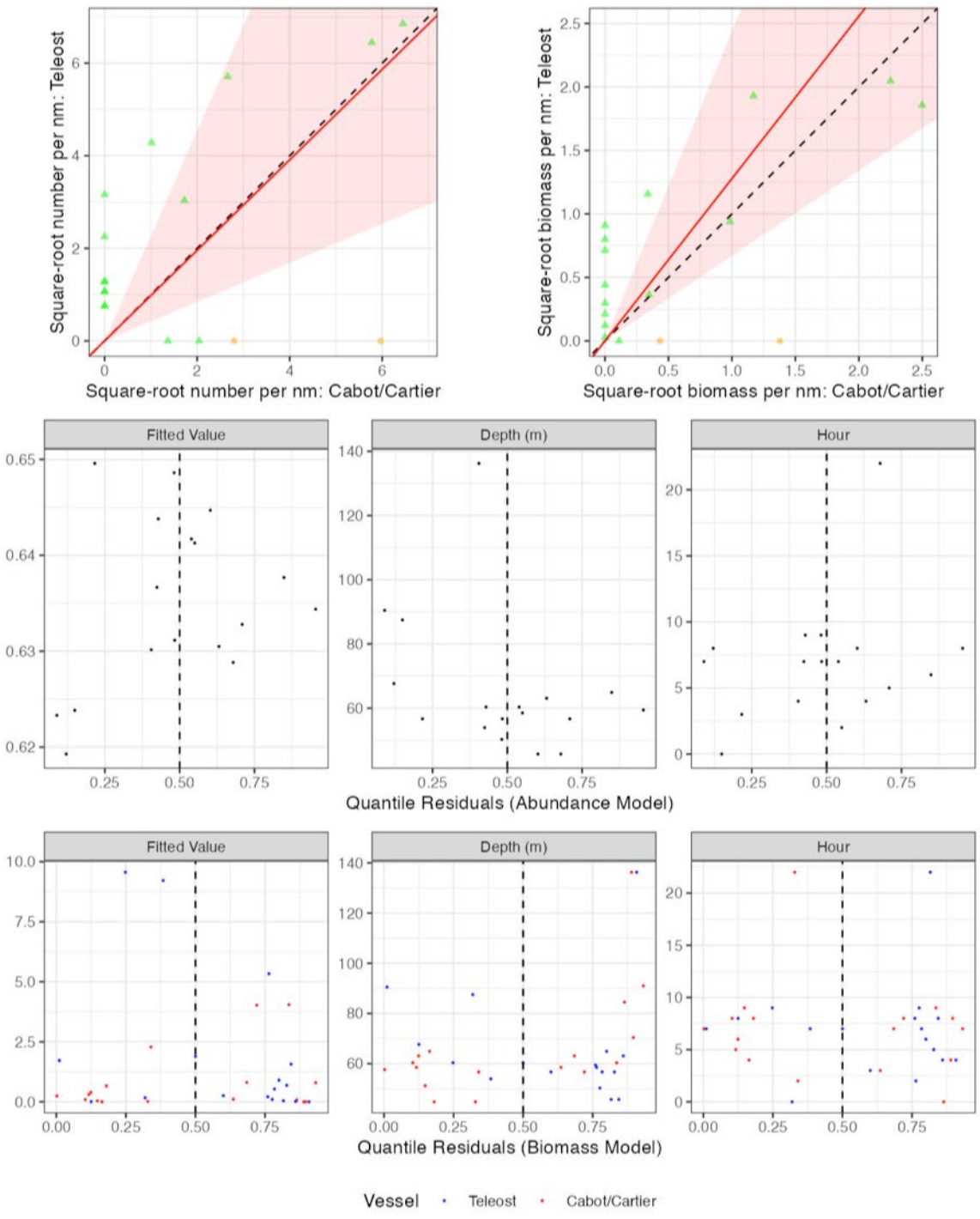

Figure 109. Visualisation of comparative fishing data, size-aggregated model predictions and residual diagnostics plots for Suberites ficus (8613).